Phytoplankton Community Structure, Photophysiology and Primary Production in the Atlantic Arctic.

by

Thomas Jackson

Thesis submitted to the University of Oxford

for the degree of Doctor of Philosophy

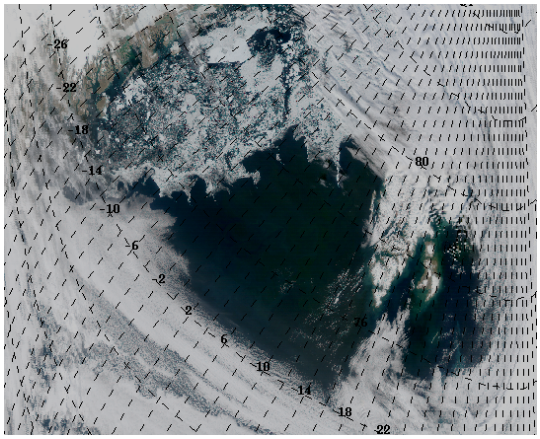

Department of Earth Sciences

St Edmund Hall

University of Oxford

September, 2013

Supervised by Dr Heather A. Bouman

Dr Shubha Sathyendranath

and

Dr Gavin Tilstone

The fact that the Arctic, more than any other populated region of the world, requires the collaboration of so many disciplines and points of view to be understood at all, is a benefit rather than a burden.

Bruce Jackson (1936 –)

Blue, green, grey, white, or black; smooth, ruffled, or mountainous; that ocean is not silent.

H.P. Lovecraft (1890-1937)

Excerpts from 'Apostrophe to the Ocean'

There is a pleasure in the pathless woods,
There is a rapture on the lonely shore,
There is society where none intrudes,
By the deep Sea, and music in its roar:
I love not Man the less, but Nature more,
From these our interviews, in which I steal
From all I may be, or have been before,
To mingle with the Universe, and feel
What I can ne'er express, yet cannot all conceal.

And I have loved thee, Ocean! and my joy
Of youthful sports was on thy breast to be
Borne like thy bubbles, onward: from a boy
I wantoned with thy breakers–they to me
Were a delight; and if the freshening sea
Made them a terror–'twas a pleasing fear,
For I was as it were a child of thee,
And trusted to thy billows far and near,
And laid my hand upon thy mane–as I do here.

Lord Byron (1788-1824)

Declaration

This dissertation is the result of my own work. It does not exceed the page limit set out by the degree committee and is not the same as any work that has been, or is being submitted to any other university for any degree, diploma or other qualifications.

Thomas Jackson

Abstract

Phytoplankton Community Structure, Photophysiology and Primary Production in the Atlantic Arctic.

Thomas Jackson, St Edmund Hall, Oxford

Trinity Term, 2013

The Arctic is a region undergoing unprecedented and unequivocal climate change. The seas of this extreme region form a major component of the oceanic thermohaline conveyor and natural carbon cycle. Using a combination of recent and historical datasets this study examines the distribution, diversity, photophysiology and primary productivity of phytoplankton in the Atlantic sector of the Arctic Ocean. CHEMTAX analysis reveals a diverse phytoplankton community structure in the Greenland Sea comprising six main phytoplankton groups. The influence of sea-ice and water column stratification are key factors in the presence or absence of groups such as haptophytes and prasinophytes. Group-specific differences are observed in spectral absorption and photophysiological parameters. However, the influence of environmental factors has a stronger influence than taxonomic composition on photophysiology. A clear division between the photoacclimatory response of algal communities beneath sea-ice and those of open-ocean stations is predominantly due to 'E_k independent' photoacclimation beneath sea-ice. This occurs due to the combined effect of sea-ice decreasing irradiance entering the water column and a positive correlation between P_m^B and temperature. This variation in photophysiology is important for primary production models as a sensitivity analysis shows that errors in these parameters propagate to give the largest final errors in primary production values. The importance of other model parameters varies with the level of biomass in the water column and the presence or absence of sea ice. Accelerated ice-melt and an increase in open water due to climate change are likely to increase primary production in the Atlantic Arctic alongside an altered distribution of phytoplankton groups, with an increase in the importance of prasinophytes or haptophytes.

Extended Abstract

Phytoplankton Community Structure, Photophysiology and Primary Production in the Atlantic Arctic.

Thomas Jackson, St Edmund Hall, Oxford

Trinity Term, 2013

The Arctic is undergoing the most rapid climate change of any region in the world. The changes in the physical environment will have important repercussions for the distribution and growth of Arctic phytoplankton. These single-celled autotrophs form the base of the marine ecosystems and play a key role in the carbon cycle of the high latitude Atlantic, which is a critical component in the global carbon cycle and is one of the major oceanic CO_2 sinks. This thesis focusses on the Atlantic sector of the Arctic and investigates the phytoplankton community structure (Chapter 2), photophysiology (Chapter 3) and primary production (Chapter 4) in relation to the physical and chemical properties of the water column, which in turn are governed by the presence sea ice.

Chapter 1 introduces the importance of marine primary production on regional and global scales. The methods used to divide the oceans into ecosystems relevant for the modelling of biogeochemistry and primary production are then described. The current hydrographic conditions for phytoplankton growth in the Arctic Ocean are summarised and the reasons for the increased interest in Arctic marine ecosystems in recent decades are discussed. Chapter 1 also introduces the diversity of phytoplankton and methods used for grouping them in relation to their taxonomic class, size or biogeochemical function. The basic requirements for primary production models are explained and the problem of model complexity is considered.

In Chapter 2, phytoplankton accessory pigments measured using High Performance Liquid Chromatography were analysed using cluster analysis and CHEMTAX. The pigment data showed that the region was host to six major phytoplankton taxonomic groups. Diatoms, cryptophytes, prasinophytes, haptophytes, dinoflagellates and chrysophytes were

each estimated to contribute >50 % of the biomass in a number of samples. Microscopy data was used to validate the CHEMTAX estimation of group-specific biomass prior to interpretation of the relationships between taxonomy and environmental variables. The correlation between phytoplankton community structure and environmental variables was investigated using principle component analysis (PCA). The results from the PCA and the spatial distribution of pigment clusters demonstrated that the presence of sea-ice plays a key role in controlling many properties of the water column that govern phytoplankton growth in the surface ocean, such as water temperature and light. The implications of a changing Arctic climate are discussed in light of the relationships identified and increased summer ice-melt is likely to lead to an increase in the importance of haptophytes or prasinophytes, depending upon the future strength of stratification and water temperature of Atlantic Arctic surface waters.

While Chapter 2 analysed the diversity and distribution of phytoplankton groups in the Atlantic Arctic, Chapter 3 assesses the variability of bio-optical and photophysiological parameters, in relation to both taxonomic group and environmental conditions. Group-specific differences in the shape of phytoplankton absorption spectra were observed which have important implications for both the identification of Phytoplankton Functional Types and the estimation of phytoplankton biomass from remotely-sensed data. Despite the diversity and heterogeneity observed in phytoplankton community structure, there were a number of persistent patterns seen in the photophysiology of the phytoplankton assemblages. There was a strong relationship between temperature and maximum photosynthetic rate (P_m^B), which was consistent with historical data covering much of the Western Atlantic Arctic. Vertical profiles of α^B between sea-ice and open-ocean stations: samples collected beneath sea ice exhibited less variation in α^B with depth due to the reduced light levels in the near surface and the limitation of maximum growth rate at low water temperatures. Irrespective of the phytoplankton groups present, an increase in surface temperatures led to an increase in the maximum photosynthetic rate of phytoplankton in these polar waters and a reduction in the extent of sea-ice may lead to a much greater variability in photosynthetic parameters. Culture

studies of Arctic phytoplankton grown over a range of temperatures also supported the field data reported in Chapter 2, that climate warming may favour prasinophytes and haptophytes over dinoflagellates and cryptophytes.

In Chapter 4 the impact of incorrectly estimating the photophysiology of phytoplankton on modelled primary production estimates was examined as part of a detailed sensitivity analysis. Prior to the sensitivity analysis, the validity of PAR data sources available for input into the model were examined. The BIRD radiative transmission model was used in the modelling study due to its high temporal resolution and good performance at low zenith angles. The results from the sensitivity analysis show that for both open-ocean and under-ice stations an incorrect assignment of the photophysiological parameters is the largest potential source of error in the final estimates of production, which is consistent with modelling studies from other regions. Factors such as the absorption efficiency of phytoplankton, absorption by CDOM, cloud cover, and the biomass profile can all cause errors of $>$30 % if incorrectly estimated for input into the model. When using parameters measured *in situ*, the model gave a range of oceanic primary production estimates of $\approx$25 - 2250 mg m^{-2} day^{-1}. A non-spectral primary production model routinely used for both regional and global studies consistently overestimated primary production. The primary production model results support the hypothesis that an increased area of open water could significantly increase primary production in the Atlantic Arctic.

This study has determined that there is a distinct shift in the phytoplankton community structure, phytoplankton photophysiology and primary production across the sea-ice boundary in the Arctic Atlantic. The analysis of HPLC pigment and photophysiology data suggests that a declining summer sea-ice extent may lead to a shift in the dominant phytoplankton groups across a broad region alongside greater photophysiological variability and increased marine primary production. Results from this body of work raise key problems that should be addressed in future Arctic research. Firstly, although all open-ocean waters encountered in this study could be modelled optically as Case-I waters, the relationship between phytoplankton and CDOM absorption appears to be

influenced by sea ice. Analysis of vertical structure in the biomass profiles showed that the presence of sub-surface maxima is predominantly a feature of under-ice stations in the Atlantic Arctic during the summer, but assignment of the parameters describing the shape of the biomass profile in this heterogeneous environment remains a challenge, though with a larger combined dataset a nearest neighbour method may prove fruitful.

Acknowledgements

Firstly, I would like to thank my primary supervisor Heather Bouman, who has been an invaluable guide and font of knowledge as I have entered into the world of scientific research. She introduced me to biological oceanography as an undergraduate and has helped me hone my research skills throughout my PhD.

I would also like offer many thanks to my co-supervisors Shubha Sathyendranath and Gavin Tilstone for their input, support and instruction. There are others at Plymouth Marine Laboratory to whom I am indebted for training and assistance; Trevor Platt, Victor Martinez and Morvan Barnes made me feel welcome and were essential to my scientific training.

Ray Leakey (SAMS), who was the PSO on the ICE CHASER 2010 expedition, and the captain and crew of the RRS *James Clark Ross* were responsible for the smooth execution of my work in the Arctic Ocean. Thanks must also be given to Colin Griffiths and Estelle Dumont (SAMS) for their technical support.

To my long suffering office mates, Mark, Maeve and Julia I would like to say thanks for the great working atmosphere and fantastic company.

Many thanks go to my parents for their continued support and assistance.

To my wife, Rebecca Jackson, I would like to offer the warmest of thanks. She has supported me when work got tough and always knew when I needed to step back and take a break or change the way I was approaching a problem. She is a constant force in the turbid world of scientific discovery and one without whom I probably would have given up long ago.

I would like to acknowledge the funding of this project by the Natural Environment Research Council, UK.

Contents

Declaration i
Abstract iii
Extended Abstract iv
Acknowledgements viii
Contents xii
List of Figures xv
List of Tables xvii

1 Introduction **1**
1.1 Overview 1
1.2 Marine photosynthesis and primary production 2
1.2.1 Global estimates of production 4
1.2.2 Phytoplankton classification and functional types 6
1.2.3 Phytoplankton blooms 8
1.2.4 Phytoplankton pigments 8
1.3 Modelling phytoplankton production 10
1.3.1 Basic requirements 10
1.3.2 Model complexity 11
1.3.3 Scaling up primary production models 12
1.4 Dividing up the oceans 13
1.4.1 Biogeochemical ocean provinces 14
1.4.2 Bio-optical water types 16

1.5 The Arctic region 17
1.5.1 Defining the Arctic 17
1.5.2 Physical conditions and extremes of the Arctic 20
1.5.3 Climate change 24
1.5.4 The Arctic and the carbon cycle 25
1.6 Summary and aims of work 27

2 Phytoplankton community structure in the Greenland Sea: validation and interpretation of CHEMTAX analysis in relation to environmental forcing 31
2.1 Introduction 32
2.2 Methods 37
2.2.1 Study area 37
2.2.2 Environmental data 40
2.2.3 Phytoplankton pigment analysis 41
2.2.4 Interpretation of pigment data 42
2.2.5 Cell counts used for CHEMTAX validation 46
2.3 Results 49
2.3.1 Environmental conditions 49
2.3.2 Phytoplankton pigment distribution 53
2.3.3 Cluster analysis 57
2.3.4 CHEMTAX: successive iterations and pigment ratios 69
2.3.5 CHEMTAX: comparison to microscopy taxonomy estimates . . 69
2.3.6 CHEMTAX: distribution of microalgal classes 74
2.4 Discussion 81
2.4.1 The use of pigment analysis for phytoplankton taxonomy in the Arctic 81
2.4.2 Phytoplankton variability and distribution 85
2.4.3 Implications for a changing climate 88
2.5 Conclusions 89

3 Variation in phytoplankton bio-optical and photophysiological properties in the Atlantic Arctic 91

3.1 Introduction . . . 93
3.2 Materials & Methods . . . 97
3.2.1 Description of the study area and data sources . . . 97
3.2.2 Sampling procedures . . . 99
3.2.3 Determination of phytoplankton spectral absorption $a_{ph}(\lambda)$ . . . 100
3.2.4 Photophysiological measurements . . . 101
3.2.5 Determination of phytoplankton pigment concentrations . . . 105
3.2.6 Pigment-based determination of phytoplankton community structure . . . 106
3.2.7 Culture experiments using Arctic strains . . . 106
3.3 Results . . . 108
3.3.1 Absorption spectra and absorption efficiencies . . . 108
3.3.2 Variation in photophysiological parameters . . . 113
3.4 Discussion . . . 122
3.4.1 Sources and implications of variation in phytoplankton absorption 123
3.4.2 Sources and implications of variations in photophysiology . . . 127
3.4.3 Projections for a changing Arctic . . . 134
3.5 Conclusions . . . 135

4 Modelling of Primary Production in the Greenland sector of the Arctic Ocean. 139

4.1 Introduction . . . 140
4.2 Methods . . . 144
4.2.1 Sampling strategy . . . 144
4.2.2 Fluorometric chlorophyll-a measurement . . . 145
4.2.3 Photophysiological parameters . . . 145
4.2.4 High-latitude PAR data sources . . . 147
4.2.5 Light attenuation coefficients . . . 148

4.2.6 Modelling primary production 149
4.3 Results 156
4.3.1 Quality of PAR data sources 156
4.3.2 Chlorophyll profiles and Case-I water assumptions 158
4.3.3 Sensitivity of primary production estimates to input variables . . 169
4.3.4 Comparison to a non-spectral VGPM model 177
4.4 Discussion 179
4.4.1 PAR data sources 179
4.4.2 Parameterization of IOPS 180
4.4.3 Parameterization of the biomass profile 181
4.4.4 Parameterization of photophysiology 182
4.4.5 Assigning model parameters for other locations 182
4.5 Conclusions 185

5 Summary **189**
5.1 Future directions 195

List of Figures

1.1 Calvin cycle for the formation of sugars 3
1.2 Size range of phytoplankton 7
1.3 CZCS detection of ice-edge bloom 9
1.4 Levels of primary production model complexity 12
1.5 Static and dynamic biogeochemical province boundaries 16
1.6 National Snow and Ice Data Center Arctic extent map 19
1.7 Ocean currents and circulation in the Arctic 21
1.8 PAR variation with time of year 23
1.9 National Snow and Ice Data Center sea-ice decline 26

2.1 Ocean currents by source type in the Greenland Sea 38
2.2 Map of stations occupied during cruise IC2010 39
2.3 Monthly composite of sea surface temperature (SST) in Greenland sea from MODIS 51
2.4 Temperature and salinity profiles for northerly ice-stations 52
2.5 Nitrate and nitrite:phosphate plot for samples from IC2010 cruise . . . 53
2.6 Depth distribution of major pigments 55
2.7 Correlation between accessory pigments and chlorophyll-a 56
2.8 Pigment composition in surface waters in the Greenland Sea 58
2.9 Accessory pigment concentrations in surface waters and at the SCM . . 59
2.10 Pigment composition profiles for each cruise station 60
2.11 Dendrogram of cluster analysis of pigment assemblages 63

2.12 Mean accessory pigment concentrations for clusters 64
2.13 Pigment clusters in relation to depth and salinity 67
2.14 Geographical map of pigment cluster distribution 68
2.15 Convergence of CHEMTAX pigment ratios for phytoplankton groups with successive iterations 70
2.16 CHEMTAX final group pigment ratios 71
2.17 Comparison of CHEMTAX microscopy estimates of algal group biomass 73
2.18 Histograms for the CHEMTAX assignment of biomass for each algal group 76
2.19 CHEMTAX group profiles for each cruise station 77
2.20 Principle component analysis of CHEMTAX groups and physical variables 80
2.21 Comparison of CHEMTAX and cluster analysis 84

3.1 National Snow and Ice Data Centre yearly sea-ice cycle 95
3.2 Combined BIO and IC2010 data station locations 98
3.3 Schematic diagram and image of photosynthetron used for P-E incubations 103
3.4 Coulter counter cell count calibration 107
3.5 Group-specific mean absorption spectra 109
3.6 Culture absorption spectra normalised to $a_{ph}(440)$ 110
3.7 Biomass-normalised absorption efficiency for combined Atlantic Arctic dataset 112
3.8 Relationship between $a_{ph}(440)$ and chl-a concentration for the IC2010 samples 113
3.9 Comparison of IC2010 photophysiological parameters to other Arctic datasets 115
3.10 Group-specific photophysiological parameters 117
3.11 Variation of cultured phytoplankton growth rates with temperature . . . 119
3.12 Correlation between P_m^B and environmental variables 120

3.13 Relationship between P_m^B and temperature for combined Atlantic Arctic dataset . . . 121
3.14 Correlation of IC2010 α^B to environmental variables . . . 122
3.15 Absorption spectra of accessory pigments . . . 125
3.16 Limitation of α^B by low water temperatures . . . 131
3.17 Effect of photo-protective carotenoids on quantum yield . . . 133

4.1 Cruise track . . . 146
4.2 Comparison of SeaWiFS and underway PAR . . . 157
4.3 Bird Model vs Underway data . . . 159
4.4 CTD Chlorophyll correction . . . 161
4.5 Chlorophyll near surface and in total water column . . . 162
4.6 Model fits to CTD profiles . . . 164
4.7 Histograms of the exponential Gaussian fit parameters for all CTD casts 165
4.8 Correlation of K_d^{PAR} with Chl-a . . . 167
4.9 Correlation of Kd with Chl-a . . . 168
4.10 Model sensitivity to optical inputs . . . 172
4.11 Model sensitivity to profile equation type . . . 174
4.12 Model sensitivity to photophysiology . . . 176
4.13 Primary production estimates for IC2010 stations . . . 178
4.14 Exponential Gaussian parameter assignment . . . 184

List of Tables

2.1 Details of pigments detected through HPLC and their distribution in algal groups . . . 43
2.2 Details of cultured algal species . . . 45
2.3 CHEMTAX initial matrices . . . 47
2.4 Details of cruise stations . . . 50
2.5 Cluster analysis mean pigment assemblages . . . 61
2.6 Mean accessory pigment ratios for pigment clusters . . . 65
2.7 CHEMTAX population summary . . . 78
2.8 Statistics for PCA of CHEMTAX groups and physical variables . . . 79

3.1 Group-specific average absorption coefficients from IC2010 field samples 111
3.2 Group-specific photophysiological parameters from IC2010 field samples 116
3.3 Carbon to Chl ratios and estimation of P_m^B for algal cultures . . . 118
3.4 Perennially ice-covered Arctic ocean area . . . 134
3.5 Symbols and units used in the study . . . 138

4.1 Production model error due to biomass profile equation, relative to baseline model . . . 177
4.2 Importance of primary production model parameters by water type . . . 183
4.3 Symbols and units used in the study . . . 188

Chapter 1

Introduction

1.1 Overview

This chapter begins by introducing the concept of primary production and the pivotal role that phytoplankton play in the global carbon cycle. It goes on to cover phytoplankton diversity and the details of algal photosynthesis. The requirements and details of modelling marine primary production are explained, first at a local scale and then on regional scales. The partitioning of the global ocean into biogeochemical regions based on differences in biological forcing factors (Section 1.4), is then discussed. To conclude, I focus on the Arctic Ocean (Section 1.5), covering its geography, climate, and seasonality. The increased interest in Arctic marine ecosystems in recent decades is also discussed (Section 1.5.3).

1.2 Marine photosynthesis and primary production

Primary production is the fixation of carbon from the atmosphere or ocean into complex organic molecules through photosynthesis. Photosynthesis is often simplified to the equation

$$\underbrace{2nCO_2}_{\text{Carbon dioxide}} + \underbrace{2nDH_2}_{\text{electron donor}} + \underbrace{photons}_{\text{energy source}} \rightarrow \underbrace{2(CH_2O)_n}_{\text{carbohydrate}} + \underbrace{2nA}_{\text{oxidized electron donor}} \tag{1.1}$$

In aquatic photosynthesis the electron donor is water and the simplified equation is

$$2nCO_2 + 2nH_2O + photons \rightarrow 2(CH_2O)_n + 2nO_2 \tag{1.2}$$

The process of photosynthesis is a complex series of reactions within a photosynthetic cell to achieve carbon fixation (Kirk, 1994). These reactions are often considered in two groups, light and dark. The light reactions remove hydrogen from water and combine it with nicotinamide adenine dinucleotide phosphate (NADP) to form $NADPH_2$, which liberates oxygen as a bi-product. During the transport of the hydrogen, adenosine diphosphate (ADP) is converted to adenosine triphosphate (ATP). In the dark reactions $NADPH_2$ is used to reduce CO_2 into a carbohydrate through repeated Calvin cycles. The energy for this reaction is provided by breaking down ATP back into ADP, and the enzyme Ribulose-1,5-bisphosphate carboxylase oxygenase (RuBisCO) is an essential enzyme for carbon fixation in all phytoplankton (Tabita et al., 2008). An illustration of the Calvin cycle is shown in Figure 1.1.

The carbohydrates formed in this reaction are then used for a number of functions within

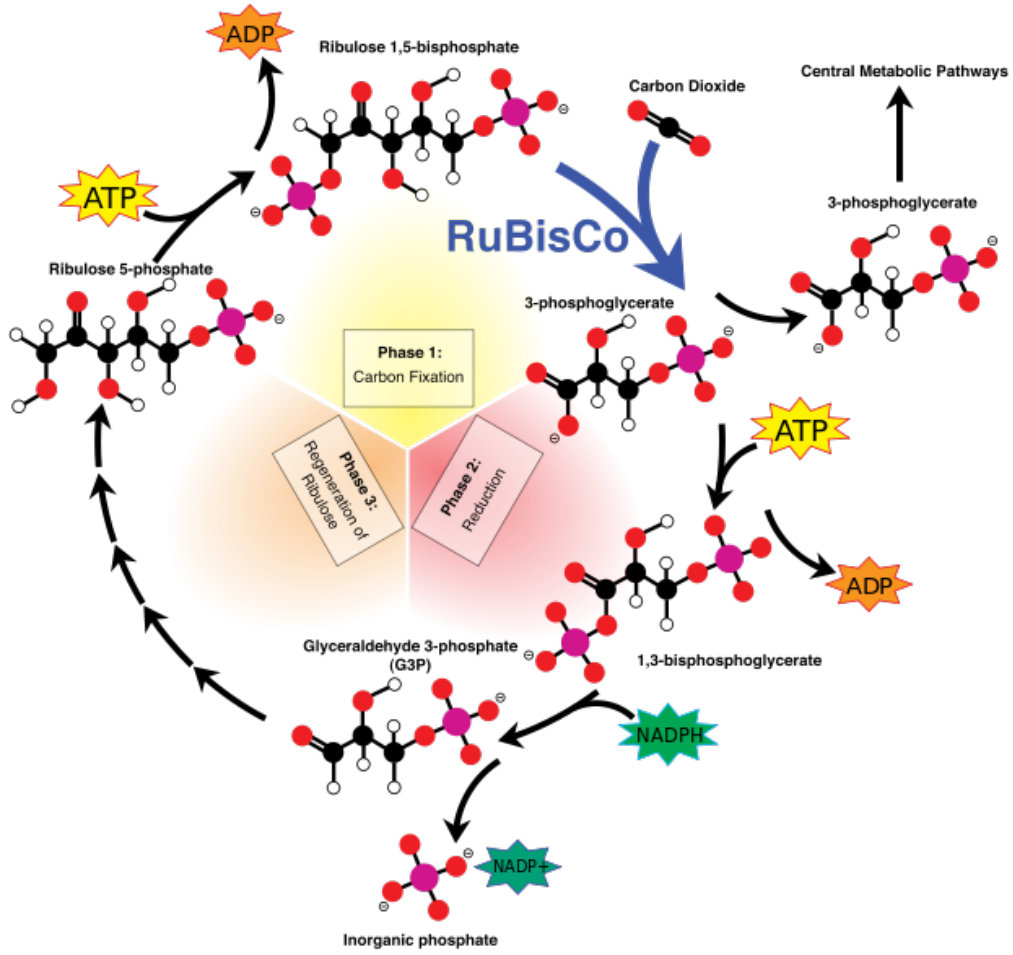

Figure 1.1: An illustration of the details of the Calvin cycle by Mike Jones. Atoms are colour coded where black is carbon, white is hydrogen, red is oxygen and pink is phosphorus.

the cell. From an ecological perspective, the carbohydrates formed by phytoplankton are a source of energy for the rest of the oceanic food chain. Thus the process of aquatic photosynthesis in the ecological literature is often referred to as primary production.

1.2.1 Global estimates of production

The process of marine photosynthesis takes place at the individual cellular level, but photosynthetic phytoplankton occur in such numbers across all the oceans of the world that changes in marine primary production are of global importance. When phytoplankton grow in sufficient numbers they can change the optical properties of the sea, making their presence detectable from air- or spacecrafts.

Global primary production estimates of the past 20 years (Longhurst et al., 1995; Field et al., 1998; Geider et al., 2001; Behrenfeld et al., 2005; Uitz et al., 2010) have converged on a value of around 50 GT of carbon fixed through oceanic photosynthesis per year. These estimates include phytoplankton size-specific estimates, chlorophyll-based models, and carbon-based models, and all used remotely-sensed fields of chlorophyll biomass. An integrated value of 50 GT for the World Ocean is approximately equal to that of the terrestrial biosphere (Field et al., 1998). The average water-column production in the oceans is around 140 g C m^{-2} yr^{-1}, but values can range from near zero to $>$ 500 g C m^{-2} yr^{-1} depending on geographic location (Field et al., 1998). The fact that primary producers in the ocean are as productive as their terrestrial counterparts is made more impressive when one considers that the total biomass of oceanic primary producers is thought to be around 1 GT (Antoine et al., 1996), compared to hundreds of GT in the terrestrial forests. The low relative standing stock of biomass compared

to annual primary production is explained by the rapid turnover time of phytoplankton growth. Terrestrial plants and trees live from months to centuries whereas phytoplankton can double their numbers in less than a day under favourable conditions. A rapid life cycle makes it difficult to map phytoplankton abundances on large scales, as they can respond rapidly to local changes in environmental conditions. Remote sensing has recently allowed us an unprecedented temporal resolution of observation of the oceans, but interpreting the data is complex. It is noteworthy that the region of the ocean where current primary production models are least certain is the Arctic ocean (Carr et al., 2006).

The fate of the carbon fixed through marine primary production is important for biogeochemical processes and ocean/atmosphere carbon budget calculations. The biological carbon pump is defined as the export of carbon from the sea surface to the deep ocean through the sinking of organically-bound carbon. This could be particulate organic carbon or organically-secreted $CaCO_3$ from sources such as coccolithophores. The strength of this carbon pump can depend upon factors such as the taxonomy of the phytoplankton, the local and regional mixing dynamics, the water temperatures and the temporal variability in the primary production (Laws, 1991; Falkowski, 1992; Buesseler, 1998; Laws et al., 2000; Sarmiento and Gruber, 2004). In general, systems that support blooms of large phytoplankton such as diatoms will export a higher fraction of the organic carbon than those that maintain uniform biomass through the year and have a food web centred around smaller cells, which favours respiration and nutrient recycling (Buesseler, 1998).

1.2.2 Phytoplankton classification and functional types

An understanding of the importance of different phytoplankton with respect to primary production and biogeochemical cycles requires a system to differentiate and group phytoplankton, for which there are a number of methods. Phytoplankton can, for example, be grouped according to taxonomy, size, or biogeochemical function.

Phytoplankton are incredibly diverse and have representatives from the Bacteria and Chromista kingdoms. Most phytoplankton, however, fall within a small number of phyla: cyanobacteria, heterokonts, haptophytes, cryptophytes, and dinoflagellates and these phyla have within them thousands of species. To assess phytoplankton diversity at the species level requires the use of conventional light microscopy for larger cells, or molecular techniques for cells less than a 3 μm (Simon et al., 1995; Tilstone et al., 2003; Soares et al., 2011).

Another way of dividing up the phytoplankton community is by cell size. Larger cells tend to have lower maximum specific growth rates, though this relationship is more complicated when we compare different phytoplankton groups of equal size (Chisholm, 1992). Larger cells also have a smaller surface area to volume ratio, so are not as efficient at diffusive uptake of nutrients. However, larger cells tend to be less susceptible to predation and can store larger pools of nutrients during times of plenty to survive times of poor nutrient supply. The utility of a size-based classification scheme is highlighted in work of Sieburth and Smetacek (1978). Phytoplankton cell sizes can vary over many orders of magnitude, from less than 1 μm to over 1 mm (figure 1.2). Common classes used are micro- nano- and pico-plankton with size ranges of $>$20 μm, 2-20 μm, and $\leq$2 μm, respectively.

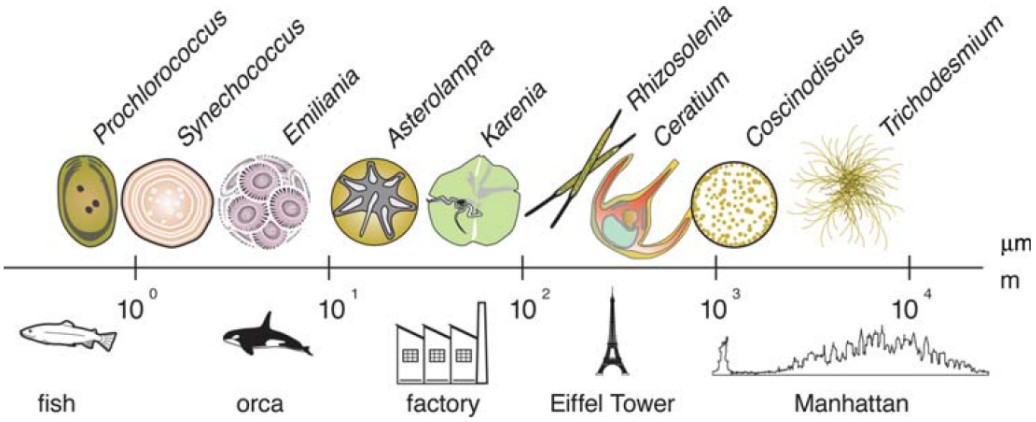

Figure 1.2: Phytoplankton size range relative to human scale objects, from (Finkel et al., 2010).

Phytoplankton perform a number of biogeochemical roles, some of which are confined to specific groups. This has led to the approach of classifying phytoplankton taxa into various Phytoplankton Functional Types (PFTs) (Steffen, 1996; Quere et al., 2005). For example, some marine cyanobacteria are diazatrophs and as such can fix nitrogen (N_2) into ammonia (NH_3). Some functional groups are associated with biomineralisation: for example diatoms are one of the primary producers of biogenic silica in the oceans, while coccolithophores produce calcium carbonate. The presence of nitrifying and silicifying phytoplankton affect the cycling and availability of macronutrients at local and global scales. The concept of PFTs is very useful for biogeochemical modelling, as it allows the key metabolic/biogeochemical processes of organisms to be modelled in the absence of detailed information on phytoplankton taxonomy at the species level (Quere et al., 2005).

1.2.3 Phytoplankton blooms

Much of the primary production by marine phytoplankton takes place during brief periods of rapid cell growth referred to as blooms. The onset of phytoplankton blooms are usually triggered by an increased supply of the resource that is limiting phytoplankton growth, which could be a macronutrient such as phosphorus, a micronutrient such as iron, or light. In the open ocean an increased supply of nutrients to the sea surface is usually due an upward flux of nutrient rich deep waters. This can be through deep surface mixing due to wind and tidal forcing or through large-scale upwelling. Upwelling occurs when winds, the Coriolis effect and Ekman transport cause water to diverge at the surface, drawing water from below and can occur along sea-ice boundaries.

Ice-edge blooms of phytoplankton frequently occur in the Arctic during spring and summer (See figure 1.3). Unfortunately due to the scarcity of data from the Coastal Zone Color Scanner (CZCS) sensor, early remote-sensing studies were to unable quantify total production of ice-edge blooms and hence assess their ecological significance (Mitchell et al., 1991). More recent studies (Perrette et al., 2011) that use data collected from modern ocean-colour sensors such as SeaWiFS and MODIS have shown that ice-edge blooms are significant contributors to annual primary production and hence are important to maintaining food-webs.

1.2.4 Phytoplankton pigments

Marine phytoplankton can be detected through remote sensing due to their spectral influence on the absorption of light in ocean waters. This influence is predominantly controlled by the pigments contained within phytoplankton cells. All phytoplankton

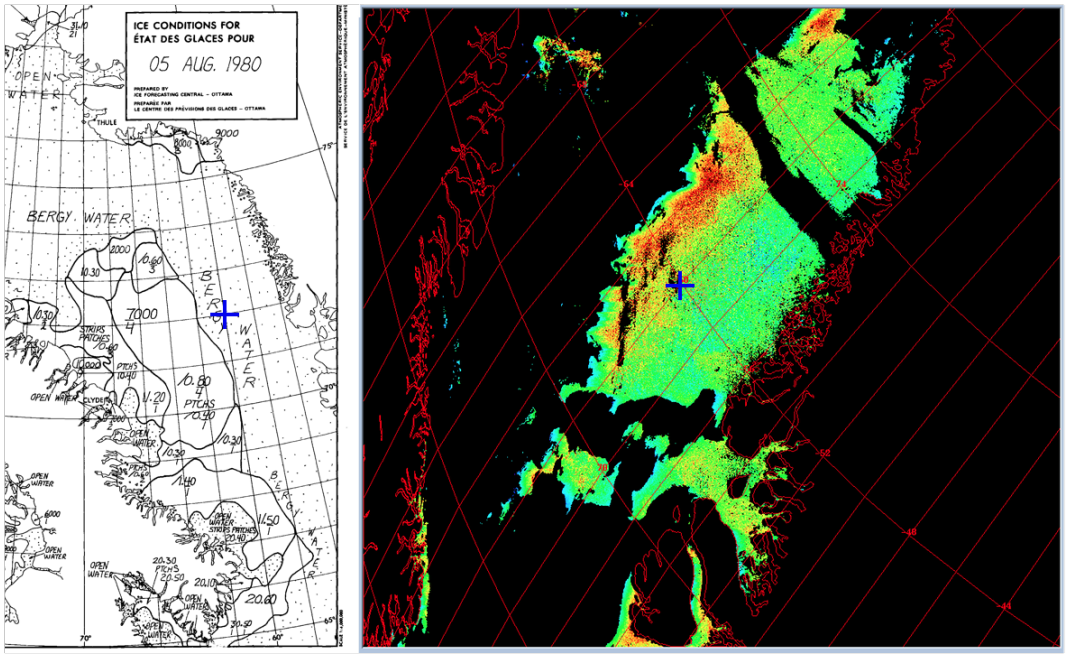

Figure 1.3: Ice edge blooms can be detected by remote sensing and shown is an example from Baffin Bay. The image on the left is taken from a Canadian ice-chart for the 5th of August 1980 and on the right is a Coastal Zone Color Scanner (CZCS) image from the 7th of August 1980. Hot colours indicate increased chlorophyll concentration, the blue cross is at the same location in both images.

contain chlorophyll-a which absorbs strongly in the red and blue regions of the visible spectrum. It is usual for additional pigments, known as accessory pigments, to be present in phytoplankton cells alongside chlorophyll-a (Roy, 2011). The accessory pigments can perform two functions, either increasing the amount of light energy absorbed and directed to photosynthetic reaction centres (photosynthetic accessory pigments) or absorbing light and dissipating it as heat to protect the photosynthetic reaction centres from being damaged by excess irradiance (photoprotective accessory pigments). While some accessory pigments are common to many phytoplankton groups, others are diagnostic of particular phytoplankton groups, leading to the development of pigment based taxonomic estimates (Vidussi et al., 2004; Roy, 2011).

1.3 Modelling phytoplankton production

1.3.1 Basic requirements

When modelling phytoplankton primary production, mathematical representations of both biological processes and the physical environment are required. Remotely-sensed models of marine primary production estimate the amount of carbon that is fixed into organic matter over a given unit of time for a given concentration of biomass within a given area or volume. There are a number of primary variables that are required. For autotrophic phytoplankton the external energy source is irradiance (E) from the sun, needs to be described. The amount of autotrophic biomass (B) contained in the water column is another key variable that is required to convert the external energy source into chemical energy, through photosynthesis. Photophysiological parameters are then used

to describe how efficiently a unit of biomass (B) uses a unit of incoming energy (E). Phytoplankton photophysiology is often described through a number of parameters. A common set of parameters is the maximum photosynthetic rate per unit biomass (P_m^B), the low light photosynthetic efficiency (α^B) and the photoadaptation parameter (E_k) which are derived from P-E experiments, where phytoplankton growth during a short incubation time is measured under a range of growth irradiances.

1.3.2 Model complexity

The complexity of primary production models can increase as the secondary factors controlling photosynthesis, are taken into account. An increase in model complexity often results in an increase in the number of state variables and the parameters used to describe them. For example, the photophysiology may be parameterized such that the production varies non-linearly with varying irradiance. Parameters can also be assigned to describe the biomass profile and how phytoplankton biomass attenuates light. In spectral models of photosynthesis, the irradiance field can also be resolved with respect to wavelength.

The work of Platt and Sathyendranath (2002) provides an in-depth explanation of the process of modelling primary production. Figure 1.4 shows how more complex models have developed and progressively eliminated assumptions about, and simplifications of, the system being modelled. The model used in this study (section 4.2.6) is at the more complex end of this spectrum. It is an available-light spectral model with non-uniform biomass, and uses a non-linear response of photosynthesis to irradiance. The effect of model complexity on estimates of production will be examined by comparing model

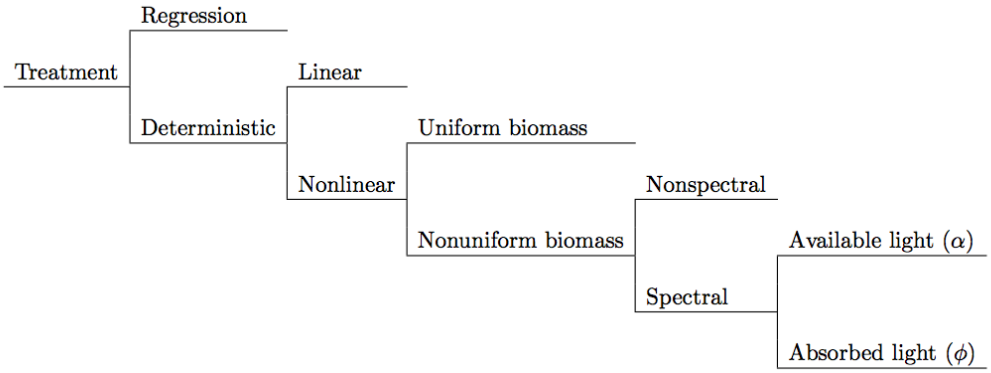

Figure 1.4: A figure from Platt and Sathyendranath (2002) illustrating various levels of complexity in primary production modelling. Models get more complex from left to right and top to bottom.

outputs from wavelength dependent, depth-resolved models of primary production, to those using non-spectral models with a uniform biomass (Section 4.3.4).

1.3.3 Scaling up primary production models

To progress from modelling the production of a water column to estimating the primary production over a large region, even the most simple models of marine primary production require estimates of surface biomass, irradiance and photophysiology. There are two sources of information used to assist in assigning model inputs over large spatial scales. The first of these is remote-sensing data and the second is global circulation models (GCMs). Remote sensing provides a dataset with high spatial and temporal resolution that provides synoptic coverage of environmental and biological variables (Platt and Sathyendranath, 1999). Remote sensing data relies on good instrument calibration,

robust data product validation and sufficient geographic coverage. By contrast, GCMs have no issues with factors such as loss of signal due to cloud cover and instrumental drift, but may fail to capture the full variability of a dynamic marine environment. The data products from GCMs must also be validated against large *in situ* datasets (including satellite data) to ensure that the results are not spurious. A review of global primary production estimates derived from both of these data sources (Carr et al., 2006) highlights the need for more studies focussing on Arctic primary production as these cold, high-latitude waters are the regions of the global ocean where there is the most disagreement between model estimates.

Although oceans cannot be considered homogeneous, some regions share a common set of physical and ecology characteristics which may aid in the estimation of primary production on basin scales (Longhurst et al., 1995; Sathyendranath et al., 1995). The partitioning of the oceans into distinct regions based on their biological, chemical and physical properties can be done using different criteria, as described below.

1.4 Dividing up the oceans

In terrestrial ecology, geographical divisions are based on large physical boundaries such as mountain ranges or rivers. However, to partition the ocean basins into large-scale ecosystems requires a different set of criteria. One approach is based on the chemical and physical forcing factors that drive ocean productivity (Longhurst et al., 1995). Another way is to divide the oceans based on the optical properties of the surface ocean which are directly related to chlorophyll estimates retrieved by ocean-colour satellites (Smith et al., 1978). The first approach is useful for the assignment of parameters in pri-

mary production models and the second is key to the assignment of fields of biomass.

1.4.1 Biogeochemical ocean provinces

There has been over 150 years of work on the biogeography of the oceans (Longhurst.A, 1998) and the partitioning of the global ocean into ecological regimes can be performed over a range of spatial scales. The largest scale partition separates the oceans into biomes: regions that are defined by a similar set of climate conditions and biological forcing.

Biome boundaries and type are predominantly determined by nutrient dynamics, primarily the supply mechanism (Sarmiento et al., 2004). The supply of nutrients, in turn, will depend upon physical forcing factors such as wind-driven mixing and upwelling, processes which can be monitored by remote-sensing. Biomes are the coarsest partitioning of the ocean and can be further subdivided into smaller ocean provinces. The subdivision of the oceans into biogeochemical provinces allows us to tackle the issue of non-linearity in the biological responses to forcing factors in the oceans (Sathyendranath et al., 1995). Moreover, the photophysiology of one group of phytoplankton is likely to differ from that of another (Platt and Sathyendranath, 1988). If we assume only a selection of algae are known to exist within a province at a given time, it becomes simpler to describe their physiological response based on geographic location by assuming it is constant over the province in question.

In the work of Longhurst et al. (1995) there are four principle biomes which are then subdivided into 57 ocean provinces. For the sake of brevity and relevance, we will discuss only those provinces pertinent to the Atlantic Arctic. Longhurst assigned one

biome (Polar Biome) to cover both the Arctic and Antarctic with three provinces assigned for each. The Polar Biome is defined as a marine domain that is influenced by the brackish waters produced during the melting of winter sea ice and snow. The three Arctic provinces encompass all the oceans north of the polar front. The Arctic Polar provinces according to Longhurst are:

BPLR-Boreal Polar.
Comprises the Arctic Ocean, Baffin Bay and the Canadian archipelago, and the coastal Greenland and Labrador Currents. It is dominated by permanent ice cover which opens significantly during summer only in some coastal and archipelagic regions.

ARCT-Atlantic Artic.
This province lies between the Polar Front, lying seawards of the Greenland coastal currents, and the oceanic Polar or Subarctic Front, which often cannot be traced at the sea surface.

SARC-Atlantic Subarctic.
Comprises the poleward limb of the polar gyre, characterized by warm Atlantic water as it is carried north across the Iceland-Faroes ridge and thence by the Norwegian Offshore Current into the Barents Sea.

Longhurst's criteria suggest that even at province level, a range of ocean conditions can occur over an annual cycle. When assigning province boundaries, a balance must be struck between the upper and lower limits used to define the geographical boundaries of the province and that the province size is sufficiently large to be of use in global studies of primary production. While the boundaries of the biogeochemical provinces of Longhurst et al. (1995) were originally rectilinear and held constant, recent studies

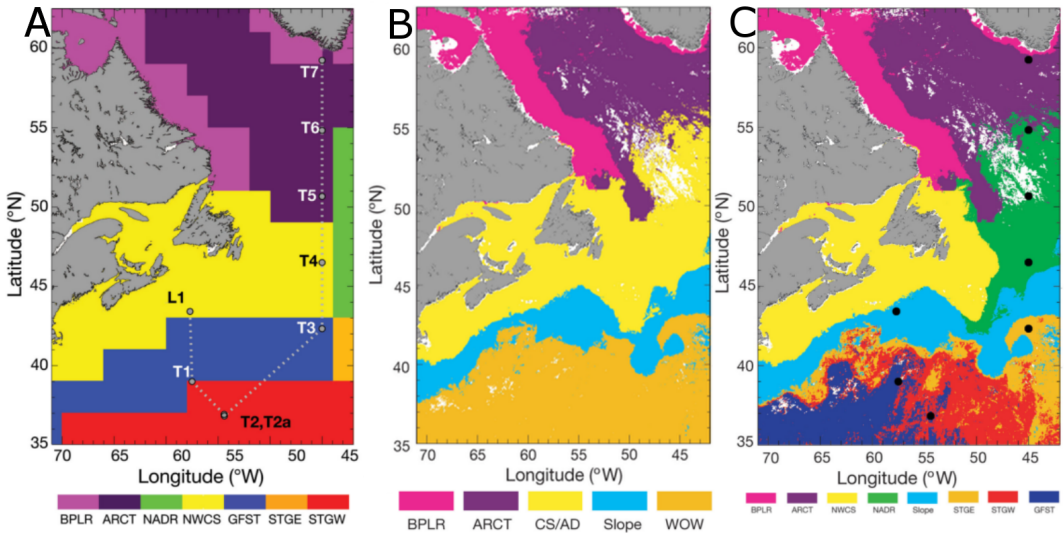

Figure 1.5: A compilation of province boundary estimates from (Devred et al., 2007) for the North-west Atlantic Ocean and Labrador Sea. Provinces defined using Longhurst (A), cluster analysis (B) and dynamical definition of ecological province borders based on the static classification (C). The province abbreviations are: Arctic (ARCT), Boreal Polar (BPLR), N. Atlantic Drift (NADR), NW Atlantic Shelves (NWCS), Gulf Stream (GFST), N. Atlantic Subtropical Gyral Province (East) (STGE), N. Atlantic Subtropical Gyral Province (West) (STGW), Continental Shelf province/Atlantic Drift (CS/AD), and Warm Oligotrophic Waters (WOW).

have used a dynamic assignment of province boundaries through the use of remotely-sensed data fields (Devred et al., 2007, 2009).

1.4.2 Bio-optical water types

Although the Longhurst provinces serve as a useful tool for partitioning the global oceans depending on physical forcing factors, the oceans have also been classified based on their bio-optical properties (Morel and Prieur, 1977). The reason behind this partitioning is not to assign parameters for use in models of primary production, but to aid in

the retrieval of chlorophyll biomass from satellite. In optical oceanography the simplest partitioning divides the oceans into two categories: Case-I and Case-II waters. In Case-I waters, optical properties are dominated by phytoplankton and their derived products (Morel, 1988). Case-II waters are those for which sediments, or dissolved yellow substances, contribute significantly to, or dominate the optical properties. Since the seminal work on the subject by Morel and Prieur (1977), there has been a number of models and algorithms developed based upon this classification scheme (Prieur and Sathyendranath, 1981; Gordon and Morel, 1985; Morel, 1988; Mobley et al., 2004). The bio-optical category of a body of water will influence biomass and primary production estimates derived from remotely-sensed data due to both the chlorophll retrieval algorithm used and the parameterization of light attenuation in the primary production model. Much of the Arctic is often considered to be Case-II waters, with optical properties dominated by coloured dissolved organic matter (CDOM). Therefore, chlorophyll-retrieval algorithms for the Arctic using ocean colour satellite data have tried to account for this CDOM influence (Mustapha et al., 2012).

1.5 The Arctic region

1.5.1 Defining the Arctic

The Arctic covers a large geographical area comprising a number of environments including kilometre thick ice-sheets, vast expanses of frozen tundra, mountainous glacial regions, large rivers, thick multi-year sea ice, and open-ocean waters. To analyse the diversity and primary production of phytoplankton in the Arctic we must define the

boundaries of the Arctic Ocean.

A simple definition is that everything above the Arctic circle (66°33'N) is classified as the Arctic. The Arctic circle is set by the tilted axis of the Earth's rotation, which means that above a latitude of 66°33'N both polar night and polar day take place. The ocean to the north of this latitudinal boundary comprises an area of a little over 14 Million km^2. Another common criterion used to define Arctic waters is based on sea-surface temperature, where the mean warmest monthly temperature does not exceed 10 °C. Predicted ocean warming, resulting from climate change, will therefore lead to a shrinking of Arctic waters in the future if they are defined by mean sea-surface temperature. It is also worth noting that the 10 °C isotherm shows a much greater latitudinal range in the oceans that it does on land. This is due to the large transport of heat by surface currents, especially the Gulf Stream in the North Atlantic.

A comparison of these two methods for marking the boundaries of the Arctic is shown in figure 1.6. Although the first approach is simple to implement, it bears little value for the modelling of Arctic primary productivity as it has no relation to ecological regimes. In this work I will adopt the latter method of defining the Arctic region.

For more detailed study of primary production dynamics, the Arctic Ocean is often further subdivided into regional seas. There are eight such regions distinguished inside the Arctic Circle (Baffin Bay, Greenland Sea, Barents Sea, Kara Sea, Laptev Sea, East Siberian Sea, Chukchi Sea and the Beaufort Sea) and three regions further south (Norwegian Sea, Davis Strait and Bering Strait/Sea) (Pabi et al., 2008).

Figure 1.6: Adapted from an NSIDC map of the Arctic (based upon a map in the The Perry-Castaeda Library Map Collection). The tree-line was added by NSIDC based on information from National Geographic 1983, Armstrong et al. 1978, and Young, 1989. Here the Arctic circle is further highlighted.

1.5.2 Physical conditions and extremes of the Arctic

The Arctic Ocean has a drainage basin that is larger than the ocean itself (Fasham, 2003). The freshwater flux from the runoff is estimated at 3300 $km^{-3}yr^{-1}$, much of this entering via the Yenisei (603 $km^{-3}yr^{-1}$), Ob (530 $km^{-3}yr^{-1}$), Lena (520 $km^{-3}yr^{-1}$) and Mackenzie (340 $km^{-3}yr^{-1}$) rivers (Aagaard and Carmack, 1989). These rivers are not only a source of buoyant freshwater to the Arctic Ocean but also of nutrients, sediments and dissolved organic matter (Macdonald et al., 1998). The annual cycle in sea ice also has a strong influence on salinity fluxes and mixing. During the summer, melting sea ice acts to stratify the upper water column, whereas in the winter, sea ice formation and brine rejection lead to deep mixing. The sinking of cool salty water in the Arctic is a key component of the thermohaline conveyor and the major ocean currents of the Arctic are shown in figure 1.7. It has been suggested that changes in the Arctic region could affect the strength of the Meridional Overturning Circulation, the poleward transport of heat and, therefore, the global climate (Vellinga and Wood, 2002).

As seen in figure 1.7, the deep waters of the Arctic originate from two sources. The fresher Pacific waters sit above the saline Atlantic waters and a strong front separates the water masses at depth near the Losomonov Ridge. It is believed that this front has recently moved towards the Alpha-Mendeleev Ridge (Pabi et al., 2008). The Pacific-sourced waters are richer in macronutrients (phosphate in particular) than Atlantic-sourced waters (Jones et al., 1998) and should be able to support greater phytoplankton productivity (Pabi et al., 2008).

The presence of sea ice influences the upwelling and mixing of nutrients from subsurface waters in two ways. First, sea ice isolates surface waters from wind stress (Carmack

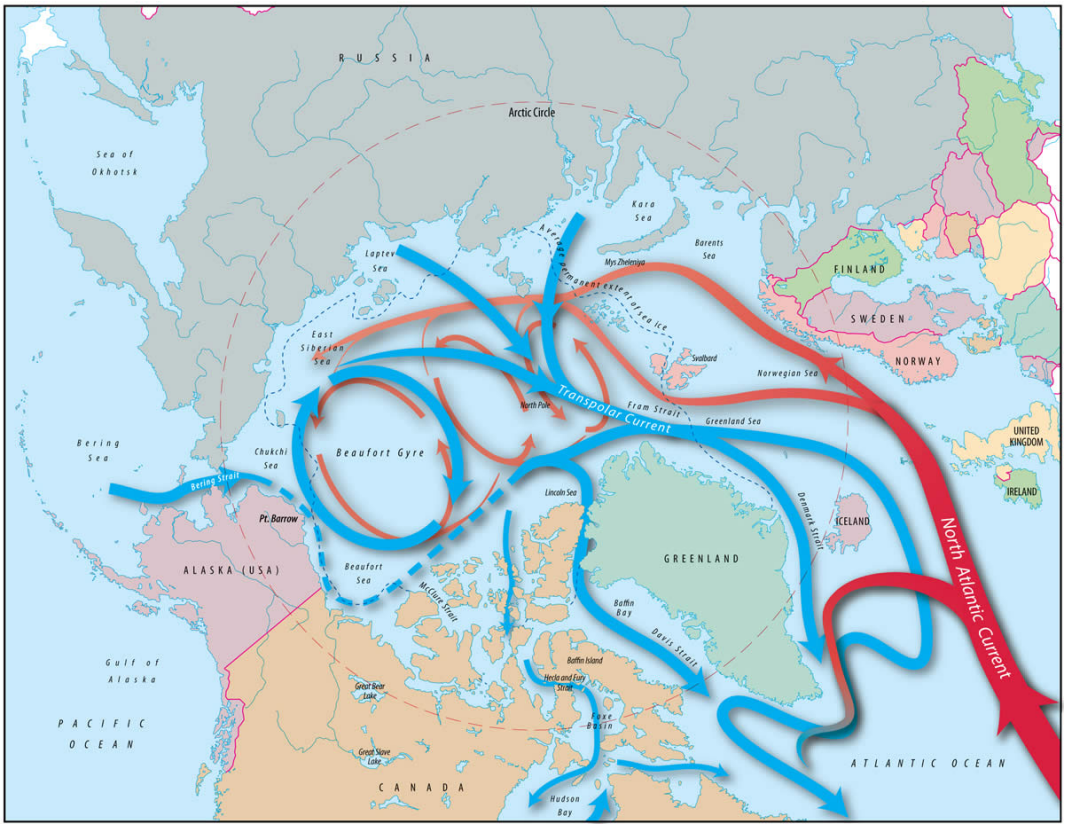

Figure 1.7: A diagram from Jack Cook (WHOI) showing the currents and circulation within the Arctic Ocean. Warm, saline, water from the Atlantic penetrates into the Arctic region but remains partially trapped beneath cold fresh waters, preventing the melting of sea ice. Water from the Pacific is colder and fresher than that from the Atlantic and, after entering through the Bering Strait, pass into the Beaufort Gyre.

and Chapman, 2003) which prevents the mixing of surface waters and the replenishment of nutrients from depth. Along the ice edge, however, there is the potential for increased upwelling when water is blown away from the ice edge (Mundy et al., 2009). This is similar to coastal upwelling through Ekman transport, driving an increase in nutrient supply along the ice edge. The formation of large open water areas within the sea ice, called polynyas, can occur where the ice is pushed away from a landmass. These areas are also regions of upwelling and increased nutrient supply to surface waters.

The Arctic is characterized by freezing winters and cool summers with a low level of precipitation. Air temperatures can reach approximately -70 °C in the winter but less extreme temperatures are seen in oceanic regions due to a net heat flux from the ocean to the atmosphere. Sea ice also acts to insulate the surface waters from the freezing atmospheric temperatures above. In addition to acting as a barrier between atmosphere and surface ocean, sea ice forms an optically-thick layer between the sun's rays and the ocean waters below. Cloud cover, fog and re-suspension of snow in strong winds are common which produce a high range of incident irradiance conditions even before light is transmitted through sea ice. With increasing latitude the seasonal variation in irradiance becomes more extreme. At the North Pole the sun remains above the horizon from March to September before setting for 6 months. The sun will however only reach a maximum zenith angle of 23.5° in midsummer. Combining low sun angles with a highly reflective (high albedo) surface can produce unique light environments.

Due to the extreme annual variation in light and temperature, phytoplankton bloom dynamics in the Arctic are characterised by a strong summer peak in biomass, primary production and carbon export (Kahru et al., 2011). Data from the Arctic Ocean suggest integrated annual primary production is controlled by nutrient availability, as post

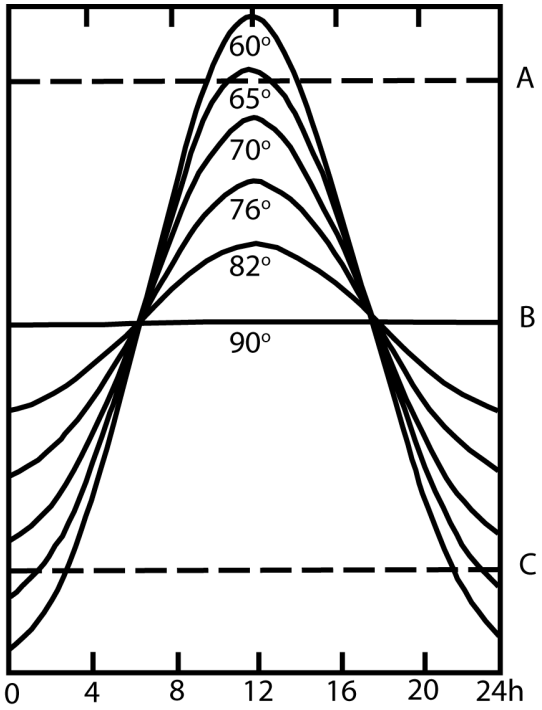

Figure 1.8: Variation in daily solar orbit from different latitudes at Earth's surface, reproduced from Stein and MacDonald (2004). The orbit can be regarded as fixed for a given latitude and seasons arise from vertical movements of the horizon (horizontal line) due to declination. Position (A) represents the Winter solstice (23.5° above B) and (C) the Summer solstice (23.5° below B).

bloom waters show levels of nitrate, phosphate and silicic acid close to the limit of detection (Stein and MacDonald, 2004). The North Atlantic is known to be depleted in phosphorus relative to nitrate (N:P ratio greater than 16), whereas the opposite is true in the Pacific (Wu, 2000). As the Arctic Ocean waters include Pacific, Atlantic and fluvial sources, we would expect a range in N:P ratios. Generally the N:P ratio varies from around 11-16:1 (Stein and MacDonald, 2004), showing that most of the Arctic appears to be nitrate limited.

1.5.3 Climate change

Over the past 30 years there has been a dramatic reduction in the summer extent of the Arctic sea ice (Figure 1.9). The volume of ice has decreased even more dramatically as a larger fraction of the ice present in winter is now thinner first-year ice, rather than thicker multi-year ice. The onset of melting is beginning earlier in the year and the freeze up is becoming later, giving an increased period of open water. In the last 3-4 years there has been a reduction in the maximum extent of the winter ice, which until 2005 had remained relatively constant (Comiso, 2006).

Though there is a wealth of observational evidence to show warming of the climate in the Arctic region, the question arises as to whether recent observations are depicting an enhanced greenhouse-warming signal or merely natural decadal and multidecadal variability (Polyakov and Johnson, 2000; Polyakov et al., 2002). Nevertheless, there is an overall consensus within the scientific community that the dramatic changes observed are a response to anthropogenic forcing (Johannessen et al., 2004). With each passing year the trends in sea-ice extent become more pronounced and the warming signal be-

comes stronger and better constrained (Comiso et al., 2008). Not only is current climate change more rapid in the Arctic than any other region, small changes in temperature have the potential to induce a greater response due to the ubiquity and importance of ice in the region. In addition to temperature, changes in ice distributions are one of the most obvious manifestations of climate change and have important consequences for the local biota. It has been predicted that the Arctic may be completely free of sea ice in the summer by 2050 if current trends continue (Overland and Wang, 2007). These changes will lead to an increased growing season and recent estimates from satellite data suggest this may lead to an increase in annual primary productivity in the Arctic (Arrigo et al., 2008). However, estimates of pan-Arctic primary production have converted satellite detected chlorophyll fields into productivity rates using a model that assigned photosynthetic parameters based on field measurements made in the Southern Ocean. Though both regions have a light-limited winter these two polar regions differ in many important respects, such as nutrient supply (both micro and macro), mixing dynamics and dominant phytoplankton species. As a result, adopting physiological relationships from the Southern Ocean may lead to errors in the productivity estimates for the Arctic. Moreover, these estimates assume productivity beneath sea ice is negligible, which is in contradiction to recent observations of large under-ice blooms (Arrigo et al., 2012).

1.5.4 The Arctic and the carbon cycle

Though the Arctic Ocean is around 1 % of the global ocean volume, 53 % of the Arctic seas are on continental shelves, giving a favourable environment for carbon burial. This means that the Arctic will punch above its weight with regard to it importance for global climate change. Approximately 1,000,000 tonnes of CO_2 dissolve into the global oceans

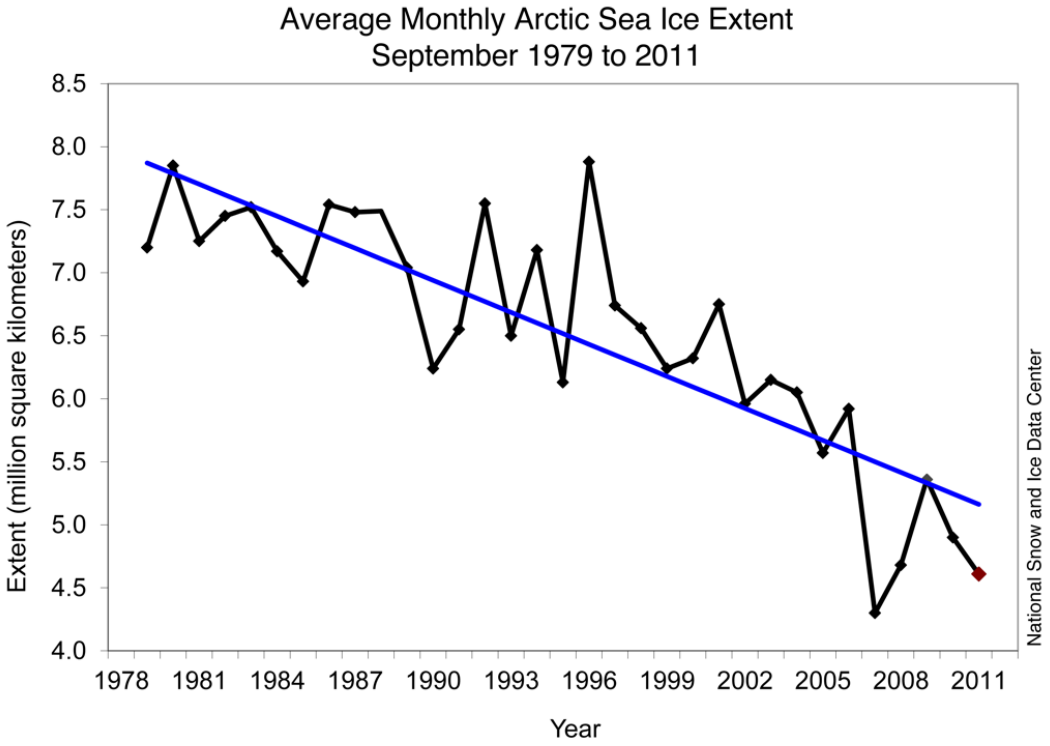

Figure 1.9: Minimum sea-ice area per year from the National Snow and Ice Data Center (NSIDC) as detected by Defence Meteorological Satellite Program (DMSP) the Special Sensor Microwave Imager/Sounder (SSMIS). The linear trend is 12% per decade.

every hour and it is estimated that the Arctic may be up to three times more important for CO_2 sequestration than its area implies (Fasham, 2003). It is estimated that the ocean-atmosphere CO_2 exchanges in the Arctic currently sum to a net flux from the atmosphere to the ocean of $\approx$ 66-199 Tg C yr^{-1} (Bates and Mathis, 2009). Some fraction of the carbon dioxide that dissolves into the surface ocean is fixed into organic carbon through primary production. The carbon cycle in the Arctic is influenced by a number of organic and inorganic processes. The various pathways of carbon transport are covered by Bates and Mathis (2009), but the biological carbon pump is of particular relevance to this study. A recent study combining remote sensing data and a mechanistic food-web model estimated global export production as $\approx$ 6 Pg C yr^{-1} (Siegel et al., 2014), though this excluded the high latitude seas. Though large uncertainties are attached to estimated rates of Arctic new and export production, $\approx$ 135 Tg C yr^{-1} (Macdonald et al., 2009), it is clearly of a similar order of magnitude to the regional ocean-atmosphere flux and is $> 2\%$ of the global export estimate. Increased Arctic primary productivity in a warming Arctic (Arrigo et al., 2008) will likely lead to an increase in the importance of the Arctic for carbon export. Without a strong understanding of the variability of phytoplankton physiology and the resulting distribution of primary production in the Arctic we cannot accurately predict the coming changes in the regional carbon cycle.

1.6 Summary and aims of work

In summary, the Arctic seas are extreme environments that are challenging for biological monitoring and modelling. They are responding rapidly to climate change and the biological response to a changing environment will have important feedbacks on the

global carbon cycle. It is essential that we continue to monitor this system and improve our ability to understand and predict its state under future climate scenarios. The following chapters aim to contribute towards this goal.

Chapter 2 aims to investigate the distribution of phytoplankton taxa in the Atlantic Arctic, with a focus on the transition across the ice-edge boundary. This will involve the following tasks:

1. Analyse the pigment assemblage and distribution of phytoplankton pigments in the Greenland Sea.

2. Compare estimates of cell abundance/taxonomy using CHEMTAX methods with cell count data.

3. Investigate the biogeography of phytoplankton taxa and its relationship to environmental variables.

Chapter 3 aims to scrutinise the relationships between environmental variables and photophysiological parameters to explore the possibility of using estimates of environmental conditions to inform the modelling of primary production. This will require:

1. An examination of the variability in bio-optical and photophysiological parameters of Arctic phytoplankton using field and culture data.

2. An assessment how the bio-optical and photophysiological properties of Arctic phytoplankton relate to the primary factors governing phytoplankton growth (light, nutrients and temperature).

3. Determination of whether relationships between environmental variables and photophysiology are consistent across the Atlantic Arctic and if they differ from other

oceanic regions.

Chapter 4 aims to improve modelling of Arctic primary production by considering the importance of variability in each of the parameters used to model primary production in an Arctic setting. To achieve this goal we:

1. Estimate marine primary production in the Greenland Sea using a combination of modelling and *in situ* data.
2. Analyse the sensitivity of a spectral primary production model to variations in input parameters and determine which parameters are most significant.
3. Discuss the level of model complexity required for Arctic waters.
4. Propose ways of improving estimates of primary production for the Arctic region.

Chapter 2

Phytoplankton community structure in the Greenland Sea: validation and interpretation of CHEMTAX analysis in relation to environmental forcing

Abstract: The distribution of different phytoplankton groups is a result of competition for resources under a given set of environmental conditions. Shifts in the phytoplankton community structure can serve as an indicator of environmental change and alter the bio-optical and photophysiological properties of the phytoplankton. In this study phytoplankton pigment concentrations are used to estimate the distribution of taxa in the Greenland Sea, through the utilization of CHEMTAX (CHEMical TAXonomy) analysis. The CHEMTAX MATLAB subroutine was used iteratively and the results were stable within a range of seed matrices. Biomass estimates from microscope counts were

in general agreement with the group-specific estimates of major phytoplankton classes using CHEMTAX. Six algal classes were shown to dominate within the study area: diatoms, haptophytes, cryptophytes, prasinophytes, chrysophytes and dinoflagellates. Multivariate statistical analysis (cluster and principle component analyses) revealed that patterns in the distribution of phytoplankton groups were related to environmental forcing and sea ice presence. Cryptophytes, chrysophytes and prasinophytes were dominant groups under sea ice. Haptophytes dominated many of the open ocean stations where stratification was weak due to the presence of warm Atlantic waters lying beneath the surface mixed layer and reduced melt-water input. Diatoms were ubiquitous in the study region, and dominated in both sea-ice and open-ocean samples. Across the study region phytoplankton populations were generally mixed at depth and tended to be dominated by a single taxonomic group in the near surface, possibly a result of the presence of strong environmental gradients within the surface layer.

2.1 Introduction

In recent decades our understanding of phytoplankton diversity and abundance has increased due to methodological advances in microscopy (Roy et al., 1996), flow cytometry (Zubkov et al., 2000), genetic (Díez et al., 2001; Not et al., 2009) and chemical (Mackey et al., 1996; Stuart et al., 1998; Uitz et al., 2006) analyses. It has been suggested that phytoplankton diversity in the Arctic may not be as high as other ocean regions (Baldwin et al., 2005). Yet recent identification of endemic or undersampled taxa in the Arctic Ocean (Lovejoy et al., 2007; Mock and Thomas, 2008) highlights the need for further study. Arctic marine ecosystems are characterised by large annual

variations in irradiance, low temperatures, strong salinity-driven stratification and the physical barrier of sea ice separating the ocean from the atmosphere. These conditions create a number of distinct ecological niches within the euphotic zone and necessitate strong physiological acclimation (Bursa, 1963; Gradinger, 1996). Arctic sea-surface temperatures are rising, sea ice is retreating, and terrestrial run-off and permafrost melt is increasing, all of which have important repercussions for biology in the region. As the Arctic is undergoing significant climate change, it is essential to understand how environmental change will alter phytoplankton biogeography (IPCC, 2007), as different groups of phytoplankton play different biogeochemical and ecological roles in Arctic marine systems.

Snow and ice cover of Arctic terrestrial systems, combined with a large fraction of the Arctic being ocean, means that much of the primary production in the Arctic is due to aquatic photosynthesis (Field et al., 1998; Geider et al., 2001; Mock and Thomas, 2008). The response in Arctic phytoplankton communities to climate change is of interest for two reasons. Firstly, phytoplankton respond rapidly and non-linearly to subtle changes in local conditions and therefore can act as sentinels of environmental change (Newton, 2007; Li and Harrison, 2008). Secondly, changes in phytoplankton community structure will have a series of important feedbacks on the local environment. These may include changes in the rate and fate of carbon fixed through primary productivity due to the shifts in the dominant phytoplankton groups (Buesseler et al., 2003; Quere et al., 2005; Tamelander et al., 2009). There is some evidence of a waning in the dominance of diatoms and an increase in the abundance of prymnesiophytes (Harrison et al., 2013) and picoeukaryotes (Li et al., 2009) in Arctic regions. In highly productive waters, carbon export decreases rapidly as temperatures cross the 10 °C threshold, in less

productive waters this threshold is at even lower temperatures (Laws et al., 2000). Also warmer water temperatures favour smaller celled phytoplankton (Daufresne et al., 2009; Li et al., 2009), which also promotes a reduction in the biological pump. Rising temperatures and shifting phytoplankton communities could promote a shift from classical to microbial food webs (Legendre and Rassoulzadegan, 1995). To understand and predict the changes in phytoplankton community structure we must first understand the current biogeography and the primary factors influencing it. This requires detailed estimation of group specific phytoplankton abundances and an understanding of the primary factors controlling the distribution of groups that serve important biogeochemical and ecological functions in the Arctic Ocean.

Phytoplankton groups that are important in Arctic and Subarctic seas include diatoms, chrysophytes, prymnesiophytes, dinophytes, cryptophytes and green flagellates (prasinophytes + chlorophytes) (Stein and MacDonald, 2004). Phytoplankton diversity is normally greatest in the summer, when a transition from a few diatom species to a diverse assemblage of (small) flagellates takes place (Booth and Jr., 1997; Stein and MacDonald, 2004; Harrison et al., 2013). However, seasonal and geographical changes in community structure are also observed in Arctic seas. What follows is a summary of our current understanding of the distribution of phytoplankton taxonomic groups in relation to particular environmental conditions.

Diatoms are abundant in both the water column and sea-ice algal mats (Vincent, 2010) and are known to form ice-edge blooms in polar seas (Coupel et al., 2012). Diatoms also have an additional nutrient requirement for silica, and thus the availability of silicate is believe to play an important role in controlling their distribution. Chrysophytes are nanoplankton predominantly found in lower salinity waters (Stein and MacDonald,

2004). Prymnesiophytes are also mainly nano-plankton and some (e.g. *Pheocystis*) produce Dimethyl-sulphide (DMS) which is an important atmospheric aerosol (Becquevort et al., 2005). Prymnesiophytes have been found to be more common in open and mixed polar waters (Wright and van den Enden, 2000). Coccolithophorids, a prymnesiophyte sub-group present in the Arctic, have calcium-carbonate tests which give them significantly different optical and biochemical properties compared to other phytoplankton (Ackleson et al., 1994). Coccolithophores are typically found in temperate and Subarctic waters, but are thought to be encroaching further north with warming sea temperatures (Smyth et al., 2004). Dinoflagellates can be found as both autotrophs and heterotrophs in the Arctic. Some dinoflagellates can even combine the two life modes, becoming mixotrophic (Jones, 2000). In addition to being mixotrophic, dinoflagellates can be either armoured (thecate) or naked (athecate), the latter normally being found in waters influenced by sea ice (Stein and MacDonald, 2004). Cryptophytes are usually found in environments influenced by melt waters, be those melt-ponds, within-sea-ice or near-ice surface waters. The Arctic green flagellates are endemic picoplankton whose small size allows them to compete in very low-light conditions, even persisting through the long, dark Arctic winter (Lovejoy et al., 2007). A notable absence from the list of common phytoplankton are cyanobacteria. Due to low temperatures cyanobacteria are only found in minimal concentrations in the Greenland Sea region (Marchant et al., 1987; Gradinger and Lenz, 1995; Cottrell and Kirchman, 2009).

Each of the techniques used to measure phytoplankton community structure has a number of advantages and disadvantages. Although microscopic identification of phytoplankton provides information on phytoplankton taxonomic composition to the species level, it is extremely time-consuming, requires a high level of skill and may be ineffec-

tive at detecting the presence of smaller cells (Claustre, 1994). Preservation of samples for microscopy counts can also lead to the destruction of some cells (Hill et al., 2005). Phytoplankton pigments are frequently used as biomarkers and provide information on the community structure of phytoplankton. Chlorophylls and carotenoids are typically used as indicator pigments (Wright and Jeffrey, 2006), since they are present in all photosynthetic algae. Those pigments which are restricted to particular classes are referred to as diagnostic pigments (Jeffrey, 1997). The determination of phytoplankton groups from pigment data is complicated by the presence of pigments that are found in more than one class and by the intra-specific plasticity of pigment composition with changes in growth conditions. One approach that attempts to address these problems is the CHEMTAX iterative pigment factorisation method developed by Mackey et al. (1996). CHEMTAX has been utilized across a variety of oceanic domains, including in high-latitude waters (Wright et al., 1996; Wright and van den Enden, 2000; Vidussi et al., 2004; Coupel et al., 2012). To optimally use CHEMTAX as a method of partitioning chlorophyll-a biomass into various phytoplankton taxa requires prior knowledge of the dominant phytoplankton groups, their associated pigment complement and relative pigment concentrations. To date, most Arctic studies have assigned input pigment matrices based on Antarctic studies which has led to errors such as overestimation of diatoms and underestimation of prymnesiophytes (Coupel et al., 2012). To apply CHEMTAX to a new region, microscopic cell counts should be used to validate the model outputs of group-specific biomass (Havskum et al., 2004). In addition, pigment data from strains isolated from a particular location can aid the development of a region-specific pigment ratio matrix that may be used to interpret pigment datasets from the same hydrographic area (Hill et al., 2005).

The primary goal of this study is to examine the variation in phytoplankton community structure in the Greenland Sea region using a combination of High Performance Liquid Chromatography (HPLC) pigment concentrations and cell counts by conventional microscopy. HPLC pigment data are analysed and interpreted using both cluster analysis and CHEMTAX. Group-specific biomass estimates from the CHEMTAX analyses are validated using ancillary microscopy cell count data. The physio-chemical drivers governing the distribution of phytoplankton groups are then examined using Principal Component Analysis (PCA).

2.2 Methods

2.2.1 Study area

Samples were collected during the ICE CHASER 2010 (IC2010) research cruise onboard the RRS *James Clark Ross* (NERC/BODC cruise ID JR219). The cruise track covered a transect from the North Sea to the Greenland Sea between Svalbard and the Greenland Shelf. This region is influenced by Atlantic water moving northwards and Arctic waters returning south (see figure 2.1). Twenty three stations were sampled between the 14th of June and the 11th of July, from 56.7°N to 80.7°N and from 5.6°W to 8.3°E. Sampling stations covered a sea-ice gradient from the open ocean to 75 km into the sea ice (Figure 2.2).

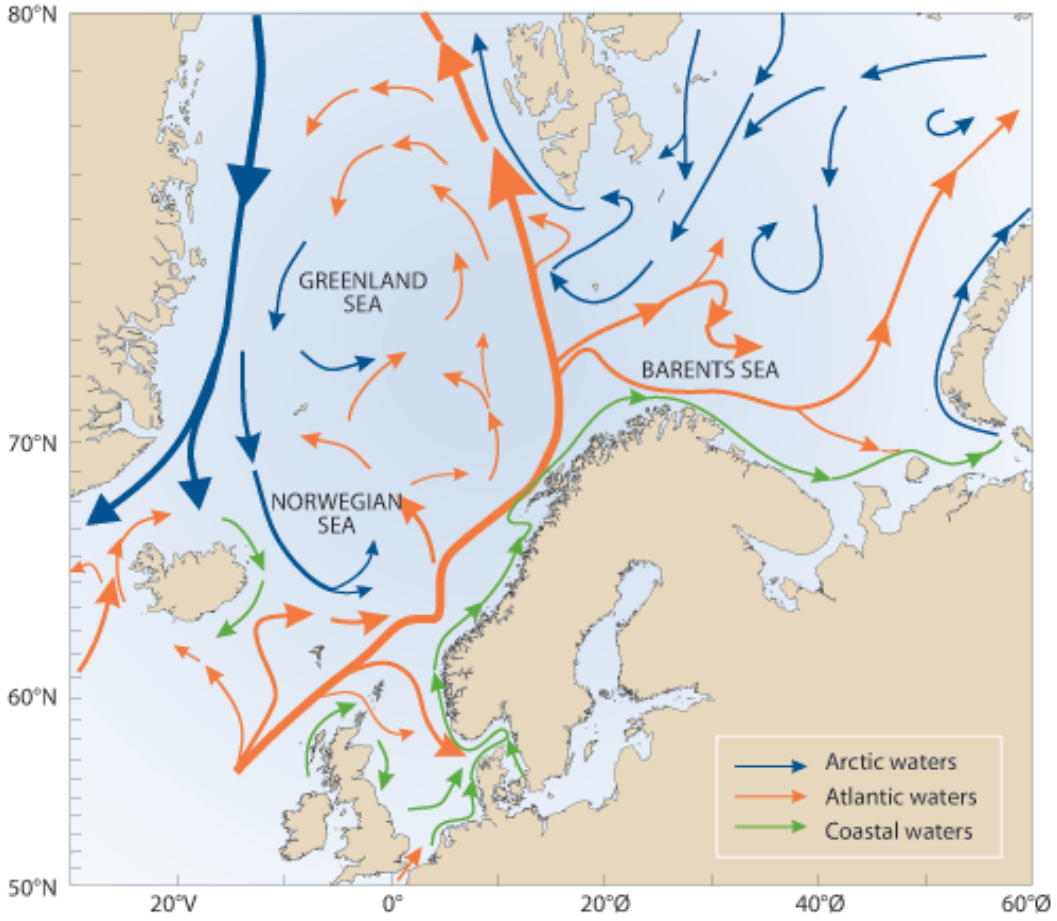

Figure 2.1: The ocean currents in the North, Norwegian, Greenland and Barents Seas. The major currents/water masses relating to this Greenland Sea study are (from west to east): the cold, southward moving East Greenland Current, the relatively warm, northward moving Norwegian Arctic Current, and the cold northward moving West Svalbard Current. Map sourced from the Norwegian Institute of Marine Research (of Marine Research, 2002).

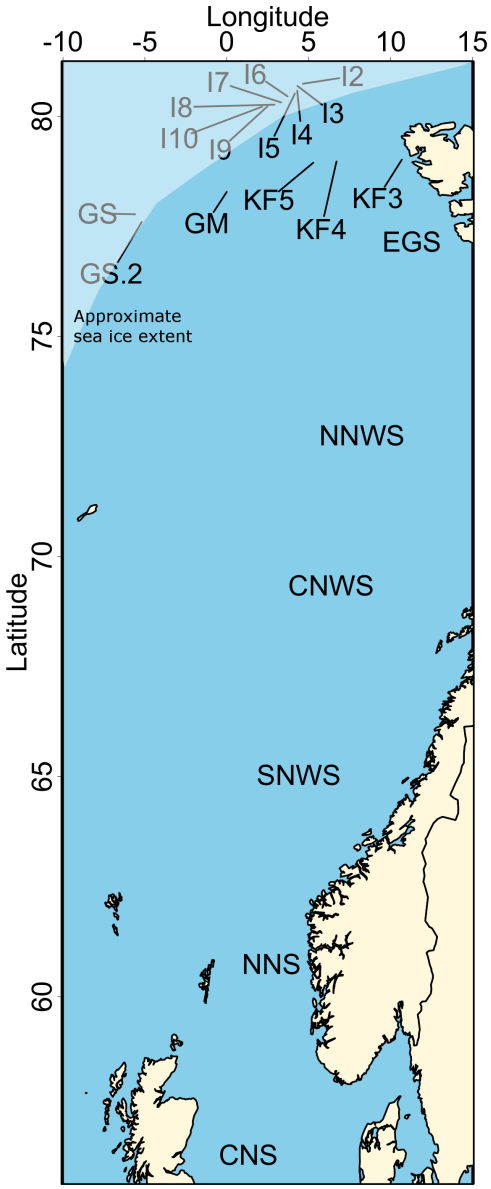

Figure 2.2: The geographical distribution of the stations sampled during the ICE CHASER 2010 cruise. Station names are offset for clarity when stations are in proximity to one another. White shaded region shows approximate extent of sea ice during research cruise.Station names: C/NNS = Central/North North Sea , S/C/NNWS = South/Central/North Norwegian Sea, I2-10 = Ice station 2-10, GS = Greenland Shelf, GM = Greenwich Meridian, KF = Kongsfjorden

2.2.2 Environmental data

Seawater samples were taken at 4-5 depths using 10 litre Niskin bottles, mounted on a CTD rosette. Sample depths were chosen to capture the vertical variability in the biomass profile through the photic zone. Samples were always collected from the near surface and the chlorophyll maximum which was determined using profiles of *in vivo* fluorescence measured using a Chelsea fluorometer. In addition to *in vivo* fluorescence, profiles of salinity (using two 4C conductivity sensors), temperature (two 3P temperature sensors) and downwelling irradiance (Biospherical Li-Cor PAR sensor) were measured and used to calculate mixed-layer depths (MLD), stratification index (SI) and euphotic depth (Z_{eu}).

Various methods exist for calculating the depth of the mixed layer from density profiles. The methods can be classified into three categories: density offset, least squares regression and integral methods (Thomson and Fine, 2003). The most commonly used method is density offset. This approach uses the depth at which the potential density is offset from the surface $\Delta\sigma_\theta(z) = \sigma_\theta(z) - \sigma_\theta(z_0)$ by a threshold value ($\Delta\sigma_\theta^T$), usually in the range 0.005 to 0.5 kg m^{-3}. In this study, the density offset method was used with a modification allowing three different thresholds, depending on the density range of the water column. Values for $\Delta\sigma_\theta^T$ were 0.05, 0.125 or 0.3 kg m^{-3} depending upon the total profiles density range $\Delta\rho$:

$$\Delta\sigma\theta(z) = \begin{cases} 0.05 & \Delta\rho \leq 0.25 \\ 0.125 & 0.25 < \Delta\rho \leq 1.4 \\ 0.3 & 1.4 < \Delta\rho. \end{cases} \tag{2.1}$$

The stratification index (kg m^{-3}) is calculated using density profiles and defined as the density difference between the surface and a reference depth. The reference depth used was 50 m, since much of the density variation occurred above this depth and increasing the reference depth further did not make a significant difference in the stratification index values and excluded profiles that did not extend beyond 60 m.

CTD downwelling irradiance profiles were used to calculate euphotic depths. The euphotic depth is defined as the depth at which downwelling irradiance was equal to 1 % of surface irradiance (I_0). To estimate the I_0, an exponential decay equation was fitted to light profiles in the upper 10 m and extrapolated to the surface (z = 0 m). For most stations Z_{eu} coincided with an absolute irradiance of 1-5 μeinsteins $m^{-2}s^{-1}$.

From a biological perspective, a useful definition of a stratified water column is one in which the euphotic depth is greater than the mixed-layer depth (Uitz et al., 2006). Therefore, information from both density and irradiance profiles were used to determine whether a given water-column was classed as 'stratified' or 'mixed'.

2.2.3 Phytoplankton pigment analysis

For each sample depth, 0.2-1 L of seawater was filtered onto 25 mm GF/F filters (Whatman Inc.) at a pressure of $<$200 mm Hg. Filters were then placed in cryovials and flash frozen in liquid nitrogen prior to storage at $\leq$-80 °C. Samples were analysed using reverse-phase HPLC as described in Barlow et al. (1997) after sonication in 90% acetone (Vibracell probe, Sonics and Materials, Newtown, CT, USA) for 30 s and centrifugation. The mobilised pigments were syringe filtered through a 0.2 μm nylon filter. Chlorophylls and carotenoids were detected by absorbance at 440 nm. Data collection

and integration utilized the Chromquest 3.0 software (Thermo Finnigan, CA, USA). Further confirmation of pigment identity was provided through on-line diode array spectroscopy. Multi-pigment standards were run at the beginning and end of batches of 24 samples and a chlorophyll-a standard was inserted between each subset of 6 samples to ensure there was no significant drift in pigment elution times and response factors. Measured marker pigments and their associated algal groups are shown in table 2.1.

To provide information on phytoplankton bulk pigment biomass during the cruise, fluorometric measurements of chlorophyll-a were made in triplicate using the method of Holm-Hansen et al. (1965). Sub-samples of 100 ml were filtered onto 25 mm GF/F filters and chlorophyll-a was extracted in 90 % acetone for 24 hours in the dark at -20 °C. The chlorophyll-a concentrations were then measured using a Turner Designs Trilogy fluorometer.

2.2.4 Interpretation of pigment data

Photosynthetic and photoprotective pigments

Phytoplankton accessory pigments can be separated into photosynthetic pigments (PP) and non-photosynthetic pigments (NPP). This distinction is important as the relative contribution of PP and NPP to total accessory pigments (TP) provides information on photoacclimation and energy transfer within the phytoplankton cells (Eisner et al., 2003). The photosynthetic accessory pigments detected were Chl-b, Chl-$c_{2,3}$, Perid, 19′-But, 19′-Hex, Fucox, and Pras. The measured non-photosynthetic accessory pigments were Diad, Zeax, Viol, Allox, and Lutein (Bricaud et al., 1995; Stuart et al., 2000; Eisner et al., 2003; Barlow et al., 2007).

Table 2.1: Details of pigments detectable during HPLC analysis of samples and the groups in which they are found (Jeffrey, 1997).

Pigment	Abbreviation	Retention time (minutes)	Relevant algal groups
Chlorophyll-c_3	Chl-c_3	2.2	Haptophytes,Chrysophytes
Chlorophyll-c2	Chl-c_2	3.08	Cryptophytes, Diatoms, Dinoflagellates, Haptophytes,Chrysophytes
Peridinin	Perid	3.73	Dinoflagellates
19′-Butanoyloxyfucoxanthin	19′-But	4.56	Haptophytes,Chrysophytes
Fucoxanthin	Fucox	4.86	Diatoms, Haptophytes, Chrysophytes
19′-Hexanoyloxyfucoxanthin	19′-Hex	5.53	Haptophytes
Prasinoxanthin	Pras	5.77	Prasinophytes
Violaxanthin	Viol	5.85	Chlorophytes,Prasinophytes
Diadinoxanthin	Diad	6.92	Diatoms, Dinoflagellates Haptophytes, Chrysophytes
Alloxanthin	Allox	7.74	Cryptophytes
Zeaxanthin	Zeax	9.34	Chlorophytes
Lutein	Lut	9.88	Chlorophytes, Prasinophytes
Chlorophyll b	Chl-b	18.14	Chlorophytes, Prasinophytes
Chlorophyll a	Chl-a	23.87	All phytoplankton

Cluster analysis

Cluster analysis was used to compare the major accessory pigments and identify any trends in the distribution of similar assemblages. Cluster analysis was conducted on pigment data using Euclidean distance in m-dimensional space, where m is the number of accessory pigments under consideration. The analysis was performed using the R statistical analysis software with functions from the 'stats' package. Unlike CHEMTAX analysis, cluster analysis makes no assumptions about group-specific pigment content or ratios. Pigments that are found in many groups, such as diadinoxanthin, were excluded from the cluster analysis dataset due to their poor diagnostic capabilities. All accessory pigment concentrations were normalised to chlorophyll-a concentration. Through

examining the resulting dendrogram and the change in the group sum of squares with changing cluster number, six major clusters were identified and k-means analysis was performed using the six clusters.

CHEMTAX initialization and processing

The relative contribution of phytoplankton groups to chlorophyll-a biomass was calculated using the MATLAB version of the CHEMTAX program. For CHEMTAX matrix factorization an initial pigment ratio matrix must be assigned, known as a seed matrix. To constrain the values used in the input matrix, pigment data from Arctic phytoplankton cultures were used and compared to previous CHEMTAX studies (Mackey et al., 1996; Wright et al., 1996; Jordan and Chamberlain, 1997; Vidussi et al., 2004).

HPLC measurements were made on Arctic phytoplankton cultures from six phytoplankton groups: Bacillariophyceae, Chlorophyceae, Cryptophyceae, Dinophyceae, Prasinophyceae and Prymnesiophyceae. These cultures were sourced from the National Centre for Marine Algae and Microbiota (NCMA), Bigelow Laboratory, Maine. Details of cultured species are given in table 2.2. All strains were cultured in a Sanyo MLR-352 incubator using a cool-white fluorescent light source. Cultures were incubated with a 16:8 light:dark cycle, at 5 °C, to represent Arctic summer growth conditions. With the exception of *Micromonas*, all cultures were exposed to an irradiance of 100 μmol quanta m^{-2} s^{-1}. The irradiance for *Micromonas* was modified to represent conditions deeper in the water column, as it was isolated from a depth of 55 m. For *Micromonas* growth flasks a combination of neutral-diffusing and blue filters reduced irradiance to 35 μmol quanta m^{-2} s^{-1}. Samples were taken for HPLC analysis during exponential growth phase by filtering cells onto 25mm GF/F filters.

Table 2.2: Details of species cultured. Cell sizes are means from 15 cell measurements per species. Biovolumes are calculated using the species-specific equations of Hillebrand et al. (1999). Sample depths refer to the depth of the sample from which the culture was originally isolated.

Species	Group	Cell size(μm)	Biovolume (μm^3)	Sample depth (m)	Growth Media
Cylindrotheca sp.	Bacillariophyceae	70x7μm	1800	6m	f/2
Rhodomonas sp.	Cryptophyceae	13x9μm	275	11m	f/2(no Si)+soil sol.
Unidentified sp.	Prymnesiophyceae	10x9μm	450	11m	f/2(no Si)+soil sol.
Polarella Glacialis	Dinophyceae	12x10μm	630	11m	f/2(no Si)
Chlamydomonas sp.	Chlorophyceae	14x8μm	470	ice core	f/2(no Si)+soil sol.
Micromonas sp.	Prasinophyceae	2x2μm	5	55m	f/2(no Si)

The CHEMTAX seed matrix used in this study followed recommendations put forward by Mackey et al. (1996): that the number of pigments were greater than the number of groups by at least two and that no group was assigned a single non-zero pigment ratio (table 2.3). The matrix defined a total of seven algal classes using thirteen accessory pigments. To confirm that the CHEMTAX output was not significantly biased by the seed matrix, CHEMTAX analyses were also performed using seed matrices with twice and half the initial matrix ratio values (table 2.3).

For the seven algal classes, further subdivisions were required to discriminate between members of the same algal class that possess significantly different pigment assemblages (Jeffrey and Wright, 1994). The prasinophyte group was split into two subgroups; those that contain prasinoxanthin and those that do not, such as *Micromonas puscilla* (Vidussi et al., 2004). Prasinophytes that do not contain prasinoxanthin also tend to have higher concentrations of other accessory pigments(Vidussi et al., 2004). The haptophytes were also split into two subgroups: type 3 contain 19′-Hex and fucoxanthin, such as *Chrysochromulina* (Barlow et al., 1993), and type 4 contain 19′-But, 19′-Hex, and fucox (Vidussi et al., 2004). This gave a total of nine algal functional

groups, based upon pigment content.

Since factors such as nutrient concentration and growth irradiance can result in significant variations in accessory pigment/chl-a ratios (Vidussi et al., 2004), samples were grouped into surface and deep samples based on irradiance profiles. Samples 2 m above the euphotic depth ($Z_{eu}-2$) and below were classified as deep. The depth horizon Z_{eu}-2 was chosen to allow for small discrepancies between the downward CTD profiles (used to calculate Z_{eu}) and upward CTD profiles (which correspond to when samples were collected). Using this approach, 24 samples were classified as deep and 59 as shallow.

CHEMTAX ratio limits were set to a default value of 500 %, which allowed the initial pigment ratio, *r*, to vary from *r*/5 to 5*r*. As in Mackey et al. (1996) the data were weighted according to the reciprocal of the mean pigment concentration in the sample subset being analysed to ensure the residual is a measure of relative rather than absolute fit to the data, thereby increasing the relative fit to the minor pigments at the expense of the major pigments. CHEMTAX was run iteratively as in (Latasa, 2007) to allow CHEMTAX to correctly adjust pigment ratios. The iterative process consisted of using the output pigment matrix from the previous CHEMTAX run as a new input matrix for the same set of samples until the pigment matrix stabilised (maximum change in pigment ratio between iterations is $<$10 % of previous ratio).

2.2.5 Cell counts used for CHEMTAX validation

At four stations, cell counts were conducted by light and epifluoresence microscopy to validate CHEMTAX estimates of group-specific biomass. The four stations covered a range of sea-ice conditions: under-ice, transitional and open-ocean waters. Microscopy

Table 2.3: Initial (seed) matrix used for CHEMTAX analysis of sample pigments. Matrix A ratios were determined from literature and cell cultures. Matrix B has doubled the ratios from matrix A, matrix C has halved the ratios of matrix A. All ratios are the amount of accessory pigment per unit chl-a for the chemo-taxonomic group.

Acc Pigment:Chl-a / Group	$Chlc_3$	Chlc2	Peri	But	Fuco	Hex	Pras	Viol	Ddx	Allo	Zea	Lut	Chlb
Matrix A													
Prasinophytes 1	0	0	0	0	0	0	0.8	0.01	0	0	0	0	0.4
Prasinophytes 2	0	0	0	0	0	0	0	0.06	0	0	0.09	0.01	0.7
Chlorophytes	0	0	0	0	0	0	0	0.06	0	0	0.1	0.2	0.5
Dinoflagellates	0	0.1	0.7	0	0	0	0	0	0.3	0	0	0	0
Cryptophytes	0	0.07	0	0	0	0	0	0	0	0.3	0	0	0
Haptophytes 3	0.2	0	0	0	0.2	0.9	0	0	0.2	0	0	0	0
Haptophytes 4	0.2	0	0	0.01	0.5	0.01	0	0	0.1	0	0	0	0
Diatoms	0	0	0	0	0.8	0	0	0	0.2	0	0	0	0
Chrysophytes-Pelagophytes	0.15	0	0	0.5	0.4	0	0	0	0.5	0	0	0	0
Matrix B													
Prasinophytes 1	0	0	0	0	0	0	1.6	0.02	0	0	0	0	0.8
Prasinophytes 2	0	0	0	0	0	0	0	0.12	0	0	0.18	0.02	1.4
Chlorophytes	0	0	0	0	0	0	0	0.12	0	0	0.2	0.4	1.0
Dinoflagellates	0	0.2	1.4	0	0	0	0	0	0.6	0	0	0	0
Cryptophytes	0	0.14	0	0	0	0	0	0	0	0.6	0	0	0
Haptophytes 3	0.4	0	0	0	0.4	1.8	0	0	0.4	0	0	0	0
Haptophytes 4	0.4	0	0	0.02	1.0	0.02	0	0	0.2	0	0	0	0
Diatoms	0	0	0	0	1.6	0	0	0	0.4	0	0	0	0
Chrysophytes-Pelagophytes	0.3	0	0	1.0	0.8	0	0	0	1.0	0	0	0	0
Matrix C													
Prasinophytes 1	0	0	0	0	0	0	0.4	0.005	0	0	0	0	0.2
Prasinophytes 2	0	0	0	0	0	0	0	0.03	0	0	0.045	0.005	0.35
Chlorophytes	0	0	0	0	0	0	0	0.03	0	0	0.05	0.1	0.25
Dinoflagellates	0	0.05	0.35	0	0	0	0	0	0.15	0	0	0	0
Cryptophytes	0	0.035	0	0	0	0	0	0	0	0.15	0	0	0
Haptophytes 3	0.1	0	0	0	0.1	0.45	0	0	0.1	0	0	0	0
Haptophytes 4	0.1	0	0	0.005	0.25	0.005	0	0	0.05	0	0	0	0
Diatoms	0	0	0	0	0.4	0	0	0	0.1	0	0	0	0
Chrysophytes-Pelagophytes	0.075	0	0	0.25	0.2	0	0	0	0.25	0	0	0	0

47

samples were taken from multiple depths coincident with the samples collected for HPLC pigment analysis and preserved using Lugol's iodine solution. Cell counts by both light and epifluorescence microscopy provided taxonomic identification up to the species level. A complete description of the microscopy techniques used to identify and enumerate phytoplankton cells is given in (Davidson et al., 2007). Preserved cell volumes were converted to cell biovolumes using the equation of Menden-Deuer et al. (2001). The cell abundances were converted into carbon biomass estimates by multiplying the cell abundance by group-specific carbon conversion factors (Montagnes et al., 1994; Menden-Deuer and Lessard, 2000; Montagnes and Franklin, 2001). The conversion for diatoms is (Montagnes and Franklin, 2001):

$$\mathrm{C} = 10^{0.850(\log(\mathrm{V}))-0.420}, \tag{2.2}$$

for dinoflagellates (Menden-Deuer and Lessard, 2000),

$$\mathrm{C} = 10^{0.819(\log(\mathrm{V}))-0.119}, \tag{2.3}$$

and for cryptophytes and haptophytes (Montagnes et al., 1994)

$$\mathrm{C} = 0.109(V^{0.991}), \tag{2.4}$$

where C is carbon (pg) per cell and V is cell biovolume (μm^3).

To allow comparison to the CHEMTAX estimation of phytoplankton biomass, we summed the carbon biomass estimates determined by microscopy for each of the major autotrophic phytoplankton groups: diatoms, dinoflagellates, cryptophytes and haptophytes.

2.3 Results

2.3.1 Environmental conditions

The surface water temperatures in the study region ranged from -1.52 to 11.85 °C, although the majority of stations were in waters of 7 °C or less (figure 2.3 and table 2.4). Surface salinity varied from 31.04 to 35.24 PSU and was strongly dependent upon proximity to the ice edge. The mixed-layer depth ranged from 6.2 to 25.8 m, with over half the stations having a mixed layer of $<$10 m. The stratification index exhibited a large range, varying between 0.069 and 2.26 kg m^{-3}. Much of this density change took place in the upper 20 m of the water column and was predominantly related to the presence of low salinity ice melt rather than thermal forcing. Two water-column structures were observed beneath sea ice; 1) a shallow surface layer above warmer Atlantic water and 2) a cold halocline layer up to a depth of 80 m, observed at IS 6, IS 7 and IS 8 (figure 2.4).

Surface irradiance varied from 53 μeinsteins $m^{-2}s^{-1}$ beneath sea ice to 1280 μeinsteins $m^{-2}s^{-1}$ in the open waters. The majority of surface irradiance values (> 85 %) were less than 400 μeinsteins $m^{-2}s^{-1}$. The mean euphotic depth in the under-ice and ice-edge stations (50.2 $\pm$ 20.2 m) was nearly twice that of the open ocean stations (32.5 $\pm$ 9 m). This is due to a tendency for lower values of integrated biomass in the euphotic zone beneath sea ice than for open ocean stations. Using the Uitz et al. (2006) criteria for a stratified water column, 95 % of stations were classified as stratified, which implies that the phytoplankton within the mixed layer are much more likely to be nutrient limited than light limited (Yentsch, 1981).

Table 2.4: Station details for the IC2010 research cruise. Chl_{max} represents the highest chlorophyll-a concentration detected in the station profile and Z_{Cmax} is the depth at which that maximum concentration was located. Sea surface temperature (SST) and surface salinity values are averaged from the upper 5 m of the water column. Mixed-layer depth (MLD) is calculated according to equation 2.1 and euphotic depth (Z_{eu}) estimation is covered in section 2.2.2.

Station	Latitude (North)	Longitude (East)	Chl_{max} (mg/m^3)	Z_{Cmax} (m)	SST (°C)	Surface salinity	MLD (m)	Z_{eu} (m)
CNS	56°24.73'	001°18.85'	1.13	28	11.85	35.07	19.0	31.5
NNS	60°44.59'	002°43.67'	1.64	17.5	11.20	33.63	8.1	20.5
SNWS	65°02.42'	004°24.02'	1.39	17.5	9.96	34.31	18.1	28.5
CNWS	69°20.46'	006°22.42'	1.73	11	7.28	35.24	23.1	37.0
NNWS	72°45.21'	008°15.93'	0.81	12	5.90	35.19	25.8	44.0
EGS	77°09.42'	011°17.53'	3.88	20.5	5.75	35.03	31.7	21.0
I2	80°44.48'	004°39.05'	0.31	15	-0.78	32.98	13.0	56.5
I3	80°41.50'	004°19.09'	0.24	26.5	-1.13	32.79	15.4	51.5
I4	80°35.10'	004°18.29'	0.51	58	-1.10	32.65	11.3	50.0
I5	80°31.09'	004°09.87'	0.61	54.5	-1.35	32.55	9.9	52.0
I6	80°27.32'	003°43.04'	0.25	21.5	-1.52	33.10	6.2	100.5
I7	80°18.98'	003°19.39'	0.25	20	-1.52	33.06	7.7	76.0
I8	80°15.98'	002°55.15'	5.48	32	-1.32	32.46	9.6	36.0
I9	80°13.78'	002°29.79'	3.86	25	-1.18	32.20	8.0	36.0
I10	80°13.19'	002°09.94'	3.56	30	-1.13	32.18	7.7	32.5
KF3	79°01.00'	010°42.05'	0.26	18	4.51	33.79	9.7	50.0
KF3	79°00.91'	010°41.28'	2.97	29	2.32	33.93	9.9	34.0
KF4	78°58.52'	006°42.39'	3.85	21.5	6.38	35.07	22.9	27.0
KF4	78°58.51'	006°42.38'	3.21	28	6.45	34.61	9.2	28.5
GS	77°46.63'	-005°35.77'	1.31	14.5	-1.01	31.04	7.8	35.0
GS	77°36.05'	-005°11.43'	0.47	6	-0.93	31.21	9.0	41.0
GM	78°17.00'	000°00.02'	7.15	20	-0.64	33.51	7.4	35.0
KF5	78°56.85'	005°17.30'	2.82	19.5	7.42	35.00	9.6	36.0

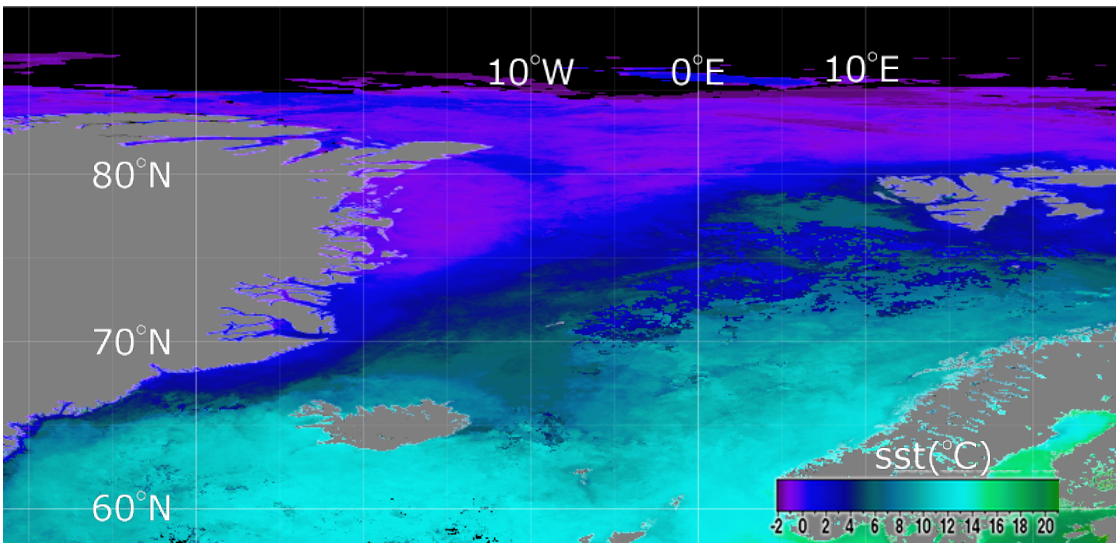

Figure 2.3: Monthly composite SST map of Greenland sea from MODIS, night-time 11μm data from July 2010. Study stations were sampled between the 14th of June and the 11th of July so this map represents an upper temperature estimate.

Nitrate concentrations were observed from below the limit of detection (0.01) to 12.55 μM, though concentrations above 8 μM were only seen in waters below 30 m. Phosphate concentrations varied from below the detection limit to 1.13 μM. The N:P ratio was generally close to 16:1 (Redfield ratio), although stations on the Greenland Shelf exhibited N:P ratios indicative of nitrate limitation at depths of up to 30 m (figure 2.5). Silicate concentrations ranged from 0.02 to 4.72 μM and correlate with nitrate ($r^2 = 0.6$) with an N:Si ratio of 3.3:1, indicating that silicate may be limiting diatom growth (Gilpin et al., 2004).

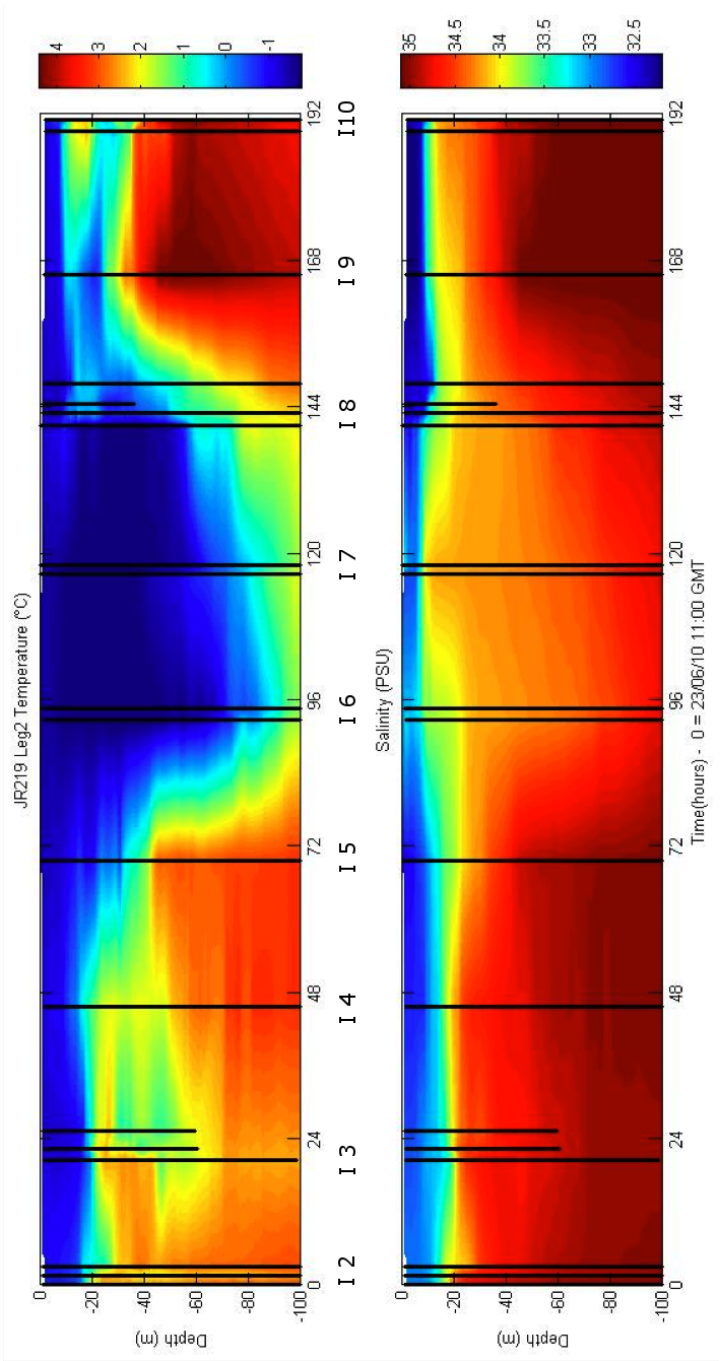

Figure 2.4: Temperature and salinity profiles for the northern ice-stations. For stations IS 1-5 and IS 9-10 a shallow surface water layer lies above warm saline Atlantic water. Stations IS 6, 7 and 8 exhibit a cold halocline layer beneath the surface layer, increasing water column stability. Black lines are single CTD casts used for each station in this study.

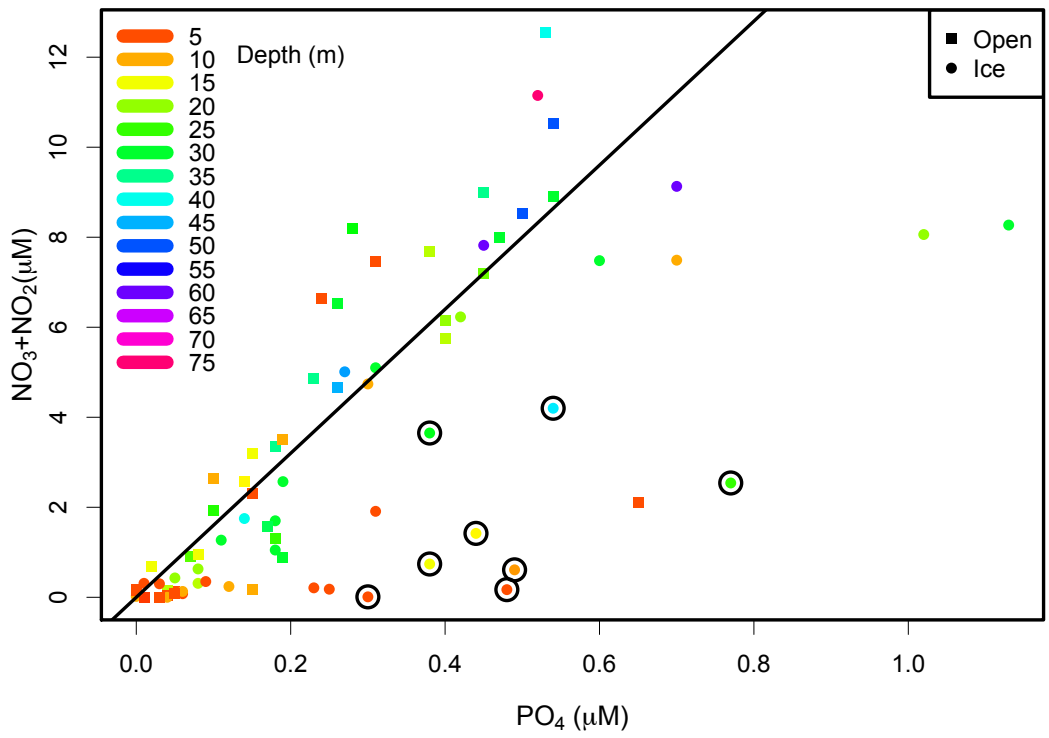

Figure 2.5: NO_3 + NO_2 concentrations plotted against the PO_4 concentrations and coloured according to sample depth. The line shows the Redfield ratio (16:1). Points circled below the Redfield ratio are all from samples taken at the two Greenland Shelf stations.

2.3.2 Phytoplankton pigment distribution

Surface chlorophyll-a concentrations varied from 0.12 to 2.3 mg m^{-3} with higher concentrations primarily found in open-ocean waters. Inspection of chlorophyll-a profiles revealed that chlorophyll-a concentrations at depth were often greater than surface values and subsurface chlorophyll-a concentrations reached a maximum of 7.15 mg m^{-3}. Subsurface maxima were also present in a number of accessory pigments (figure 2.6). A strong correlation was observed between concentrations of chlorophyll-a and total

accessory pigments (r^2 =0.83) with the majority of Chl-a:TP lying close to 1. Photoprotective pigment to photosynthetic pigment ratios ranged from 0.04 to 1.3, with a mean of 0.4 in the upper 10 m of the water column and mean values below 0.2 for each 10 m increment below this. The accessory pigments chl-$c_{2,3}$, 19′-But, fucox, 19′-Hex, viol, diad, allox, and chl-b were all detected in surface waters (figure 2.8).

Fucoxanthin showed the strongest correlation with total chlorophyll-a (r^2=0.81). There is a poor correlation for peridinin (figure 2.7), but a strong correlation exists for 19′-Hex. Therefore, in this region phytoplankton biomass, and thus primary production, correlates with diatom and haptophyte abundance rather than diatom and dinoflagellate abundance.

Fucoxanthin was present at all stations and is the dominant accessory pigment, constituting between 10 % and 91 % of the TP. The next most prevalent pigment was diadinoxanthin, detected in 97 % of samples. This photoprotective pigment is present in four algal groups and its concentration is strongly correlated to the summed concentration of fucoxanthin and its derivatives (r^2=0.75). The next most prevalent photosynthetic pigments were 19′-Hex and 19′-But. Over 95 % of samples contained one of these two pigments and 70 % contained both. A higher proportion of the samples contain 19′-But (88 %) but at most it constituted 31% of the TP. Samples containing a significant proportion of 19′-But tended to be at depths around 15-20 m. The pigment 19′-Hex was detected in 78 % of samples and contributed up to 54 % of TP. This pigment also showed a peak in concentrations in the subsurface but the maxima is 3-5 m shallower than 19′-But and surface concentrations were much greater. Alloxanthin was observed in 86 % of samples and constituted up to a quarter of TP in some samples. The highest average alloxanthin concentrations were observed in surface waters (5 m) and contrasts

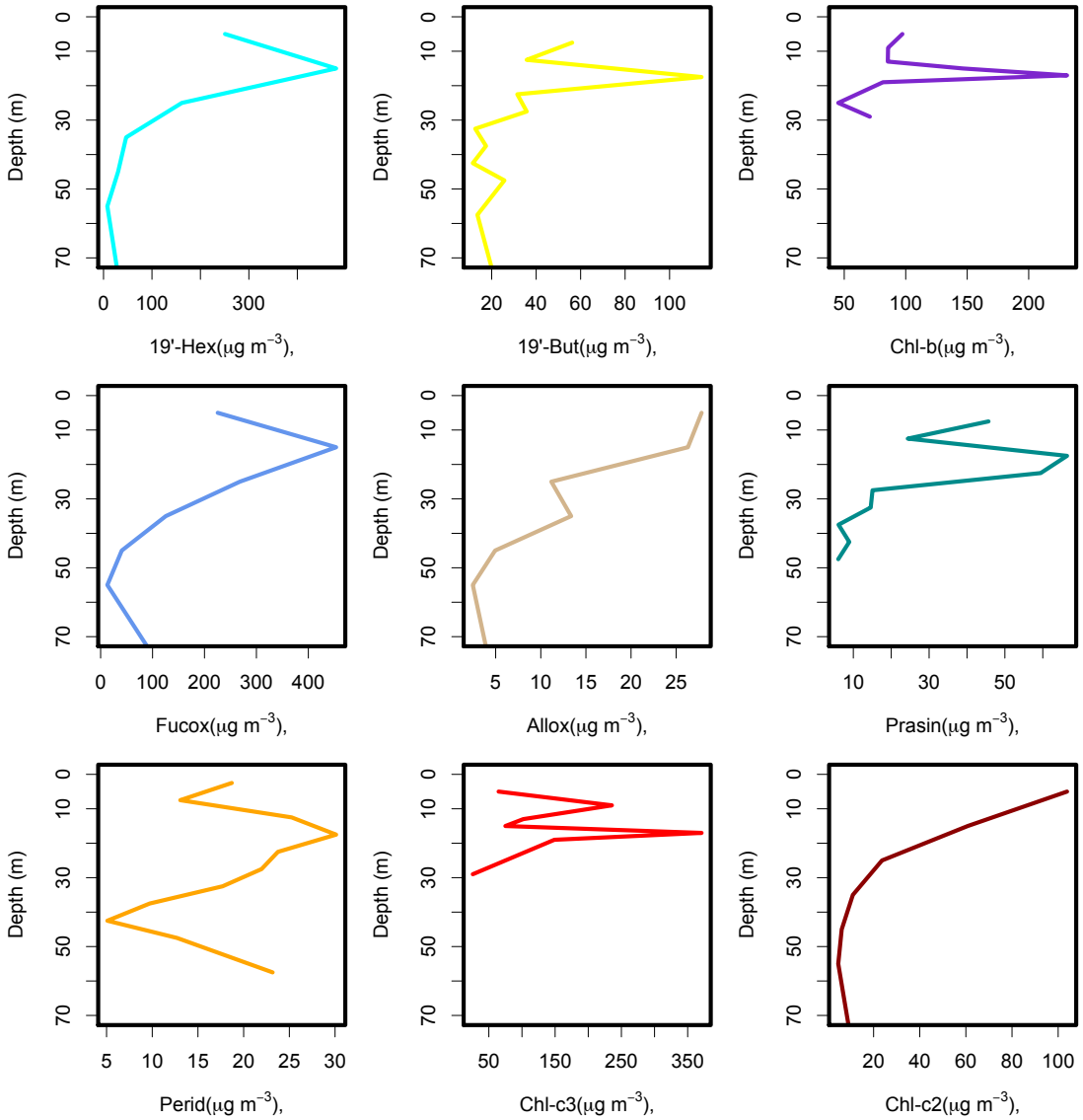

Figure 2.6: Mean concentrations of major pigments with depth, as determined by HPLC. Data from cruise samples containing each pigment were combined and binned to produce mean profiles.

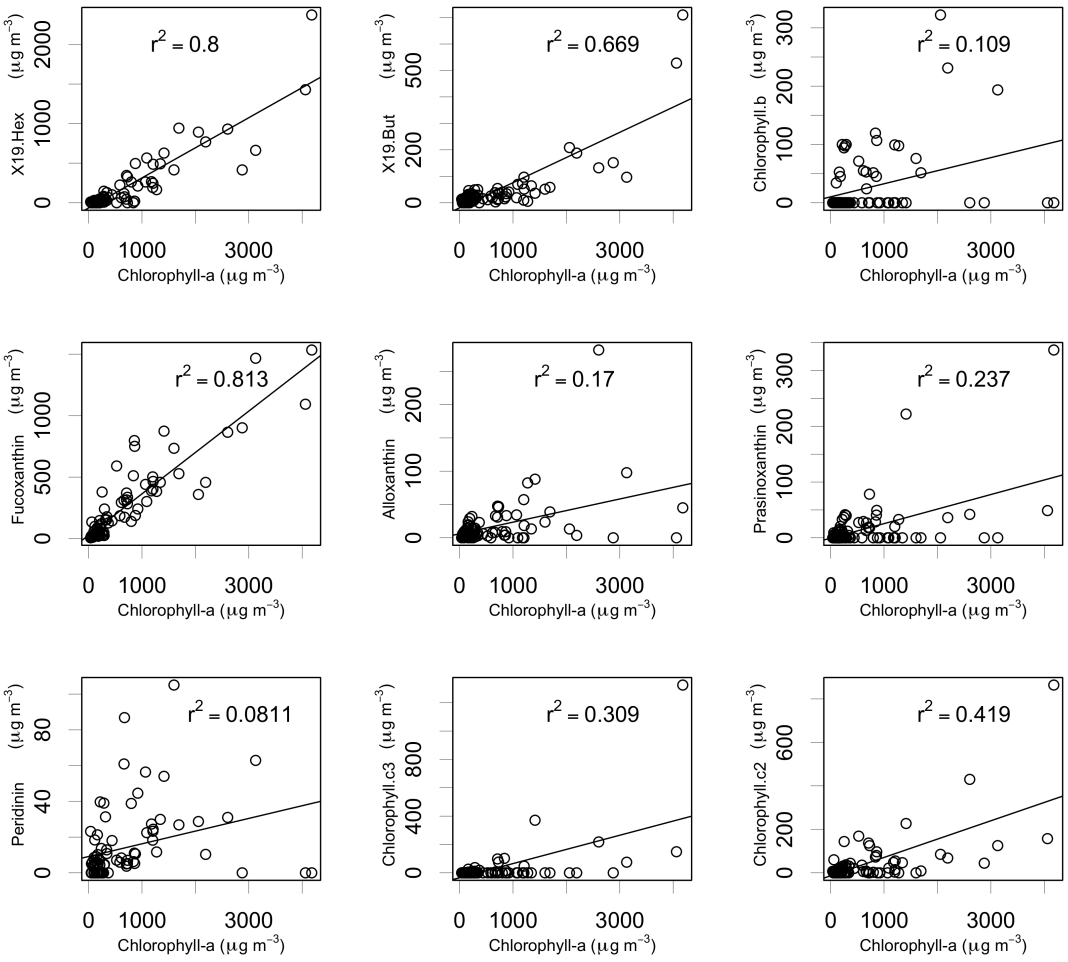

Figure 2.7: Comparison of accessory pigment concentration to the chl-a concentration. Linear regression and correlation coefficients shown for each accessory pigment.

profiles of the other accessory pigments, which showed a peak in average concentrations at depths around 10-20 m (figure 2.6). Peridinin, a pigment marker of dinoflagellates, was present in 70 % of samples, usually making up less than 10 % of TP, but reaching maxima of 40 % of TP. Chlorophyll-b was only present in 22 samples, but was detected at high absolute and relative concentrations (up to 40 % TP). Prasinoxanthin (present 37 samples) only constituted up to 22 % of TP. Average profiles for both of these pigments have a subsurface maxima at around 17 m. Zeaxanthin was only detected in a small number of samples (15 %) and never contributed more than 6% of TP. For stations were zeaxanthin was present, peak concentrations tended to fall between 15-17 m. A comparison of pigment composition (% total pigment) and concentrations at the surface and subsurface chlorophyll maximum (SCM) is shown in figure 2.9 and full profiles of pigment fractions are shown in figure 2.10. It should be noted that the cyanobacteria *Synechococcus* contain zeaxanthin, alongside phycobiliproteins (Waterbury et al., 1986), but were assumed to not be present for this study. Although the phycobiliproteins were not quantified during the HPLC analysis, co-incident absorption spectra measurements (Chapter 3) show no significant absorption peaks in field samples in the 545-565 range (absorption maxima for *Synechococcus* phycobiliproteins (Moore et al., 1995)). If this group were present then the effect would be minimal as only a small number of samples contain zeaxanthin, and never dominated the accessory pigments.

2.3.3 Cluster analysis

Cluster analysis identified six pigment clusters, as highlighted in the dendrogram shown in figure 2.11. Average cluster pigment composition, as separated by k-means analysis, are given in table 2.5 and plotted in figure 2.12. The clusters are shown in relation to

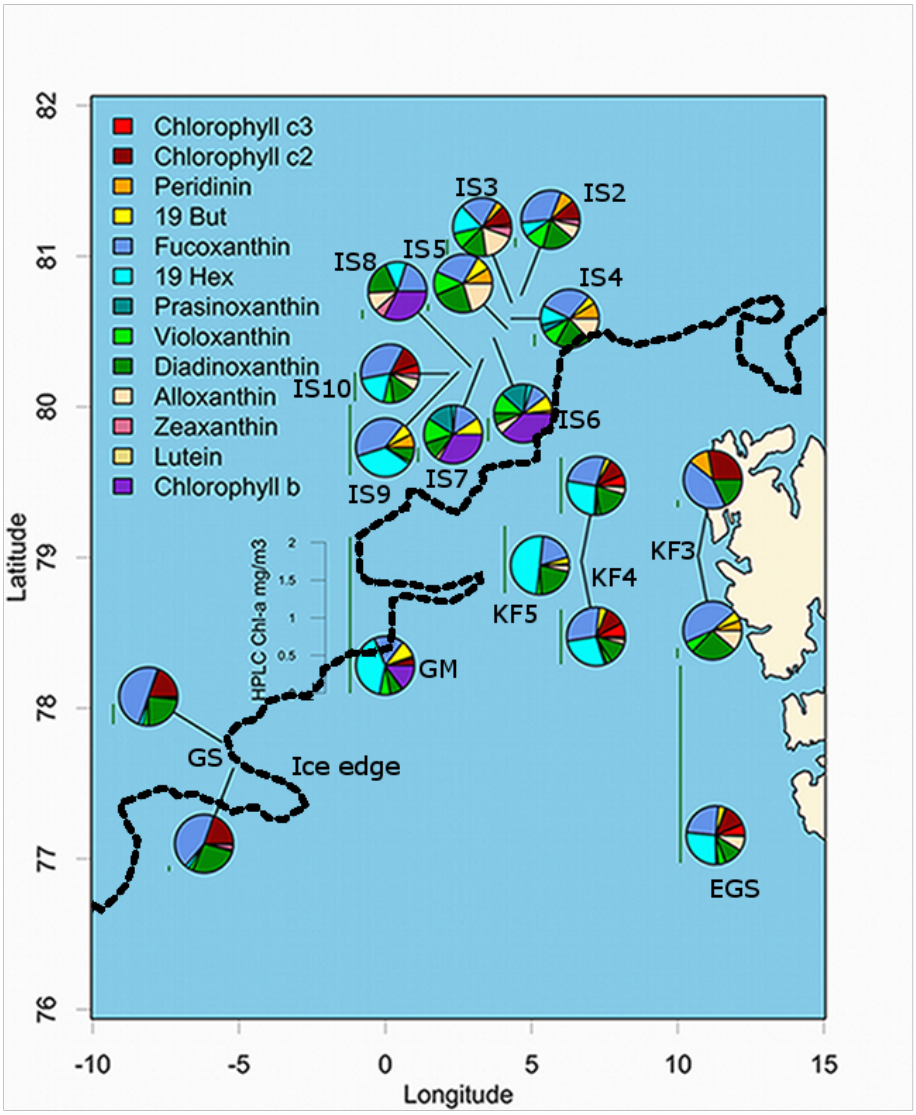

Figure 2.8: Pigment composition (pie chart) and chlorophyll-a concentrations (Green Bar) plotted in relation to the ice edge (Dashed contour). The ice edge is defined as ice concentrations > 30 %. Data shown are from the shallowest sample at the respective station.

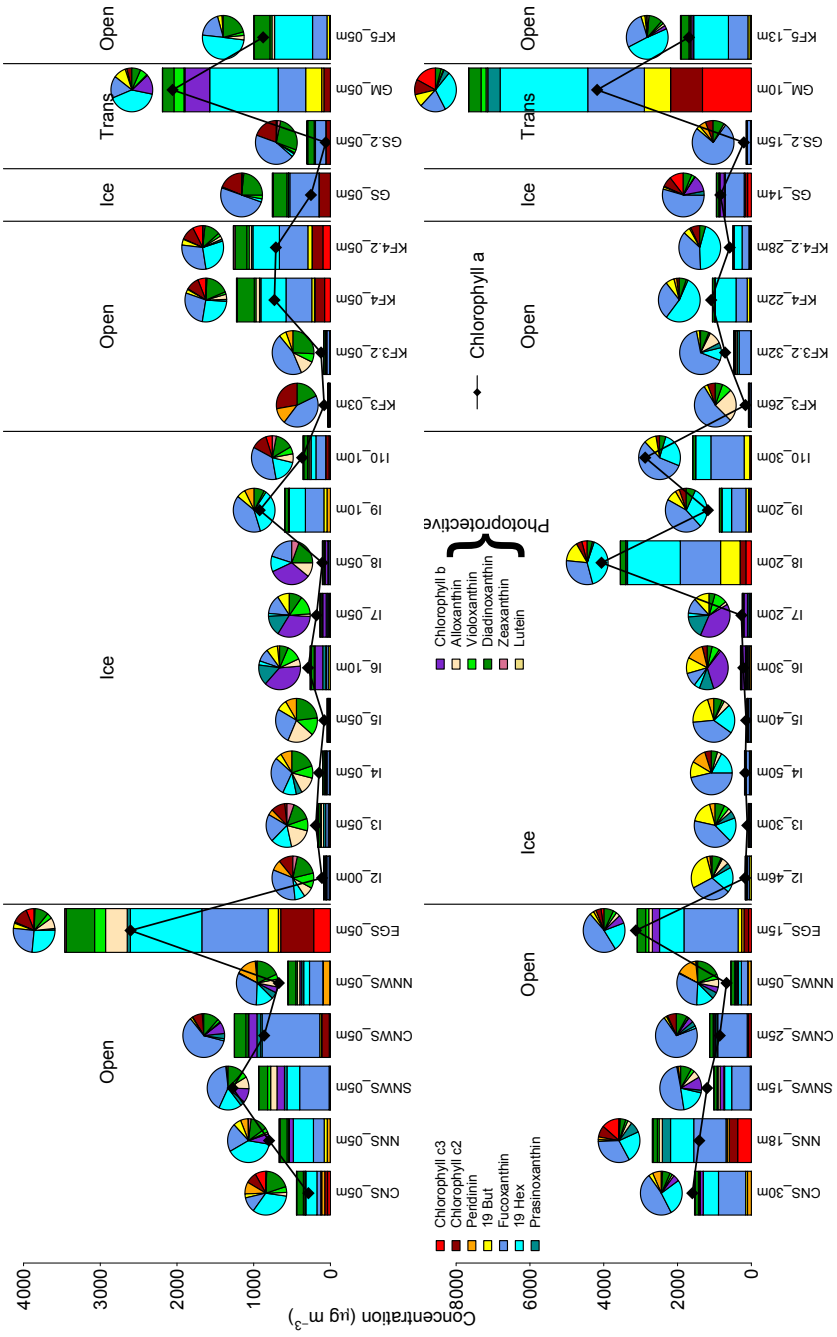

Figure 2.9: Pigment assemblages for samples closest to the surface and the chl-a maximum for each station of the cruise. Sample names are composed of the station name and sample depth. Bars show accessory pigment concentrations and pie charts show fraction of total accessory pigments. Chlorophyll-a concentrations are overlain in black.

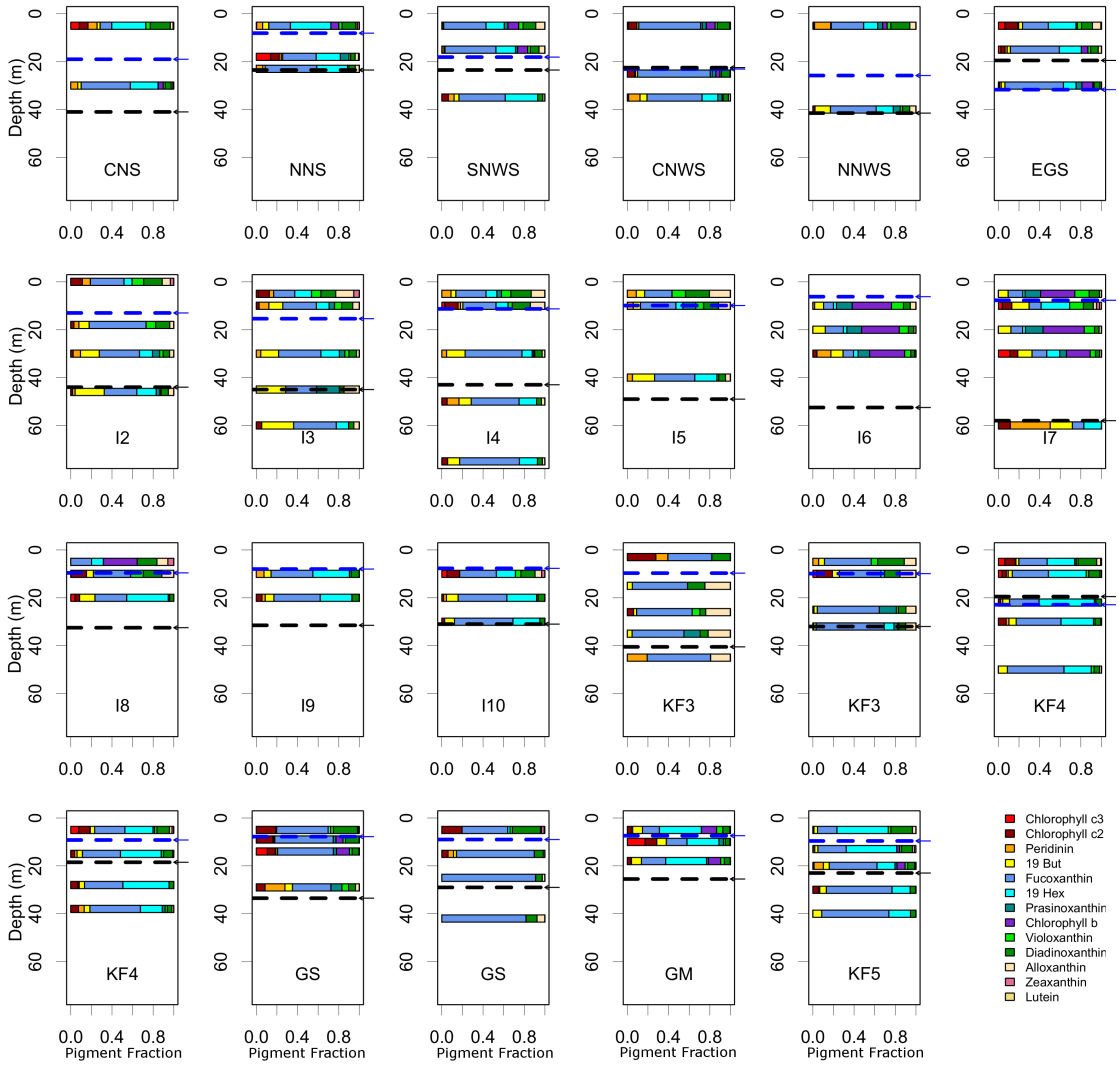

Figure 2.10: Profile of pigment composition profiles for each station with the mixed-layer depth indicated by a blue dashed line and the euphotic zone shown as a black dashed line.

depth and salinity (a proxy for sea-ice influence) in figure 2.13 and geographic location in figure 2.14.

Almost all clusters contained a significant portion of fucoxanthin ($\geq$20 %) and 19′-Hex, which indicates the presence of both diatoms and haptophytes in most samples. All clusters apart from cluster 5 also contain a small fraction of peridinin, probably representing a background presence of dinoflagellates. Small fractions of zeaxanthin and chl-b are seen in clusters 1 and 3 with a zeax/chl-b ratio of around 0.5 or less, which suggests the presence of chlorophytes (Schlüter et al., 2000; Hill et al., 2005).

Table 2.5: Mean accessory pigment fractions of diagnostic pigments for each cluster. For each cluster the two highest fractions are highlighted in bold.

Cluster	Chl-c_3	Allox	Chl-b	19′-Hex	19′-But	Fucox	Pras	Perid	Lutein	Zeax
1	0.008	**0.155**	0.010	0.070	0.081	**0.527**	0.062	0.080	0.000	0.006
2	0.004	0.034	0.018	**0.213**	0.106	**0.559**	0.019	0.046	0.000	0.002
3	0.060	0.025	0.019	**0.419**	0.086	**0.312**	0.018	0.052	0.002	0.006
4	0.017	0.008	0.057	0.094	0.054	**0.738**	0.024	0.007	0.000	0.000
5	0.000	0.012	0.000	**0.044**	0.006	**0.887**	0.000	0.000	0.013	0.039
6	0.026	0.041	**0.399**	0.075	0.121	**0.166**	0.130	0.032	0.000	0.009

Examination of the pigment composition of each cluster provided further detail on the groups of phytoplankton that were present in each cluster. The geographic distribution and environmental conditions that coincided with those samples could then be examined from an ecological perspective and provide an insight into the major drivers of Arctic phytoplankton biogeography.

Cluster 1

Cluster 1 encompassed around a fifth (22 %) of the samples analysed. The cluster was characterized by a high proportion of alloxanthin, indicating cryptophytes. It was also

the cluster that contained the largest proportion of peridinin, a diagnostic pigment of dinoflagellates. The cluster was primarily found in the near surface and at intermediate depths beneath sea ice, particularly in the extreme north-east, these waters may be influenced by the cold West Svalbard Current.

Cluster 2

Cluster 2 contained the greatest number of samples (27) and had the most diverse pigment assemblage, which implied a mixed population. High proportions of fucoxanthin, 19′-Hex and 19′-But were present alongside lesser contributions of alloxanthin, prasinoxanthin, chl-b and peridinin. The carotenoid 19′-But is often used as an indicator of type 4 haptophytes. However these samples typically had low Chl-c_3/Chl-a and Fuco/19′-Hex ratios (table 2.6), which makes the presence of type 4 haptophytes in sufficient numbers to account for the observed 19′-But concentrations unlikely. A more likely explanation for the relatively high concentrations of 19′-But is the presence of chrysophytes. Therefore, this cluster is best described as a mixed phytoplankton population with a significant fraction of diatoms, haptophytes and chrysophytes. Cluster 2 occurred under sea ice and in open-ocean waters and, with the exception of a single brine sample, contained no surface ($\leq$5 m) samples. The cluster was most abundant at depth, especially in the north-east of the study area, lying in the path of the warm, northward moving Norwegian Arctic Current.

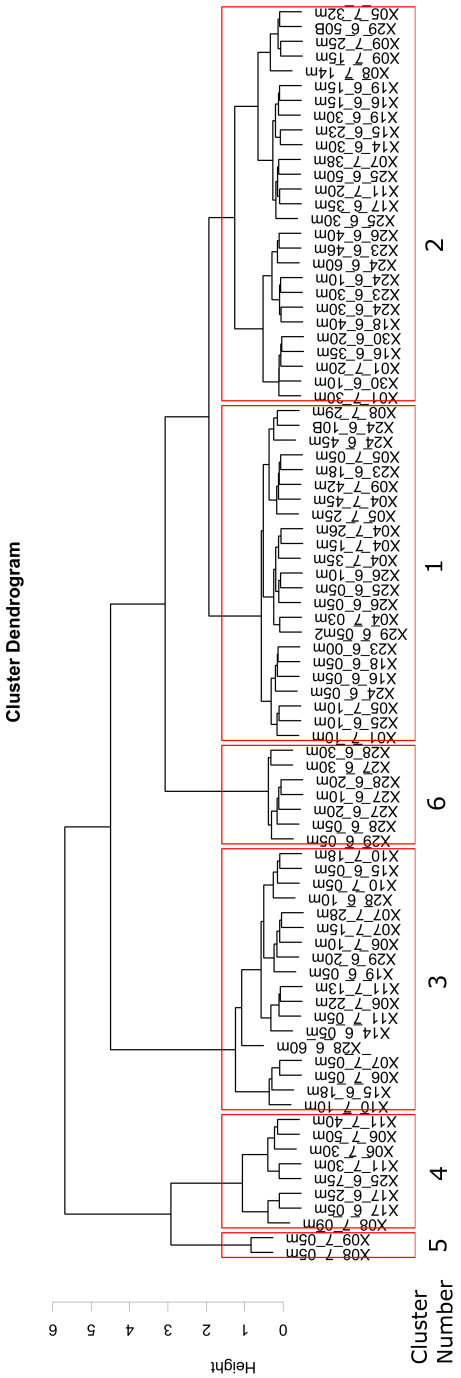

Figure 2.11: Dendrogram representation of cluster analysis of pigment samples based upon the photosynthetic accessory pigments contents normalised to chlorophyll-a. Similarity was defined as Euclidean hierarchical distance in m-dimensional space, where m is the number of accessory pigments.

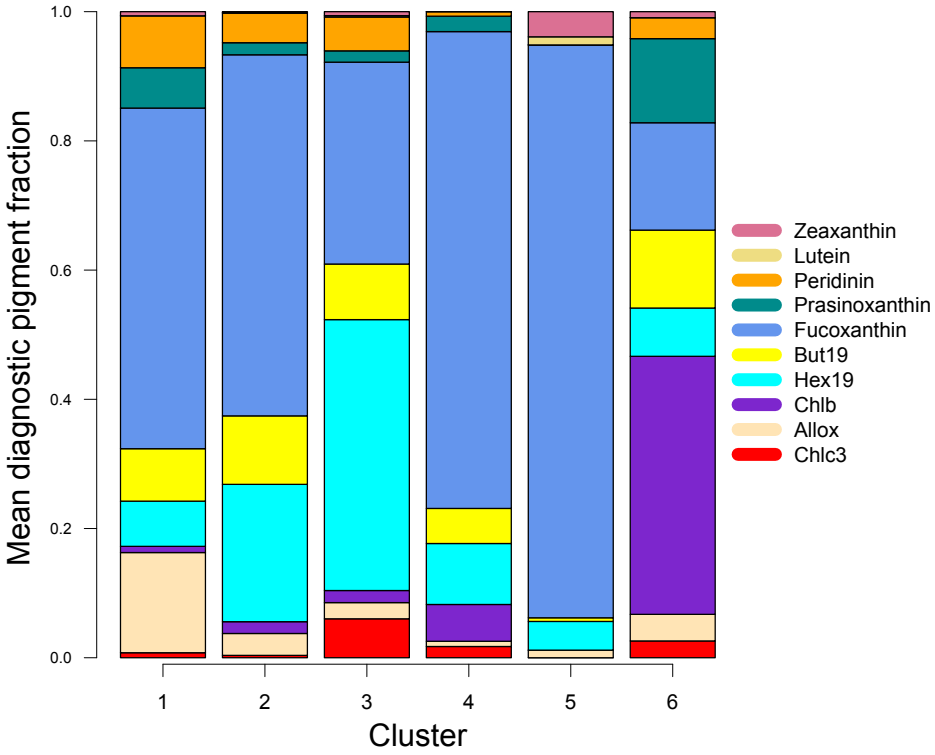

Figure 2.12: Average diagnostic pigment assemblage of samples from each cluster separated by the k-means analysis.

Cluster 3

Comprising thirteen samples, this cluster contained significant quantities of 19′-Hex, chl-c_3 and fucoxanthin, suggesting the presence of a large proportion of haptophytes in the population (Hill et al., 2005). The 19′-Hex/Fucox ratio in cluster 3 is indicative of type 3 haptophytes. The relatively minor contribution of 19′-But may be from type 4 haptophytes, or a small population of chrysophytes. Only a single sample from >30 m was present in this cluster and the remaining members were from the surface waters and intermediate waters of the open ocean stations in the Norwegian Arctic Current influenced waters to the south-east.

Cluster 4

The fourth cluster contained seven samples with a mean depth of 28 m. They were found in open ocean and under-ice stations from intermediate depths up to 75 m. This cluster contained 19′-But and chl-c_3, which suggested the presence of haptophytes. However, high Fucox/19′-Hex and Fucox/19′-But ratios implies a large proportion of the population were diatoms. There is also a small contribution of Chl-b and prasinoxanthin and the pras/chl-b ratio shows this may be from type 1 prasinophytes (Schlüter and Møhlenberg, 2003).

Table 2.6: Informative accessory pigment to chlorophyll-a and pigment to pigment ratios for each cluster.

Pigment ratio	Cluster 1	Cluster 2	Cluster 3	Cluster 4	Cluster 5	Cluster 6
Allo/Chl-a	0.0788	0.0248	0.0252	0.00926	0.0246	0.0358
Peri/Chl-a	0.0409	0.0338	0.0525	0.00797	0	0.0282
Chl-c_3/Chl-a	0.00393	0.00269	0.0605	0.0198	0	0.0226
Fuco/Hex	7.54	2.63	0.745	7.82	20	2.22
Fuco/But	6.49	5.27	3.63	13.6	157	1.38
Hex/But	0.862	2.01	4.87	1.74	7.86	0.62
Pras/Chl-b	6.5	1.02	0.936	0.419	NA	0.326
Lut/Chl-b	0	0.026	0.116	0	NA	0
Zeax/Chl-b	0.665	0.0826	0.33	0	NA	0.0233

Cluster 5

Containing only two samples, cluster 5 was the smallest cluster. The accessory pigments were almost exclusively fucoxanthin. It is therefore likely that these samples were diatom dominated. The presence of trace concentrations ($<$5 %) of 19′-Hex may suggest a small fraction of haptophytes, however chlorophyll-c_3, another diagnostic pigment of haptophytes was absent from these samples, perhaps because the levels were below the

limit of detection. These assemblages were only seen in extremely fresh surface waters in under-ice samples on the Greenland Shelf.

Cluster 6

Cluster 6 showed a dominance of Chl-b in the accessory pigments (≈40 %) with additional prasinoxanthin. There are three Chl-b containing phytoplankton groups which are found in Arctic marine systems; the chlorophytes contain Chl-b alongside Lut and Zea, type 1 prasinophytes contain both Pras and Chl-b, and type 2 prasinophytes contain Chl-b with little else (Hill et al., 2005). The ratio of Pras/Chl-b for this cluster was 0.33, which is within the range found in type 1 prasinophytes cultures (Schlüter and Møhlenberg, 2003). There was no Lutein to indicate the presence of chlorophytes, but there were trace levels of zeaxanthin, which can be found in type 2 prasinophytes. Based on the pigment profile of this cluster, it likely contains a mix of type 1 and 2 prasinophytes. Spatially these samples were distributed in the middle and upper water column of the under-ice stations in the middle of the northern ice transect. These stations were characterized by a unique water column structure; a strong cold halocline layer was present to depths of 80 m. The salinity structure of these stations differed from the other northern under-ice stations which had a thin, fresh, surface-water layer above warm saline Atlantic waters.

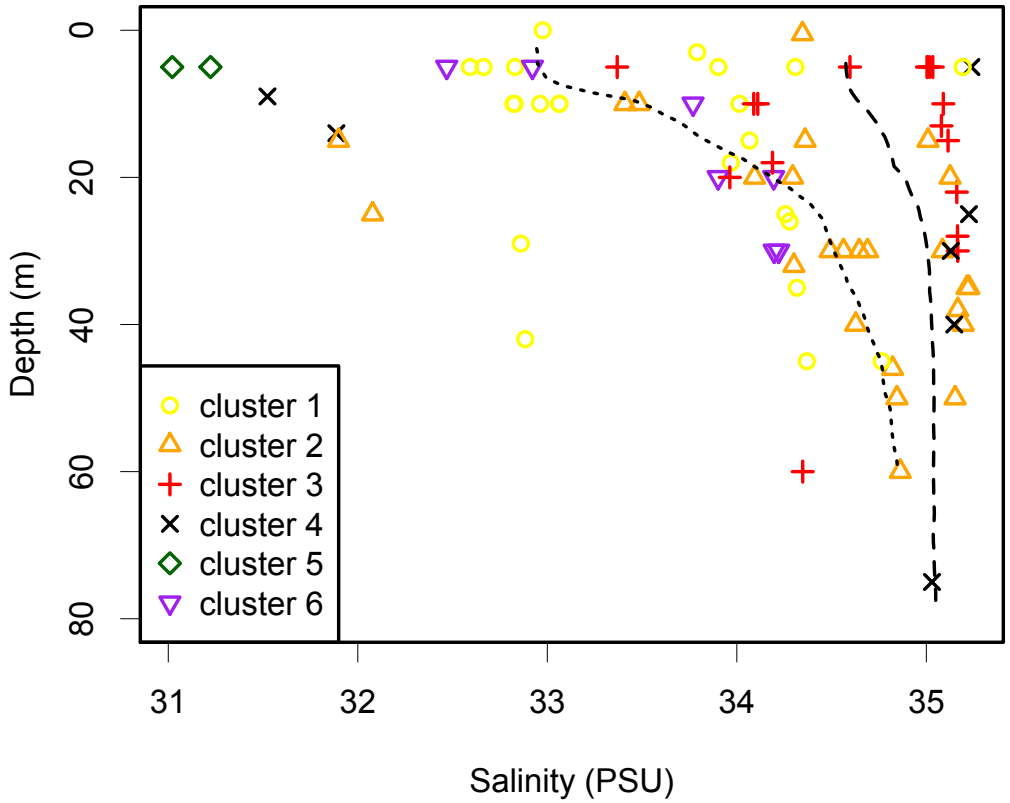

Figure 2.13: Pigment clusters distributed by depth and salinity. Average salinity profiles are shown for open (dashed) and sea-ice (dotted) stations. Lower salinity values in the near surface are due to the increasing influence of sea-ice melt and are strongly correlated with the strength of stratification.

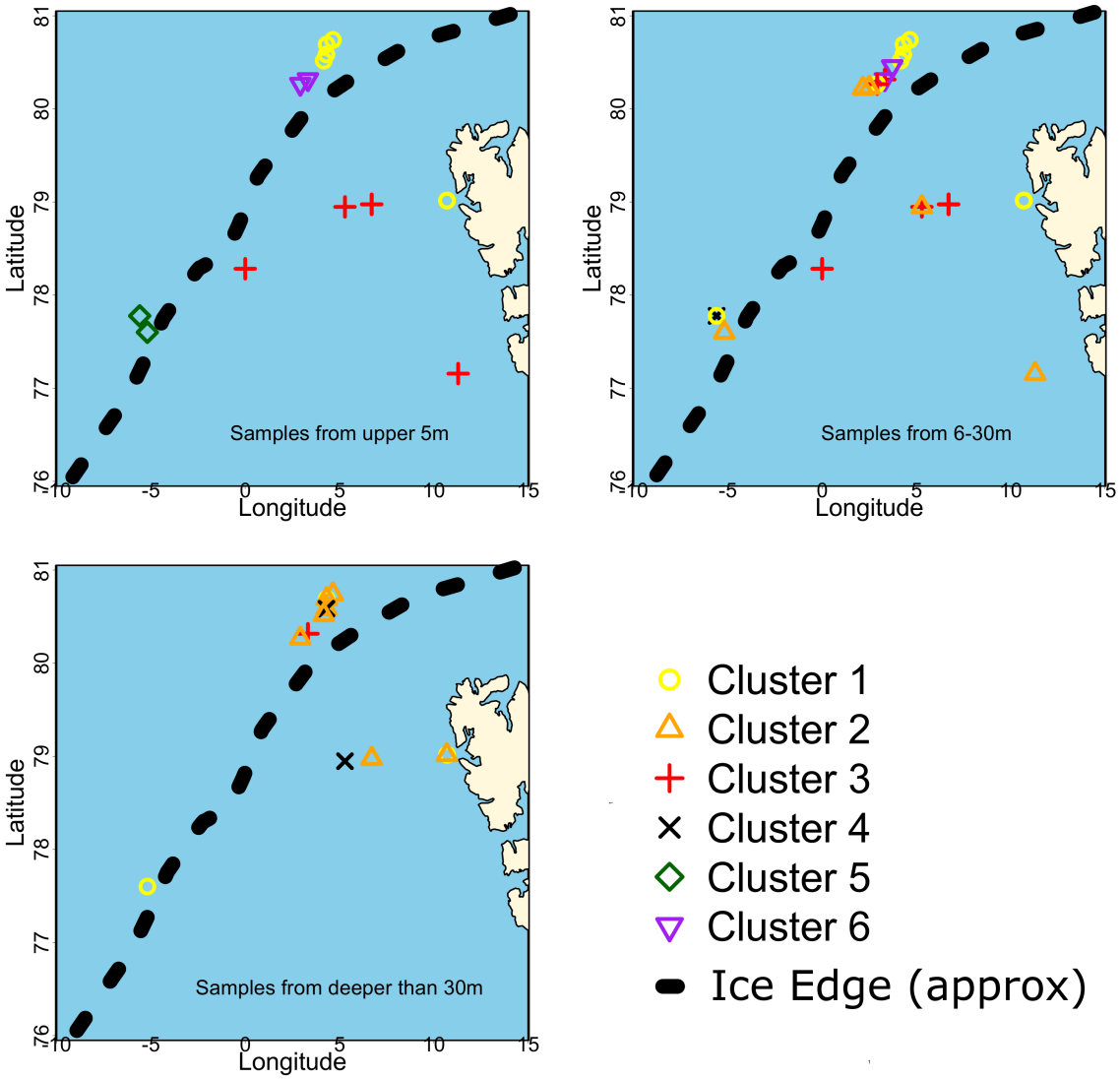

Figure 2.14: Geographic distribution of phytoplankton pigment clusters. Samples are separated into three subgroups based on depth: (A) surface samples from 5 m or less, (B) samples from intermediate depths (6-30 m), and (C) samples from >30 m.

2.3.4 CHEMTAX: successive iterations and pigment ratios

The cluster analysis highlighted regional differences in the distribution of phytoplankton groups with depth and proximity to sea ice. For a more quantitative assessment of the relative contribution of individual phytoplankton groups to phytoplankton pigment biomass, CHEMTAX analysis was used.

To achieve reasonable estimates of phytoplankton community structure, seed values should fall within 25 % of the output pigment ratios (Mackey et al., 1996). To check this, CHEMTAX was run in an iterative mode (Latasa, 2007). Multiple initial seed matrices were also used to estimate the effect of varying seed values on CHEMTAX estimates. A convergence of pigment ratios from differing initial seed matrices (figure 2.15) provides evidence that the initial seed matrix used is appropriate for the study area. The final pigment ratios (figure 2.16) were reduced relative to seed values for most pigments. A significant difference between the pigment ratios was observed between deep and shallow subsets in some accessory pigments and phytoplankton groups. This difference suggests that CHEMTAX is capturing photo-acclimatory changes in photosynthetic pigment composition with depth. Although the analysis was terminated after ten iterations, little change in the pigment ratios occurred after the sixth iteration.

2.3.5 CHEMTAX: comparison to microscopy taxonomy estimates

Since CHEMTAX biomass estimates are expressed as a chlorophyll-a concentration per group, and microscopy biomass estimates in carbon, natural variation in the C:Chl-a ratio of phytoplankton will result in some discrepancies between the two methods. Arctic phytoplankton C:Chl-a ratios (χ) can vary from around 10 to over 250, with

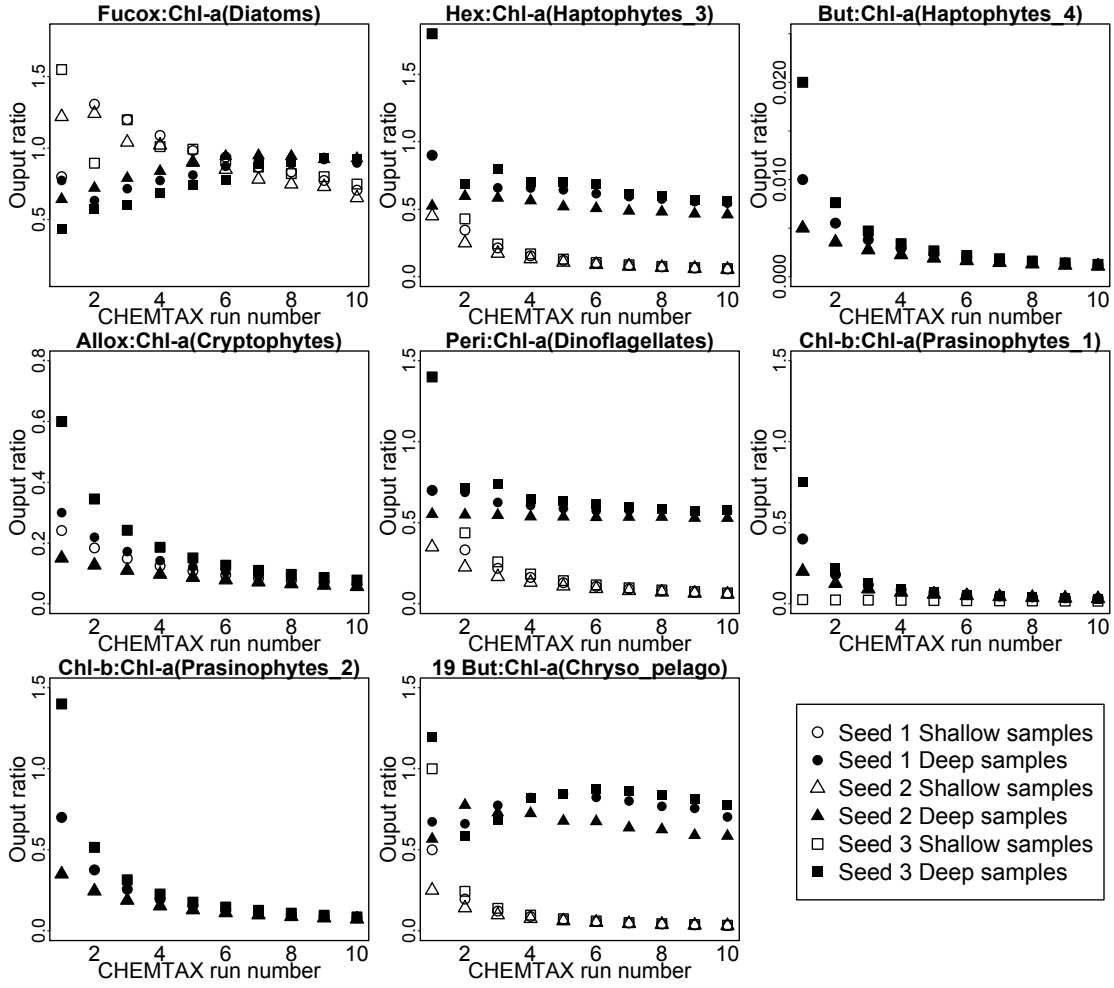

Figure 2.15: Plots of selected pigment ratios through successive iterations of CHEMTAX for major pigments in various phytoplankton groups. Deep and shallow subgroups are distinguished. The three seed matrices are those shown in table 2.3.

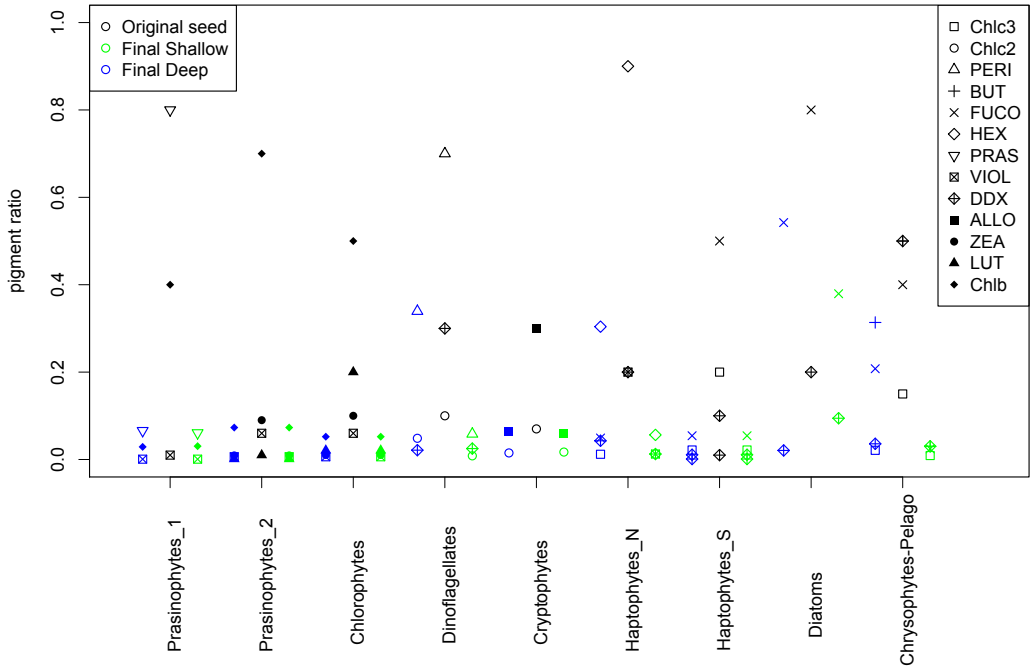

Figure 2.16: Initial and final pigment ratios for chemo-taxonomic groups following CHEMTAX analysis. The initial ratios are shown in black, with the final ratio for the deep subset shown to the left (in blue) and for the shallow subset to the right (in green).

average values around 65 (Booth and Jr., 1997), where lower values are associated with higher growth irradiance (Stein and MacDonald, 2004).

A strong, positive correlation (r^2=0.86, p-val < 0.001) is observed between the CHEMTAX and microscope estimates of haptophyte biomass. The slope of the linear regression gives a χ of 51, which is physiologically reasonable. Initial estimates of diatom biomass using microscopy and HPLC methods are weakly correlated (r^2=0.2, p-val < 0.05) and resulted in low values of χ (45). Four samples were identified diatom-dominated by CHEMTAX, whereas microscopy counts yielded low estimates of diatom biomass. Three of the four samples are from a single station (5, 10 and 18 m at station

GM) and if one excludes this station as anomalous then the r^2 increases to 0.52 (p-val $<$ 0.001) and χ increases to 92. The cryptophytes also show a poor correlation (r^2=0.18, p-val $<$ 0.05) between the two biomass estimates. A reason for this discrepancy may be the presence of *Mesodinium rubrum*, a photosynthetic ciliate which contains the carotenoid alloxanthin (Parsons and Blackbourn, 1968). The microscopy cell counts provide data on *Mesodinium rubrum* carbon biomass and when the *Mesodinium rubrum* and cryptophyte biomass estimates are summed and compared to the CHEMTAX cryptophyte estimate the r^2 increases to 0.29 (p-val $<$ 0.05). There is no apparent correlation between the two biomass estimates for dinoflagellates. This result is not surprising as there is no correlation (r^2=0.01, p-val $>$ 0.3) between the microscopy dinoflagellate biomass estimates and the HPLC peridinin measurements. Some high latitude dinoflagellates from the genera $Gymnodinium$, $Gyrodinium$ and $Peridinium$ contain fucoxanthin and its derivatives instead of peridinin (Roy et al., 1996). Cell count data show the presence of $Gymnodinium$ and $Gyrodinium$ species, but these were not included in the microscope carbon comparison estimates as they were classified as heterotrophic. A shortcoming of the comparison of pigment- and cell-based estimates of phytoplankton biomass is that enumeration of picoplankton cells was undertaken by analytical flow cytometry which cannot discriminate between most phytoplankton groups. Given the large diversity within this size class (Not et al., 2009), using microscope-based cell counts to infer the taxonomic structure of the entire phytoplankton community can lead to significant errors, especially in oligotrophic waters where small cells dominate.

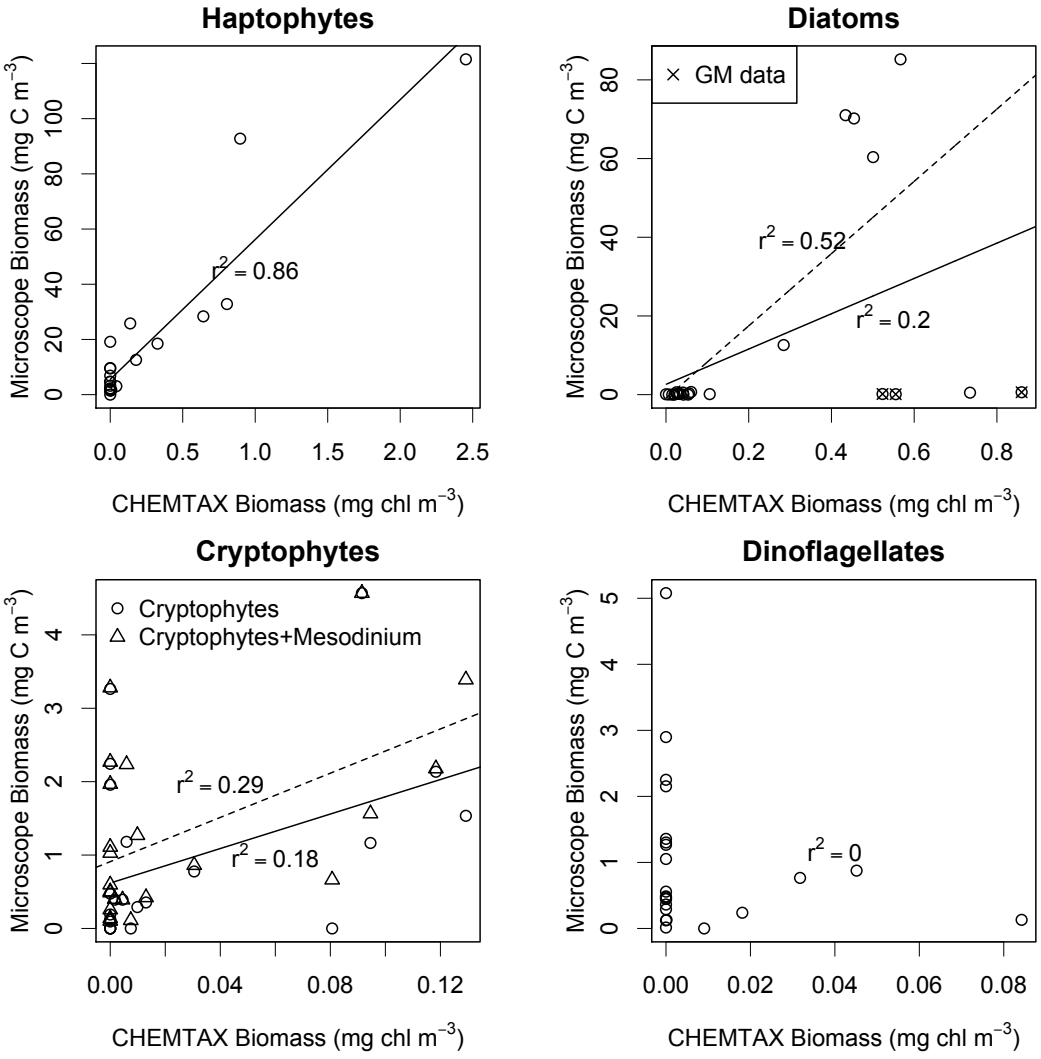

Figure 2.17: Comparison of the biomass estimates from CHEMTAX and microscopic methods. Solid lines show linear regression through data. Anomalous Greenwich Meridian (GM) data highlighted for diatoms. Dashed lines show linear regression after correction for anomalous station (diatoms) or *Mesodinium rubrum* presence (Cryptophytes).

2.3.6 CHEMTAX: distribution of microalgal classes

If one defines a mixed population as a sample in which no single phytoplankton group contributes more than 50 % of the biomass, then just over a third of the samples were classified as mixed using CHEMTAX (table 2.7). The mixed assemblages were unevenly distributed between surface and deep samples. Just over 29 % of the deep samples were dominated by a single group, whereas 78 % of surface samples had dominant groups.

As expected from the ubiquity of fucoxanthin within the field samples, diatoms were present throughout the water column at nearly all stations (figure 2.19). On average, diatoms contributed around 40 % of total biomass when present (figure 2.18), and when they dominated ($>$ 50 % of biomass), it was often in surface waters. Geographically, the samples dominated by diatoms were from waters around the sea-ice waters on the Greenland Shelf and the open-ocean waters of the North Greenland Sea.

According to CHEMTAX, type 3 haptophytes were the next most significant group contributing to phytoplankton biomass. The haptophytes were more common in open-ocean waters than under-ice waters and their contribution to biomass peaked in the near surface and at around 20-30 m. When present, type 3 haptophytes constituted 35 % of the biomass on average.

Cryptophytes and type 2 prasinophytes were equally important, with both groups being significant contributors to total pigment biomass ($>$25 %). Prasinophytes were more prevalent in shallow samples and only dominated assemblages near the sea surface. When present, prasinophytes had a very high average biomass contribution, close to 54 %. The prasinophytes were also the only group, other than diatoms, to account

for 100 % of the pigment biomass according to the CHEMTAX output. Prasinophytes were almost exclusively seen in ice-influenced stations (IS6, IS7, GS and GM). The mean contribution from the cryptophytes was around 27 % of biomass and they most often constituted $< 20\%$ of total biomass. Cryptophytes were prevalent in both open-ocean and under-ice waters. They were present throughout the water column and were especially dominant in a number of near surface samples beneath sea ice.

Chrysophytes were significant in 16 % of samples and were a common but minor (<20 %) contributor to biomass (figure 2.18). Chrysophytes were never observed in samples shallower than 10 m and were only detected above the MLD at a single station. Dinoflagellates appear to be another ubiquitous group, and although being a minor-contributor to total biomass in many of the samples, these cells did dominate a small number of samples. Unlike prasinophytes, dinoflagellates were observed to dominate deeper in the water column; some of the highest fractions of dinoflagellates were observed close to the euphotic depth in ice-covered stations (IS7 and GS). Chlorophytes and type 4 haptophytes were only present in a small number of samples and were insignificant in terms of regional biomass.

The CHEMTAX results show a diverse and complex distribution of phytoplankton groups in the study region. To understand the relationship between the observed biological variability and the physical environment, Principle Component Analysis (PCA) was performed on the six major CHEMTAX group biomass contributions and biologically-relevant physio-chemical variables (figure 2.20).

The PCA showed a correlation between the three major macronutrients (silicate, phosphate, bio-available nitrogen) and these were anti-correlated to irradiance, highlighting the depletion of nutrients in illuminated surface waters. The distribution of diatoms

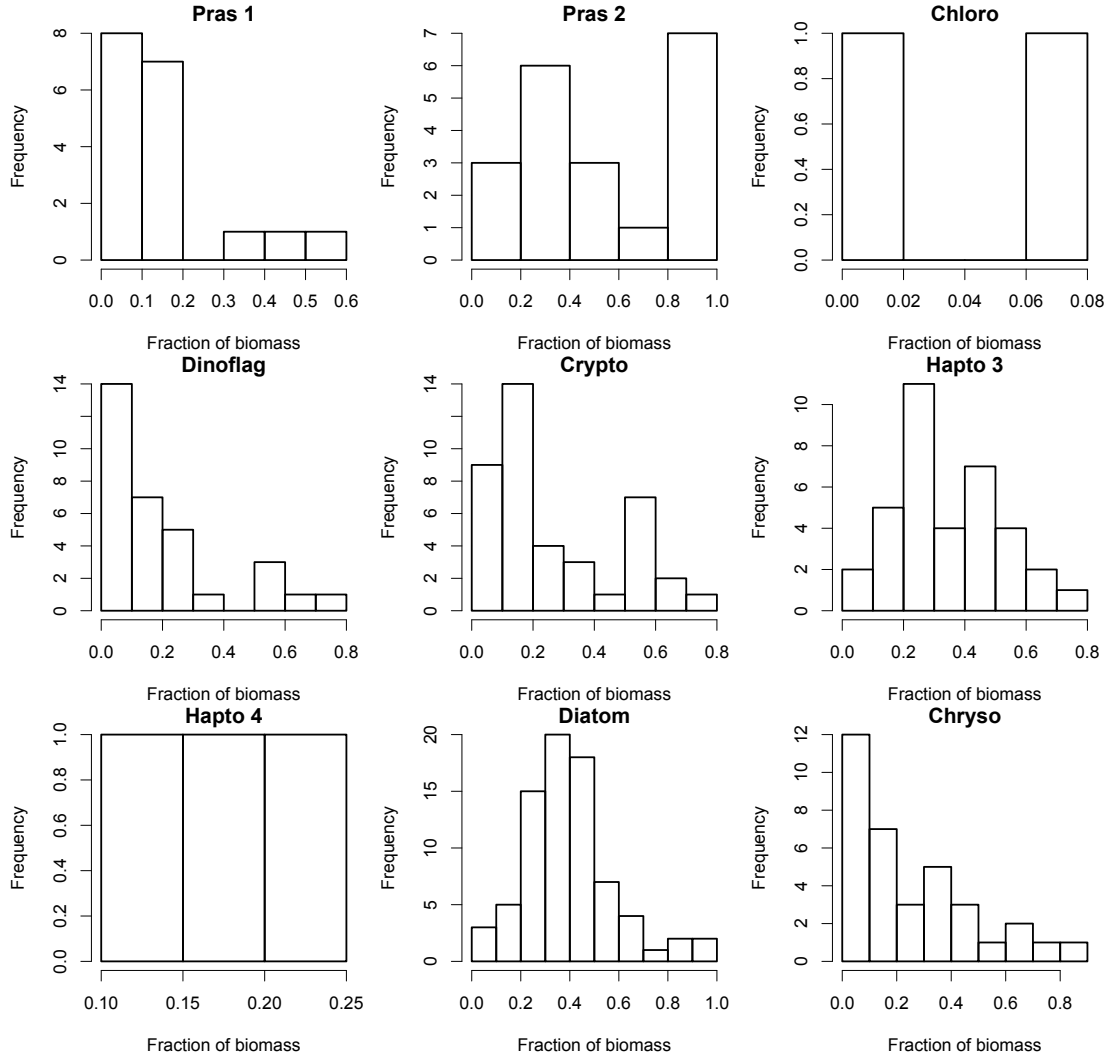

Figure 2.18: Histogram of the fraction of biomass assigned to each algal group. Only samples where the group are classified as contributing >1 % of the population were included in each histogram.

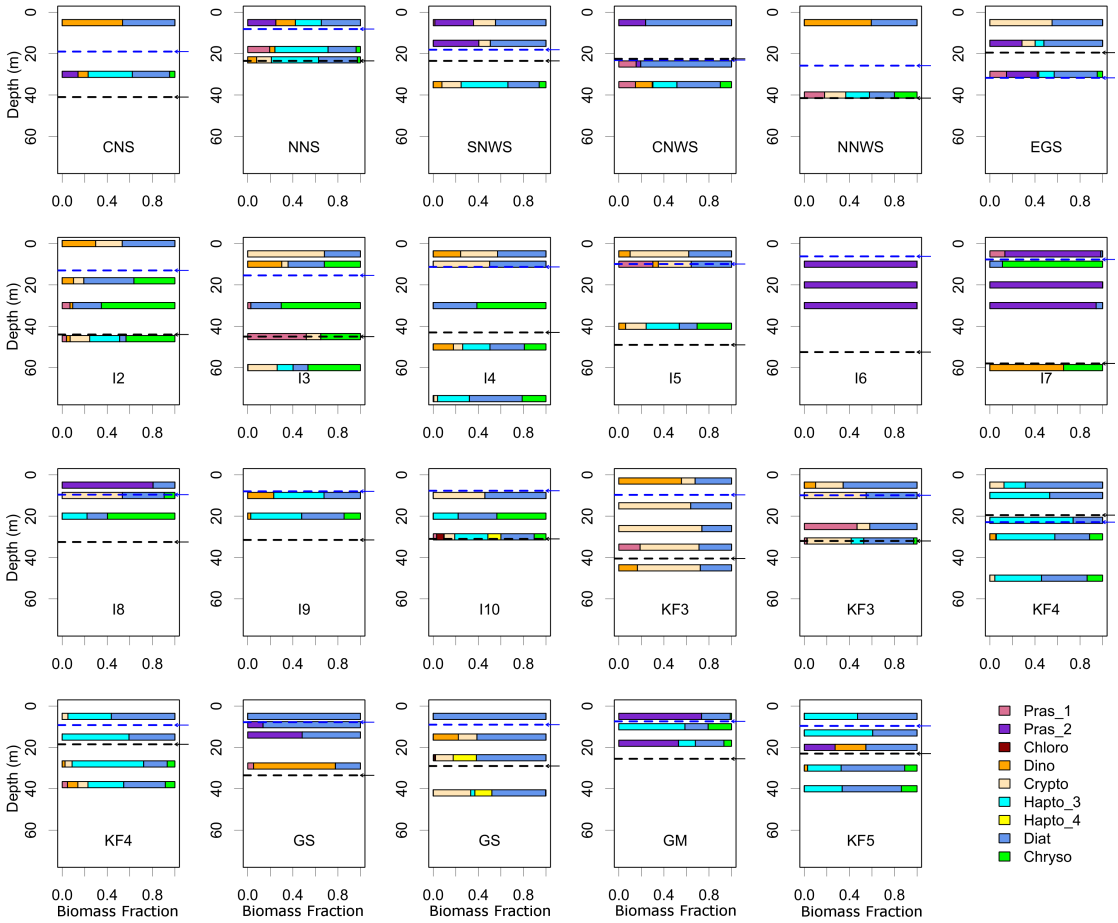

Figure 2.19: Phytoplankton groups as identified by CHEMTAX for each cruise station. Mixed layer and euphotic depth shown as in fig 2.10.

Table 2.7: Summary of CHEMTAX biomass assignment to algal groups. The total number of samples analysed was 83, split into 24 deep and 59 shallow samples. For each taxonomic group the number of samples in which they were significant (>25 % biomass) and dominant (>50 % biomass) are shown. The maximum % is the highest biomass contribution in any sample. Mean % and standard deviation (sd) were calculated from samples where the group are classified as contributing >1 % of the population.

CHEMTAX	Samples >25 % (and 50 %) Biomass			Max % of	mean %	sd
Group	All samples	Deep	Shallow	community		
Prasino 1	3(1)	1(1)	2(0)	52	15.2	14.7
Prasino 2	15(9)	1(0)	14(9)	100	53.7	34.2
Chloro	0(0)	0(0)	0(0)	62.7	37.7	35.4
Dinoflag	8(5)	1(1)	7(4)	72.7	19.7	20.2
Crypto	16(10)	4(1)	12(9)	73.8	26.8	20.4
Hapto 3	23(7)	14(2)	9(5)	73.9	34.3	17.3
Hapto 4	0(0)	0(0)	0(0)	20.6	15.8	4.6
Diatom	63(16)	16(2)	47(14)	100	39.8	19.1
Chryso	13(5)	5(0)	8(5)	88.8	25.4	22.8

was weakly correlated with water temperature or salinity as their vectors are almost orthogonal, but was strongly positively correlated with irradiance and negatively correlated with macronutrient concentrations. The cryptophyte fraction is also positively correlated with irradiance and is negatively correlated with ammonium concentration.

The population fraction of type 3 haptophytes correlates well with the MLD and salinity, which is anti-correlated with the stratification index. The depth at which haptophytes were most abundant was close to the mixed layer depth seen at the open ocean stations and they clearly prefer well-mixed, open waters.

By contrast, the type 2 prasinophytes dominated in the coolest waters, showing little correlation with irradiance or nitrate, but there appears to be some correlation between prasinophytes and phosphate. The N:P ratios from all the samples dominated by

prasinophytes were below the Redfield ratio, reaching N:P values as low as 6.2. The stations where prasinophytes dominated throughout the water column were the same stations possessing a cold halocline layer. The chrysophytes showed a strong correlation with nutrients explaining why they are predominantly found at 15-25 m, similar to the nutricline depths.

Table 2.8: Summary statistics for the principle component analysis of the CHEMTAX groups and environmental variables. Correlating variables are those who have a correlation coefficient magnitude greater than 0.6 (positive or negative) with the principle component.

Principle component	Eigenvalue	Proportion Explained	Cumulative	Correlating Variables
PC1	3.649	0.243	0.243	salinity, strat ind, NO_3+NO_2, SiO_4
PC2	2.781	0.185	0.429	temperature, PO_4
PC3	1.748	0.117	0.545	NH_4
PC4	1.422	0.095	0.640	Crypto
PC5	1.309	0.087	0.727	Diatom
PC6	1.240	0.083	0.810	Pras2, Dino
PC7	0.835	0.056	0.866	Chryso
PC8	0.511	0.034	0.900	
PC9	0.473	0.032	0.931	
PC10	0.358	0.024	0.955	
PC11	0.293	0.020	0.975	
PC12	0.166	0.011	0.986	
PC13	0.103	0.007	0.993	
PC14	0.086	0.006	0.998	
PC15	0.025	0.006	1.000	

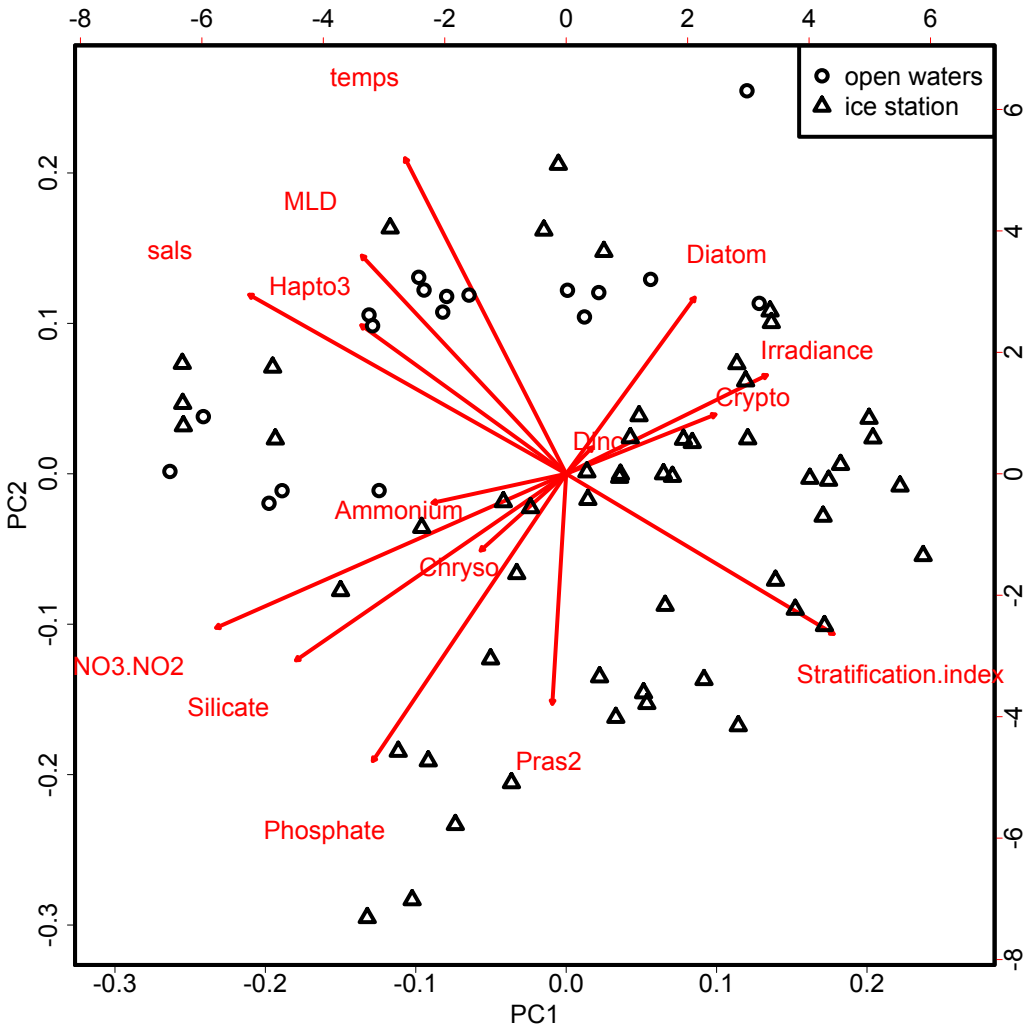

Figure 2.20: Ordination plot of the CHEMTAX phytoplankton group fractions and biologically relevant physical forcing factors. Samples are depicted for sea-ice and open-ocean stations. Only the six phytoplankton groups that were significant contributors to biomass were included.

2.4 Discussion

2.4.1 The use of pigment analysis for phytoplankton taxonomy in the Arctic

To understand how phytoplankton taxonomic distribution and physiology respond to environmental forcing in the Arctic requires a robust and consistent method for estimating group-specific biomass from routine sampling. Recent investigations in the Arctic have used microscopic taxonomic analysis (Ardyna et al., 2011), size fractionation (Gosselin et al., 1997), and pigment-based size classes (Huot et al., 2013) to identify phytoplankton groups. Yet to relate diagnostic pigments to phytoplankton taxa requires a careful comparison of both pigment and microscopy field data (Coupel et al., 2012). In this study the comparison between microscopy and CHEMTAX estimates of group-specific biomass provides encouraging results. For haptophytes and diatoms, which constitute the majority of the biomass in the region, there is good agreement between the two biomass estimates, apart from one anomalous station (Figure 2.17). Any comparison of chlorophyll-a (CHEMTAX) and carbon (microscopy) biomass estimates will include innate discrepancies due to variations in χ, which is known to differ between species and under changing growth conditions (Falkowski and Raven, 1997; Vidussi et al., 2004). Although microscopy data allowed validation of CHEMTAX using an independent dataset, it alone does not provide a complete picture of the phytoplankton composition. Conventional microscopy techniques often do not account for the smallest cells (Roy et al., 1996), whereas pigment-based approaches account for the biomass of the entire community simultaneously without the need for assumptions about carbon-biovolume relationships (Mackey and Higgins, 2001).

Photoacclimation of natural assemblages may lead to variations in pigment ratios as cells adjust their pigment complement to the prevailing light conditions (Moore et al., 2006). By using euphotic depth to account for changes in the attenuation of light between sampling stations, CHEMTAX was able to capture the variation caused by photoacclimation (figure 2.15). The ratio between euphotic depth, Z_{eu}, and MLD has been a useful predictor of photoacclimation (Kozlowski et al., 2011) in the natural environment. For most stations in the study area $Z_{eu} >$ MLD, which suggests that phytoplankton populations are contained within well-lit waters, leading to cells within the surface ocean acclimating to high light conditions (Kozlowski et al., 2011). The shallow mixed-layer depths observed in this study resulted in strong vertical changes in photoacclimation, as evidenced by the increase in the light-harvesting pigment ratios in samples from near the base of the photic zone (figure 2.9). Therefore by binning samples by light environment allowed us to account in part for the strong vertical changes in photoacclimation present in the Arctic, especially below sea ice where even summer surface irradiance can be low (Tremblay et al., 2006).

This study also supports the work of Latasa (2007), which shows that CHEMTAX should be run iteratively, even in cases where additional information on the taxonomy of the phytoplankton populations is available to assign initial pigment ratios. Figure 2.15 shows that the change in pigment ratios after the first CHEMTAX iteration is insufficient to reach a stable output. It is also important to note that the iteration process is not currently automated within the CHEMTAX MATLAB subroutine and needs to be done manually by the user (Latasa, 2007).

The agreement between the CHEMTAX and cluster analysis methods means that cluster analysis could be used to highlight the essential groups to be considered during the

construction of a CHEMTAX seed matrix. The clusters identified from the pigment data can be directly associated with the dominant taxonomic groups identified using CHEMTAX analysis (Figure 2.21). These results suggest that cluster analysis can be used to aid in the construction and refinement of CHEMTAX input matrices, alongside evaluation of pigment ratios from culture studies (Schlüter and Møhlenberg, 2003). The CHEMTAX analysis then allows a greater level of insight into the diversity and distribution of phytoplankton groups across the region than the cluster analysis, especially for stations aggregated into a 'mixed' cluster.

The estimation of the contribution of phytoplankton groups such as dinoflagellates, cryptophytes and chrysophytes to total phytoplankton biomass requires further work, as there is a disparity between the microscope and pigment estimates that cannot be explained by changes in χ or the presence of small cells which are not included in conventional microscope counts. There are eight samples for which microscopy methods estimated a dinoflagellate biomass > 1 mg C m^{-2} and CHEMTAX was unable to detect any dinoflagellate biomass. Some of the disparity between biomass estimates may be the results of some of these groups only forming a very low and relatively constant fraction of the total pigment biomass compared to diatoms and haptophytes. The highest cryptophyte biomass estimated by microscopy is < 5 mg C m^{-3}, whereas for diatoms it is > 100 mg C m^{-3}. Low group-specific biomass concentrations can lead to a low signal to noise ratio.

The presence of photosynthetic ciliates in some of the samples also complicates the comparison between cell count and pigment data. *Mesodinium rubrum* cells were present at a number of stations and should be accounted for alongside other autotrophic cells. However *Mesodinium rubrum* cells could not be accounted for using CHEMTAX as de-

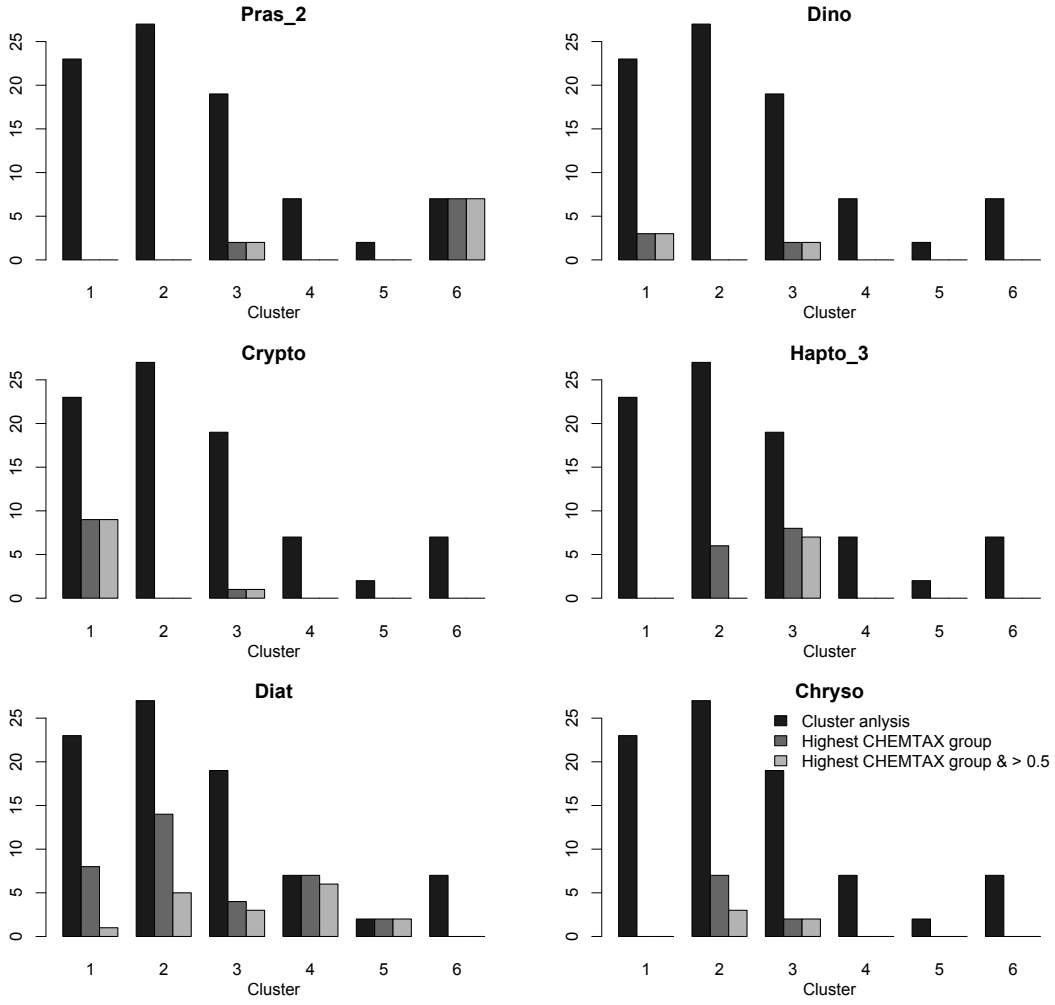

Figure 2.21: A comparison of the CHEMTAX analysis of samples and the cluster analysis. Each plot displays the cluster distribution for all samples compared to distribution of samples for which a group is the largest biomass contributor, according to CHEMTAX. The lightest bars show the distribution of samples for which the group was truly dominant (>50 % biomass rather than simply most abundant).

tailed information on variability in the intracellular pigment composition of this ciliate is lacking. As more pigment data of Arctic assemblages becomes available and our understanding of the intra- and intergroup variation in phytoplankton pigments evolves, large datasets may be revisited to improve composition estimates (Kozlowski et al., 2011).

2.4.2 Phytoplankton variability and distribution

An increase in water column stability results in the creation of a number of ecological niches (Qian et al., 2011). In a stratified water column strong gradients in nutrients, light and temperature are often accompanied by vertical changes in cell abundance, cell pigment content and phytoplankton diversity. Stratified waters are frequently characterized by a subsurface chlorophyll-a maxima, which are well documented in Arctic waters (Martin et al., 2010; Hill and Zimmerman, 2010).

Based on pigment markers, a group-level increase in assemblage diversity with depth was observed across most stations (figures 2.13 and 2.19) with samples more frequently dominated by a single phytoplankton class near the sea surface. Although this trend was not observed in the microscopy data, stations KF4 and GS did show very low species diversity in surface samples (top 25 m). This vertical pattern in community structure is likely due to phytoplankton cells being exposed to greater physical stresses (variable salinity, high UV, low nutrients, low temperature) at the sea surface, promoting the growth of phytoplankton specialized to these extreme environments

Pigment analysis identified six phytoplankton groups as contributing significantly to the regional phytoplankton biomass (table 2.7). Diatoms were ubiquitous and dominated in both low salinity, under-ice surface waters and well-mixed open-ocean waters. The

haptophytes were most abundant at depths of 5-30 m in the open ocean waters, often close to the MLD, and absent in low temperature and low salinity surface waters, especially beneath sea ice. These results are consistent with those of Arrigo and coworkers (Arrigo et al., 1998) in the high latitude waters of the Ross Sea, which found that diatoms dominate in the marginal ice zone and prymnesiophytes dominate in more unstable waters. The agreement between these two high latitude studies suggests that there may be common group-specific physiological differences allowing prymnesiophytes to out-compete other groups in less stratified waters and diatoms to flourish in the ice influenced waters. The observation that diatom dominance negatively correlated with macronutrient concentrations is likely a result of diatom growth rapidly consuming all available macronutrients.

Other taxa are seen to dominate phytoplankton biomass and this must be due to possession of a competitive advantage under a certain set of circumstances. One strategy for out-competing other phytoplankton groups is to utilise a different nutrient. Cryptophytes were negatively correlated with ammonium concentration. This group has been shown to prefer ammonium over nitrate, especially at cold temperatures and under low irradiance (Cloern, 1977; Dortch, 1990; Berg et al., 2003). Ammonium uptake is suppressed under photoinhibition (Muggli and Smith, 1993), meaning it is harder to utilize this nitrogen source in high-light environments. Low irradiance beneath sea ice may allow cryptophytes to increase their ammonium uptake, favouring their growth over other algal groups in nitrate depleted surface waters.

Prasinophytes dominated phytoplankton populations throughout the water column at a select number of stations. These cells were linked with the occurrence of surface waters lying above waters other than warm Atlantic water. This water-column structure

is associated with highly-stratified shallow mixed layers, with limited entrainment of nutrients from depth (Björk, 2002) and hence, favours the presence of small cells with high nutrient uptake efficiencies. These observations fit with our current understanding of *Micromonas* ecophysiology. Both culture and field studies show that these small prasinophytes have a narrow thermal niche and are found to dominate at cold temperatures (Hochachka and Somero, 2002; Lovejoy et al., 2007). Autotrophic dinoflagellates were only detected in small concentrations, possibly due to heterotrophic dinoflagellates being better suited to the oligotrophic, stratified conditions that prevailed during the summer. Microscopy cell count data showed that heterotrophic dinoflagellates were an order of magnitude more abundant than their autotrophic counterparts in a number of samples. Although these cells are not identified by pigment-based methods, they play an important role in the Arctic carbon cycle (Nielsen and Hansen, 1999).

The importance of vertical mixing and nutrient inputs in governing the distribution of phytoplankton communities is well documented for temperate and tropical regions (Margalef, 1978; Cullen et al., 2002). In this polar dataset, stratification also plays a key role in governing the distribution of phytoplankton groups. Yet the distribution shown here differs from that reported for the Canadian high Arctic (Ardyna et al., 2011), where mixing promoted the growth of diatoms and stratification favoured flagellates. In this study, haptophytes and diatoms co-dominated open waters, with haptophytes out-competing diatoms in more mixed waters, away from the ice edge. In stratified, under-ice waters prasinophytes, cryptophytes and diatoms co-dominated.

2.4.3 Implications for a changing climate

Phytoplankton biogeography is believed to be primarily controlled by a combination of bottom-up factors, such as temperature, irradiance and nutrient concentrations (Boyd et al., 2010). In the Arctic, these factors are largely dictated, on a regional scale, by the flow of large water masses and the location of the marginal ice zone. The transition between ice cover and open ocean waters is ecologically significant as it provides a sharp horizontal transition in environmental conditions. Crossing the relatively narrow band of water into ice-influenced waters involves rapid changes in stratification, irradiance and nutrient supply. It has been hypothesised that a warming Arctic may experience increased water column stability, leading to an increased importance of picoplankton (Li et al., 2009). Our results support the view that increased stratification would promote the growth of prasinophytes, but in addition to increased sea-ice melt, the distribution of regional water masses at depth may also be important. The waters dominated by prasinophytes were also those with the lowest contribution from diatoms, which suggests that prasinophyte-dominated waters may represent a distinct ecological niche.

The distribution of water masses, regional stratification and mixing dynamics may dictate the fate of prasinophytes, haptophytes and diatoms. Diatoms were ubiquitous (table 2.7) and it is likely that they will remain a major group in this region as they can dominate assemblages in stratified open and under-ice waters (figure 2.19), allowing them to form large ice-edge blooms that begin beneath the sea ice. The haptophytes were more prevalent in open waters but their fate will be dictated by the competing influences of stratification (both salinity and temperature driven) and wind mixing in an open Arctic Ocean. If stratification increases, due to increased summer melt-water generation,

this group may become a minor contributor to biomass. If a greater period of open water allows more wind mixing then the haptophytes could move north into the Arctic Ocean. Our observations suggest that if a larger region of the Arctic becomes ice-free in summer, there would be a significant decrease in the abundance of cryptophytes and chrysophytes as these groups were much more common beneath sea-ice. A decrease in phytoplankton diversity has been suggested as having direct detrimental effects on both the quantity and predictability of aquatic primary production (Ptacnik et al., 2008).

2.5 Conclusions

The goal of this study was to assess the variability in the community structure of phytoplankton in the Greenland Sea in relation to environmental forcing to provide an insight into drivers of phytoplankton biogeography. A prerequisite to using pigment markers to assess phytoplankton distribution is the validation of CHEMTAX using microscopy-based biomass estimates.

Six major phytoplankton groups were observed to dominate the algal biomass. The diatoms and haptophytes contributed the largest fraction of pigment biomass. Other groups which occasionally dominated the phytoplankton population were cryptophytes, prasinophytes, chrysophytes and dinoflagellates. The distribution of each phytoplankton group appears to be controlled by the structure of the water column and the presence of sea ice, which together control the light and nutrient availability. Correlation between CHEMTAX- and microscope- estimates were poor for both dinoflagellates and cryptophytes due to the presence of peridinin-lacking dinoflagellates and alloxanthin-containing *Mesodinium rubrum*.

Results from this study suggest that the taxonomic structure of phytoplankton communities is strongly influenced by the presence of sea ice, due to its influence on water-column stratification, irradiance and water temperatures. Although this dataset is confined to a given region and season, the distribution patterns reported here are consistent with several other Arctic studies and we can begin to speculate on how a changing Arctic Ocean may lead to shifts in the taxonomic structure of phytoplankton communities. A loss of sea ice may result in a decrease in populations of cryptophytes and chrysophytes, in favour of haptophytes. The fate of prasinophytes is uncertain as ice melt could produce a set of environmental conditions (strongly-stratified, cold surface layer) in which these cells are known to flourish, or an ice-free ocean may lead to increased wind-driven mixing favouring other algal groups. The ubiquity of diatoms across a range of oceanographic conditions in this dataset, suggests that this group could remain an dominant member of Arctic communities.

Chapter 3

Variation in phytoplankton bio-optical and photophysiological properties in the Atlantic Arctic

Abstract: The Arctic is an extreme environment and marine phytoplankton undergo strong acclimation in order to optimise their light-harvesting efficiency and productive potential. Understanding the bio-optical and photophysiological properties of phytoplankton is of key importance to the modelling of marine primary production. Relationships between the parameters of photosynthesis and physical variables that can be remotely-sensed, such as sea-surface temperature, can allow parameter estimation on large spatial scales. During the ICE-CHASER cruise of 2010, photosynthesis-irradiance (P-E) and spectral absorption measurements were taken to allow the estimation of photophysiological and bio-optical properties of marine phytoplankton, alongside local environmental variables in the Norwegian and Greenland Seas. This new data is combined

with data from the wider Atlantic Arctic and the regional variation in measured photophysiological parameters and phytoplankton absorption is considered in relation to environmental variables and community structure. Measurements were also taken on culture samples representing six major Arctic phytoplankton taxonomic groups for comparison with the field observations. Group-specific differences in the spectral shape of phytoplankton absorption were observed in both culture and field measurements. However, the relationship between increasing absorption efficiency with decreasing chlorophyll-a concentration for samples collected in the Atlantic Arctic was found to be invariant across taxa. Group-specific differences in photophysiology were seen in culture experiments but taxa-based variability in the photosynthetic parameters observed in field samples are likely the result of physiological responses to variations in temperature. A strong relationship between maximum photosynthetic rate (P_m^B) and temperature was observed, with values of P_m^B being significantly lower than those predicted using global models. Photosynthesis-irradiance data from this and other studies of the Atlantic Arctic suggest that the magnitude of low-light photosynthetic efficiency (α^B) is largely constrained by low assimilation numbers. Due to the strong control of sea ice on irradiance and water temperature in the Arctic region, changes in sea-ice cover will likely lead to pronounced changes in the photosynthetic efficiency of phytoplankton in the Atlantic sector of the Arctic. This work demonstrates the need to understand the response of phytoplankton physiology to the primary local forcing factors, in addition to global trends and relationships.

3.1 Introduction

Change in the spatial extent of sea ice has been used as an indicator of large-scale climate change (Perovich et al., 2008). Decades of satellite observations show a decrease in sea-ice cover during both summer and winter (Comiso, 2006) across the Arctic Basin (Lindsay et al., 2009). Reinforcing feedbacks and continually rising CO_2 mean the retreat in ice cover is likely to increase in the near future (Maslanik et al., 2007). The summer/autumn of 2012 was the lowest recorded sea-ice extent on record (figure 3.1) and a downward trend in ice cover was seen in all months (Stroeve et al., 2012). September showed the strongest trend and the rate of decline appears to be increasing with time. The latest estimate of decline for September is around 13 % per decade, meaning a loss of over 30 % since 1980. In addition to the reduced areal extent of the sea ice it is also thinning (Kwok, 2007; Maslanik et al., 2007).

Changes in sea-ice dynamics influence the environmental factors (e.g., sea-surface temperature, stratification, and irradiance) controlling phytoplankton primary production (Wassmann et al., 2011). In addition to consistently low water temperatures year round, the variation in the Arctic light environment is also extreme. Solar geometry causes annual transitions from 24-hour darkness to 24-hour daylight. The presence of sea ice and shallow mixed layer depths result in a wide range in irradiance within the surface mixed layer. On short time scales, the underwater light field can undergo rapid changes due to melting or migration of sea ice. Alongside low temperatures and rapid changes in light, Arctic phytoplankton must also overcome strong salinity gradients and large seasonal variations in nutrient concentrations.

Such strong variability in the growth conditions of Arctic phytoplankton is reflected in

the seasonal cycle of marine primary production. An increase in both water-column stability and the light penetration in the surface ocean result in the formation of ice-edge blooms, which follow a retreating sea-ice front (Sakshaug and Slagstad, 1992; Engelsen et al., 2002; Perrette et al., 2011). These blooms begin as soon as the ice thins and can be extensive (Gradinger, 1996; Arrigo et al., 2012). Where perennial ice cover is not present, the North Atlantic experiences a spring bloom as temperature-driven stratification begins to reduce the mixed layer depth (MLD) and the mean light received by phytoplankton in the mixed layer increases (Sverdrup, 1953; Smetacek and Passow, 1990).

In addition to changes in the gross phytoplankton biomass, shifts in phytoplankton community structure also depend upon light history, water-column stability, nutrient availability, and temperature (Coupel et al., 2012). Given that unicellular autotrophs form the base of the pelagic food chain, changes in sea-ice cover and the co-variables it governs may cause a subsequent shift in the structure and function of marine primary producers that will cascade to higher trophic levels(Smetacek and Nicol, 2005).

There are contrasting theories as to how a large-scale reduction in sea ice will affect primary production in the Arctic. As the fraction of open water in the Arctic increases, wind-driven surface mixing will become enhanced, leading to a higher supply of nutrients from depth, and consequently increased productivity (Arrigo et al., 2008; Zhang et al., 2010). A reduction of ice cover will also provide more light in the surface ocean, and may result in a longer growth season. However, this enhancement of light within the surface layer will only hold true if wind-driven mixing does not lead to light limitation. A competing hypothesis is that fresher surface waters, created by the accelerated melting of sea ice and increased fluvial input from thawing tundra, may lead to a stronger buoy-

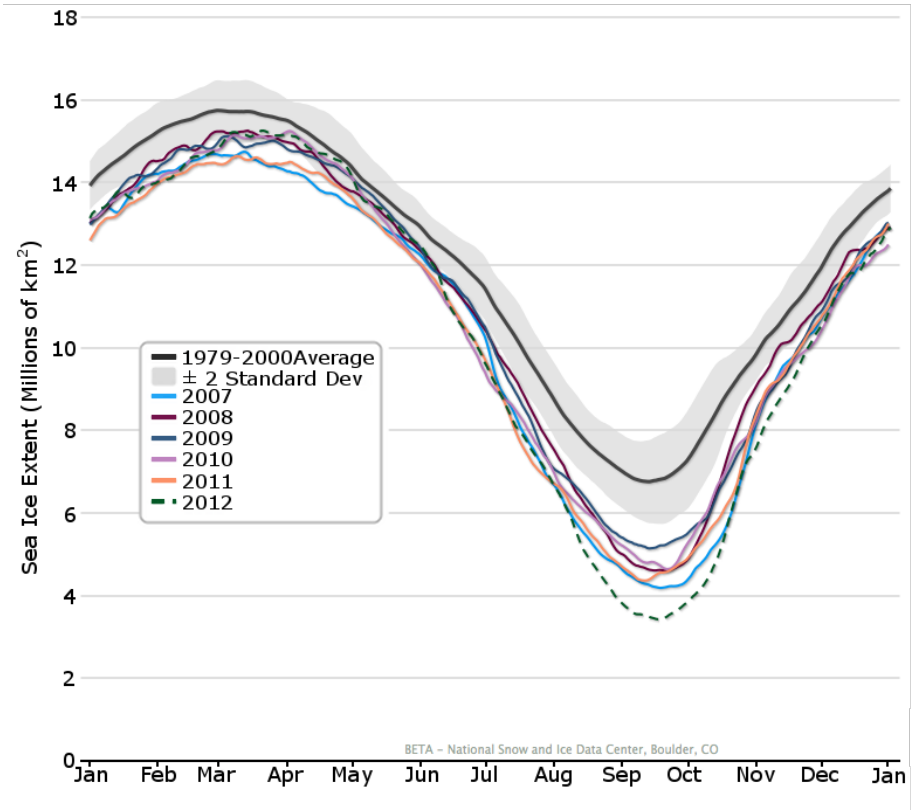

Figure 3.1: Pan-Arctic sea-ice extent over the past six years compared to historical average. Figure created using data and software from the National Snow and Ice Data Centre (NSIDC).

ancy gradient and very shallow surface mixed layers. Increased salinity-driven stratification would limit nutrient fluxes to surface waters and promote the growth of smaller, more nutrient efficient phytoplankton (Li et al., 2009). It is likely that either hypothesis may hold true for different regions (Wassmann and Reigstad, 2011) and changes in primary production will not necessarily correlate with changes in open water in all sectors of the Arctic Basin (Pabi et al., 2008). Unfortunately, a scarcity of data (Wassmann and Reigstad, 2011) means that current estimates of marine primary production in the Arctic Ocean remain uncertain. Moreover, our inability to provide a definitive baseline of marine primary production means that we cannot confidently predict the productivity

potential under a future climate scenario. This view is supported by a recent inter-model round robin comparison of primary production, which found poor agreement between model estimates for the Arctic (Carr et al., 2006).

Primary production depends upon three main factors: (1) the phytoplankton biomass present, (2) the light and nutrient resources available to those phytoplankton, and (3) the efficiency with which the phytoplankton biomass can utilise light energy, which in turn depends on the optical and photophysiological characteristics of the phytoplankton cells. The bio-optical characteristics of phytoplankton can vary spatially and temporally according to the species present, nutrient availability and light history (Cullen and Lewis, 1988; Bidigare et al., 1989; Sakshaug et al., 1997; Huot et al., 2013). Photoacclimation of phytoplankton occurs through a number of mechanisms. These include changes in pigment content, pigment composition, and the number of photosynthetic units per cell (Richardson et al., 1983). These cellular strategies of photoacclimation can influence the spectral absorption efficiency, the optimum irradiance for photosynthesis, the efficiency of light harvesting and ultimately the CO_2 utilization under light limitation of phytoplankton (Platt and Jassby, 1976; Falkowski and Owens, 1980; Richardson et al., 1983; Platt and Sathyendranath, 2002). To model marine primary production in the Arctic using satellite data, it is essential that we fully understand the primary factors governing variability in the bio-optical and photosynthetic characteristics of polar marine phytoplankton. It is also essential to determine whether robust relationships between the photophysiological parameters and environmental variables, especially those accessible by remote sensing, can be established on regional to basin scales. Obtaining such information will improve models of marine primary production for the current Arctic state and aid predictions of change for the future.

In this chapter I will examine the variation in the absorptive and photosynthetic properties of natural phytoplankton assemblages in the Atlantic Arctic and Subarctic (Greenland and Norwegian Seas) and compare them to culture experiments on strains isolated from the Canadian Archipelago with the aim of gaining an understanding of the natural variability and primary forcing factors on phytoplankton photophysiology in this region. If strong relationships to environmental variables are observed then it may be possible to estimate the photophysiology of phytoplankton in this region through the use of a proxy or remotely measured variable. Results of this study show that variability in the photosynthetic parameters is related to environmental conditions, geographical location, and water-column structure. Patterns observed in this dataset are compared to data from Baffin Bay and the Labrador Sea to ascertain if the trends are consistent across the Atlantic Arctic and can be used in remote-sensing algorithms of marine primary production.

3.2 Materials & Methods

3.2.1 Description of the study area and data sources

The Atlantic sector of the Arctic covers a number of sub-regions that experience similar annual cycles in light, nutrients and species succession. The hydrographic region examined in this study encompasses a subset of Longhurst's provinces (Longhurst et al., 1995): ARCT, the Atlantic Arctic Province; SARC, Atlantic Subarctic Province; and a part of BPLR, Boreal Polar Province. The *in situ* photophysiological parameter data are sourced from a series of cruises conducted by the Marine Environment Laboratory

(MEL) at the Bedford Institute of Oceanography (BIO) during the periods 1978 to 1983 and 1996 to 2000, and the 2010 ICE CHASER expedition. Only data north of 55°N were used from the BIO dataset. These datasets provide over 600 sets of photophysiological parameters and environmental co-variables collected from a number of ocean environments (ice edge, under ice, open ocean and coastal regions) as shown in figure 3.2.

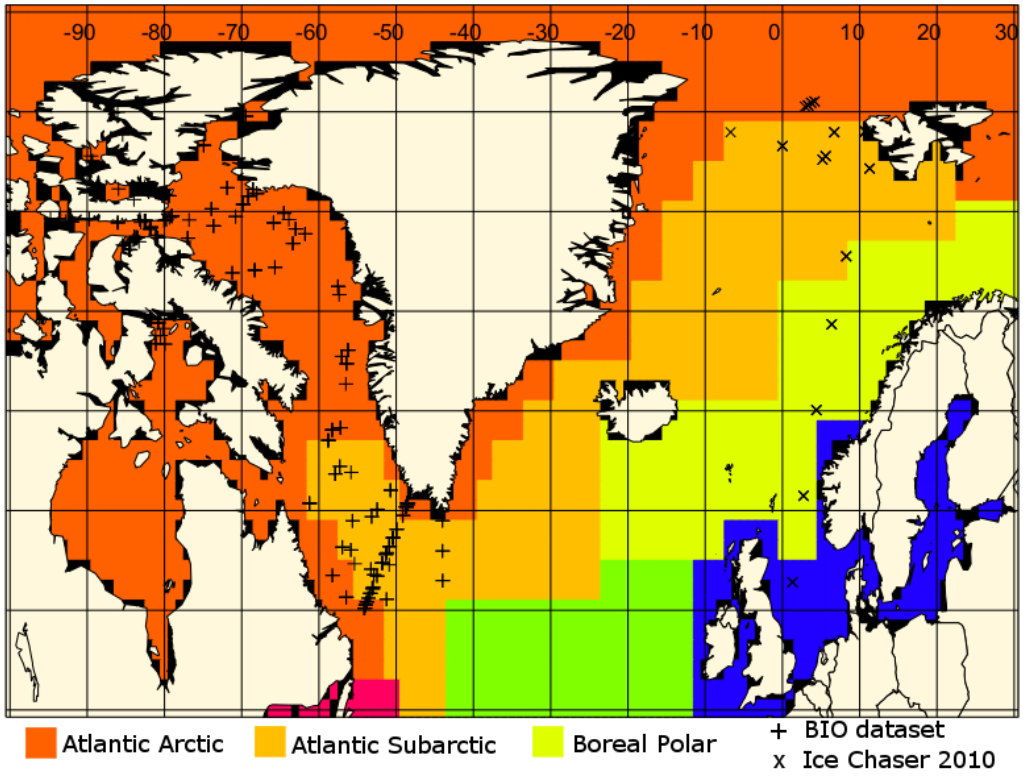

Figure 3.2: The station locations of the combined BIO (+) and ICECHASER 2010 (x) datasets. Background colours show the distribution of Longhurst's provinces at a 1° resolution.

3.2.2 Sampling procedures

The ICE CHASER 2010 (IC2010) cruise took place from the 14th June to the 21st July 2010 aboard the RRS *James Clark Ross*. Seawater samples were collected at 23 stations covering sea-ice, transitional-zone, and open-ocean conditions. Sampling depths were selected based on *in vivo* chlorophyll-a fluorescence profiles to capture the vertical structure in phytoplankton biomass. Seawater samples were collected in 10 litre Niskin bottles and sub-sampled for bio-optical, pigment and photophysiological measurements. Measurements included accessory pigment concentrations, using High Performance Liquid Chromatography (HPLC), fluorometric determination of chlorophyll-a, spectral absorption by phytoplankton cells, and ^{14}C-based photosynthesis-irradiance (P-E) incubations. At each station, profiles of temperature, salinity, and downwelling irradiance were recorded using a Sea-Bird 9plus CTD equipped with two 3P temperature sensors, two 4C conductivity sensors, a dissolved oxygen sensor, a Chelsea fluorometer sensor and a Biospherical Li-Cor PAR sensor. Underway measurements of salinity, sea-surface temperature (SST), air temperature, and fluorescence were taken using an Oceanlogger system and photosynthetically available radiation (PAR) and windspeed were continuously measured using the ships meteorological instruments.

The BIO dataset is a compilation of data from the Canadian Archipelago and the Labrador Sea. The sampling depths, size of Niskin bottles used and suite of measurements taken varied slightly from cruise to cruise. A more detailed description of the data collection procedures for the Canadian Archipelago is provided in Harrison and Platt (1986). The Labrador Sea data is from six cruises which took place from 1996 to 2000 (Sathyendranath et al., 2004). The Canadian Archipelago data provides additional measurements of photophysiology and physical conditions, but not spectral absorption or HPLC pig-

ment markers, whereas the Labrador Sea dataset provides measurements of photophysiology, spectral absorption and concentrations of phytoplankton accessory pigments.

3.2.3 Determination of phytoplankton spectral absorption $a_{ph}(\lambda)$

Seawater samples were filtered onto Whatman 25 mm GF/F filters, flash frozen in liquid nitrogen and stored at -80 °C until analysis. The optical density of total particulates (OD_T) and bleached detritus (OD_d) were determined following the method of Tassan and Ferrari (1995) using sodium hypochlorite (NAClO, 1% active chloride) as a pigment extraction agent. Spectral measurements of optical density were made using a dual-beam Perkin Elmer Lambda 800 spectrophotometer equipped with a spectralon coated integrating sphere. Scans were performed from 750 nm to 350 nm. To estimate the optical density of cells in suspension (OD_s) from samples concentrated onto glass fiber filters (OD_f) requires the application of a β-correction factor (Hoepffner and Sathyendranath, 1992) to account for pathlength amplification by the filter. In this study an empirically-derived β-correction factor was used (Hoepffner and Sathyendranath, 1992):

$$OD_s = 0.31OD_f + 0.57OD_f^2 \tag{3.1}$$

To calculate absorption in suspension (a_s), optical densities were divided by geometric pathlength and multiplied by 2.3 (conversion from decimal to natural logarithm):

$$a_s = 2.3OD_s\frac{S}{V}, \tag{3.2}$$

where S is the absorption cross section area of the filter and V is the volume of filtered seawater. The *in vivo* absorption coefficient of phytoplankton $a_{ph}(\lambda)$ was then calculated by subtracting $a_d(\lambda)$ from $a_T(\lambda)$. The mean absorption value between 735 and 740 nm was used as a baseline and subtracted from the values at all other wavelengths. The rationale for using these wavelengths is that phytoplankton pigments do not absorb in this region of the visible spectrum ((Sathyendranath et al., 1987)).

To compare the relative shapes of phytoplankton absorption spectra, phytoplankton absorption coefficients in the visible range (400 to 750 nm) were normalised to the value at 440 nm, which corresponds to the absorption peak of chlorophyll-a (Cleveland, 1995).

3.2.4 Photophysiological measurements

Photosynthesis-irradiance (P-E) curves were obtained for samples collected at multiple depths at each station using an incubator design similar to that of Tilstone et al. (1999) (see Figure 3.3). For each P-E curve, 14 sub-samples of 60 ml were taken from a Niskin bottle and poured into polycarbonate bottles, inoculated with 200 μl $NaH^{14}CO_3$ stock solution under low light conditions and placed in the linear incubator. We maintained *In situ* temperatures using a circulating water bath and for sub-zero water temperatures, ethylene glycol was added to the water bath to prevent freezing. The bottles were subjected to a light gradient with intensities ranging from 0 (dark bottle) to $\approx$ 1500 μE m^{-2} s^{-1}. Light measurements were taken before and after each experiment at each bottle position using a Li-Cor Biospherical PAR sensor. After an incubation time of 90-120 minutes, samples were filtered onto Whatman 25 mm GF/F filters, under a vacuum of $<$200 mm Hg. Filters were placed in a desiccator with fuming acid to drive off adsorbed

carbon from the filter or cells. Scintillation cocktail was added to fumed filters and disintegrations per minute (DPM) were determined using a shipboard liquid scintillation counter (Tri-Carb 3100, Perkin Elmer, Shelton, USA). For each set of incubations, 20 μl of stock solution were pipetted into vials with scintillation cocktail (4 ml) and carbosorb (1 ml) to estimate the total activity added to the sample bottles.

Biomass-normalised primary production (P^B) was calculated for each bottle with corrections for alkalinity, dark radiocarbon uptake and isotopic discrimination;

$$P^B = \frac{1.05(DPM_{light} - DPM_{dark})TIC}{N(DPM_{add})Chl}, \tag{3.3}$$

where DPM_{light} is the count in a given light bottle, DPM_{dark} is the count in the dark bottle, TIC is the total inorganic carbon, 1.05 is the isotope discrimination factor, DPM_{add} is the amount of radiocarbon added, N is the duration of the incubation in hours and Chl is the chlorophyll concentration in mg m^{-3}.

P-E curves were then fitted with the equation of Platt et al. (1980)

$$P^B = P_s^B(1 - exp(\frac{-\alpha^B I}{P_s^B}))exp(\frac{-\beta^B I}{P_s^B}), \tag{3.4}$$

where P_s^B is the maximum photosynthetic rate in the absence of photoinhibition, α^B is the initial slope and β^B is the photoinhibition parameter. The biomass-normalised maximum photosynthetic rate P_m^B was derived using the following equation:

$$P_m^B = P_s^B(\frac{\alpha^B}{\alpha^B + \beta^B})(\frac{\beta^B}{\alpha^B + \beta^B})^{\frac{\beta}{\alpha}}. \tag{3.5}$$

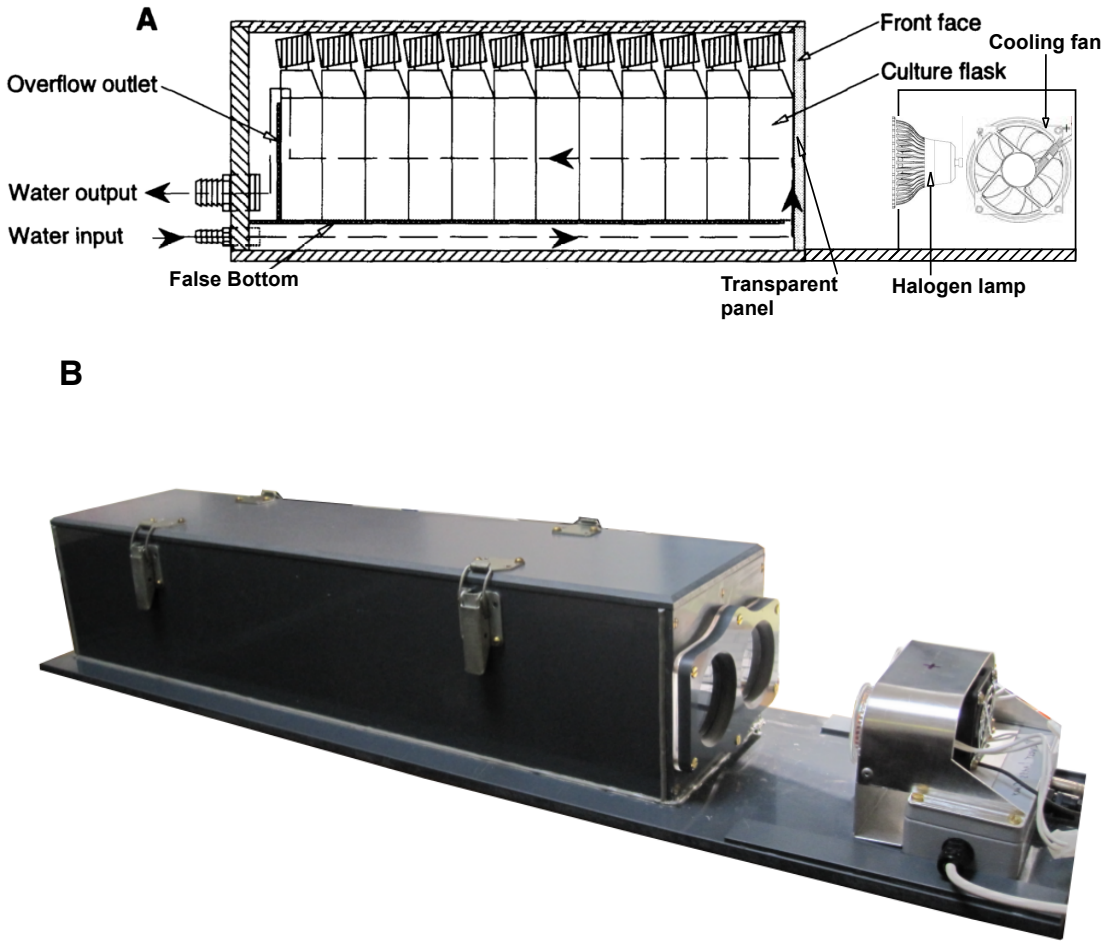

Figure 3.3: A schematic diagram (A) and image (B) of the P-E incubator set up used in this study. The diagram is adapted from (Babin et al., 1994). Water-column temperatures were maintained using a circulating water bath.

Values of α^B retrieved from the incubations are biased due to the emission spectra of the light source (Stuart et al., 2000), and therefore were corrected using the phytoplankton absorption spectrum for each sample (Kyewalyanga et al., 1997). The correction is performed by multiplying each α^B value by a factor X, derived from the unweighted mean absorption spectra ($\bar{a}_p$) and the weighted mean absorption spectra ($\bar{a}_T$) of the phytoplankton,

$$X = \frac{\bar{a}_p}{\bar{a}_T}, \tag{3.6}$$

and,

$$\bar{a}_p = \frac{\int_{400}^{700} a_p(\lambda)}{\int_{400}^{700}} d\lambda, \tag{3.7}$$

$$\bar{a}_T = \frac{\int_{400}^{700} a_p(\lambda) I_T(\lambda)}{\int_{400}^{700} I_T(\lambda)} d\lambda, \tag{3.8}$$

where $I_T(\lambda)$ is the spectral irradiance from the tungsten halogen light source.

The photoadaptation parameter (E_k) is a measure of the irradiance to which the phytoplankton population is acclimated and is the projection of α^B to its intersection with P_m^B:

$$E_k = P_m^B / \alpha^B \tag{3.9}$$

Measurements of phytoplankton absorption were used to determine the maximum quan-

tum yield (ϕ_m) of photosynthesis. According to the equation of Tilzer et al. (1985) ϕ_m is calculated as;

$$\phi_m = \frac{0.0231\alpha^B}{\bar{a}_{ph}}, \tag{3.10}$$

where $\bar{a}_{ph}$ is the mean spectral absorption coefficient of phytoplankton in the range of 400-700 nm, and 0.0231 is used to convert mgC h^{-1} to μmol C s^{-1}.

3.2.5 Determination of phytoplankton pigment concentrations

Fluorometric chlorophyll-a measurements were made in triplicate using the Holm-Hansen et al. (1965) method after filtering 100 ml of seawater onto 25 mm GF/F filters. Samples were immediately placed in 90 % acetone under dark conditions maintained at -20 °C for 24 hours. Measurements were taken using a Turner Designs Trilogy fluorometer.

Samples for HPLC pigment analysis were also filtered onto GF/F filters, flash frozen in liquid nitrogen and stored at -80 °C until analysis. Filter volumes varied between 200 and 1000 ml depending upon the level of biomass in the water sample, with high biomass samples requiring a lower filtration volume. Pigments were quantified using reverse-phase HPLC after sonication and centrifugation to separate the pigments into solution. The solvent, mobile phase mix and elution times are covered in the paper of Barlow et al. (1997).

3.2.6 Pigment-based determination of phytoplankton community structure

To compare the bio-optical and photophysiological properties of different phytoplankton groups, a method was required to ascertain the taxonomy of samples. This was done using CHEMTAX analysis of HPLC pigment data, as covered in section 2.2.4. A sample was classified as being dominated by a particular group if it contributed > 50 % of the total chlorophyll-a biomass as determined by CHEMTAX.

3.2.7 Culture experiments using Arctic strains

Six Arctic phytoplankton cultures were sourced from the National Center for Marine Algae and Microbiota (NCMA), Bigelow Laboratory, Maine. Details of the strains and growth media are shown in table 2.2 in section 2.2.4. The strains were selected to cover the range of phylogenetic groups encountered in the Atlantic Arctic. Incubation temperatures were varied from 2.5 to 7.5 °C and phytoplankton were acclimated over two growth cycles prior to maximum growth rate determination. Cell concentrations were measured using a Beckman coulter counter at 1-3 day intervals. During the exponential growth, phase counts were made daily and the growth rates (μ) were calculated from the daily change in cell counts. Coulter counter cell counts were checked against haemocytometer measurements and this method was found to perform slightly better than the spectrophotometric method of Lovejoy et al. (2007) which utilizes optical density at 750 nm (see Figure 3.4). Given the accuracy and precision of cell counts using the coulter counter method, especially at low cell densities, these data were used to derive growth rates.

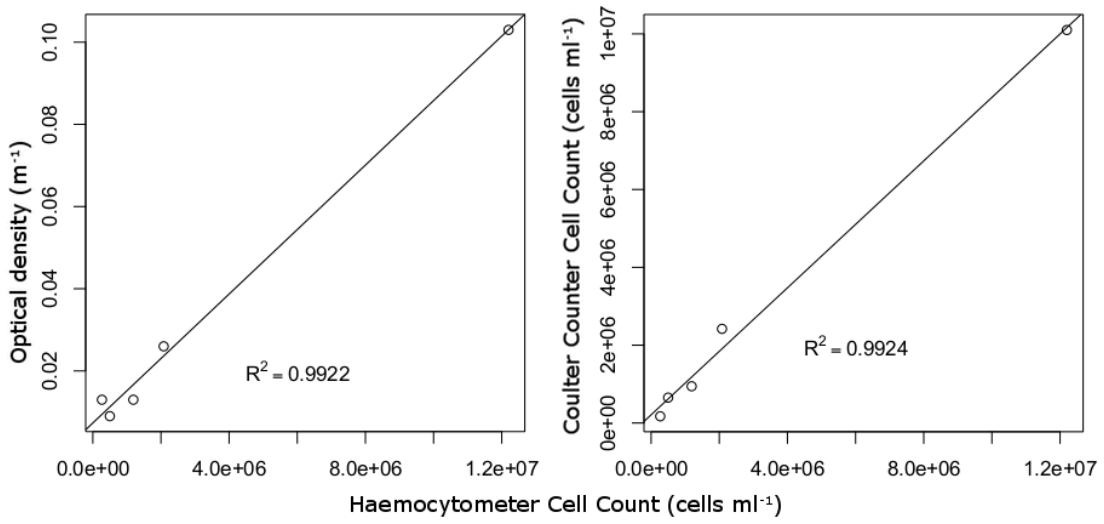

Figure 3.4: A comparison of cell count estimates for prasinophyte cultures from coulter counter and optical density measurements against haemocytometer counts. Correlation is slightly better for coulter counter data, especially at low cell densities.

Samples for phytoplankton absorption coefficient, HPLC and fluorometric pigment concentration and cell carbon measurements were taken during the exponential growth phase when cell counts reached a cell density threshold sufficient to allow organic carbon measurements. The threshold was different for each species; for example, the threshold for *Micromonas* was 3,000,000 cells ml^{-1}, for the *Cylindrotheca* it was 40,000 cells ml^{-1}. Carbon content measurements were made by electrolytic titration using a Coulomat 702 Analyser.

Variation of culture P_m^B between groups and with temperature was estimated by combining the μ and C:Chl (χ) data, as covered by Saux-Picart et al. (2012):

$$P_m^B = \chi\mu\frac{1}{\Delta t}. \tag{3.11}$$

Alternatively, if we wish to account for respiration we can re-arrange the empirical

equation of Cloern et al. (1995):

$$\mu = 0.85 \times P^B(\frac{1}{\chi}) - 0.015, \tag{3.12}$$

to give

$$P^B = (\mu + 0.015) \times \frac{\chi}{0.85} \times \frac{1}{\Delta t}, \tag{3.13}$$

where Δt is the time increment over which growth has occurred.

3.3 Results

3.3.1 Absorption spectra and absorption efficiencies

Group-specific variation in the spectral shape of absorption

The mean absorption spectra for field samples dominated by each of the six major phytoplankton groups detected are shown in figure 3.5. The normalised absorption spectra for cultured Arctic taxa are shown for comparison in figure 3.6. Though the field sample spectra do not show as striking differences in their spectral shape when compared to the cultures, similarities can be seen between culture and field spectra for samples representing prasinophytes, dinoflagellates, prymnesiophytes, and diatoms.

Variability in the spectral absorption shape for the dominant phytoplankton groups is greatest within the 460-500 nm and 560-610 nm wavebands. The group-specific absorption spectra from the field samples show three main features within the 400-550

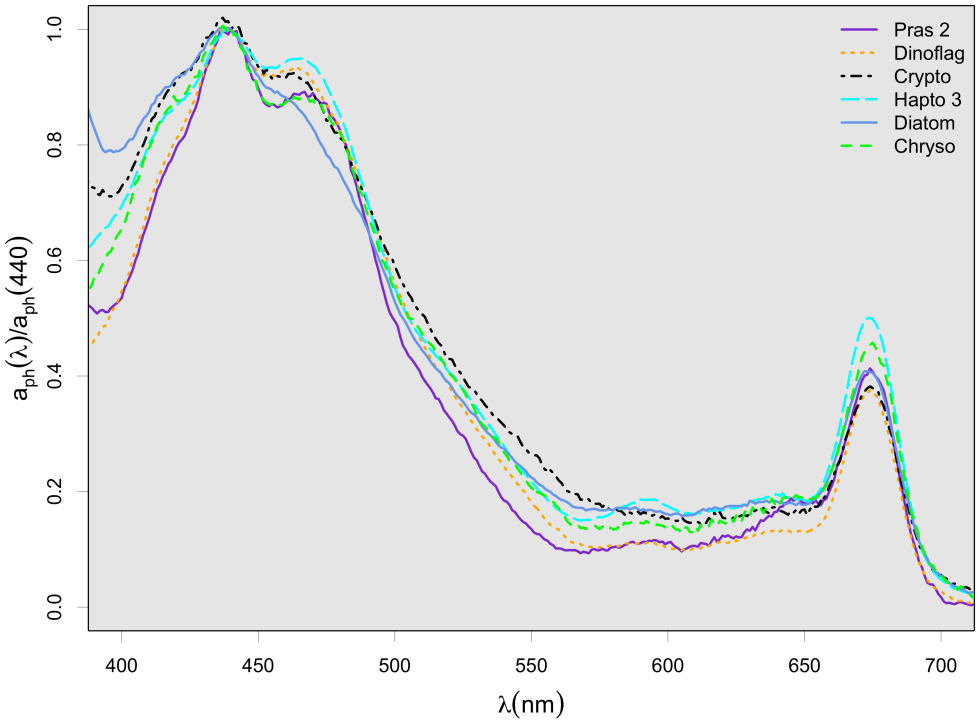

Figure 3.5: Average absorption spectra for field samples dominated by phytoplankton groups from IC2010 data. Means for each group were calculated from samples that were estimated to have $>$ 50 % of biomass being contributed by a particular class according to CHEMTAX analysis. Spectra were normalised to $a_{ph}(440)$ prior to averaging.

nm region: a chl-a absorption peak centred around 440 nm, a narrow peak around 465 nm and a shoulder of a broad peak in the range of 510 to 550 nm. These features led to variability in the spectral gradient from 465 to 550 nm, with diatoms having the shallowest gradient, followed (in increasing order) by cryptophytes, chrysophytes, haptophytes, dinoflagellates and prasinophytes.

Group-specific mean spectra also show variation in absorption ratios between absorption maxima and minima; the a_{ph}(490):(555) ratio was significantly different for the prasinophytes but remarkably similar for the diatoms, haptophytes and chrysophytes (Table 3.1). The difference between diatoms and prasinophytes was not as significant for the ratio between chlorophyll absorption peaks, a_{ph}(443):(676). The largest differ-

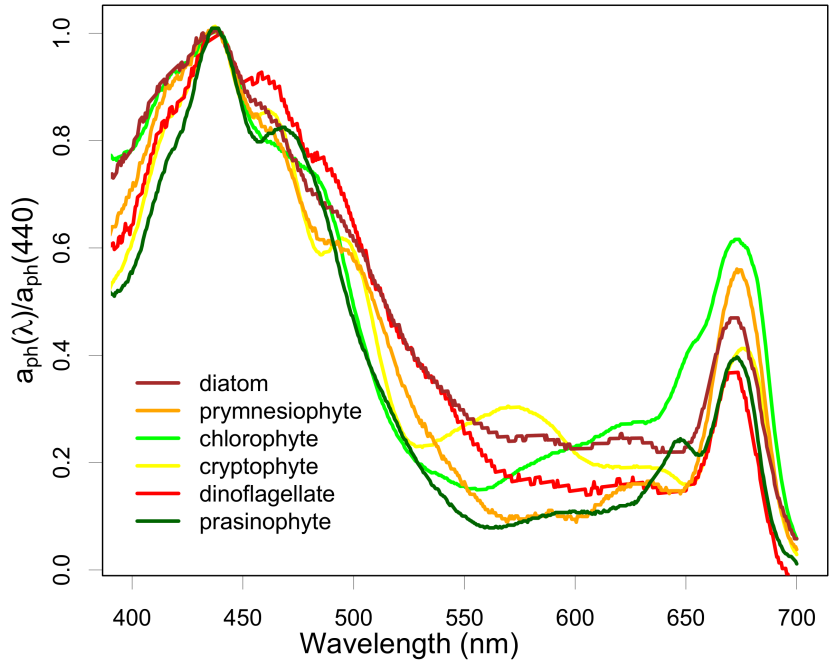

Figure 3.6: Culture species absorption spectra normalised to absorption at 440 nm. As for figure 3.5 spectra were normalised prior to averaging.

ence in a_{ph}(443):(676) ratios was between cryptophytes and haptophytes.

Absorption efficiency

The chl-a-specific absorption coefficient of marine phytoplankton at 443 nm (a^B_{ph}(443)) for the IC2010 cruise ranged from 0.026 to 0.105 m^2 mgChl-a^{-1} with the highest values observed at low chl-a concentrations (see Figure 3.7). The range of specific absorption coefficients is smaller than that observed in the Labrador Sea data (<0.008 to 0.126 m^2 mgChl-a^{-1}). However, the IC2010 data lie close to the lower limit of the Labrador Sea absorption efficiencies at low chl-a concentrations (< 0.3 mgChl m^{-3}), especially for samples from mixed phytoplankton communities.

No significant difference in the relationship between specific absorption coefficient and

Table 3.1: Group-specific mean absorption coefficients from field samples collected from the IC2010 expedition. Group identification was performed by CHEMTAX pigment analysis.

	Pras(10)		Dino(1)		Crypto(7)		Hapto(6)		Diatom(10)		Chryso(4)	
	mean	sd	mean	sd	mean	sd	mean	sd	mean	sd	mean	sd
$a_{ph}^{B}(443)$	0.063	0.026	0.066	NA	0.066	0.016	0.035	0.0055	0.051	0.021	0.074	0.019
$a_{ph}^{B}(676)$	0.026	0.0078	0.026	NA	0.025	0.0028	0.018	0.0022	0.021	0.0043	0.034	0.0085
$a_{ph}(490):(555)$	5.59	1.49	4.61	NA	3.17	0.88	3.81	0.656	3.81	1.58	3.81	1.52
$a_{ph}(443):(550)$	7.33	1.88	6.07	NA	4.1	1.23	4.75	0.743	5.21	1.87	5.39	2.75
$a_{ph}(443):(676)$	2.45	0.672	2.55	NA	2.66	0.426	2.02	0.0974	2.48	0.675	2.22	0.174

chlorophyll-a concentration was found between the phytoplankton groups. Haptophyte-dominated samples possess a much lower mean $a_{ph}^{B}(443)$ but this is a consequence of haptophyte samples being from waters with higher chlorophyll-a concentrations.

The relationship between chlorophyll-a concentration and absorption has been described by a number of linear and non-linear equations (Prieur and Sathyendranath, 1981; Lutz et al., 1996; Bricaud et al., 1998; Sathyendranath et al., 2004). The IC2010 data is compared to the global equation of Prieur and Sathyendranath (1981), the equation of Bricaud et al. (1998) for case-I waters and the regional (Northwest Atlantic) equations of Sathyendranath et al. (2004) in figure 3.8.

A majority of the IC2010 data lies below the global equation of Prieur and Sathyendranath (1981) with points falling between the curves of Sathyendranath et al. (2004) which describe the relationship between chlorophyll and phytoplankton light absorption at 440 nm for both diatom-dominated and mixed population samples. The IC2010 samples dominated by diatoms were not systematically closer to the Atlantic diatom equation, probably owing to the large range in cell sizes observed within the diatom

group over the sampling period. Mean species cell volumes within the diatoms identified ranged from 20.1 μm^3 (*Pseudo-Nitzchia delicatissima*) to >47,000 μm^3 (*Coscinodiscus sp.*). The global equation given by Bricaud et al. (1998) is a better fit to the IC2010 data than that of Prieur and Sathyendranath (1981) but is still too high at low chlorophyll-a concentrations. A two-part linear equation was fitted to the IC2010 data, whose coefficients are shown in equation 3.14:

$$a_{ph}(440) = \begin{cases} 0.005 + 0.043\mathrm{B} & \mathrm{B} \leq 1 \\ 0.026 + 0.022\mathrm{B} & \mathrm{B} > 1. \end{cases} \tag{3.14}$$

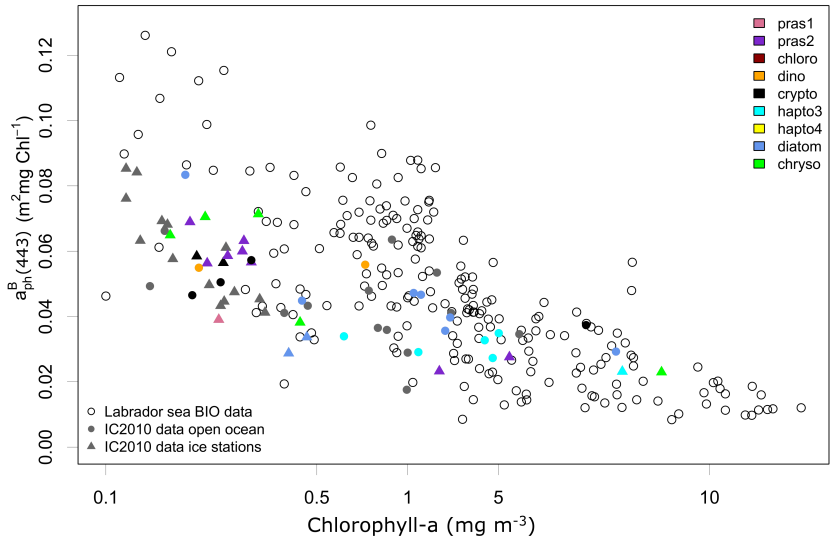

Figure 3.7: Biomass-normalized absorption coefficient for marine phytoplankton at 443 nm for the IC2010 samples. Also shown are data from the Labrador Sea (BIO dataset). Grey points show IC2010 data that were classified as mixed (i.e not dominated by a single phytoplankton group according to pigment analysis). Points are marked differently for IC2010 samples that were from ice-covered and open-ocean stations.

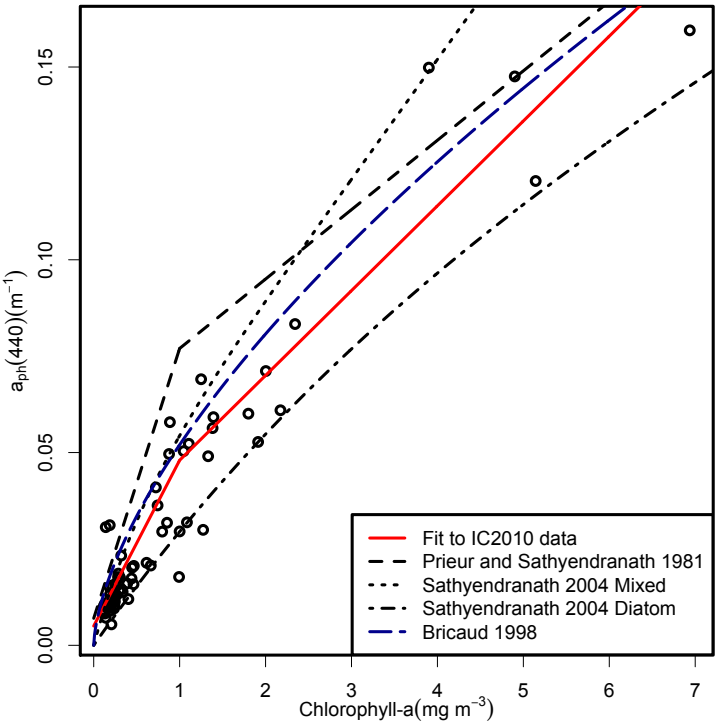

Figure 3.8: Absorption coefficients for marine phytoplankton plotted against chlorophyll-a concentration for the IC2010 cruise. Best fit of two-part linear equation to IC2010 data is shown along with equations used in the studies of Prieur and Sathyendranath (1981), Bricaud et al. (1998), and Sathyendranath et al.(2004).

3.3.2 Variation in photophysiological parameters

P_m^B values for IC2010 varied from 0.54 to 12.27 mg C (mg chl-a)$^{-1}$ h^{-1}, which is well within the range of values reported by Sakshaug and Slagstad (1991) for polar phytoplankton (0.1-15 mg C (mg chl-a)$^{-1}$ h^{-1}). The IC2010 data also shows good agreement with the BIO dataset (0.1-12.84 mg C (mg chl-a)$^{-1}$ h^{-1}), see figure 3.9(A). The dependence of α^B and E_k on the emission spectra of the light source utilized for the P-E incubation makes it difficult to directly compare these parameter values from multiple datasets (Sakshaug and Slagstad, 1991; Huot et al., 2013). Both the IC2010

and BIO incubations used a tungsten halogen light source, but the light source for the range of values cited by Sakshaug and Slagstad (1991) is unknown. Values of α^B from IC2010 samples varied between 0.009 and 0.069 mg C (mg chl-a)$^{-1}$ h^{-1} (μ mol quanta m^{-2} s^{-1})$^{-1}$ and were also in agreement with values reported by Sakshaug and Slagstad (1991))(0.001-1 mg C (mg chl-a)$^{-1}$ h^{-1} (μ mol quanta m^{-2} s^{-1})$^{-1}$) and were of similar magnitudes to the BIO data (0.0039-0.56 mg C (mg chl-a)$^{-1}$ h^{-1} (μ mol quanta m^{-2} s^{-1})$^{-1}$), see figure 3.9(B). The IC2010 E_k values were between 22 and 261 μ mol quanta m^{-2} s^{-1} with most values in the range of 20-150, which is in good agreement with the 30-200 μ mol m^{-2} s^{-1} given by Sakshaug and Slagstad (1991) for polar waters and those reported for the Labrador Sea (Stuart et al., 2000). The BIO dataset showed a range of 2-299 μ mol m^{-2} s^{-1} for E_k with most values between 5 and 185 μ mol m^{-2} s^{-1} with a skewed distribution towards lower values, see figure 3.9(C).

Having established that the IC2010 values are consistent with other high-latitude studies, the relationship between photophysiological parameters and phytoplankton taxonomic composition and environmental variables is examined. Using the same assignment of samples to taxonomic groups as for absorption, the group-specific variation in photophysiological parameters was assessed (table 3.2, figure 3.10).

The mean P-E parameters differ between the various phytoplankton groups, especially E_k and ϕ_m (Welch t-test p-val ≤ 0.05). Diatoms have the highest P_m^B and E$_k$ values, while prasinophytes and chrysophytes have low values of P_m^B. The standard deviations highlight the overlap in the photophysiology between groups as the phytoplankton acclimate to local forcing factors. To ascertain if the observed group-specific differences are taxonomic or a response to changes in temperature we used the growth rates, carbon:chlorophyll-a and irradiance data from the algal cultures (equations 3.12 and

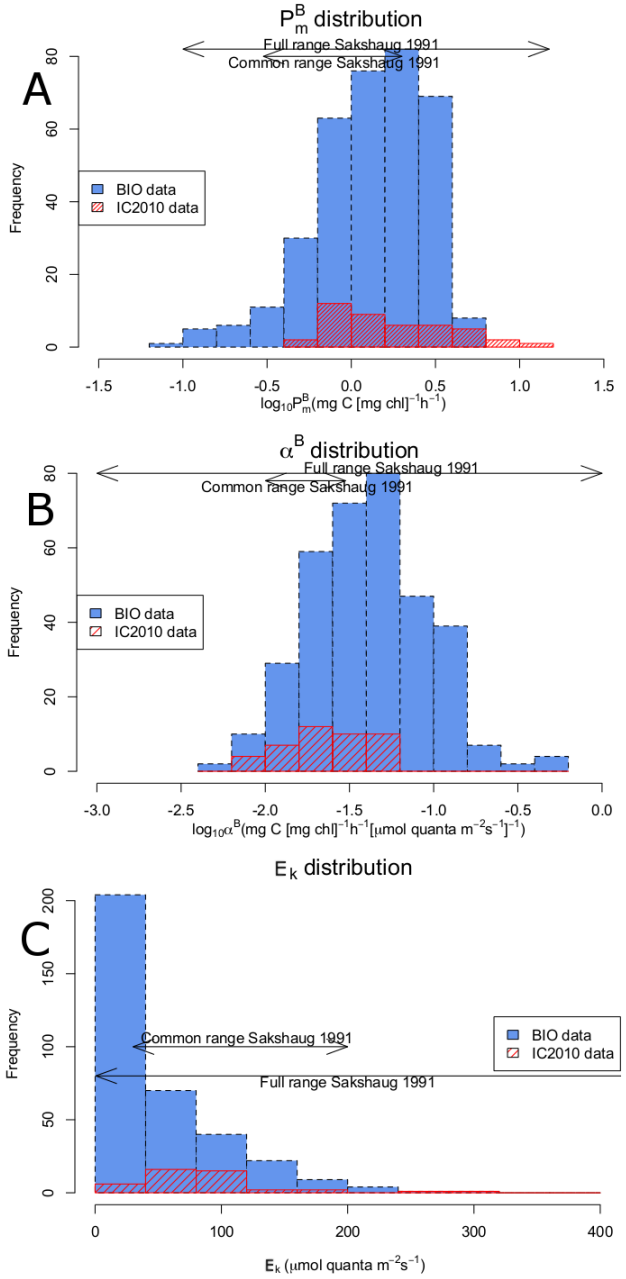

Figure 3.9: Ranges of measured P_m^B (A), α^B (B), and E_k (C) for samples collected during the IC2010 cruise. Also shown are ranges from the BIO dataset and the review of polar phytoplankton photophysiology by Sakshaug and Slagstad (1991). Note that some of the BIO data is included in the pan-Arctic review of Sakshaug and Slagstad (1991).

Table 3.2: Group-specific mean photophysiological parameters for samples collected during the IC2010 cruise. The number of samples contributing data to the average value for each group is shown in parentheses. The minimum p value for a Welch t-test between any two groups is shown for each parameter.

	Pras(10)		Dino(1)		Crypto(7)		Hapto(6)		Diatom(10)		Chryso(1)		t-test
	mean	sd	mean	sd	mean	sd	mean	sd	mean	sd	mean	sd	min p
α^B	0.0170	0.0060	0.0384	NA	0.0206	0.0149	0.0312	0.0118	0.0275	0.0148	0.0228	NA	0.10
P_m^B	0.988	0.178	3.20	NA	2.18	1.62	1.19	0.116	3.88	4.45	0.746	NA	0.08
E_k	63.5	19.7	83.4	NA	110	31.4	40.6	9.74	124	106	32.7	NA	0.05
ϕ_m	0.0251	0.0192	0.0392	NA	0.0259	0.0274	0.0577	0.0144	0.0433	0.0296	0.0190	NA	<0.01

3.13), to calculate the maximum photosynthetic rate, as direct measurements of P_m^B from ^{14}C incubation experiments were not available.

Estimates of P_m^B for the Arctic cultures ranged from 1.5 to 6.0 mg C (mg chl-a)$^{-1}$ h^{-1} depending on species, temperature, and equation used to estimate P_m^B (see table 3.3). Group-specific differences are apparent with assimilation numbers varying by a factor of three between taxa at 7 °C (see table 3.3). The culture data also clearly illustrates the influence of temperature on P_m^B through changes in both growth rates and χ. The response in μ to incubation temperature varied between the different phytoplankton groups (Figure 3.11) but each species showed a consistent response between culture replicates. For *Micromonas*, μ increased with increasing temperature, which is consistent with the work of Lovejoy et al. (2007), although the values of μ measured here are slightly higher. For example the μ was 0.55 at 6 °C in the Lovejoy (2007) study and 0.73 for this study. The elevated μ observed in this study may be due to a longer period of illumination than that of the work by Lovejoy et al. (2007), although differences in growth media (F/2 vs K) or acclimation times between the studies cannot be ruled

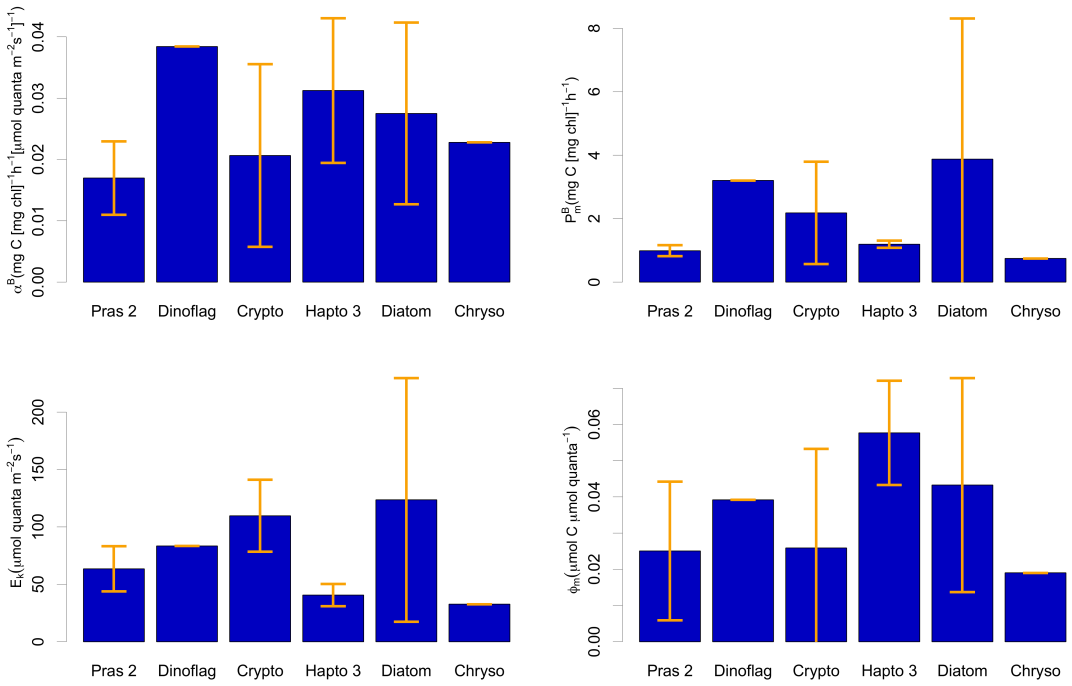

Figure 3.10: Average photophysiological parameters for IC2010 samples dominated by key phytoplankton taxonomic groups. Group values determined from a single observation are those which have no reported standard deviation (values shown in table 3.2).

out. The prymnesiophyte strain exhibited a temperature-growth relationship that is very similar to that of *Micromonas*, and its larger size may explain the lower absolute μ. The cryptophyte and dinoflagellate cultures show a strong decrease in μ with increasing temperature. Diatoms and chlorophytes exhibited little change in μ with temperature.

The culture results highlight that in addition to group-specific differences, local forcing factors such as temperature must also be considered. Correlations between the photophysiological parameters and environmental variables for the IC2010 cruise are shown in figures 3.12 and 3.14.

For P_m^B, the strongest correlation was found with temperature (r^2=0.45, p-val < 0.001).

Table 3.3: Culture photophysiology data. Growth rate calculated from daily cell counts. P_m^B estimated according to Saux-Picart et al. (2012) and Cloern et al. (1995).

ID	Temp(°C)	χ	μ	Saux-Picart P_m^B	Cloern P^B
Diatom	3°	86	0.60	3.24	3.91
	5°	87	0.64	3.50	4.21
	7°	87	0.66	3.60	4.33
Cryptophyte	3°	55	0.53	1.82	2.20
	5°	55	0.43	1.49	1.81
	7°	288	0.27	4.83^h	6.00^h
Prymnesiophyte	3°	106	0.39	2.61	3.18
	5°	106	0.55	3.61	4.37
	7°	106	0.67	4.45	5.35
Dinoflagellate	3°	82	0.80	4.11	4.91
	5°	82	0.51	2.59	3.14
	7°	160	0.27	2.73^h	3.39^h
Chlorophyte	3°	40	0.71	1.78	2.13
	5°	40	0.55	1.36	1.65
	7°	40	0.60	1.48	1.79
Prasinophyte	3°	60	0.52	1.94	2.35
	5°	60	0.69	2.57	3.09
	7°	60	0.78	2.94	3.52

^{h} species increased C:Chl at high temperatures, raising P^B

The open-ocean stations of the IC2010 data exhibit a clear decrease in P_m^B with depth, a pattern not seen in the under-ice data. The P_m^B data were also compared to nutrient concentrations (nitrate, phosphate, silicate and ammonium), but correlations were weak.

To determine if the P_m^B-temperature relationship observed in the IC2010 data is consistent with other measurements made within the Atlantic Arctic region, the IC2010 measurements were combined with P-E data from the Canadian Archipelago and Labrador Sea. The combined dataset was then binned by temperature (see Figure 3.13) and a steady rise in P_m^B from sub-zero to temperatures around 10°C is observed.

Figure 3.13 shows that at temperatures above 2 °C, the mean of the field observations

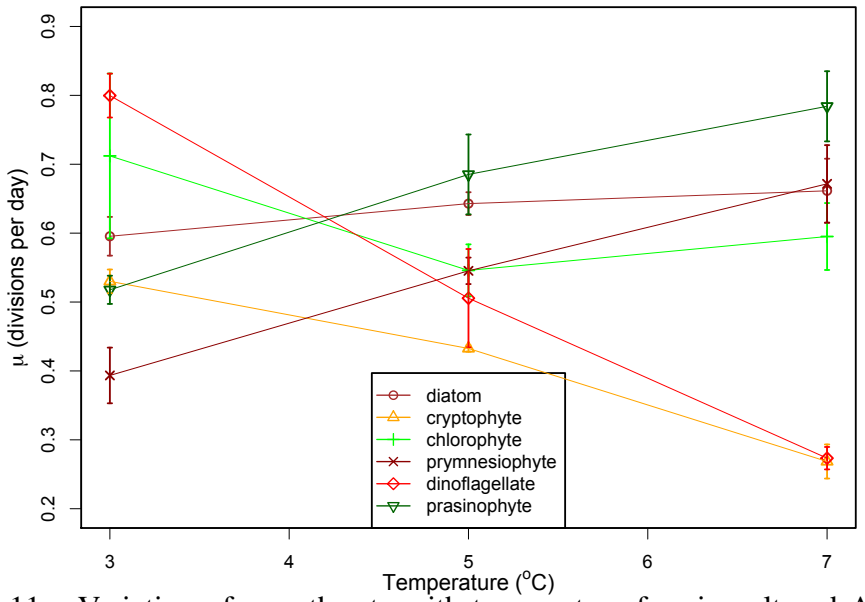

Figure 3.11: Variation of growth rate with temperature for six cultured Arctic algal groups. Growth rates were determined from daily cell counts and averaged between duplicate cultures grown at each temperature.

lies between the maximum photosynthetic rate predicted using the 7th order polynomial of Behrenfeld and Falkowski (1997b) and the Eppley (1972) growth curve, normalised as per Behrenfeld and Falkowski (1997b), such that production at 20 °C is 4.65 mg C (mg chl-a)$^{-1}$ d^{-1}. Below 2°C, the majority of data points fall below both curves.

Values of α^B decreased with latitude from 65°N to 80°N (Figure 3.14). Values of α^B also show a positive relationship with temperature. Clear differences in the depth profiles of α^B were observed between the IC2010 under-ice and open-ocean stations. The open-ocean profiles show an increase in α^B with increasing depth, whereas no clear vertical trend is present for samples collected beneath the sea ice. The α^B values are also consistently lower for the under-ice samples when compared with those collected in open-ocean waters. Similar to P_m^B, α^B showed little correlation with any of the macronutrients measured, regardless of whether samples were collected at ice-covered or ice-free stations.

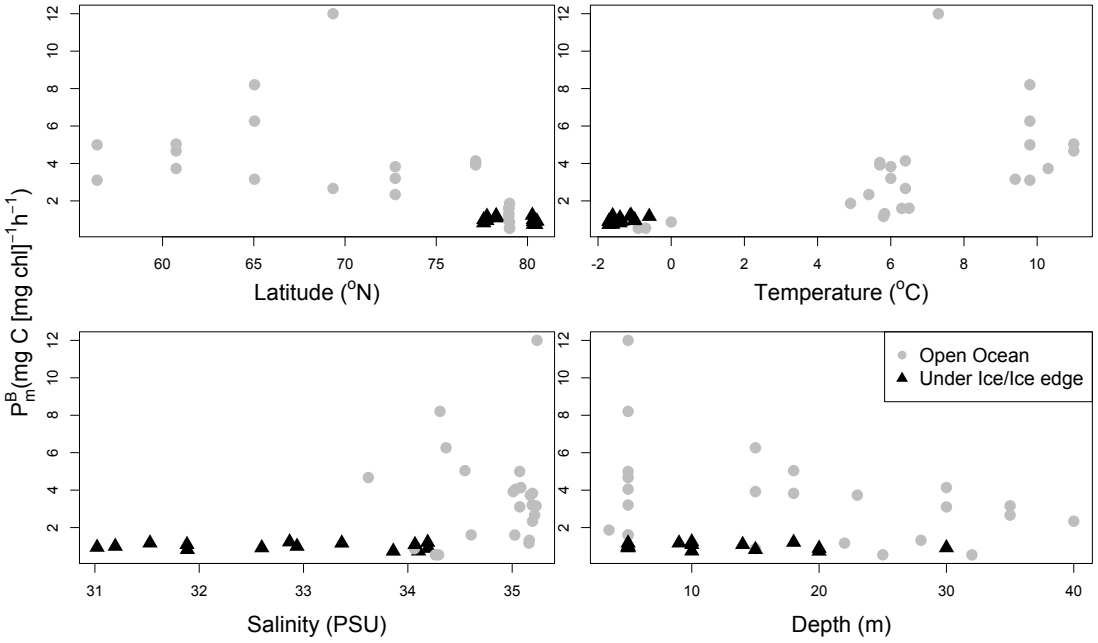

Figure 3.12: Correlation between P_m^B and environmental co-variables for the IC2010 cruise. Both under-ice (▲) and open-ocean (●) stations are shown.

The IC2010 dataset also showed a high number of samples that exhibited photo-inhibition. In a review of Arctic phytoplankton photophysiology, Sakshaug and Slagstad (1991) noted that the majority of β^B values in pan-Arctic samples were less than 0.0003. Half the IC2010 samples had β^B values greater than this, and most of these were from open-ocean samples collected from below 10 m.

Quantum yield (ϕ_m)

ϕ_m was calculated for IC2010 samples using matched measurements of phytoplankton spectral absorption ($a_{ph}(\lambda)$) and light-limited photosynthetic rates (α^B) using equation 3.10. ϕ_m values ranged from 0.005 to 0.096 μmol C(μmol photons)$^{-1}$ with most values falling within the range of 0.02 to 0.08 μmol C(μmol photons)$^{-1}$. All estimates of ϕ_m

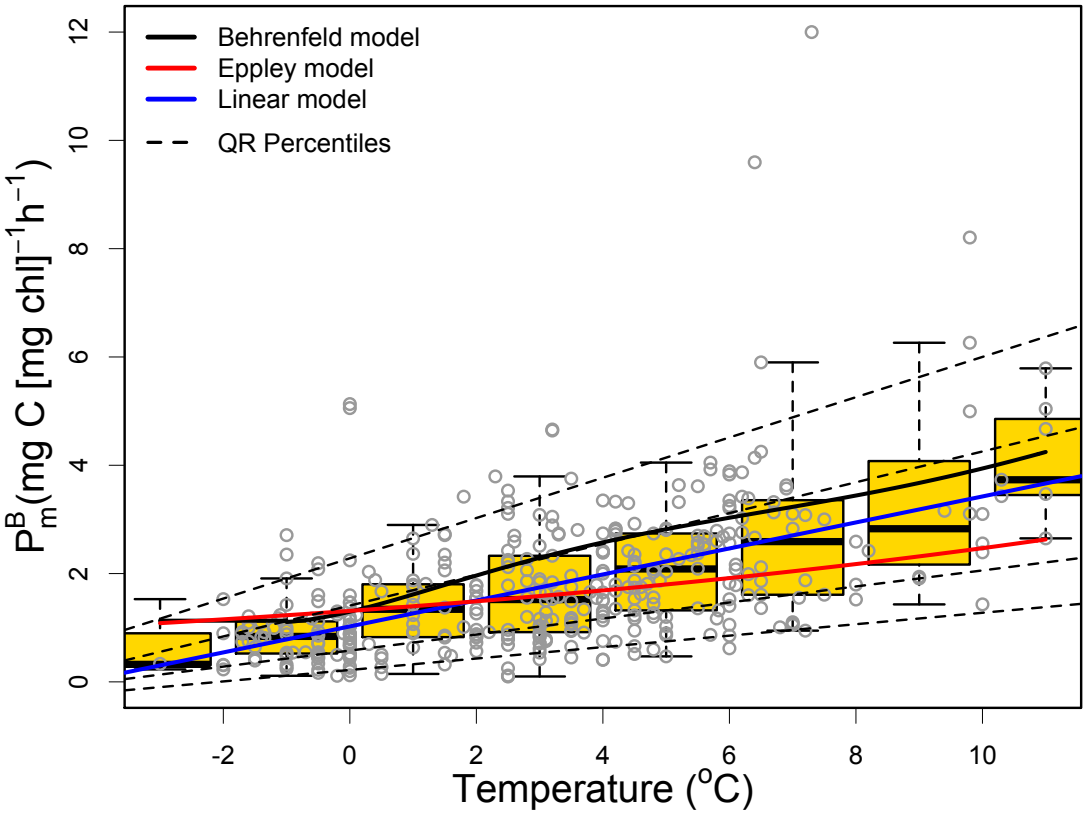

Figure 3.13: Variation of P_m^B with temperature for the combined IC2010 and BIO dataset. Only data from stations above 55°N and with water temperatures < 11°C were included. Equations plotted are a linear fit through the data, the Behrenfeld and Falkowski (1997b) P_{opt}^B, and Eppley equations. Also shown are the 95 %, 75 %, 25 % and 5 % quantile regressions.

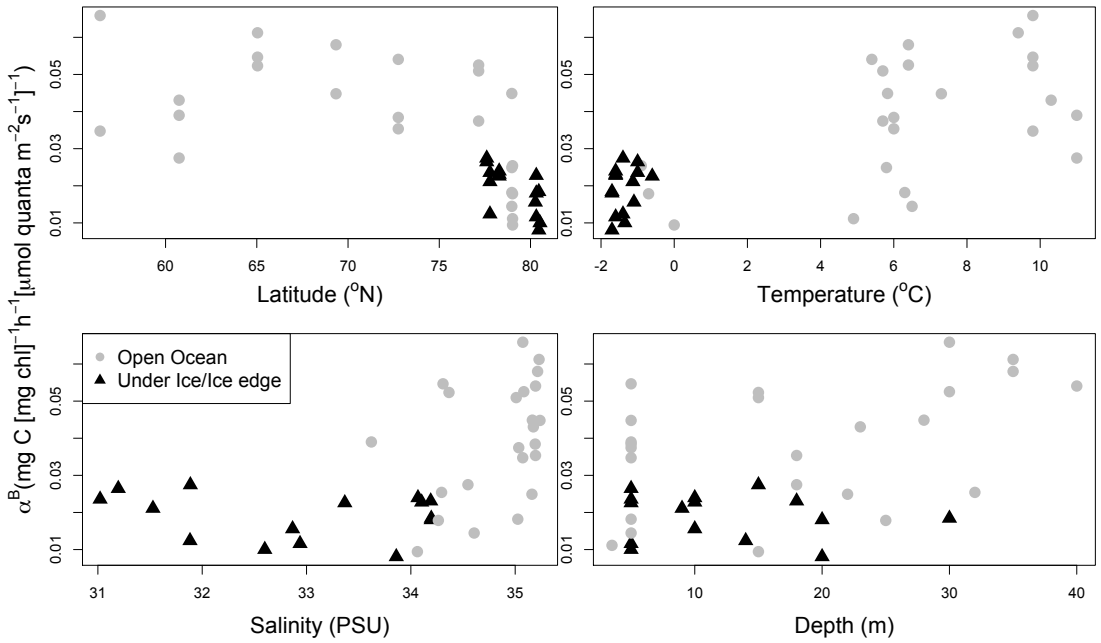

Figure 3.14: Comparison of α^B to environmental variables for the IC2010 data. Under-ice (▲) and open-ocean (●) stations are indicated separately.

fell below the theoretical maximum (0.125 $(\mu$mol C$)(\mu$mol photons$)^{-1}$) and the lowest values were within the lower range of reported values (Sakshaug and Slagstad, 1991). Of the six values of ϕ_m below 0.0125 (10 % theoretical maximum) observed in this study, four are from beneath sea ice and one is from a brine sample (the lowest value of ϕ_m in the dataset).

3.4 Discussion

Optical measurements are critical to remotely-sensed estimates of phytoplankton biomass and primary productivity using ocean colour data. Therefore it is critical that the sources of variation in the bio-optical and photophysiological properties of phytoplankton within

and between different ocean regions are understood to ensure our estimates are accurate.

3.4.1 Sources and implications of variation in phytoplankton absorption

The largest variations in phytoplankton spectral absorption of the IC2010 samples were seen in two wavebands (460-500 nm and 560-610 nm) as seen in culture studies, and field data from the Atlantic and Pacific oceans (Sathyendranath et al., 1987; Lutz et al., 1996; Stuart et al., 2004).

Group-specific differences in the spectral shape and efficiency of phytoplankton absorption are important for ocean-colour remote sensing (Stuart et al., 2000), as the 440, 490, 510 and 555 nm wavebands are used to estimate chl-a concentrations from water-leaving radiance (Reilly et al., 1998). Thus, regional variability in the spectral shape of absorption caused by shifts in the community structure of marine phytoplankton may cause errors in estimates of both chlorophyll-a biomass (Gordon and Morel, 1983) and primary production from space. Taxonomic differences in the absorptive properties of phytoplankton have been shown to influence the performance of ocean-colour algorithms at high latitudes (Stuart et al., 2000; Sathyendranath et al., 2001). In addition to variation in spectral shape, taxonomic differences in the chlorophyll-specific absorption coefficient of marine phytoplankton can lead to significant errors in estimates of surface chl-a concentration (Stuart et al., 2000; Sathyendranath et al., 2001). The retrieval of phytoplankton functional groups using satellite data also relies on exploiting differences in both the shape and magnitude of $a^B(\lambda)$. Since the Arctic is a region of rapid environmental change, understanding the sources of variability in the absorptive

properties of Arctic phytoplankton assemblages will improve our ability to use the bio-optical properties of marine phytoplankton as a tool to monitor shifts in the distribution of Phytoplankton Functional Types that play key ecological and biogeochemical roles in Arctic marine systems (Nair et al., 2008; Hirata et al., 2008).

Two primary factors govern group-specific differences in the spectral shape and magnitude of $a^B(\lambda)$. The first is the package or flattening effect, which reduces the absorption efficiency of pigments contained within a cell (Kirk, 1976). The package effect is greatest at the absorption maxima (Morel and Bricaud, 1981; Bouman et al., 2000), acting to dampen the spectral variability in an absorption spectrum, thus "flattening" the spectrum. The second factor governing both the shape and efficiency of phytoplankton absorption is the composition of the accessory pigment assemblage. In the spectral region centred around 465 nm the non-photosynthetic carotenoids (alloxanthin, zeaxanthin, diadinoxanthin) and chlorophylls -b and -$c_{1,2}$ absorb strongly. Accessory pigments that absorb light significantly in the spectral region of 525 to 550 nm are the photosynthetic carotenoids peridinin, fucoxanthin, 19′-Hex and 19′-But (Figure 3.15). The influence of the phytoplankton community structure on variation in spectral absorption in field samples collected during the IC2010 cruise is indicated by changes in the spectral gradient of absorption between 465 and 550 nm, with the prasinophytes (small cells with high relative concentrations of chlorophyll-b) possessing the steepest gradient and the diatoms (large cells with high relative concentrations of the photosynthetic carotenoid fucoxanthin) possessing the shallowest gradient. Note, the largest difference in the ratio of chlorophyll-a absorption peaks, a_{ph}(443):(676), is not between prasinophytes and diatoms, but between haptophytes and cryptophytes, which highlights the importance of accessory pigments rather than pigment packaging in driving variations in the shape of

the absorption spectra. Increased absorption at 676 nm due to the presence of a chl-b absorption shoulder would act to decrease the $a_{ph}(443)$:(676) values for prasinophytes relative to phytoplankton lacking chl-b.

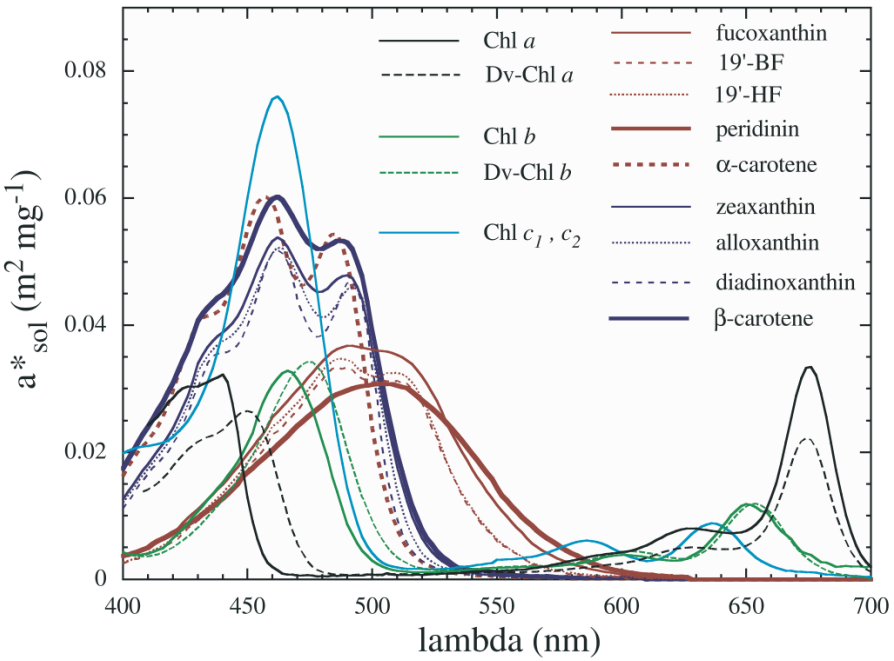

Figure 3.15: Weight-specific *in vivo* absorption spectra of major accessory pigments, $a^*_{sol,i}(\lambda)$ (m^2 mg^{-1}), as given in Bricaud (2004). Absorption spectra of photosynthetic and non-photosynthetic carotenoids are shown in red and blue.

Cell size, intracellular pigment concentration, and the presence of various auxiliary pigments can also influence absorption efficiency (Morel and Bricaud, 1981; Sathyendranath et al., 1987). A comparison of absorption efficiency for Greenland Sea and Labrador Sea data (Figure 3.7) shows a relationship of decreasing chl-a specific absorption at 440 nm with increasing chl-a concentration, a trend consistent with other global datasets (Bricaud et al., 1995, 1998). The greater range in absorption efficiencies in the Labrador Sea data, compared to the IC2010 data, is likely due to the BIO dataset covering a larger range of oceanographic conditions, as the data were acquired

over a larger range of the seasonal cycle (May to October) and over multiple years. The relationship between the absorption coefficient at 440 nm and chlorophyll-a concentration (Figure 3.8) is non-linear due to the common association of smaller cell sizes with low chlorophyll-a concentrations (Bricaud and Stramski, 1990; Bricaud et al., 1995; Lutz et al., 1996), both of which promote increased absorption efficiency (Kirk, 1976). Though the Labrador Sea and Greenland Sea datasets show a consistent trend in absorption efficiency with chl-a concentration, the best fit two-part linear equation of absorption to chl-a, compared to the equations of Prieur and Sathyendranath (1981) and Bricaud et al. (1998), highlight the need to consider regional differences in absorption efficiency, since these parameters are used in remote-sensing estimates of chlorophyll-a concentration (Astoreca et al., 2006) and solar-induced fluorescence (Behrenfeld et al., 2009).

Despite significant differences in cell size and pigment assemblage observed across the sampling region, no group-specific changes in specific absorption coefficient at 440 nm were found, although samples identified as mixed assemblages tended to have lower $a^B_{ph}(443)$ values at low chlorophyll-a concentration. The lower absorption efficiencies for mixed assemblages could be explained by the persistence of diatoms in the mixed populations. Surprisingly, the diatom-dominated samples are not distinguished by especially low absorption efficiencies, which may suggest that bloom forming cells were smaller in size, a hypothesis supported by cell count data showing small diatoms (cell volumes $<$750 μm^3) contributing $>$50 % of diatom biomass in samples from four stations. The majority of samples with low chlorophyll-a concentrations and higher $a^B_{ph}(443)$ in the Greenland Sea data were collected from ice-covered stations. The algal class that commonly dominated under sea-ice was the prasinophytes. Despite their

small cell size ($<2\ \mu m$), the prasinophytes do not possess absorption efficiencies significantly greater than other dominant groups encountered during IC2010. One reason for the similarity in absorption efficiencies across communities of varying size structure could be that the low light beneath sea ice leads to cells increasing their pigment content. This increase in intracellular pigment concentration may offset the effect of cell size on pigment packaging, resulting in a population dominated by small cells having an unusually low absorption efficiency. This supports the theory that prasinophytes such as *Micromonas* can out-compete other phytoplankton due to both their high growth rates in cold waters, especially when nutrient supply is low, and their ability to increase their pigment content to harvest more light to support photosynthesis (Lovejoy et al., 2007).

3.4.2 Sources and implications of variations in photophysiology

Field and culture data reported here support previous studies that report a relationship between phytoplankton taxonomic structure and photophysiology (Suggett et al., 2009; Huot et al., 2013) with higher estimates of P_m^B for microphytoplankton, such as diatoms and prymnesiophytes, than picophytoplankton, such as prasinophytes and chlorophytes. However, our field observations illustrate that in natural assemblages, such group-specific differences are difficult to distinguish from variations in physiology resulting from light and temperature effects, which may explain why in some datasets, diatoms show lower P_m^B values than smaller cells (Bouman et al., 2005). Thus, the physiological plasticity of Arctic phytoplankton may confound establishing global group-specific photophysiological parameter values from field observations alone. Only through the use of mechanistic models of phytoplankton physiology (Geider et al., 1996) will we be able to reconcile trends between the P-E parameters we observe in the field

with metabolic processes we examine through controlled culture studies.

Due to its influence on P_m^B, predominantly through enzyme kinetics, temperature has been used to predict P_m^B in some global primary production models (Antoine and Morel, 1996; Behrenfeld and Falkowski, 1997a). The exact nature of the relationship, however, is not the same for all oceanic regions. Eppley (1972) originally limited the application of his temperature-dependent model for phytoplankton growth to shallow coastal and estuarine waters, which may be considered to be nutrient replete. The influence of multiple factors means that regional variability in the physiological rates of marine phytoplankton is likely embedded in all single-factor correlations, such as that between P_m^B and temperature(Platt and Sathyendranath, 2002).

In the Atlantic Arctic, as in other regions of the global ocean (Sathyendranath and Platt, 1993; Bouman et al., 2005), temperature is the strongest environmental predictor of P_m^B. At low temperatures, P_m^B is low and shows little variability. A strong reduction in P_m^B at low temperatures irrespective of phytoplankton group calls into question some measurements of photophysiology in the Arctic where P_m^B values of > 10 have been reported from waters below 2 °C (Cota et al., 1994). The relationship between P_m^B and temperature observed is consistent across datasets spanning different geographical regions and years, yet differs from global empirical models derived from data collected at lower latitudes (Behrenfeld and Falkowski, 1997b). The 7^{th} order polynomial that is commonly used in primary production studies is close to the quantile regression of the 75^{th} percentile of the Arctic data and would produce an overestimate of primary production if used in the Arctic region.

As a result of the control of temperature on P_m^B and different temperature profiles between under-ice and open-ocean stations we observe a different correlation between P_m^B

and depth in the two regimes. Open-ocean stations showed a decrease in temperature (and therefore a decrease in P_m^B) with depth while under-ice waters often exhibited very little variation, or even an increase in temperature at depth due to the presence of a cold, low-salinity surface layer overlying a warmer saline Atlantic layer, which led to low variability in P_m^B values.

Variation is expected in photophysiological parameters as phytoplankton acclimate their photosynthetic machinery to achieve optimal growth rates at a particular light level. Observed variations in photophysiological parameters can be classed as 'E_k-dependent', leading to a change in E_k, or 'E_k-independent', where E_k remains unchanged due to simultaneous changes in both α^B and P_m^B (Behrenfeld et al., 2004). Variation in α^B is a function of changes in accessory pigment concentrations and modification of the PSI:PSII ratio while P_m^B is predominantly altered by changes in enzyme kinetics and electron transport rates (Behrenfeld et al., 2004). Thus if phytoplankton are trying to optimise their photosynthetic performance for a particular light level, 'E_k-dependent' variation is observed (photoacclimation). An example of 'E_k-dependent' variation is correlation between depth and α^B for the IC2010 open-ocean stations. However, limited variability in both P-E parameters, leading to a low variation in E_k, and relatively low values of α^B are seen at the sea-ice stations. This pattern has also been reported for the Canadian Arctic (Palmer et al., 2011). A decrease in light-limited photosynthetic efficiency may seem counter-intuitive, since the sea ice creates a lower surface light level than in open-ocean waters and one would expect phytoplankton cells to respond by increasing their photosynthetic efficiency at low light intensities.

The limited variability in α^B may be related to the restricted range in under-ice light levels. As Arctic water temperatures are consistently low, and this will result in a re-

duction in enzyme kinetics and thus low P_m^B values, in order for cells to acclimate to a given E_k (P_m^B/α^B) i.e'E_k-independent' variation, the cells must also exhibit low values of α^B. This also explains the temperature-dependence of α^B, where the light-limited photosynthetic rates are lower in the cold Greenland Shelf waters than in the warmer waters of the Norwegian Sea, as shown schematically in figure 3.16. Using CTD PAR and density profiles from IC2010, the average light in the upper 15 m of under-ice stations was estimated to be around 40-50 μ mol quanta m^{-2} s^{-1}. The P_m^B for the under ice stations was around 1 mg C (mg chl-a)$^{-1}$ h^{-1}, which means that in order for cells to acclimate to a growth irradiance (E_k) of 40-50 μmol quanta $m^{-2}s^{-1}$ would require an α^B of around 0.02-0.025 mg C (mg chl-a)$^{-1}$ h^{-1} (μ mol quanta m^{-2} s^{-1})$^{-1}$, which is the value observed in this dataset. These magnitudes of E_k reported here are also consistent with those measured under sea ice in the Beaufort Sea (Palmer et al., 2011). An alternative explanation for consistently low α^B values beneath sea ice is that normalising α to chlorophyll can result in low values for shade-acclimated communities due to the strong packaging effect caused by high intracellular pigment concentrations (Sakshaug et al., 1997; Harrison et al., 2013). However, if an increased chlorophyll-a content was responsible for low α^B values, one would expect that these samples would also have lower absorption efficiencies. Yet no consistent pattern between absorption efficiency and sea-ice cover was observed. The remaining cause that could explain the correlation between α^B and temperature is the influence of mixed-layer depth on light history. Cold melt waters lead to the formation of a shallow mixed layer that will confine the phytoplankton cells to a high-light environment, resulting in a decrease in light-limited photosynthetic efficiencies (Richardson et al., 1983). This mechanism may be responsible for the latitude-dependent variation of α^B, as day-length increased and mixed-layer depth decreased. However, this photoacclimatory mechanism fails to explain the low-

temperature, low-α^B data observed beneath sea ice where the near surface irradiances are low.

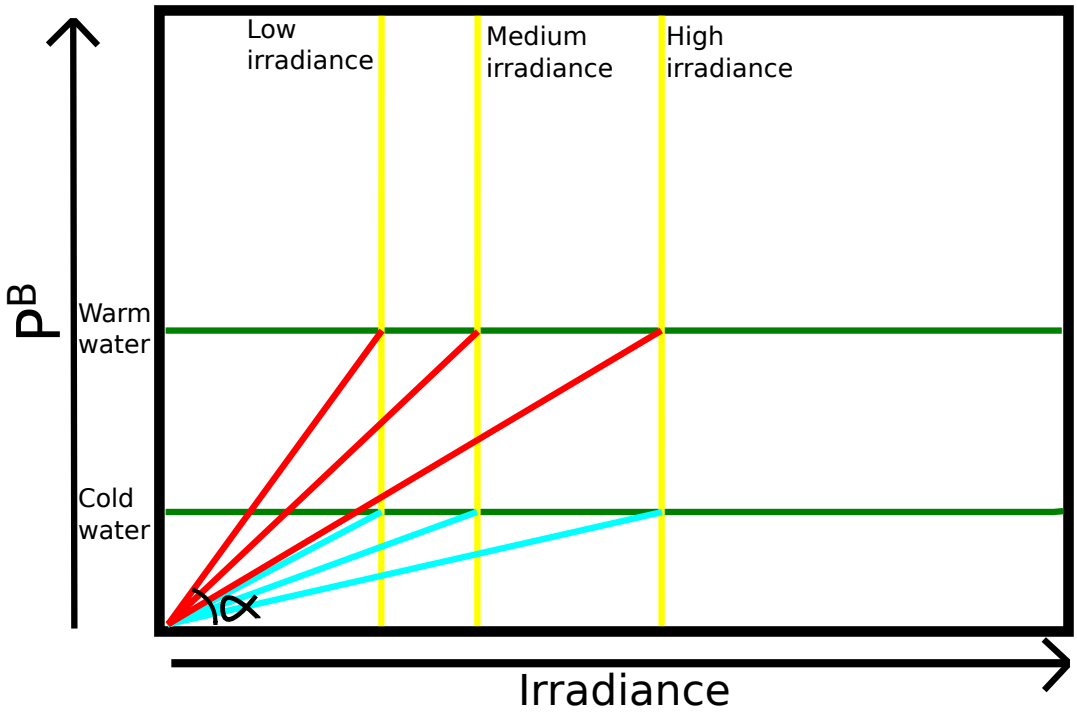

Figure 3.16: A schematic diagram showing the effect of cold temperatures on the magnitude of α^B assuming an E_k-independent relationship (Behrenfeld et al., 2004).

Our data therefore support the view that the likely dominant environmental control on polar algal photophysiology is water temperature (Palmer et al., 2011). The low temperatures place a strong constraint on P_m^B, which leads to a suppression of α^B. Consequently samples taken beneath, or proximal to, sea ice have markedly less depth-dependent variability in α^B compared to open-ocean samples. A shift from under-ice to open-ocean conditions will likely lead to an increase in P_m^B, E_k and α^B as sea surface temperature and irradiance increase.

By combining information on the absorptive and photophysiological characteristics of the natural assemblages, estimates of ϕ_m were derived. The magnitudes of ϕ_m were in agreement with previous data from the Arctic region (Sakshaug and Slagstad, 1991), however a number of samples exhibited extremely low values. The theoretical maximum quantum yield for phytoplankton is 0.125 mol C (mol quanta)$^{-1}$ and estimates of ϕ_m from carbon uptake experiments are usually lower than those using O_2 release (Sakshaug and Slagstad, 1991). Bannister and Weidemann (1984) proposed that values greater than 0.1 mol C (mol quanta)$^{-1}$ for carbon-based measurements of ϕ_m are likely caused by methodological error. There are three reasons why ϕ_m falls below the theoretical maximum (Babin et al., 1996). First, the transfer of absorbed energy to the reaction centres of photosynthesis may be less efficient within high-light acclimated cells due to the presence of photoprotective pigments (Dubinsky et al., 1986; Bidigare et al., 1989). Second, the number of healthy photochemical reaction centres can change in response to environmental factors such as light (Vassiliev et al., 1994), nutrients (Sosik and Mitchell, 1991; Falkowski, 1992) and temperature (Sosik and Mitchell, 1994). Third, the cycling of electrons through either PSI or PSII expends absorbed energy in the absence of carbon fixation (Slovacek et al., 1980). Unfortunately, this dataset can only examine the light harvesting efficiency by looking at the proportion of photosynthetic to photoprotective pigments.

Low values of ϕ_m could be due to a large fraction of the light harvested by phytoplankton cells being dissipated as heat by photoprotective pigments. The importance of photoprotection has been raised before for Arctic estimates of ϕ_m by Sakshaug and Slagstad (1991). A decrease in the proportion of photoprotective carotenoids with increasing ϕ_m is shown by the IC2010 data in figure 3.17. However, the presence of photoprotective

pigments is insufficient to explain all of the variability in ϕ_m, as some samples have both low relative concentrations of photoprotective carotenoids and low values of ϕ_m. Three of the lowest ϕ_m samples were found under sea ice and exhibit low levels of photoprotection with NPC: NPC+PPC ratios of less than 0.3 (samples 45,47 and 63). Sample 63 had extremely low NO_3 + NO_2 and phosphate concentrations, and the remaining two have phosphate concentrations around 0.3 μM and NO_3 + NO_2 concentrations around 2 μM which may suppress maximum growth rates (Tyrrell, 1999), so nutrient limitation may explain the low value of ϕ_m for these samples. However, samples 46, 48 and 49 have relatively high macronutrient concentrations yet low corresponding values of ϕ_m and NPC:NPC+NPP ratios. Therefore, these under-ice assemblages are limited by an unmeasured micronutrient, such as iron, or have a very high proportion of cyclic electron transport.

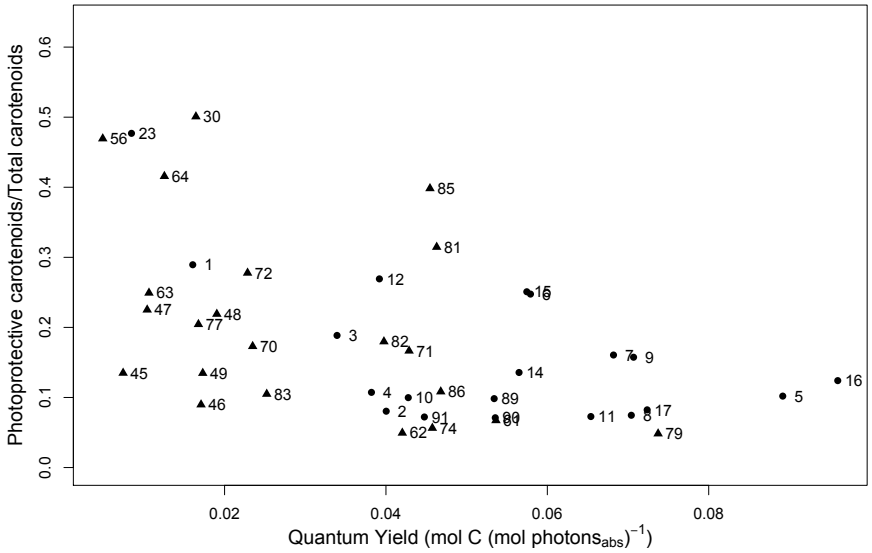

Figure 3.17: Relationship between quantum yield (ϕ_m) and relative contribution of photoprotective carotenoids to accessory pigments. Points are numbered for ease of reference. Under-ice (▲) and open-ocean (●) stations are also indicated separately.

3.4.3 Projections for a changing Arctic

Since the decrease in sea-ice extent during the Arctic winter is not as large as in the summer months, the region of the Arctic Ocean that undergoes a transition from ice-covered to open waters is increasing (table 3.4). This means that improving our understanding of the photophysiological response of marine phytoplankton across sea-ice gradients is critical.

Table 3.4: Perennially ice-covered Arctic ocean area. Data sourced from the NSIDC (http://nsidc.org/cryosphere/sotc/)

September/March (minimum/maximum)	September Average Extent (millions of km^2)	March Average Extent (millions of km^2)	Perennially Covered Region (millions of km^2)
19792000 mean	7	15.7	8.7
1999/2000	6.2	15.3	9.1
2000/2001	6.3	15.6	9.3
2001/2002	6.8	15.4	8.6
2002/2003	6	15.5	9.5
2003/2004	6.2	15.1	8.9
2004/2005	6.1	14.7	8.6
2005/2006	5.6	14.4	8.8
2006/2007	5.9	14.7	8.8
2007/2008	4.3	15.2	10.9
2008/2009	4.7	15.2	10.5
2009/2010	5.4	15.1	9.7
2010/2011	4.9	14.6	9.7
2011/2012	4.6	15.2	10.6
2012/2013	3.6	15	11.4

The presence of sea ice influences underwater light, temperature and stratification. Hence a change in the extent and thickness of sea-ice cover will likely lead to significant changes in the physiological status of Arctic phytoplankton assemblages. Here we re-

port clear differences in the photophysiology of the phytoplankton growing beneath the sea ice and in open-ocean waters. With the Arctic predicted to be ice free in the summer within 50-100 years, temperature and light in the surface of ocean is set to increase. The combination of warmer waters and greater penetration of light will lead to higher values of P_m^B and greater depth-dependent variation in α^B. The culture experiments reported here also show that warmer waters are likely going to effect phytoplankton taxa in different ways and lead to shifts in the taxonomic structure of Arctic communities, reducing cryptophyte and dinoflagellate distributions and increasing the distribution of prasinophytes and prymnesiophytes.

If some species are exhibiting low ϕ_m due to micronutrient availability, understanding how the distribution of both micro and macronutrients may shift in an ice-free Arctic Ocean may be fundamental to knowing how Arctic ecosystems may respond in a changing climate. Although it is beyond the scope of this thesis to estimate these changes, modelling studies predict that riverine fluxes of micronutrients to the Arctic could double under a warming climate (Pokrovsky et al., 2012).

3.5 Conclusions

Group-specific differences in the shape of the phytoplankton absorption spectrum observed in this study may be used in remote sensing algorithms to detect Phytoplankton Functional Groups in the Atlantic Arctic using both earth-orbiting satellites and *in situ* optical platforms. The non-linear relationship between chlorophyll concentration and phytoplankton absorption at 440 nm obtained in this dataset showed lower absorption for a given chlorophyll concentration than for global estimates (Prieur and Sathyen-

dranath, 1981; Bricaud et al., 1998). Since it is widely known that regional differences in the relationship between chlorophyll concentration and absorption caused by changes in phytoplankton community structure can lead to the poor performance of global algorithms at high latitudes(Stuart et al., 2000; Sathyendranath et al., 2001), there should be an increased emphasis on developing regional optical algorithms for the Arctic.

By combining P-E parameter data from studies across the Atlantic Arctic (Greenland Sea, Baffin Bay, Labrador Sea) spanning a period of 30 years, relationships between temperature and the photophysiological parameters were observed. At very low temperatures the variation in and magnitude of P_m^B was low, and could be explained by the temperature-dependent constraints on enzyme-mediated dark reactions of photosynthesis. There is, however, a trend of increasing P_m^B with rising temperatures. Although this relationship between temperature and P_m^B has been exploited in remotely-sensing models of primary production, our results show that models parameterized using global datasets will likely overestimate primary production at low temperatures, which are characteristic of Arctic Seas. Data collected in the Greenland and Norwegian Sea show that a reduction of P_m^B, that we believe to be caused by low temperatures, restricts the variability in α^B, through 'E_k-independent' variation (Behrenfeld et al., 2004).

Variation in ϕ_m appears to be strongly influenced by the presence of photoprotective pigments, although this mechanism could not explain some samples which displayed extremely low ϕ_m values. Macronutrients explained some of this additional variability in ϕ_m, and another limiting factor, possibly micronutrient availability, must be responsible for the remaining low values of ϕ_m. Group-specific variation in phytoplankton growth and photosynthesis was also examined using culture and field experiments, respectively. Culture experiments showed varying responses in the temperature-dependent changes

in growth rates across the taxonomic groups studied. Although the field data revealed some differences in the photosynthetic characteristics of Arctic communities dominated by different taxa, the strong influence of physical factors on the physiology of the natural assemblages, in particular temperature and light history, make the interpretation of these differences complex.

It is likely that different biogeographic regions of the Arctic may respond independently to climate change (Ardyna et al., 2011). Here we have shown that variation in the bio-optical and photosynthetic properties of phytoplankton is consistent across the Atlantic Arctic, but that this region can be divided into at least two distinct domains. In the under-ice domain, depth-dependent variation in the P-E parameters is markedly reduced when compared to the open-ocean domain. This has important implications for the geographical and vertical distribution of primary production in the Atlantic Arctic. The limited range in P-E parameters may allow a simple physiological model of phytoplankton production to perform well for under-ice conditions, provided the vertical biomass and irradiance profile are correctly estimated.

These results highlight the need to measure bio-optical and photophysiological measurements in the grossly undersampled marginal ice zone, as understanding variability across the sea-ice boundary will provide insight into a region of spatial heterogeneity in terms of both phytoplankton biogeography and water-column structure. The group-specific differences in the shape of phytoplankton absorption spectra are encouraging for the identification of Phytoplankton Functional Groups from remote sensing in this region. If we can disentangle the photoacclimation response of phytoplankton from the group-specific photophysiological variation then we may be able to create a robust group-specific primary production model for Atlantic Arctic waters.

Table 3.5: Symbols and units used in the study

Symbol	Units	Description
E	μmol quanta $m^{-2}s^{-1}$	Irradiance
α^B	mgC mgChl^{-1}h^{-1}(μmol m^{-2}s^{-1})$^{-1}$	Low light efficiency of carbon fixation.
$a_{ph}(\lambda)$	m^{-1}	Absorption by phytoplankton at wavelength λ.
$a^B_{ph}(440)$	m^{-1} mgChl^{-1}	Absorption by phytoplankton (440 nm) normalised to chl.
β^B	mgC mgChl^{-1}h^{-1}(μmol m^{-2}s^{-1})$^{-1}$	Photo-inhibition at high irradiance.
E_k	μmol quanta $m^{-2}s^{-1}$	Light saturation intensity
PAR	μmol quanta $m^{-2}s^{-1}$	Photosynthetically available radiation (400-700nm).
P^B_s	mg C (mg chl a)$^{-1}$h^{-1}	Maximum photosynthetic rate without photo-inhibition.
P^B_m	mg C (mg chl a)$^{-1}$h^{-1}	Maximum photosynthetic rate with photo-inhibition.
ϕ_m	μmol C (μmol photons)$^{-1}$	Quantum yield

Chapter 4

Modelling of Primary Production in the Greenland sector of the Arctic Ocean.

Abstract: Modelling of primary production in the Arctic is challenging due to a number of factors. These are predominantly focused around few validation studies of remote sensing at high latitudes, due to a scarcity of both *in situ* and remote sensing data, and the optical complexity of the environment. This is partly compounded by potential errors associated with ocean colour data at high latitudes due to low sun angle, continuous daylight and highly variable above and below water irradiance. This study first examines the quality of input data sources and the assumptions necessary for the utilisation of a high-latitude spectral primary production model. Remote sensing estimates of photosynthetically available radiation (PAR) are shown to have a time dependent error and poor coverage, whereas modelled PAR estimates miss extreme values but otherwise

provide useful data for primary production modelling. A positive correlation between chlorophyll-a and light attenuation in the open ocean stations suggests the optical properties of the water column for the study region can be modelled using modified Case-I assumptions, i.e spectral attenuation of light is proportional to phytoplankton biomass concentration. We then investigate the sensitivity of a spectral model of primary production to input parameters, such as phytoplankton absorption spectra, phytoplankton absorption efficiency, CDOM contribution to total absorption, vertical biomass profile parameters and photophysiology. Modelled primary production errors range from 0.5 % to >80 % depending on the parameter and water column characteristics. It is also of note that common features of the chlorophyll-a *in vivo* fluorescence profiles were near surface quenching and a sub-surface maximum. The sub-surface maxima was an important contributor to the primary production beneath sea ice, but its current contribution to annual integrated production may be less significant.

4.1 Introduction

Global ocean productivity estimates of the past 20 years have converged on a value of around 50 GT of carbon fixed through oceanic photosynthesis per year (Longhurst et al., 1995; Field et al., 1998; Geider et al., 2001; Behrenfeld et al., 2005; Uitz et al., 2010). Although these estimates have been derived using different approaches (chlorophyll-a-based, carbon-based, and phytoplankton group-specific models) all have utilized satellite observations of ocean colour. However, these models are reported to under-perform in high latitude waters (Carr et al., 2006). Satellite ocean colour data has shown that the

high, sub-polar latitudes have one of the largest and most variable annual phytoplankton growth cycles, especially the North Atlantic (Harrison et al., 2013). Cold water temperatures, strong pulses of algal growth and convective mixing make this region one of the fundamental oceanic carbon sinks (Bates and Mathis, 2009). It is therefore essential that our modelling of primary production is accurate for this region as it plays an important role in the global carbon cycle and will be significantly altered by future climate warming.

In its most basic form, a one-dimensional primary production model will require three key inputs: 1) the concentration of phytoplankton biomass present in the water column at a given depth; 2) the amount of light available at a given depth; and 3) the efficiency with which the light energy absorbed by phytoplankton pigments is converted into organic carbon (Behrenfeld and Falkowski, 1997b; Sathyendranath and Platt, 2001). The level of model complexity may increase as more parameters are added to represent the vertical structure of light and biomass as well as the spectral nature of the underwater light field and phytoplankton absorption (Sathyendranath et al., 1989a; Morel and Berthon, 1989; Antoine and Morel, 1996; Sathyendranath et al., 2007). One can also introduce carbon fixation by different phytoplankton size classes or functional groups (Uitz et al., 2010). Due to the high latitude, the Arctic light environment shows strong variability throughout the year. There is a long-term (annual) cycle in solar irradiance from 24-hour darkness in the winter to 24-hour daylight in the summer. Local surface conditions can vary from clear skies and ice-free waters to thick sea mist, cloud, and sea-ice covered. These elements combine to produce a large range in instantaneous and daily integrated irradiance values throughout the year (Curry et al., 1996).

Recent estimates of pan-Arctic primary production have been based on subdividing the

Arctic Ocean into smaller geographical regions (Pabi et al., 2008), including eight regions inside the Arctic Circle (Baffin Bay, Greenland Sea, Barents Sea, Kara Sea, Laptev Sea, East Siberian Sea, Chukchi Sea and the Beaufort Sea) and three regions further south (Norwegian Sea, Davis Strait and Bering Strait/Sea). This geographical division is related to the annual sea-ice dynamics, source water inputs and regional ocean currents. The waters of the Arctic can be considered to have four main sources of nutrients: the Pacific Ocean; the Atlantic Ocean; fluvial input from North America; and fluvial input from Eurasia. These source regions will input water of differing nutrient content, salinity, and concentration of dissolved organic compounds. The boundaries assigned for this study region were set to select surface waters influenced by one of these sources, the Atlantic Ocean (Jones et al., 1998). This study focusses on the regions that border onto the eastern Atlantic Ocean, encompassing two of the previously mentioned regions (Greenland Sea and the Barents Sea) which together run from 40° W to 55° E. This region shall be referred to as the 'Atlantic Arctic'.

Significant regional differences in phytoplankton production dynamics across the Arctic are related to the spatial heterogeneity in macronutrient concentrations, the presence of sea ice and shallow mixed-layer depths (Wheeler et al., 1997; Gosselin et al., 1997; Mock and Thomas, 2008). A large portion of the Atlantic Arctic experiences perennial cover by sea ice that melts back in the spring/summer leading to open-ocean conditions (Comiso, 2006). Ice-edge blooms often follow a retreating sea-ice front (Sakshaug and Slagstad, 1992; Engelsen et al., 2002; Perrette et al., 2011) due to the increase in the water-column stability and irradiance level experienced by phytoplankton in the upper water column. Such ice-edge blooms can begin as soon as the ice thins and can be extensive beneath thin ice regions (Gradinger, 1996; Arrigo et al., 2012). Where perennial

ice cover is not present, the high-latitude Atlantic experiences a spring bloom driven by thermal-stratification which reduces the mixed-layer depth and increases the mean light received by phytoplankton within the surface ocean (Sverdrup, 1953).

A recent study of error propagation in primary production models (Milutinović and Bertino, 2011) concluded that the main sources of the error in primary production estimates are the assignment of parameters that describe vertical structure in the biomass profile and the photophysiology of the phytoplankton. This agrees with the earlier work of Platt et al. (2008) which concluded that incorrect assignment of physiological parameters could introduce errors up to 27 %, even when using data from a single biogeochemical region, and incorrect estimation of the vertical biomass profile led to errors of up to 20 % in primary production estimates (Platt et al., 1991). The assignment of other input variables, such as coloured dissolved organic matter (CDOM) absorption and photosynthetically available radiation (PAR) estimates, are also known to cause issues in the Arctic region (Stuart, 2011). As covered in section 2, the distribution of algal pigments with depth in the study region is non-uniform, so it is likely this will be an important factor in modelling primary production for this region. The phytoplankton photophysiology is also unique for high latitudes as shown in section 3, which means this will likely be significant for primary production estimates.

This chapter aims to elucidate the sensitivity of a spectral primary production model to input parameters for high latitude seas and estimate, as accurately as possible, the production in the ice edge area of the Atlantic Arctic during the summer months. As many primary production models require an input of irradiance, we also examine the validity of multiple PAR data sources by comparing them to *in situ* datasets and considering the accuracy, quality and coverage of the data. The spectral primary production model is

initially parameterized using field observational data, as covered in the chapters 2 and 3. The parameters are then varied with the aim of answering the following questions: 1) what level of error is introduced if we incorrectly parameterize the bio-optical properties of the water column (spectral phytoplankton absorption, phytoplankton absorption efficiency and CDOM contribution to total absorption)? 2) what is the effect of using different mathematical models for the vertical biomass profile on primary production estimates? 3) what is the error associated with incorrectly assigning photophysiological parameters? The spectral-model primary production estimates are also compared to those of a non-spectral model to ascertain the level of discrepancy between simple and complex models.

4.2 Methods

4.2.1 Sampling strategy

The cruise track for the ICE-CHASER 2010 cruise (organised by the Scottish Association of Marine Sciences (SAMS)) is shown in Figure 4.1. Along this transect, 23 stations were occupied. Profiles of downwelling light, temperature, salinity, and fluorescence were recorded at each station using a Sea-Bird CTD instrument package equipped with a Biospherical Li-Cor PAR sensor, two temperature sensors, two conductivity sensors, and a Chelsea fluorometer. The temperature and salinity data were used to calculate mixed-layer depths and the fluorescence data was used to describe vertical biomass profiles. Seawater samples were collected using 10 litre Niskin bottles, which were sub-sampled for photosynthesis-irradiance (P-E) incubations and optical

measurements. Sampling depths were chosen to capture the vertical structure in the phytoplankton biomass profile, usually requiring between four and eight sample depths. Analysis of algal pigments by both high performance liquid chromatography (HPLC) and fluorometry were performed and phytoplankton *in vivo* absorption spectra were measured. The 23 stations were chosen to cover a range of environments, such as beneath sea ice, in recently-melted waters, and open-ocean (ice-free) waters.

4.2.2 Fluorometric chlorophyll-a measurement

For chlorophyll-a measurements, 100 ml of seawater were filtered onto 25 mm GF/F filters at vacuum pressures of $\leqslant$200 mm Hg and immediately placed into 10 ml of 90 % acetone. These were stored in the dark at -20 °C overnight. Chlorophyll-a concentrations were then measured using a Turner Designs Trilogy fluorometer, fitted with a chlorophyll-a acidification module, following the method of Holm-Hansen et al. (1965).

4.2.3 Photophysiological parameters

A full description of the determination of photophysiological parameters from photosynthesis-irradiance (P-E) experiments is given in section 3.2.4 but a summary is given here for ease of reference. A linear temperature-controlled incubator containing 14 polycarbonate bottles was used to quantify carbon fixation in a light gradient from dark to around 1500 μEinsteins m^{-2} s^{-1} during a period of 90 minutes. Each bottle was then filtered through a 25 mm Whatmann GF/F filter and exposed to concentrated HCl fumes overnight to remove inorganic carbon. Radiocarbon activity was then analysed using a Perkin Elmer Tri-Carb 3100 liquid scintillation counter. Final P_m^B, α^B and β^B

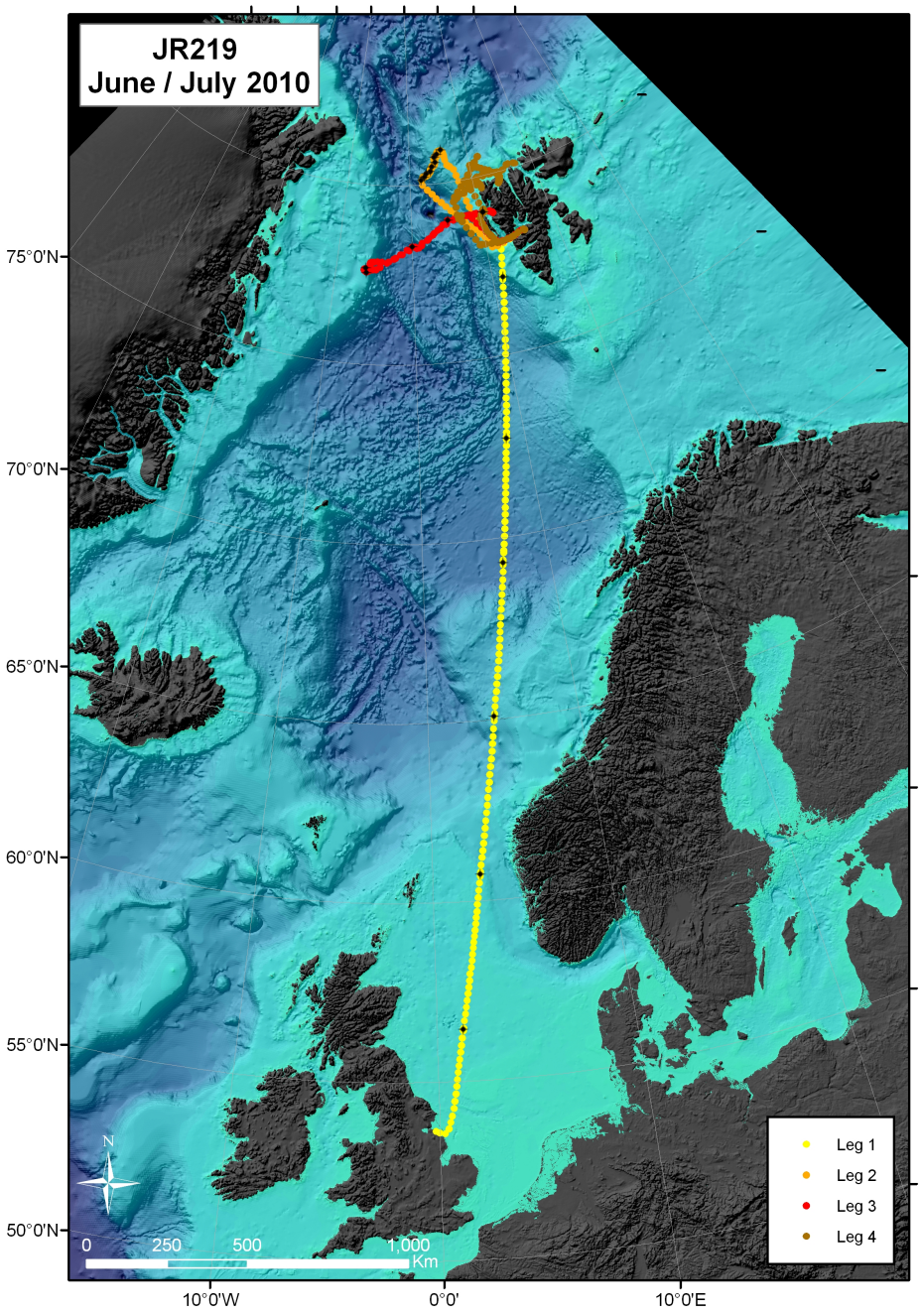

Figure 4.1: ICE-CHASER 2010 cruise track and bathymetry of the study area with sampling stations shown by black points.

values were determined after corrections for the spectral emission of the lamp and phytoplankton absorption spectra, following the method of Kyewalyanga et al. (1997) using equations 3.6 to 3.8.

4.2.4 High-latitude PAR data sources

At high latitudes, the accuracy of satellite-derived PAR data used in primary production models is uncertain (Stuart, 2011). Long day-lengths, high zenith angles, and sea ice can affect the accuracy of modelled and remotely-sensed PAR estimates. To assess this problem, we compared the underway data to the SeaWiFS PAR data product to see if the remote sensing product was a valid source for PAR to input into primary production models on a large scale. The underway data was recorded using a Kipp and Zonen PAR *LITE* quantum irradiance sensor and provided a near-continuous record of surface irradiance during the 38 day cruise. The remote-sensing data used in this work are SeaWiFS level 2 daily products provided by NASA GSFC/DAAC at http://oceancolor.gsfc.nasa.gov/. This SeaWiFS product provides an estimate of daily PAR based on an image capturing conditions at a particular time of day. PAR data was extracted on a pixel-by-pixel basis for comparison to the ICE-CHASER 2010 underway data to allow a very high temporal and spatial resolution for match-up. The SeaWiFS data used was from the valid pixel closest to the ship position at the time of satellite overpass and had to be within 0.1° of the ships position. To calculate the reference underway measurement from the underway data, we averaged the data from a ten-minute period centred at the time of the satellite overpass.

To assess the suitability of using modelled PAR in primary production models at high

latitudes, a comparison is also made between the Bird Model (Bird and Riordan, 1986) estimate of PAR and surface PAR data taken during the ICE CHASER 2010 expedition.

4.2.5 Light attenuation coefficients

Two datasets collected during the ICE CHASER 2010 expedition were used to calculate the attenuation of light within the water column. The first of these was from an upward-looking downwelling PAR (Biospherical Li-Cor) sensor attached to the CTD instrument package. Since the CTD irradiance measurements are not spectrally resolved, surface deck measurement and vertical profiles of spectral irradiance were recorded at a number of stations on the third leg of the cruise. Direct measurements of underwater downwelling spectral irradiance were made with RAMSES ACC-VIS hyperspectral radiometers (TriOS Mess and Datentechnik GmbH) and were carried out prior to, or just after, CTD casts. The RAMSES radiometer consists of sensors with an advanced cosine collector performing in a range of 320-950 nm with a spectral resolution of ≈3.3 nm. A simultaneous use of two sensors allowed tracing of major changes in incident solar radiation due to changing cloud cover. The surface sensor was placed in front of the research vessel, whilst the underwater sensor attached to a frame designed to minimize inclination and was lowered with a side crane 4-5 m away from the hull of the vessel to minimize shadowing effects. Observations were always performed on the illuminated side of the vessel. Depth increments of scans for underwater profiles ranged from ≈1 m in the subsurface layer to ≈0.5 m in the uppermost layer to obtain a better vertical resolution. Profiles were taken up to 40 m, unless the light level dropped below detection at a shallower depth. The limit of detection was 0.5 mW m^{-2} nm^{-1}, below this the signal to noise ratio became too low. Irradiance data was quality checked and then interpolated

into a 1 nm grid with vertical steps of 0.5 m. Underwater profiles were then normalised by dividing each value at depth by the coincident surface reading, giving a fraction of surface irradiance at depth. These *in situ* measurements of the underwater light field allowed us to ascertain whether the spectral light profiles generated in the primary production model were representative of the true underwater irradiance profiles.

4.2.6 Modelling primary production

The primary production model used in this study is based on the spectral model of Sathyendranath et al. (1989a) including the modifications made in Sathyendranath et al. (1995). The transmission of light was resolved at 61 wavelengths from 400 nm to 700 nm, every 5 nm, and all calculations were computed with a model temporal resolution of one hour.

Inherent optical properties and the underwater light field

The spectral radiative transfer model used was developed for Case-I waters where absorption in the water column is dominated by phytoplankton and pure water, with a small proportional contribution to total absorption by non-algal substances such as CDOM and particulates, which co-varies with algal biomass,

$$a(z,\lambda) = a_w(\lambda) + a_c^*(\lambda)C(z) + a_y^*(\lambda)Y(z). \tag{4.1}$$

where $a_w(\lambda)$ is the absorption coefficient of pure water (Pope and Fry, 1997), $a_c^*(\lambda)$ is the specific absorption of chlorophyll, C is chlorophyll concentration, $a_y^*(\lambda)$ is the

specific absorption of CDOM and particulates, Y is the concentration of CDOM and particulates and z is depth. CDOM absorption was scaled to chlorophyll-a absorption such that,

$$a_y^*(440)Y(z) \propto a_w(440) + a_c^*(440)C(z). \tag{4.2}$$

These inherent optical properties (IOPs) were modified during the sensitivity analysis to better fit *in situ* measurements of light attenuation and absorption spectra.

Chlorophyll biomass profiles

Several models of marine primary productivity that use satellite ocean-colour data require an equation to describe the vertical distribution of chlorophyll-a in the water column (Platt and Sathyendranath, 1988; Sathyendranath and Platt, 1993). Different equations have been proposed to describe the chlorophyll-a profile (Platt and Sathyendranath, 1988; Morel and Berthon, 1989; Longhurst et al., 1995; Antoine and Morel, 1996; Arrigo et al., 2008; Mignot et al., 2011). Some profile descriptions are very simple, such as uniform chlorophyll-a irrespective of depth (Antoine and Morel, 1996), but when a pronounced subsurface peak exists, a more complex equation that better describes the profile using as few parameters as possible would be more suitable (Arrigo et al., 2008). In this study, we tested four ways of modelling the vertical biomass profile and their effects on estimating primary production (PP). The following section summarises the models used.

Uniform Profile

The simplest representation of the depth dependence of chlorophyll-a would be to set

the chlorophyll-a biomass (B) to be constant from the surface to the depth of the photic zone (Antoine and Morel, 1996). This approach works well in regions with deep mixed layers, within which the phytoplankton biomass is homogeneously distributed. The chlorophyll-a concentration within the mixed layer and photic zone could, for example, be set to the value at the surface. If the chlorophyll-a value is based on a satellite-derived estimate then this is equivalent to using the weighted mean value within the first optical depth ($\bar{B}_{sat}$) such that in the model

$$B(z) = \bar{B}_{sat}. \tag{4.3}$$

Uniform mixed layer followed by exponential decay profile

A slightly more complex representation of the chlorophyll-a profile proposed by Pabi et al. (2008) maintains the chlorophyll-a biomass as uniform in the near surface and then chlorophyll-a decreases exponentially to zero with increasing depth. The depth dependence of chlorophyll-a can be described using three parameters: the concentration in the uniform section ($\bar{B}_{ML}$); the depth of the uniform section (MLD) and the rate of decrease with depth below the mixed layer:

$$B(z) = \begin{cases} \bar{B}_{ML} & \text{if } z \leq \text{MLD}, \\ \bar{B}_{ML} * e^{0.033*(z-MLD)} & \text{if } z > \text{MLD}. \end{cases} \tag{4.4}$$

Pabi et al. (2008) set the upper layer to a uniform value of $\bar{B}_{sat}$ and set the bottom of the uniform layer to 20 m (an assumed constant mixed-layer depth). Due to the constant depth of the uniform layer, this model only has one variable, the surface chlorophyll-a concentration. The biomass profile does not take into account factors such as a variable

photic or mixed-layer depth. Although this equation is a better description of most biomass profiles than a constant value, with only one input parameter it cannot capture the variability in the shape of all biomass profiles.

Shifted Gaussian profile

The shifted Gaussian model provides a more detailed description of the vertical structure of chlorophyll-a with respect to depth. This Gaussian equation was first used by Lewis et al. (1983) and was subsequently improved by Platt et al. (1994) and implemented in Sathyendranath et al. (1995); Longhurst et al. (1995) and references therein. The shifted Gaussian requires four input parameters. The first is the background concentration of chlorophyll-a, which is uniform with depth (B_0). Superimposed on top of this background concentration is a chlorophyll peak, which can be described using three parameters: the peak biomass (h), the peak width (σ) and the depth of the maxima (z_m)

$$B(z) = B_0 + \frac{h}{\sigma\sqrt{2\pi}} \exp -\frac{(z - z_m)^2}{2\sigma^2}. \tag{4.5}$$

As the peak biomass (h) includes the background concentration, it is beneficial to define a parameter for the height of the peak above the background (B_m) where:

$$B_m = \frac{h}{\sigma\sqrt{2\pi}}, \tag{4.6}$$

therefore, equation 4.5 becomes

$$B(z) = B_0 + B_m \exp -\frac{(z - z_m)^2}{2\sigma^2}. \tag{4.7}$$

The shifted Gaussian fits most profiles and performs well both in regions with surface chlorophyll-a peaks and with deep chlorophyll-a maxima (such as the subtropical gyres).

Shifted Gaussian with exponential background

Arctic marine ecosystems are sometimes characterised by a complex vertical profile of chlorophyll-a concentration (Martin et al., 2010; Hill and Zimmerman, 2010), with many profiles showing a sub-surface maxima (SCM) that is similar to the deep chlorophyll maximum (DCM) seen in oligotrophic gyres, but the peak usually occurs at much shallower depths (20-50 m). This subsurface maximum has been attributed to the unique environmental forcing seen in sea-ice influenced areas. The light intensity at intermediate depths (≈40 m) beneath sea ice is similar to that seen at the DCM in the oligotrophic gyres (Stein and MacDonald, 2004). A key difference between the Arctic SCM and the DCM in the subtropical gyres is that in the Arctic the SCM corresponds to a peak in particulate carbon and primary production (Martin et al., 2010; Hill et al., 2013), whereas in the gyres it is a result of the photoacclimatory response of cells increasing their chlorophyll-a content (Cullen, 1982). It is also usual that the background biomass (excluding the SCM) will be higher at the surface compared to that at depth.

Mignot et al. (2011) proposed a set of equations which can be used for profiles with a biomass peak superimposed upon a non-uniform background profile. The model consists of an exponential decay as the background and then adds a shifted Gaussian, which allows more complex profiles to be parameterized and gives a better fit to the *in situ* observations. This equation requires the same three Gaussian peak parameters and instead of a single background chlorophyll-a value, a surface value (F_0) and a half-saturation depth (z_2) is assigned. The parameter z_2 defines where the background exponential has

reached half of its surface concentration. The chlorophyll-a profile can therefore be described by the following equation:

$$B(z) = F_0 \exp\left[\frac{-\ln 2}{z_2} z\right] + B_m \exp\left[-\frac{(z - z_m)^2}{2\sigma^2}\right]. \quad (4.8)$$

Photosynthetically-available radiation (PAR) data

PAR used in the primary production calculations was estimated using the clear-sky model of Bird and Riordan (1984), corrected following Bird and Riordan (1986). This model has been shown to reproduce irradiance spectra at low solar elevation angles (10°) in previous studies (Bird and Riordan, 1986; Campbell and Aarup, 1989). The output from the Bird model was then corrected for seasonal variation in incoming solar radiation (Thekaekara, 1977), cloud cover (Platt et al., 1990), sea-surface reflection (Sathyendranath et al., 1989a) and sea-ice presence. The effect of sea-ice cover on the light available to phytoplankton in the water column was approximated by passing the sea surface irradiance through 30 m of clear seawater (Stein and MacDonald, 2004). Sea ice and snow transform the light field in the surface waters into one which would be found at 30-100 m in open waters, with pure sea ice and snow being almost spectrally identical to pure water (Light et al., 1998; Stein and MacDonald, 2004). Though this is a simplification of the optics of sea ice, it is a starting point which can be adapted once regional transmission estimates begin to improve through the inclusion of variable ice thickness, melt pond size and shape distributions (Ehn et al., 2011) and optically-active substances within the sea ice (Light et al., 1998).

Comparison to a simple primary production model

All of the model variations described thus far are based around a spectral, non-uniform biomass model, parameterized using *in situ* data. It is of interest to compare the estimates of a much simpler model to ascertain the benefit of the increased complexity. The simple model chosen for comparison was the VGPM model of Behrenfeld and Falkowski (1997a). Two variants of this model were run, both requiring 4 inputs: 1) surface chlorophyll-a concentration, 2) PAR, 3) sea surface temperature (SST), and 4) daylength. The surface chlorophyll-a was set to $\bar{B}_{sat}$, the SST was set to the mean temperature within the upper 10 m unless a distinct pycnocline was present at a shallower depth. The day-length and daily irradiance were derived from the BIRD model mentioned previously. For sea-ice stations the optical effect of sea ice was again approximated by 30 m of clear seawater using a non-spectral seawater K_d^{PAR} of 0.042 m^{-1}. The difference for the two model variants was the equation used to describe the relationship between temperature and P_{opt}^B. The first variant uses the seventh order polynomial equation of (Behrenfeld and Falkowski, 1997a):

$$\begin{aligned} P_{opt}^B =& 1.2956 + 0.2749T + 0.0617T^2 - 0.0205T^3 + 2.462 \times 10^{-3}T^4 \\ & - 1.348 \times 10^{-4}T^5 + 3.4132 \times 10^{-6}T^6 - 3.27 \times 10^{-8}T^7, \end{aligned} \tag{4.9}$$

while the second uses the equation of Eppley (1972):

$$P_{opt}^B = 1.54 \times 10^{0.0275 \times (T - 0.07)}, \tag{4.10}$$

where T is water temperature.

4.3 Results

4.3.1 Quality of PAR data sources

A comparison of the remotely sensed estimate of daily PAR to both the integrated daily underway data and the instantaneous underway measurements of PAR are given in Figure 4.2. For SeaWiFS images there were often multiple passes for a given day, due to the polar orbit of the satellite, which should increase the accuracy (Frouin et al., 2003). However, the remotely sensed estimates of daily PAR were consistently higher for images taken closer to midnight than those taken close to mid-day. The synchronous underway data show that, as expected, instantaneous measurements of downwelling irradiance were higher closer to noon. To attempt to correct this we applied a weighting to the remote sensing estimates based on the solar geometry. The remotely sensed estimates were weighted by the cosine of the suns zenith angle before being averaged for each day. This reduced the disparity between the satellite and underway values to around 30 %, with the weighted satellite result usually being an overestimate.

The remaining variation in satellite estimation of PAR could be explained by rapid changes in cloud cover, which is not accounted for in the SeaWiFS PAR product, but is registered in the underway data. The diurnal cloud variability in the Arctic tends to be characterised by thicker cloud cover around mid-day than in the evenings and early morning (Tjernström, 2007). Consequently, satellite passes occurring later in the day are more likely to have reduced cloud cover, which may lead to an overestimate of incident irradiance, whereas the opposite may be true for passes close to local noon. This is consistent with the results shown in figure 4.2.

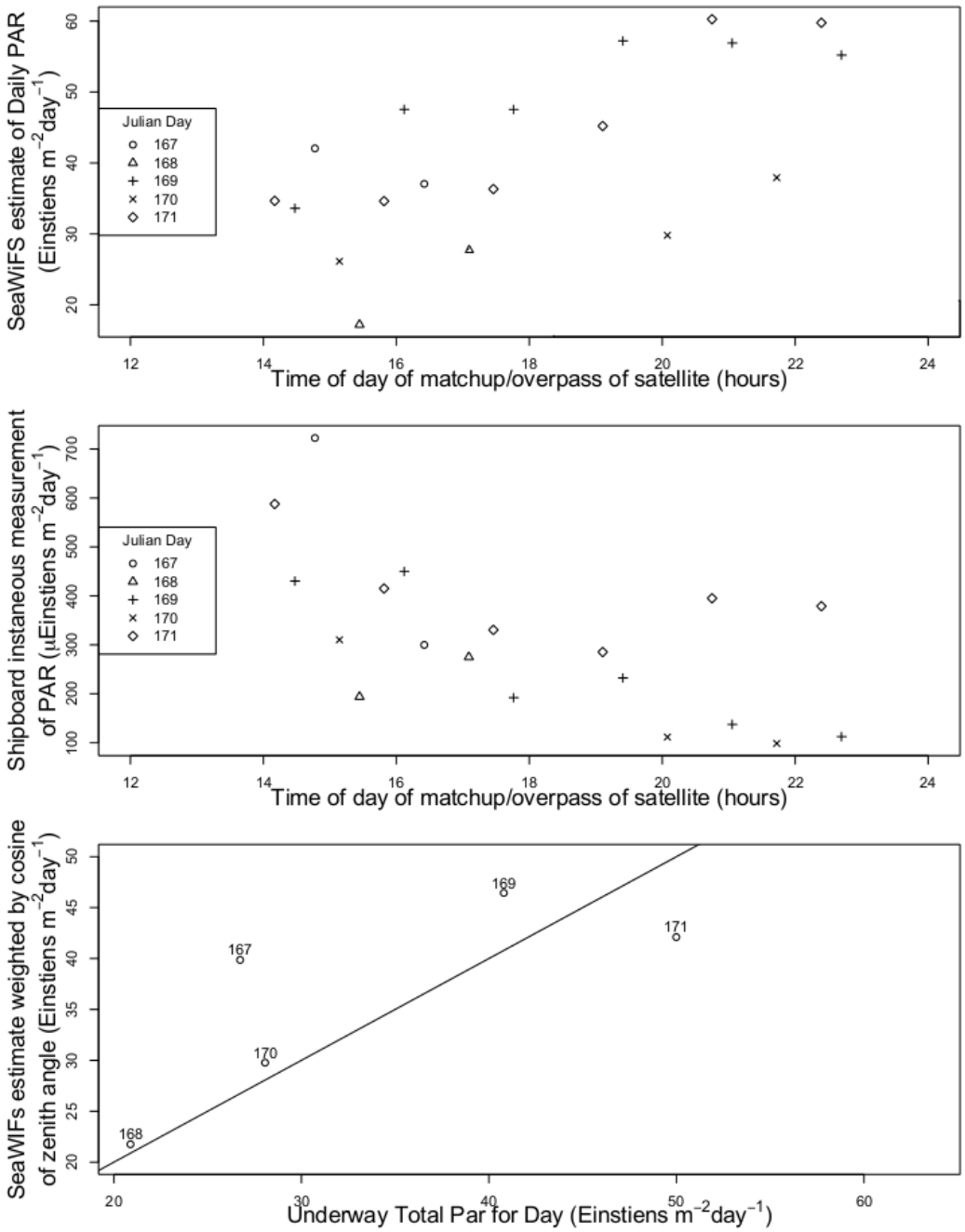

Figure 4.2: A) SeaWIFs PAR estimates separated by day and time of overpass. B) Instantaneous underway data at times of satellite overpass. C) Remote sensing composite estimate weighted by time of overpass compared to daily summed underway data.

Comparison of the Bird PAR model with the underway data (Figure 4.3) showed a general agreement for a large portion of the data, over a wide range of incident irradiances. At latitudes greater than 70°N, the range of model values were 100-1000 μEinsteins $m^{-2}s^{-1}$, depending on cloud cover. A greater range of values were observed at lower latitudes, as the sun has a greater diel range in zenith angles. The underway data for latitudes greater than 70°N varied from 60-1800 μEinsteins $m^{-2}s^{-1}$, although the highest observed values were often short fluctuations. These peaks represent a small fraction of the underway data with 85 % of the measurements in the range of 100-1000 μEinsteins $m^{-2}s^{-1}$. The agreement is also better between the modelled and underway data closer to midnight than midday. This shows that the low zenith angles are probably not the main source of discrepancy between the model and underway data as this is when the zenith angles are most extreme.

4.3.2 Chlorophyll profiles and Case-I water assumptions

In vivo flourescence profiles

We compared *in vivo* fluorescence from the CTD fluorometer with fluorometric measurements of extracted chlorophyll-a *in vitro* in order to derive profiles of phytoplankton biomass at a higher depth resolution than our bottle sampling. Figure 4.4A shows that the CTD *in vivo* fluorescence usually underestimates chlorophyll-a concentration for depths less than 15 m, especially at low chlorophyll-a concentrations. This underestimate is due to daytime fluorescence quenching in surface waters, as the 24-hour daylight and shallow mixed layers lead to a high-light environment at the near surface, which results in diminished fluorescence yields per unit chlorophyll-a (Cullen and Lewis, 1995;

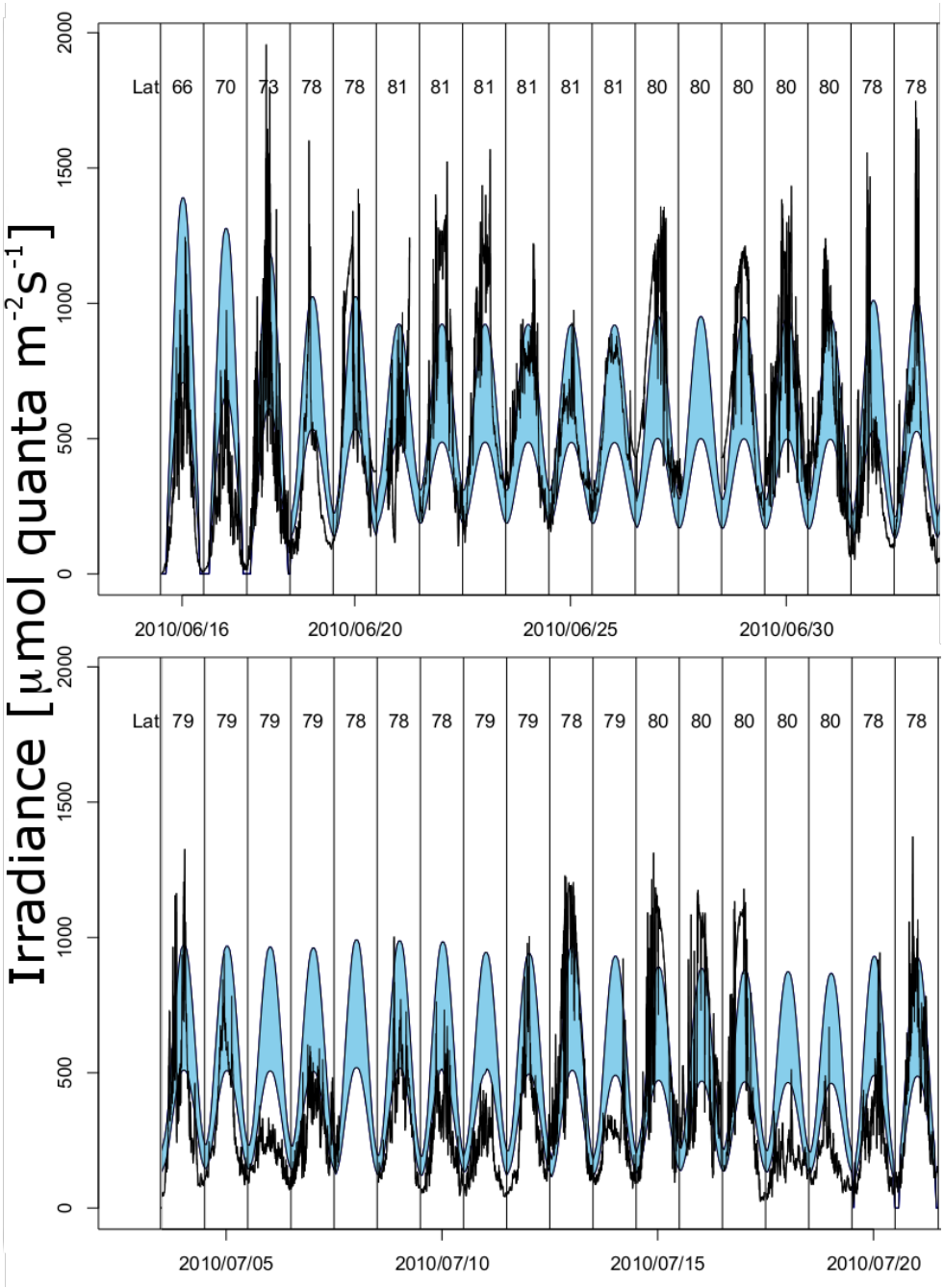

Figure 4.3: Comparison of the underway PAR data (shown in black) and the Bird model PAR output (blue shaded region, upper limit = 1 % cloud cover, lower limit = 99 % cloud cover).

Holm-Hansen et al., 2000; Sackmann et al., 2008; Mignot et al., 2011). To correct for this near-surface underestimate of chlorophyll-a, a linear equation was fitted through the log-transformed data from $\leq$15 m depth. This linear equation allows a correction (ΔB) to be added for underestimation due to quenching,

$$\Delta B = 1.71189 * B(z)^{0.65} - B(z). \tag{4.11}$$

Given that this error is greatest at the surface and decreases exponentially with depth (in the same manner as light transmission), the increase in chlorophyll-a (ΔB) was multiplied by an exponential decay with depth, with a decay constant of 1/20:

$$B(z) = B(z) + \Delta B * e^{-z/20}. \tag{4.12}$$

The agreement between observed pigment extracts and corrected *in vivo* fluorescence using equation (4.12) is shown in Figure 4.4B. The improvement is greatest at shallow depths and where chlorophyll-a concentrations are low. The overall r^2 of regression between *in vivo* and in vitro chlorophyll-a fluorescence estimates increased from 0.71 to 0.81 (p-val $<$ 0.0001), the intercept decreased from 0.125 to 0.045 and the slope increased from 0.68 to 0.92. These corrected fluorescence profiles were then used to estimate the light transmission through the water column and primary production using a spectrally-resolved model.

In addition to the diminished fluorescence yields in the near surface, we also observed high variability in the shape of the chlorophyll-a profiles. The profiles can be split into two types, those that show a pronounced sub-surface maximum and those that exhibit a

H]

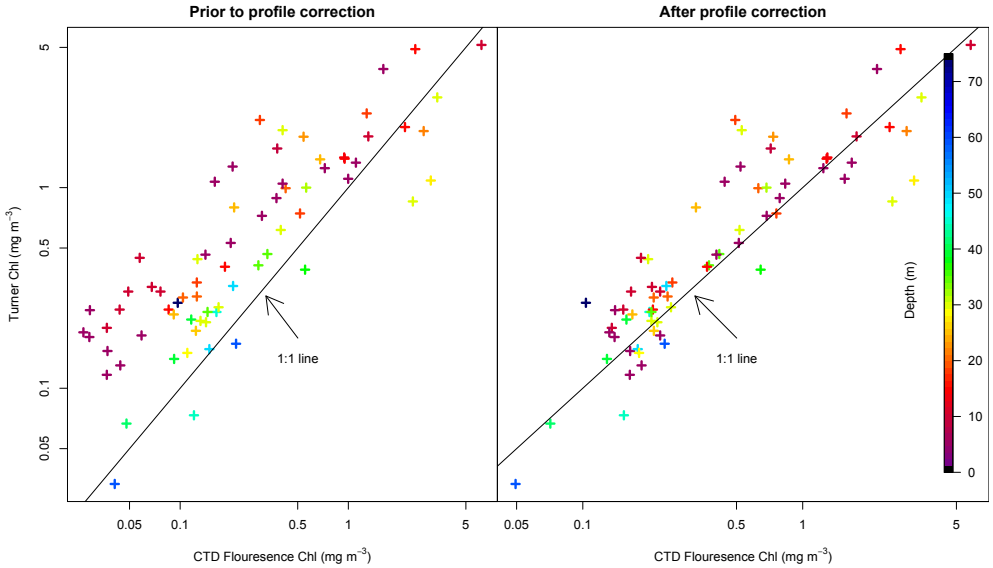

Figure 4.4: Comparison of the CTD fluorescence and Turner Chl-a estimates before and after correction factor was applied to correct for near surface saturation.

more uniform profile.

The prevalence of the subsurface biomass peak is apparent when we compare the mean chlorophyll-a concentration within the surface waters ($[\text{Chl}]_{surf}$) to that integrated over the euphotic zone ($<\text{Chl}>_{Zeu}$), where surface waters were defined by the first optical depth. Although a positive correlation between the two values was found, figure 4.5 shows that the IC2010 data lies above the trends reported by Uitz et al. (2006) for the global oceans. There is therefore a larger fraction of integrated chlorophyll-a that does not lie within the first optical depth in these Arctic waters. This is especially prominent in the stations beneath sea ice and those with lower mean surface chlorophyll-a concentrations (4.5).

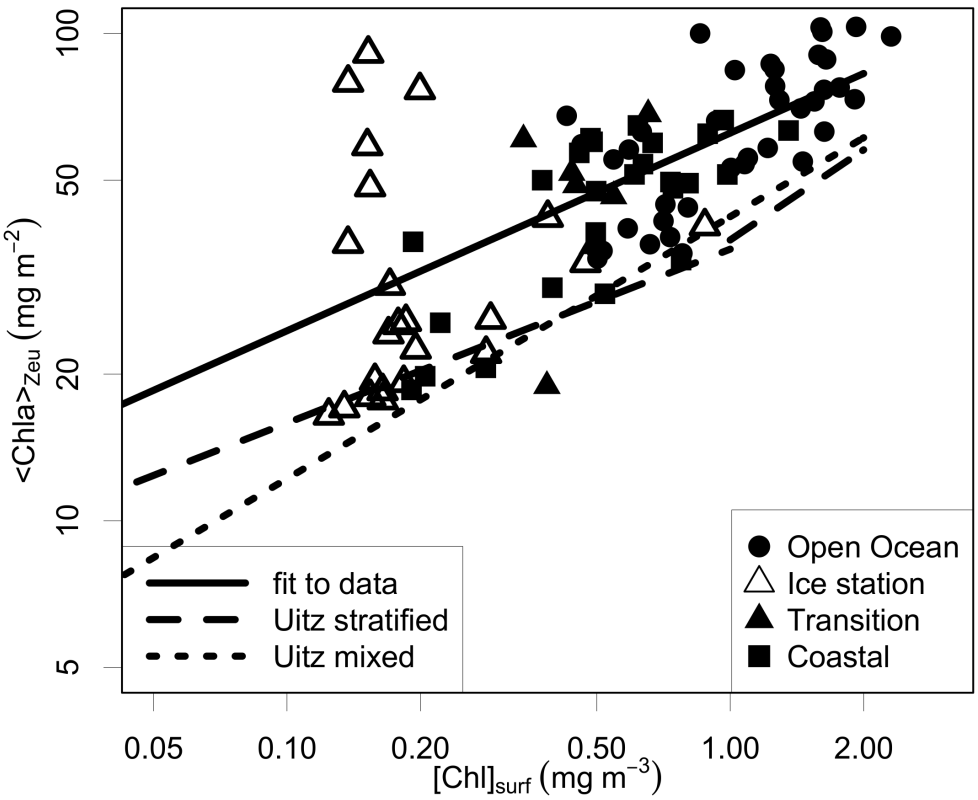

Figure 4.5: Comparison of Chlorophyll integrated over the euphotic zone and the mean value within the first optical depth.

Profiles that do not possess a strong subsurface peak show a very strong correlation between surface chlorophyll-a values and the mean chlorophyll-a in the upper 50 m of the water column (r^2 =0.9, p-val < 0.001), whereas those with a subsurface peak have a poor correlation between these two variables (r^2 =0.27, pval < 0.1). As mentioned previously, deep chlorophyll maxima in the oligotrophic subtropical gyres are a result of photoacclimation (Cullen, 1982). However, subsurface peaks in Arctic waters are usually biomass and productivity maxima (Martin et al., 2010; Hill and Zimmerman, 2010) and are typically not simply a result of changes in the pigment content of phytoplankton cells. This is supported by our model results, where chlorophyll-a peaks at

30 m contributed up to 84 % of the integrated primary production beneath sea ice and up to 26 % at open ocean stations. This is in very good agreement with the work of Hill et al. (2013) who estimated that in the Greenland sea production beneath the mixed layer could account for up to 90 % of integrated primary production.

Sub-surface peaks were present in all the different stages of ice melt (under-ice, transitional and open-ocean) as well as in some coastal waters (Figure 4.6). A number of stations had surface chlorophyll-a concentrations (B_0) $>$ 1 mg m^{-3}, in addition to a subsurface chlorophyll-a maxima. Sub-surface peaks were usually located at around 20 m in the water column (figure 4.7) but were seen as deep as 60 m at some stations. Peak concentrations ranged from 1-5 mg m^{-3} with a near-normal distribution centred just below 3 mg m^{-3}. The peaks were usually narrow (σ $\leq$10 m) though some broad peaks with σ values of 30 m were observed.

Light attenuation

To derive estimates of marine primary production it is important that the propagation of light through the water column is accurate. Modelled and measured light profiles were compared to determine whether the simple light attenuation model for Case-I waters (Sathyendranath et al., 1989b) was valid for the ICE CHASER 2010 sampling stations. It is often assumed that much of the Arctic is not Case-I due to its large drainage area and high proportion of shelf-sea coastline (Kahru et al., 2011). A comparison of downwelling light attenuation (Figure 4.8) to chl-a, using the CTD PAR data and fluorometric chlorophyll-a measurements, shows that the K_d^{PAR} is correlated with chlorophyll-a concentration. It is expected that the CTD PAR attenuation coefficients will be higher at the surface than at depth as the strong absorption of red photons by water influences

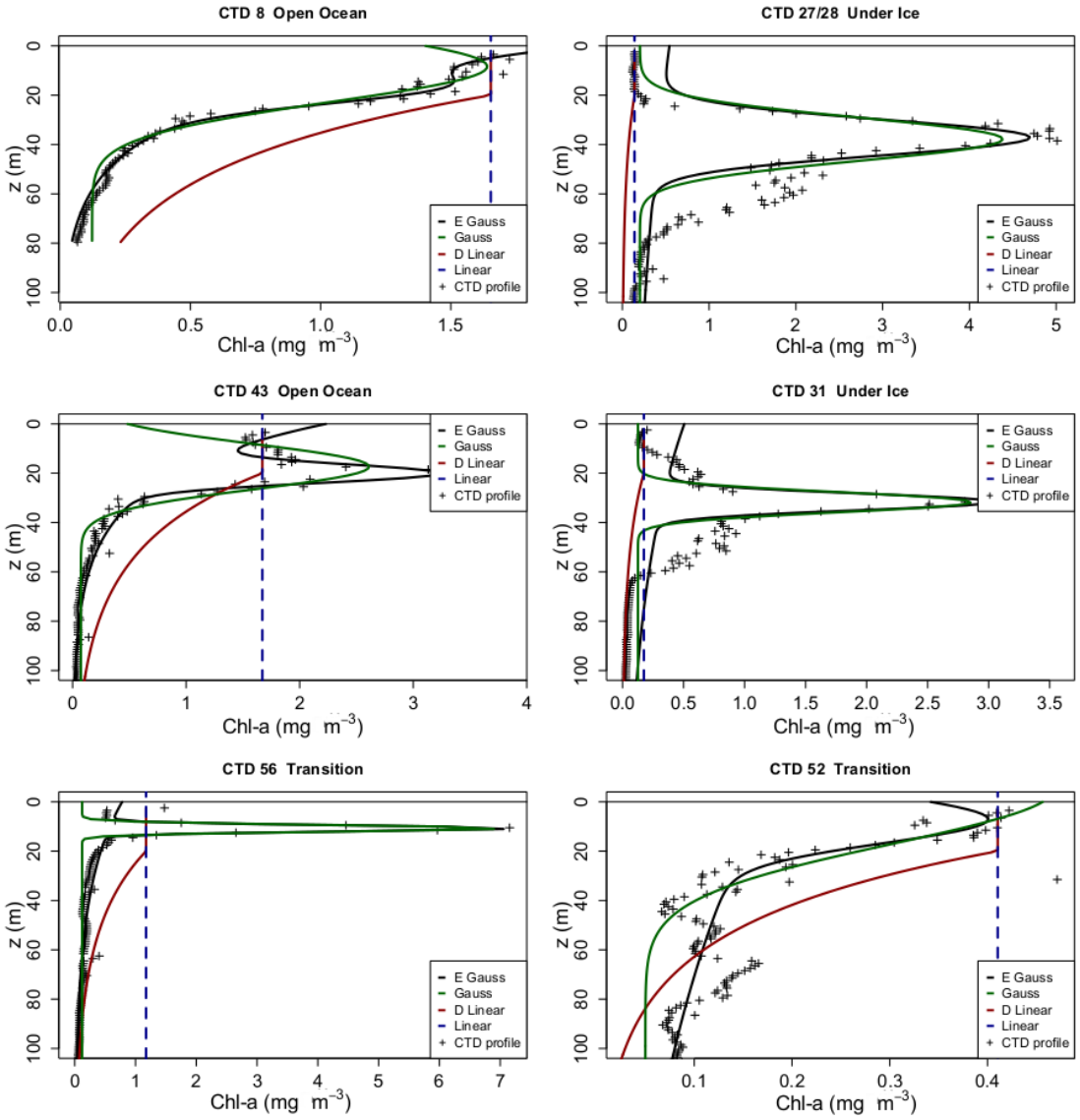

Figure 4.6: The comparative fits of the four biomass profile equations to CTD profiles. This shows the level of performance in a variety of water column situations.

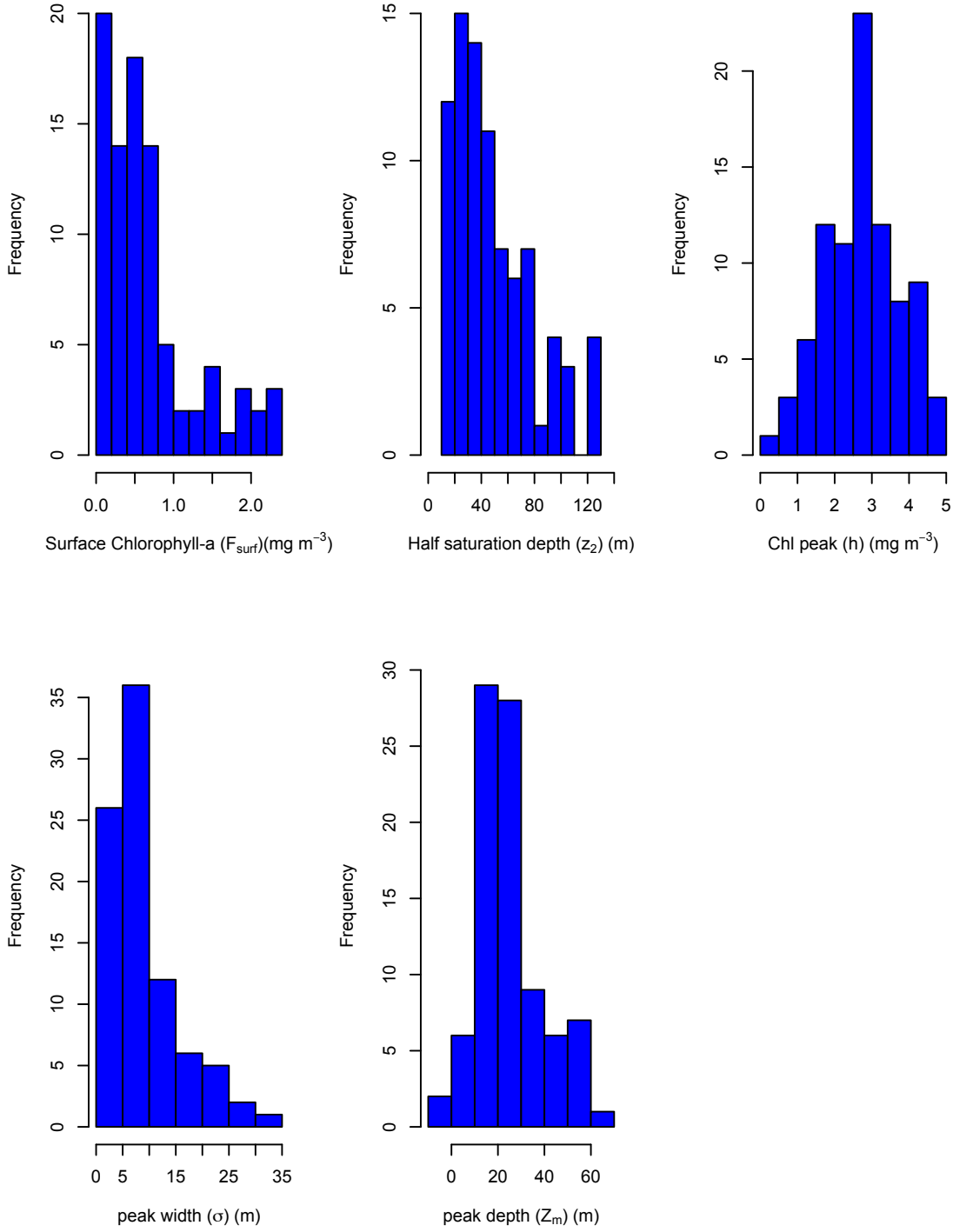

Figure 4.7: Histograms of the exponential Gaussian fit parameters for all CTD casts.

the spectral distribution of PAR (Kirk, 1994). This is shown in figure 4.8 as a general decrease in K_d^{PAR} with depth for a given chlorophyll-a concentration. The relationship is non-linear due to reduced absorption efficiencies in high concentration solutions through self shading (Kirk, 1994).

By comparing the light profiles generated using the Sathyendranath et al. (1989a) model to the hyperspectral profiles measured during the ICE-CHASER 2010 cruise, we can assess the accuracy of the model in describing the spectral properties of the underwater light field and examine whether there is a potential bias due to the assumption that these waters are Case-I. For the assumption of Case-I waters to hold true, the contribution of CDOM on the underwater light field should not be independent of the contribution from chlorophyll-a.

To examine whether adjusting CDOM absorption in proportion to the chlorophyll-a absorption may lead to a better agreement between the modelled and measured light profiles, we varied the relationship between CDOM and phytoplankton absorption. The coefficient of proportionality between a_{CDOM}(440) and a_{Chl}(440)+a_w(440) was set to 0.2 (baseline model), 0.25, 0.75 and 1.0. The first two station profiles available for comparison are from coastal waters near to Svalbard and as expected, the attenuation derived from the hyperspectral radiometer shows a poor agreement with the baseline Case-I water model (Figure 4.9A). Raising the CDOM absorption relative to phytoplankton absorption adjusts the estimates in low K_d waters but is still not high enough in regions of the water column with a high K_d. This means that the CDOM absorption is varying independently from the chlorophyll-a concentration and is contributing significantly to total absorption.

Moving to the open-ocean stations, estimates of K_d for all wavelengths from the Case-

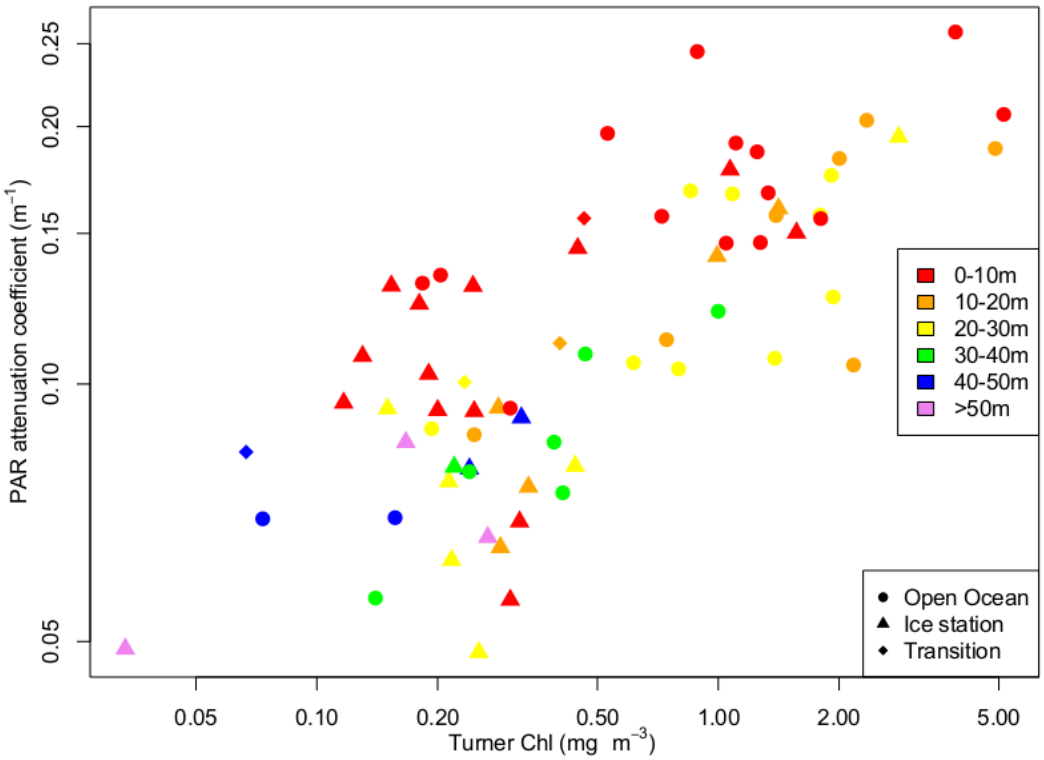

Figure 4.8: K_d^{PAR} from CTD downwelling irradiance data plotted against chlorophyll-a concentration.

I light attenuation model are in good agreement with the radiometer profiles when a_{CDOM}(440)=0.25*(a_{Chl}(440)+a_w(440)) (Figure 4.9B). The under-ice stations show a more complex relationship between modelled and measured light (Figure 4.9C). The strong attenuation of blue light suggests CDOM is contributing significantly to total light attenuation in these waters. By increasing the contribution of CDOM total absorption to 50 % (a_{CDOM}(440)=a_{Chl}(440)+a_w(440) we bring the K_d estimate closer to the *in situ* observations.

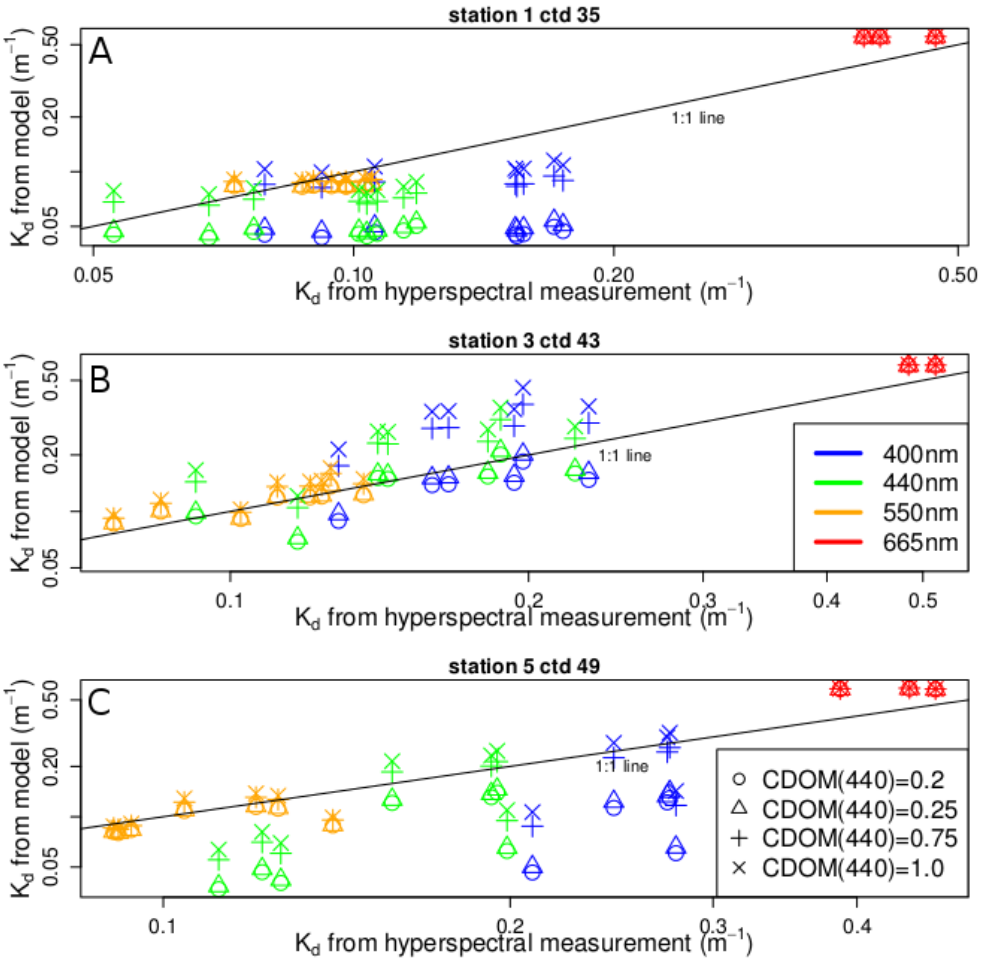

Figure 4.9: A comparison of modelled and measured light attenuation at 4 wavelengths and multiple depths (every 5 m until 40 m or light level below detection limit). Symbol denotes $A_{CDOM}(440)$ relationship to $A_{Chl}(440)$ and the colour denotes the wavelength of light.

Although these data point to CDOM as a potential contributor to strong attenuation in the blue wavebands, attenuation by mycosporine-like amino acids (MAAs) cannot be ruled out. The presence of high levels of MAA-containing phytoplankton in Arctic waters near to Svalbard has been reported by Ha et al. (2012). Some of our absorption samples did show very high absorption in the near UV, supporting the case for MAA presence but we could not quantify the MAAs as the samples had been frozen (Sosik, 1999).

4.3.3 Sensitivity of primary production estimates to input variables

The initial spectral model of primary production Sathyendranath et al. (1989a) was run using a generic spectral shape of phytoplankton absorption. The relationship between phytoplankton absorption at 440 nm ($a_{ph}(440)$) and total biomass was taken from Prieur and Sathyendranath (1981). The CTD fluorescence profile, corrected for quenching using equation 4.12, was used as the biomass profile. Each of the input parameters was then modified and the model was re-run for each of the 19 station profiles to observe the effect on the estimation of primary production for each water type (open, under ice, transition etc). The response in integrated primary production for a profile following a change in model parameters (ΔPP) is given as a percentage and calculated as:

$$\Delta PP = \frac{PP_{mod} - PP_{unmod}}{P_{unmod}} * 100, \tag{4.13}$$

where PP_{unmod} is the primary production estimated prior to the modification of any parameters and PP_{mod} is the primary production following a parameter change.

The primary production modelling results can be split into three groups based on integrated primary production (figure 4.10); 1) under-ice stations with low chlorophyll-a concentrations, yielding very low values of integrated primary production; 2) open ocean waters with high chlorophyll-a concentrations, yielding high primary production; 3) waters that are either ice-covered and possess high chlorophyll-a concentrations or open ocean with low chlorophyll-a concentrations, yielding intermediate primary production. A summary of the potential relative errors from the factors discussed is shown in table 4.2.

The effect of varying IOPs

The first input to be varied was the shape of the phytoplankton absorption spectra ($a_{ph}(\lambda)$). It was changed to the mean of the normalised absorption spectra from the samples taken during the ICE-CHASER 2010 cruise. The resulting difference in integrated production was minimal with a maximum ΔPP of 6.3 %, average ΔPP of 2.5 % and higher ΔPP in stations with larger initial production estimates. We also ran a model with a regional relationship between absolute phytoplankton absorption ($a_{ph}(440)$) and total chlorophyll-a concentration based upon field observations. This allowed us to correct the absorption efficiency of the phytoplankton. Our data show that the Arctic phytoplankton have markedly different absorption efficiencies than proposed by Prieur and Sathyendranath (1981), with Arctic assemblages having lower absorption coefficients per unit chlorophyll-a pigment.

Prieur and Sathyendranath (1981) describes $a_{ph}(440)$ as a two-part function:

$$a_{ph}(440) = \begin{cases} 0.007 + 0.07B & B \leq 1 \\ 0.059 + 0.018B & B > 1. \end{cases} \tag{4.14}$$

Whereas the best fit to the ICE-CHASER 2010 absorption data gives:

$$a_{ph}(440) = \begin{cases} 0.005 + 0.043B & B \leq 1 \\ 0.026 + 0.022B & B > 1. \end{cases} \tag{4.15}$$

Correcting the absorption efficiency had a significant effect on the primary production estimates at all modelled stations, consistently resulting in an increase in the integrated water-column primary production. The average increase using the Arctic equation (4.15) rather than the global equation (4.14) is 26.2 %, with the highest ΔPP being 47.9 %. The magnitude of ΔPP is not related to the total productivity, as with changing the shape of the absorption spectra. Instead, the increase is greatest for stations with a strong subsurface chlorophyll-a maxima, especially if the peak is beneath sea ice.

The model of Sathyendranath et al. (1989a) scales the CDOM absorption spectra such that the absorption by CDOM at 440 nm (a_{CDOM}(440)) is 20 % of the absorption by phytoplankton at 440 nm (a_{ph}(440)). At some stations this assumption was leading to the model predicting a deeper penetration of blue light than was seen in the hyper spectral irradiance profiles. By increasing the a_{CDOM}(440) absorption from 20 % of the a_{ph}(440) to 25 %, 75 % and 100 % of the a_{ph}(440), we could match different irradiance profiles (as in section 4.3.2). This led to a decrease in primary production since the CDOM absorbs light that would otherwise be available for photosynthesis (see figure 4.10). The effect of increasing the a_{CDOM}(440)/a_{ph}(440) to 0.25 is minimal and only ef-

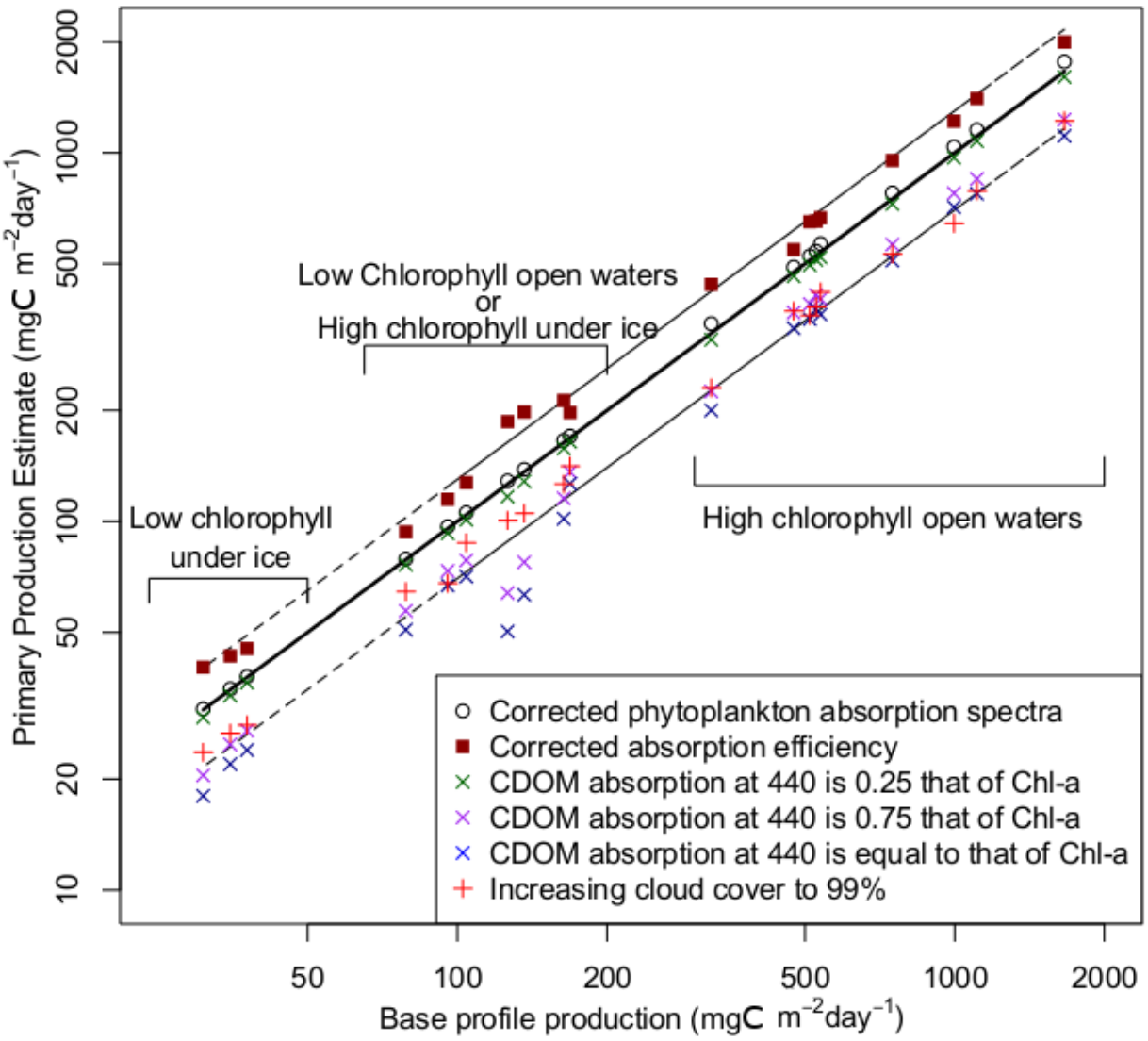

Figure 4.10: The change in the spectral model estimate of primary production when the optical properties of the phytoplankton and water column are brought in-line with regional measurements.

fects production estimates by around 3.5 %. With an increase in $a_{CDOM}(440)/a_{ph}(440)$ to 0.75, primary production decreased by 28 % on average. When $a_{CDOM}(440)$ equals that of phytoplankton, the ΔPP was around -35 % on average. The ΔPP was higher for the under-ice profiles and the most extreme reduction of primary production (-60 %) was seen at a station that also had a strong SCM.

Effects of vertical variability in the biomass profile

Primary productivity at the 19 stations was calculated using each of the four profile types mentioned previously (equations 4.3 4.4, 4.7 4.8). We consider the most accurate estimate of primary production to be derived using binned data from the calibrated CTD fluorescence profile. The primary production estimates from the four models are shown in comparison to this in figure 4.11.

Some stations show good agreement between different representations of the chlorophyll-a profile (from uniform biomass to exponential Gaussian) with ΔPP values of $<$10 %. Stations that show a discrepancy between model estimates tend to have low surface chlorophyll-a concentrations and a pronounced subsurface chlorophyll-a peak. At these stations, estimates can differ by a factor of three between the linear-decay and exponential-Gaussian models. For most stations, the biomass profile chosen can effect the estimate by $\approx$30 %, though in extreme cases it can be higher. Most of the errors introduced by fitting equations to the biomass profiles lead to underestimates of primary production, though in a couple of cases the estimated primary production does increase. The largest error (ΔPP of -69.2 %) was due to the use of the Arrigo style profile.

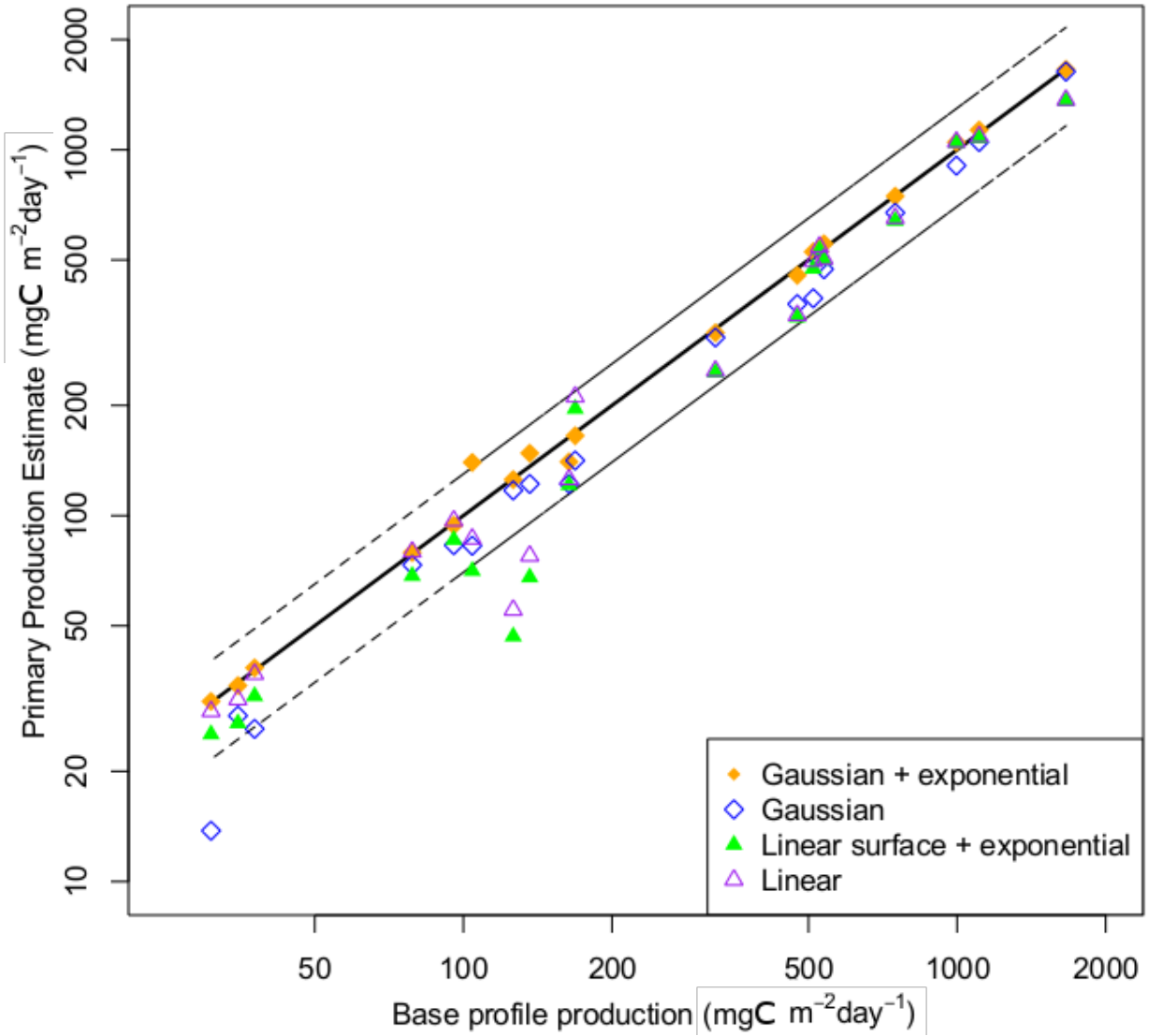

Figure 4.11: The change in the spectral model estimate of primary production when different equations are used to describe the vertical profile of chlorophyll.

Effects of photophysiological parameters and irradiance levels

Thus far, all the production model runs have used photophysiological parameters for each station measured by *P-E* incubations. If one were to incorrectly assign the *P-E* parameters then how much error could be introduced? The model was run using the extreme photophysiology values from the IC2010 data, P_m^B (0.55–9.60 mg C (mg chl-a)$^{-1}$ h^{-1}) and α (0.007–0.052 mg C (mg chl-a)$^{-1}$ h^{-1} (μ mol quanta m^{-2} s^{-1})$^{-1}$). Figure 4.12 shows that errors in the assignment of the *P-E* parameters can cause the largest errors in the estimation of integrated primary production (ΔPP $\pm$ 80 %) of any of the parameters examined. The range in primary production estimates caused by changes in α^B is greater than those produced by changes in P_m^B. The stations beneath sea ice also showed a stronger sensitivity to variation in α^B, likely because the natural range in values is lower.

As surface irradiance is a modelled variable input to the primary production model, we can also assess the sensitivity of primary production estimates to varying cloud cover (incident irradiance).

The model was run under conditions of 1 % and 99 % cloud cover to see the effect of varying incident light on the different production estimates. As expected, the PP is decreased with increasing cloud cover. However, the change in the PP caused by increasing cloud cover (16-35 % decrease in PP), is least pronounced for stations with sea ice. The insensitivity of the sea-ice stations to the quantity of incident irradiance is related to the adaptation of these phytoplankton communities to low-light conditions. One way of assessing whether a community of phytoplankton are dark adapted is to use the photo-acclimation parameter E_k, which is a measure of the optimum light level for

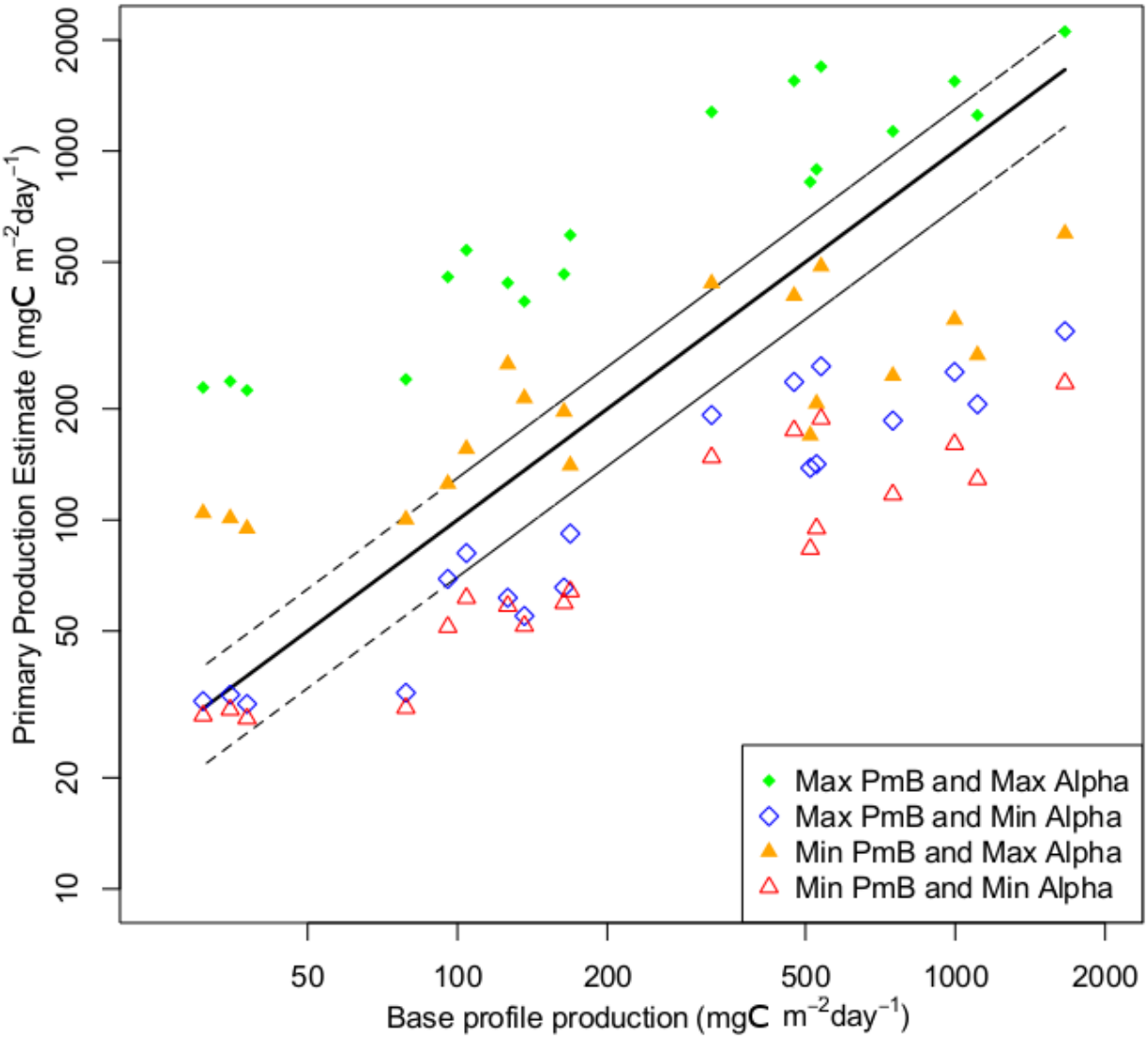

Figure 4.12: The change in the spectral model estimate of primary production when photophysiological parameters are set to extreme values.

Table 4.1: Production model error due to biomass profile equation, relative to baseline model. Profile equation abbreviations are: Exponential Gaussian (EGa), Gaussian (Ga), Linear (Lin) and Arrigo (Ar). The Behrenfeld model (Be) and Eppley model (Ep) errors are also shown. A suffix of 1 or 99 indicates 1 % or 99% cloud cover respectively.

	EGa1	EGa99	Ga1	Ga99	Lin1	Lin99	Ar1	Ar99	Be1	Be99	Ep1	Ep99
Mean error	2.8	2.7	-18.5	-18.5	-8.1	-7.8	-16.4	-16.5	156.6	207.4	119.1	158.0
Open error	2.1	2.0	-15.5	-15.4	-6.7	-6.1	-13.7	-13.2	128.7	187.3	60.1	99.2
Ice error	4.1	4.0	-24.1	-24.1	-10.7	-10.9	-21.6	-22.6	208.3	244.8	228.5	267.4

growth of the phytoplankton. The ICE CHASER 2010 data shows that the under-ice phytoplankton possess a low E_k, most commonly around 50 μEinsteins. The attenuation of light by sea-ice acts to dampen the change in under-ice irradiance variations associated with large changes in absolute surface irradiance.

4.3.4 Comparison to a non-spectral VGPM model

A comparison of the spectral model estimates to independent deck incubations and the VGPM is shown in figure 4.13. The modified VGPM models showed a reduced sensitivity to variations in cloud cover, and therefore a reduced sensitivity to incident irradiance (figure 4.13), when compared to the spectral models for open-ocean stations. The parameterization of Behrenfeld and Falkowski (1997a) consistently overestimates production and the mean overestimate is 156 % for 1 % cloud cover and 207 % for 99 % cloud cover. Assigning P^B_{opt} using the Eppley temperature response curve resulted in a lower mean error than the Behrenfeld and Falkowski 7th order polynomial (table 4.1) but the improvement is exclusively in the open-ocean waters.

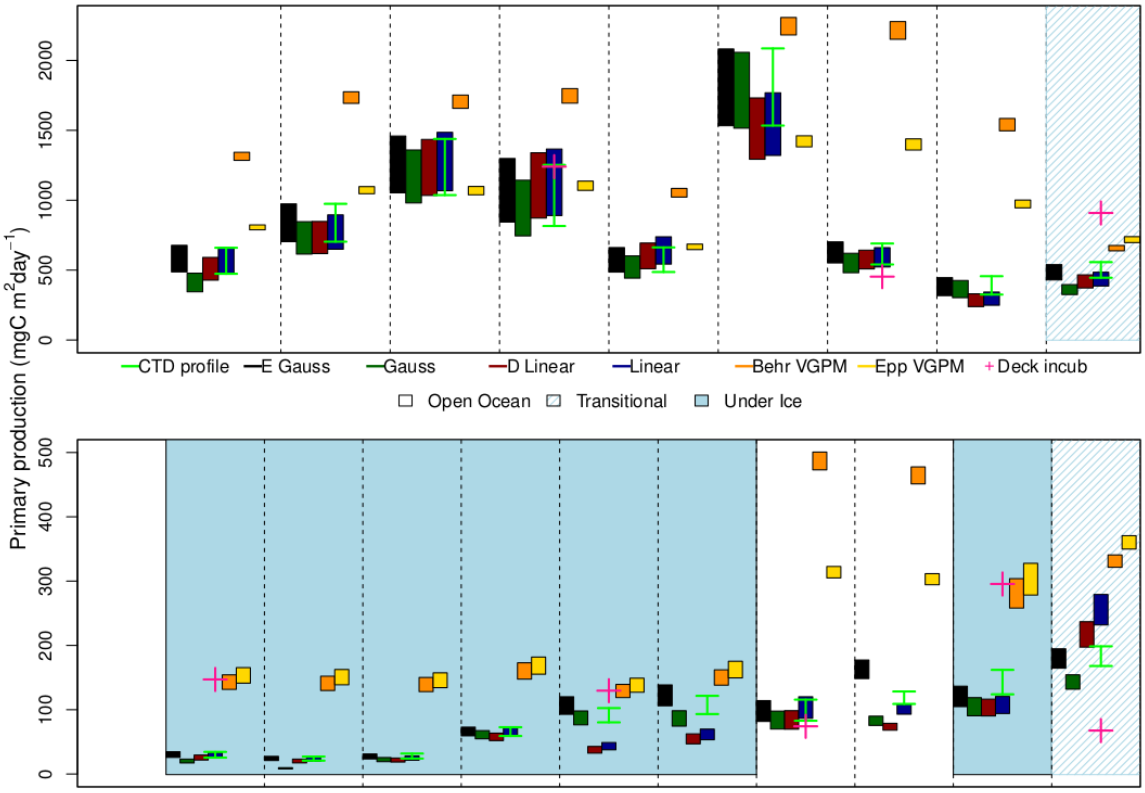

Figure 4.13: Calculated primary production for 19 Arctic stations using adapted a phytoplankton absorption spectra and absorption efficiency to chl-a relationship derived from in-situ measurements. The CDOM contribution to absorption(440) was scaled to 0.2 * chl-a(440) plus water(440) absorption in open ocean waters and 0.75 beneath sea ice. Each station has an estimate for each of the profile types, where the bar depicts the production range from cloud covered to clear skies. The production using the actual fluorescence profile is shown in light green and independent deck incubation estimates are shown in pink.

4.4 Discussion

4.4.1 PAR data sources

Although there is agreement between the cosine-weighted SeaWiFS PAR and underway data, the variation in cloud cover and small percentage of days with valid remotely sensed data (5 days of remote sensing estimates from over 25 days of cruise data) mean that this data source does not have sufficient coverage for input into primary production models.

In general the BIRD PAR model reproduces much of the surface irradiance seen at high latitudes, especially during periods of high cloud cover. The model, however, does not match the highest light observed near noon under very clear skies. The Bird model has been previously shown to reproduce irradiance spectra at low solar elevation angles (Bird and Riordan, 1986; Campbell and Aarup, 1989), with errors of less than 10 % for the visible spectrum. This work supports the conclusion that the model is suitable for high latitudes, though it also suggests some adjustment may be needed for clear-sky conditions.

In summary, the Bird model tends to consistently underestimate the underway observations at the highest intensities. It does, however, give a high temporal resolution and describes the majority of the observational data. The SeaWiFS PAR data product provides a reasonable estimate of daily PAR reaching the sea surface. However our results suggest that diel variability in the daily PAR estimates should be considered, especially when only a single valid data point exists for the day of interest, i.e. only one valid image for a given day.

4.4.2 Parameterization of IOPS

In all stations, subtle changes in the average phytoplankton absorption spectra does not produce a significant change in the level of primary production. That is not to say that specific phytoplankton absorption spectra would not be beneficial in certain light regimes (Hickman et al., 2010), merely that for modelling purposes a general phytoplankton absorption spectra does not introduce errors to the same level as other parameters.

The absorption efficiency of phytoplankton is equally important in all stations and is known to vary due to factors such as cell size and pigment assemblage. A decrease in absorption efficiency acts to increase total production as PAR propagates further into the water column.

Increasing the relative absorption by CDOM acts in opposition to decreasing the absorption efficiency, attenuating light. However, this is not necessary in all environments and does not mean that we cannot use a model dependent upon chlorophyll concentration. Beneath sea ice and close to the ice-edge, we observe a high contribution of absorption by CDOM. Unlike coastal waters, CDOM absorption co-varies with chlorophyll-a and as such the waters can still considered as Case-I. Thus, our results suggest that we can model the under-ice and open-ocean waters during the ICE-CHASER 2010 cruise using a Case-I model, with a higher CDOM contribution to total absorption beneath the sea ice. There are two possible explanations for the increased CDOM absorption beneath sea ice. There is either increased production of CDOM or better preservation of CDOM beneath sea ice. Recent estimates of the distribution of fluvial inputs of DOM in the Arctic show that there is little input into the Greenland Sea from terres-

trial sources (Fichot et al., 2013). It is likely that the CDOM is organically produced (Steinberg et al., 2004), but it is unclear as to why this would preferentially increase the CDOM contribution to absorption beneath sea ice. Photobleaching and photomineralization can act to reduce CDOM absorption in Arctic waters (Osburn et al., 2009) and would be inhibited by the presence of sea ice. If the CDOM is predominantly organically produced and is protected from photobleaching beneath sea ice then this would explain the correlation of CDOM absorption with phytoplankton biomass and the different coefficients of proportionality between under-ice and open-water stations. The a_{CDOM}(440)/(a_{Chl}(440)+a_w(440)) ratio remains variable for coastal waters and a separate model is still required for those regions.

4.4.3 Parameterization of the biomass profile

The most complex representation of *B*(z)(equation with the highest number of parameters) provides the best fit to a given profile (figure 4.6). But is such complexity required for primary production estimates? The more complex profile gives a similar primary production estimate to the simple profile under uniform mixed-layer conditions, but for a complex vertical biomass distribution the simple profiles underestimate water-column productivity. Examining the magnitudes of integrated water column primary production across the stations, it becomes clear that the model results can be grouped into pairs. The linear-profile model and the Arrigo-profile model show the same trend from station to station and have a nearly identical magnitude at all locations. Similarly, the shifted Gaussian and the exponential-Gaussian have similar primary production estimates.

The exponential-Gaussian equation provides the best fit to the profile data and shows

excellent agreement to the estimates using the CTD biomass profiles. The on-deck incubation results show a slightly better agreement with the two Gaussian-based estimates of primary production than the linear and linear + decay estimates.

The errors associated with an incorrect profile and exclusion of an SCM estimated here are similar to the estimates of Hill et al. (2013) (up to 90 % of profile production contained in the SCM in the Greenland Sea) and slightly larger than those by Arrigo et al. (2011).

4.4.4 Parameterization of photophysiology

As found in the work of Milutinović and Bertino (2011) the largest errors in primary production estimates were due to variation in the parameterization of photophysiology. Here, however, we see that the effect of α^B variation is greater than that produced by changes in P_m^B, particularly for stations beneath sea ice. The values used here were not outside of the natural variation seen in field samples. Trying to assign these parameters remotely could introduce even larger errors unless the relationship used is robust and verified for this region. We are most likely to over-estimate production for low-chl under-ice conditions (which usually have low P_m^B and α^B) and under estimate production for high-chl open-ocean waters.

4.4.5 Assigning model parameters for other locations

The exponential-Gaussian model best describes the variability in the shape of the biomass profiles over a range of sea-ice conditions in the Greenland Sea and when used in primary production models provides the most accurate estimates. However, in order to use

Table 4.2: Importance of primary production model parameters by water type

Input Parameter		ΔPP range	Open Ocean High Chl	Open Ocean Low Chl	Under Ice High Chl	Under Ice Low Chl
a_{ph} Spectra		+0.5 to +6.3%	Low	Low	Low	Low
Absorption efficiency		+15.1 to +47.8%	High	High	High	High
Cloud Cover		-16.0 to -35.5%	High	High	High	High
Biomass Profile Equation		-69.2 to +34%	Low	High	High	Low
Photophysiological	(P_B^m)	± (15 to >80%)	High	High	Low	Low
Parameters	(α_B)	± (15 to >80%)	High	High	High	High
	(0.25)	-2.4 to -7.5%	Low	Low	Low	Low
CDOM Scaling with Chl	(0.75)	-19.2 to -49%	Low	Low	High	High
	(1.00)	-24.9 to -60.1%	Low	Low	High	High

this profile equations across broad spatial and temporal scales in conjunction with remote sensing data, the biomass profile parameters need to be assigned in the absence of *in situ* data. Assignment of biomass profile parameters has been done using a number of approaches, including using 1) correlation between biomass parameters and remotely-sensed variables (Platt and Sathyendranath, 1999), 2) climatologies (Morel and Berthon, 1989), 3) nearest neighbour parameter assignment (Platt et al., 2008), 4) look-up tables (Antoine et al., 1996) and 5) assignment based on biogeochemical provinces (Longhurst et al., 1995).

We investigated whether the five parameters required for the exponential-Gaussian profile show any relationship to environmental variables that are accessible using remote sensing. The surface chlorophyll-a variable B_{surf} is strongly correlated with the remote sensing detected chlorophyll-a concentration. As B_{surf} increases, z_2 decreases, meaning that for biomass profiles with a high surface chlorophyll concentration, the decrease of chlorophyll-a with depth is more rapid. This may be due to the strong attenuation

of light in higher biomass waters. The surface chlorophyll-a concentration, sea-surface temperature, and salinity (available remote sensing variables) showed no strong correlation with the parameters used to describe the sub-surface peak and do not show any relationship to water-column 'type' (Figure 4.14). One way forward might be to adopt a nearest-neighbour approach to the assignment of biomass profile parameters (Platt et al., 2008). However, this approach requires a very large database, which is lacking in this sector of the Arctic at present. Thus, in the absence of field observations, the best approach would be to use a simple combination of predictor variables accessible to remote sensing (such as mixed layer depth) and simpler profile types.

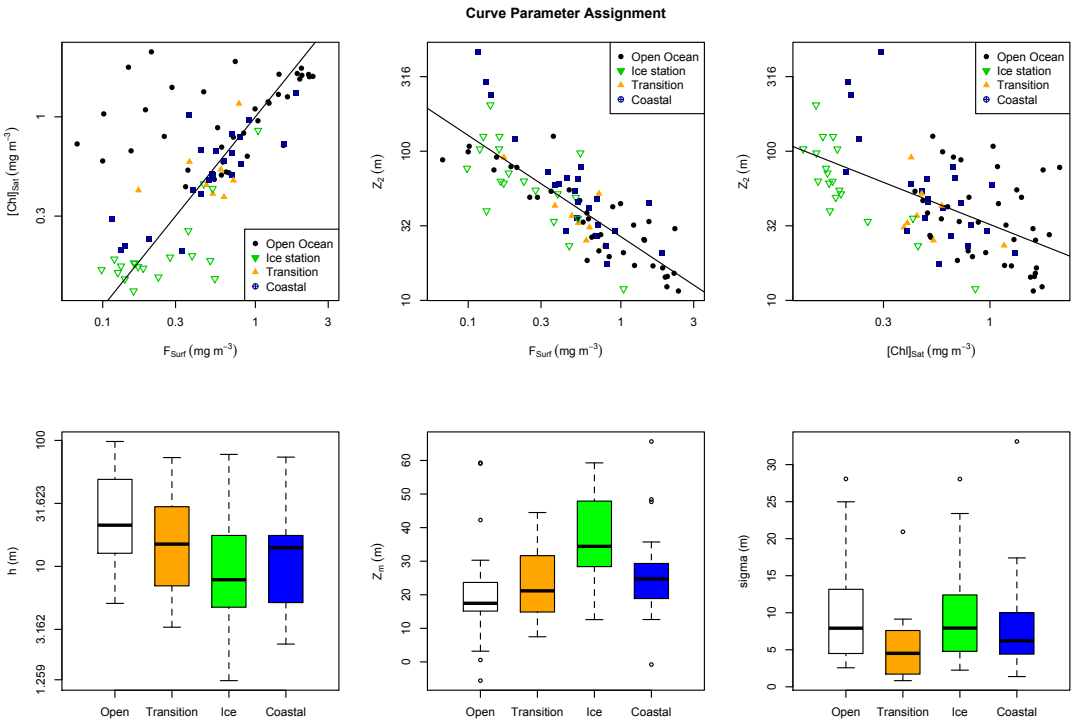

Figure 4.14: Plots showing the relationship between curve parameters and proxy variables/province types for the exponential Gaussian curve fits.

4.5 Conclusions

It is thought that the predictive power of large scale GCMs for the Arctic may decrease in a warming Arctic ocean due to a decoupling of light and nutrient controls with retreating sea ice (Popova et al., 2012). Well parameterized optical models should not be affected in a similar way, but our ability to assign variable parameters needs to improve if we are to have confidence in our primary productivity estimates. The most important parameters to constrain depend upon the conditions of the water column, namely the presence of sea ice and the level of biomass.

The important sources of error for under-ice low-chlorophyll-a stations deal with factors relating to light availability and utilization, including the absorption efficiency of phytoplankton, attenuation of light by CDOM and cloud cover. The factors can independently result in errors greater than 30 %. However, due to the low biomass and hence primary production at these stations during the summer months, errors will likely not lead to significant changes in the estimation of annual primary production.

Under-ice stations with a significant subsurface peak (Chlorophyll-a >1 mg m^{-3}) can be subject to large relative errors in primary production. Changes in the phytoplankton absorption efficiency can increase the production estimates by nearly 50 %, whereas using simple biomass profiles causes an underestimation of primary production by as much as 62 %. Correctly estimating the contribution of absorption from CDOM is also very important under sea ice, since any factor which decreases the availability of PAR at depth reduces the productive potential of a deeper chlorophyll-a peak.

The open ocean stations show a similar sensitivity to input parameters whether they are high or low chlorophyll-a. Phytoplankton absorption efficiency and cloud can affect

primary production estimates by around 25-30 %. Increasing the CDOM decreases primary production by up to 38 % and shows a stronger effect in the low chlorophyll-a waters. These waters did not actually have CDOM contents this high and so this factor is not currently important in non-coastal, open waters. Although a warming Arctic may increase terrestrial inputs of CDOM to Arctic surface waters, which would significantly reduce primary productivity. The importance of the profile equation used was generally low (mean 6 % error for linear profile), but for stations with a subsurface chlorophyll-a peak the errors were up to 25 % for using a linear model.

The P-E parameter assignment has the largest effect on the production estimates across all stations. It is of note that α^B has a stronger affect than P_m^B and was more influential for under-ice stations.

To consider the importance of the error in input parameters, we must combine the sensitivity of the model with our confidence in our estimates. Some factors such as cloud cover can cause a significant variation in the estimate of primary production (up to 35 %) but can be quantified or estimated from remote sensing data for regional production estimates. Other factors such as the photophysiological parameters and biomass profile types are difficult to assign, yet have a significant impact on our estimate of primary production.

Despite Arctic marine environments providing a unique set of challenges to modelling primary production, this study shows that some factors are more important than others when estimating the primary production across gradients of sea-ice cover. Our results suggest that accurate assignment of the photophysiological parameters in this region is critical, especially beneath sea ice. The absorption efficiency of the phytoplankton and the cloud cover/incident irradiance are also important as they affect all the production

estimates by around 30 %. The complexity in the vertical profile of chlorophyll-a is less important in high-production open waters, where biomass is focussed near the surface, but can be important in under-ice and marginal ice zones as they can exhibit a subsurface maxima in chlorophyll-a. Although CDOM is clearly important when modelling light attenuation in Arctic waters, this study shows that the non-coastal summer waters of the Atlantic Arctic appear to be Case-I waters where the optical properties can be modelled using chlorophyll-a concentration as the only variable.

It is likely that we currently underestimate summer production, due to the failure to include subsurface biomass peaks and under ice production. These can act as a significant contributor to total production in ice-influenced regimes for the post bloom period. The spring bloom phase in the Arctic can be short and followed by an extended period of post bloom conditions (Hill and Zimmerman, 2010), so the relative contribution of the subsurface production when summed over the total growing season is not insignificant. Moreover, this open-ocean low-chlorophyll-a condition may become more prevalent if sea ice melts back earlier in the year, causing oligotrophic conditions in the surface layer.

This study also highlights the need to improve the radiative transmission models in the Arctic, so that they capture the full range of irradiances observed in the region. In particular, there is a pressing need to develop models that can estimate spectral light transmission through various sea-ice conditions.

Table 4.3: Symbols and units used in the study

Symbol	Units	Description
α^B	mgC mgChl^{-1} h^{-1}(μ mol m^{-2}s^{-1})$^{-1}$	Low light efficiency of carbon fixation.
a$_{CDOM}(\lambda)$	m^{-1}	Absorption by coloured dissolved organic matter at wavelength λ.
a$_{Chl}(\lambda)$	m^{-1}	Absorption by chlorophyll-a at wavelength λ.
β^B	mgC mgChl^{-1} h^{-1}(μ mol m^{-2}s^{-1})$^{-1}$	Photo-inhibition of photosynthesis at high irradiance intensities.
B$_0$	mgChl m^{-3}	Background chlorophyll-a concentration for shifted Gaussian profile.
$\bar{B}_{sat}$	mgChl m^{-3}	Mean depth weighted chlorophyll-a concentration (1st optical depth).
ΔChl	mgChl m^{-3}	Chlorophyll correction applied for near surface fluorescence quenching.
ΔPP	mg C m^{-2}	Change in primary production in response to a change in model parameters.
F$_{surf}$	mgChl m^{-3}	Surface Chlorophyll parameter for Gaussian plus exponential model.
h	mgChl m^{-3}	Magnitude of biomass peak in Gaussian biomass profile equations.
I	μEinsteins m^{-2}s^{-1}	Irradiance
k$_d$	m^{-1}	downwelling attenuation co-efficient
PAR	μEinsteins m^{-2}s^{-1}	Photosynthetically available radiation (400-700nm).
P^B_m	mg C (mg chl a)^1 h^1	Maximum photosynthetic rate with photo-inhibition.
σ	m	Width of chlorophyll peak in Gaussian biomass profile equations.
z$_2$	m	Depth at which background chlorophyll reaches half F$_{surf}$.
z$_m$	m	The centre of the peak in Gaussian biomass profile equations.

Chapter 5

Summary

The Arctic marine environment plays an important role in global biogeochemical cycling (Bates and Mathis, 2009). Recent observations show a strong physical response to climate change in the Arctic (Johannessen et al., 2004) but the biological repercussions of this environmental forcing are poorly understood. Changes in the distribution and physiology of phytoplankton in the region are important for both geochemical budgets and regional ecology through their influence on primary production dynamics. This thesis has aimed to provide an insight into the current variability of phytoplankton community structure and photophysiology with a view to understand how the ecosystem might respond under future climate warming. It has also considered the level of complexity required to best model primary production in this region and key variables to constrain when modelling primary production in the region.

Chapter 2 presented an assessment of the distribution of phytoplankton in the Atlantic Arctic. Six major phytoplankton groups were seen to dominate phytoplankton assemblages in the study region; diatoms, haptophytes, cryptophytes, chrysophytes, dinoflag-

ellates and prasinophytes. The groups contributing the largest fraction of integrated biomass were diatoms and haptophytes. Group distributions were correlated with presence of sea ice, the strength of water-column stratification and nutrient concentrations. There was a regional trend for phytoplankton populations to be of a mixed taxonomic composition at depth, with assemblages dominated by single groups in surface waters, due to increased environmental stress and selection pressure.

During the examination of phytoplankton community variability in Arctic waters, CHEMTAX pigment methods were validated against microscopy data. This study demonstrates that CHEMTAX can correctly identify groups contributing the majority of phytoplankton biomass in the Arctic, using a regionally-tailored seed matrix. Separation of samples based on optical depth and conducting multiple iterations of the subroutine allowed CHEMTAX to account for photoacclimatory variation in group-specific pigment ratios. This work also highlighted issues that may need to be addressed in future work, such as the presence of photosynthetic ciliates that contains phytoplankton accessory pigments and dinoflagellates that do not possess the marker pigment peridinin.

Group-specific differences in the shape of phytoplankton absorption spectra and absorption ratios were observed in both Arctic field and culture samples. The relationship between absorption efficiency and chlorophyll-a appeared to be consistent across the Atlantic Arctic, irrespective of dominant phytoplankton group, and was markedly different from the relationship documented at lower latitudes (Prieur and Sathyendranath, 1981; Bricaud et al., 1998). This has important implications for remote sensing studies of phytoplankton at high latitudes (Stuart et al., 2000; Sathyendranath et al., 2001; Nair et al., 2008) as regional and group-specific differences in bio-optical properties can influence both biomass and primary production estimates based on ocean colour data.

Chapter 3 investigated the sources of variation in photophysiology in the Atlantic Arctic and compared data from the Greenland Sea to other sectors of the Arctic to establish whether physiological parameter to environmental variable relationships were local or regional. Our field data agreed with the work of Huot et al. (2013) that larger cells (diatoms) possess higher P_m^B values than other phytoplankton groups, though culture data highlighted the significance of temperature on photophysiological rates. The photophysiological parameters measured in the field seem to be primarily controlled by physical factors rather than inter-group variation. For all waters phytoplankton P_m^B was strongly influenced by temperature and in open-ocean waters α^B varied with depth (irradiance). The variation of α^B with depth was minimal beneath sea ice due to the constraints imposed by low absolute-irradiance variability and suppression of P_m^B by low temperatures. Strong stratification beneath melting sea ice causes stable environmental conditions. This stability, in combination with the low level of irradiance penetrating the sea ice and persistent low temperatures, leads to a reduced range in phytoplankton photophysiology beneath sea ice.

Changes in bio-optical properties, photophysiological parameters and environmental conditions all influence marine primary production. If the variation in these parameters is systematic across an area then a single set of equations or relationships may be applied. Given that the photophysiology seems to be dominated by water temperature and the presence of sea ice and the absorption efficiency of phytoplankton was relatively constant across the Atlantic Arctic, it should be possible to treat the Atlantic Arctic as a single region from the perspective of modelling primary production in relation to the major forcing factors.

In chapter 4 the measurements of phytoplankton absorptive and physiological proper-

ties were combined with a spectral primary production model developed by Sathyendranath et al. (1995). The modelling of primary production using multiple biomass profile equations, measured and estimated photophysiological parameters and spectral and non-spectral models allowed the importance of different parameters on primary production estimates to be assessed. This study demonstrated that the most important parameters to constrain in primary production models in the Arctic depend upon: 1) the amount of biomass in the water column and 2) the presence of sea ice. In general, the phytoplankton photophysiology and the vertical structure of biomass in the water column have the largest influence on primary production estimates, as seen in previous studies (Platt et al., 1991; Milutinović and Bertino, 2011). However, the equation used to describe the biomass profile is less important in high-biomass, open-ocean waters since most of the primary production is concentrated near the surface. Of the bio-optical properties, phytoplankton absorption efficiency is more important to correctly estimate than the details of the shape of the absorption spectrum. Chapter 4 also demonstrated that the optical modelling of some Arctic waters may be possible with a modified Case-I water type, where absorption by CDOM is higher than in normal Case-I waters but remains proportional to chlorophyll-a concentration.

The estimates of primary production using a spectral model for Arctic waters ranged from 21 to 161 mg C m^{-2} d^{-1} at under-ice stations and from 80 to 2086 mg C m^{-2} d^{-1} in the open-ocean waters. The SCM was a prevalent feature in this region and contributed up 84 % of integrated primary production beneath sea ice. The simplest primary production models had significant errors in their estimates of primary production. The Behrenfeld and Falkowski (1997) model, for example, systematically over-estimated primary production and performed particularly poorly at sea ice stations. This error

was partially due to an overestimation of maximum photosynthetic rate. These results mean that we should be wary of interpreting the results of simple models of primary production in the Arctic as they are unlikely to capture the complexity of the system, introducing significant error.

The data presented here on community structure, physiology and primary production highlight that the boundary between sea-ice and open-ocean waters leads to a marked change in multiple aspects of the marine ecosystem. The dominant phytoplankton groups, variation in photophysiology through the water column, and average primary production all change dramatically across this boundary. The formation of sea ice in the winter and its retreat in the summer is one of the defining features of the Arctic Ocean and the area of perennially ice-covered Arctic Ocean is increasing under the influence of climate change.

From our insights into the variability in the distribution and physiology of phytoplankton in the Atlantic Arctic, we can speculate on about the likely response of phytoplankton in this region to future climate change.

The key factors likely to influence phytoplankton are: 1) the loss of sea ice in the summer, both the extent of open water and the timing of the sea-ice retreat, 2) a warming of ocean surface temperatures, 3) changes in the stratification of surface waters through increased melt-water input and wind-stress.

Our data shows that the loss of sea ice will likely increase the variation in phytoplankton photophysiological parameters due to greater light penetration into the water column. Increasing water temperatures will also raise P_m^B values and allow a greater variation in photoacclimation through variation in α^B values. Our data also suggest that a larger

region of open water in the summer will lead to an increase in primary production, though under-ice production should be taken into account in these calculations, as sea-ice covered areas are productive prior to ice retreat (Gradinger, 1996; Arrigo et al., 2012).

If increased melt-water input and sea-ice melt results in increased Arctic stratification, we will likely see a widespread and extreme depletion of nutrients in surface waters, promoting the formation of productive sub-surface biomass maxima in open waters. If stratified open waters persist for long periods over the summer, the subsurface biomass peak could be important in relation to integrated annual primary production. If wind stress increases and overcomes melt-water and thermal stratification, productivity in the surface layer could increase greatly. Changes in the stratification may also lead to a transition in the dominant phytoplankton groups. Increased open water mixing and rising water temperatures may favour the growth of haptophytes in the region but increase melt-water input may lead to the dominance of prasinophytes in strongly stratified, cold surface layers. If an increase in production is co-incident with a shift in dominant phytoplankton group, away from diatoms, there may not be a synchronous increase in carbon export, as diatoms are more efficient at exporting carbon than many other phytoplankton groups (Buesseler, 1998). The extent and boundaries between regional water masses may also play a large role in the biological response to climate change. Shifts in the boundaries between Atlantic and Pacific halocline layers below the polar mixed layer could influence nutrient supply and water column stability due to different temperature and salinity profiles.

Overall, it appears that primary production will increase in a warming Arctic due to an increase in the areal extent of open waters and higher maximum photosynthetic rates.

Alongside this increase there will likely be an altered distribution of phytoplankton groups, which may lead to changes in ecosystem dynamics and biogeography. The location of the ice-edge is of great importance, not only as it promotes the upwelling of nutrients but because of the biological transitions that take place in the ice-edge zone.

5.1 Future directions

The diversity of phytoplankton observed here highlights the need for further high-resolution investigation of phytoplankton biogeography in the Arctic Ocean. Questions remain regarding dominance of particular phytoplankton groups, e.g are the prasinophytes commonly associated with the presence of a strong halocline layer and is this association related to regional nutrient and water-mass dynamics?

The routine use of CHEMTAX in the Arctic will aid our understanding of the biological response to climate forcing. The Arctic-tailored seed matrix used in this study could be used for larger datasets to assess phytoplankton variability on larger spatial or temporal scales. It would be of interest to perform a similar analysis of the performance of the CHEMTAX matrix using pigment and taxonomic data from another Arctic region. In general the use of CHEMTAX in the Arctic still requires validation against other coincident taxonomic data and the quantification of dinoflagellates and cryptophyte biomass requires further investigation.

This study has highlighted the unique photophysiology of the Atlantic Arctic with region-specific relationships between; P_m^B and temperature, α^B variability and sea-ice presence, and absorption efficiency with total Chl-a. Future work involving the use of techniques such as FRRf could allow a greater insight into observations of low quantum

yields and photoacclimation strategies beneath sea ice. It would also be worth comparing these results to those from the Pacific influenced Arctic.

To improve future estimates of Arctic primary production it is essential that we can reasonably parameterize the photophysiology and biomass profile for a given water column. This work has shown that some of these parameters may be estimated from proxy variables but others may require the use of alternative approaches, such as nearest-neighbour methods, after the construction of a larger database of measurements. It would also be of use to integrate a more realistic sea-ice optical layer into the radiative transmission model, which could account for factors such as melt ponds and changing snow cover on the underwater light field.

Bibliography

Aagaard, K. and Carmack, E. C. (1989). The role of sea ice and other fresh water in the Arctic circulation. *Journal of Geophysical Research*, 94(C10):14485–14498.

Ackleson, S., Balch, W., and Holligan, P. (1994). Response of water-leaving radiance to particulate calcite and chlorophyll a concentrations: A model for Gulf of Maine coccolithophore blooms. *Journal of Geophysical Research:Oceans*, 99:7483–7499.

Antoine, D., Andre, J., and Morel, A. (1996). Oceanic primary production, II, Estimation at global scale from satellite (Coastal Zone Color Scanner) chlorophyll. *Global Biogeochemical Cycles*, 10(1):57–69.

Antoine, D. and Morel, A. (1996). Oceanic primary production, 1, Adaptation of a spectral light-photosynthesis model in view of application to satellite chlorophyll observations. *Global Biogeochemical Cycles*, 10(1):43–55.

Ardyna, M., Gosselin, M., Michel, C., Poulin, M., and Tremblay, J. (2011). Environmental forcing of phytoplankton community structure and function in the Canadian High Arctic: contrasting oligotrophic and eutrophic regions. *Marine Ecology Progress Series*, 442:37–57.

Arrigo, K. R., Matrai, P. a., and van Dijken, G. L. (2011). Primary productivity in

the Arctic Ocean: Impacts of complex optical properties and subsurface chlorophyll maxima on large-scale estimates. *Journal of Geophysical Research*, 116(C11):1–15.

Arrigo, K. R., Perovich, D. K., Pickart, R., Brown, Z., van Dijken, G. L., and Lowry et al., K. E. (2012). Massive Phtoplankton Blooms Under Arctic Sea Ice. *Science*, 336(6087):1353–1472.

Arrigo, K. R., van Dijken, G., and Pabi, S. (2008). Impact of a shrinking Arctic ice cover on marine primary production. *Geophysical Research Letters*, 35(19):1–6.

Arrigo, K. R., Weiss, A. M., and Smith, W. O. (1998). Physical forcing of phytoplankton dynamics in the southwestern ross sea. *Journal of Geophysical Research: Oceans*, 103(C1):1007–1021.

Astoreca, R., Rousseau, V., and Lancelot, C. (2006). Specific phytoplankton absorption variability and implication for chlorophyll a retrieval in Belgian waters (Southern North Sea). *ESA Special Publications*, 615:1–5.

Babin, M., Morel, A., Claustre, H., Bricaud, A., Kolber, Z., and Falkowski, P. G. (1996). Nitrogen- and irradiance-dependent variations of the maximum quantum yield of carbon fixation in eutrophic, mesotrophic and oligotrophic marine systems. *Deep Sea Research Part I: Oceanographic Research Papers*, 43(8):1241–1272.

Babin, M., Morel, A., and Gagnon, R. (1994). An incubator designed for extensive and sensitive measurements of phytoplankton photosynthetic parameters. *Limnology and Oceanography*, 39(3):694–702.

Baldwin, A. J., Moss, J. A., Pakulski, J. D., Catala, P., Joux, F., and Jeffrey, W. H. (2005). Microbial diversity in a Pacific Ocean transect from the Arctic to Antarctic circles. *Aquatic Microbial Ecology*, 41(1990):91–102.

Bannister, T. and Weidemann, A. (1984). The maximum quantum yield of phytoplankton photosynthesis in situ. *Journal of Plankton Research*, 6(2):275–294.

Barlow, R., Cummings, D., and Gibb, S. (1997). Improved resolution of mono- and divinyl chlorophylls a and b and zeaxanthin and lutein in phytoplankton extracts using reverse phase C-8 HPLC. *Marine Ecology Progress Series*, 161:303–307.

Barlow, R., Mantoura, R., Gough, M., and Fileman, T. (1993). Pigment signatures of the phytoplankton composition in the northeastern Atlantic during the 1990 spring bloom. *Deep Sea Research Part II: Topical Studies in Oceanography*, 40(1-2):459–477.

Barlow, R., Stuart, V., Lutz, V., Sessions, H., Sathyendranath, S., Platt, T., Kyewalyanga, M., Clementson, L., Fukasawa, M., Watanabe, S., and Devred, E. (2007). Seasonal pigment patterns of surface phytoplankton in the subtropical southern hemisphere. *Deep Sea Research Part I: Oceanographic Research Papers*, 54(10):1687–1703.

Bates, N. R. and Mathis, J. T. (2009). The arctic ocean marine carbon cycle: evaluation of air-sea co_2 exchanges, ocean acidification impacts and potential feedbacks. *Biogeosciences*, 6(11):2433–2459.

Becquevort, S., Stefels, J., and Lancelot, C. (2005). Phaeocystis blooms in the global ocean and their controlling mechanisms : a review. *Journal of Sea Research*, 53:43 – 66.

Behrenfeld, M. and Falkowski, P. (1997a). Photosynthetic rates derived from satellite-based chlorophyll concentration. *Limnology and Oceanography*, 1(1):1–20.

Behrenfeld, M. J., Boss, E., Siegel, D. A., and Shea, D. M. (2005). Carbon-based ocean

productivity and phytoplankton physiology from space. *Global Biogeochemical Cycles*, 19.

Behrenfeld, M. J. and Falkowski, P. G. (1997b). A Consumer's Guide to Phytoplankton Primary Productivity Models. *Limnology and oceanogrpahy*, 42(7):1479–1491.

Behrenfeld, M. J., Prasil, O., Babin, M., and Bruyant, F. (2004). In Search of a Physiological Basis for Covariations in Light-Limited and Light-Saturated Photosynthesis. *Journal of Phycology*, 40(1):4–25.

Behrenfeld, M. J., Westberry, T. K., Boss, E. S., O'Malley, R. T., Siegel, D. a., Wiggert, J. D., Franz, B. a., McClain, C. R., Feldman, G. C., Doney, S. C., Moore, J. K., Dall'Olmo, G., Milligan, a. J., Lima, I., and Mahowald, N. (2009). Satellite-detected fluorescence reveals global physiology of ocean phytoplankton. *Biogeosciences*, 6(5):779–794.

Berg, G., Balode, M., Purina, I., Bekere, S., Béchemin, C., and Maestrini, S. (2003). Plankton community composition in relation to availability and uptake of oxidized and reduced nitrogen. *Aquatic Microbial Ecology*, pages 263–274.

Bidigare, R. R., Schofield, O., and Przelin, B. B. (1989). Influence of zeaxanthin on quantum yield of photosynthesis of Synechococcus clone WH7803. *Mar. Ecol. Prog. Ser*, 56:177–188.

Bird, R. E. and Riordan, C. (1984). Simple Solar Spectral Model for Direct and Diffuse Irradiance on Horizontal and Tilted Planes at the Earth's Surface for Cloudless Atmospheres. *Solar Energy research Institute Technical Report*, (SERI/TR-215-2436).

Bird, R. E. and Riordan, C. (1986). Simple Solar Spectral Model for Direct and Dif-

fuse Irradiance on Horizontal and Tilted Planes at the Earth's Surface for Cloudless Atmospheres. *Journal of Climate and Applied Meteorology*, 25(1):87–97.

Björk, G. (2002). Return of the cold halocline layer to the Amundsen Basin of the Arctic Ocean: Implications for the sea ice mass balance. *Geophysical Research Letters*, 29(11):1513.

Booth, B. and Jr., W. S. (1997). Autotrophic flagellates and diatoms in the northeast water polynya, greenland: summer 1993. *Journal of Marine Systems*, 10(1):241 – 261.

Bouman, H., Platt, T., Sathyendranath, S., and Stuart, V. (2005). Dependence of light-saturated photosynthesis on temperature and community structure. *Deep-Sea Research*, 52:1284–1299.

Bouman, H. A., Kraay, G. W., Sathyendranath, S., and D, B. (2000). Bio-optical properties of the subtropical North Atlantic . I . Vertical variability. *Marine Ecology Progress Series*, 200:3–18.

Boyd, P. W., Strzepek, R., Fu, F., and Hutchins, D. a. (2010). Environmental control of open-ocean phytoplankton groups: Now and in the future. *Limnology and Oceanography*, 55(3):1353–1376.

Bricaud, A. (2004). Natural variability of phytoplanktonic absorption in oceanic waters: Influence of the size structure of algal populations. *Journal of Geophysical Research*, 109(C11):1–12.

Bricaud, A., Babin, M., Morel, A., and Claustre, H. (1995). Variability in the chlorophyll-specific absorption coefficients of natural phytoplankton: Analysis and parameterization. *Journal of Geophysical Research*, 100(C7):13321.

Bricaud, A., Morel, A., Babin, M., Allali, K., and Claustre, H. (1998). Variations of light absorption by suspended particles with the chlorophyll a concentration in oceanic (Case 1) waters : analysis and implications for bio-optical models. *Journal of Geophysical Research*, 103(C13):31033–31044.

Bricaud, A. and Stramski, D. (1990). Spectral absorption coefficients of living phytoplankton and nonalgal biogenous matter : A comparison between the Peru upwelling area and the Sargasso Sea. *Direct*, 35(3):562–582.

Buesseler, K. O. (1998). The decoupling of production and particulate export in the surface ocean. *Global Biogeochemical Cycles*, 12(2):297–310.

Buesseler, K. O., Barber, R. T., Dickson, M.-l., Hiscock, R., Keith, J., and Sambrotto, R. (2003). The effect of marginal ice-edge dynamics on production and export in the Southern Ocean along 1701W. *Deep-Sea Research*, 50:579–603.

Bursa, A. (1963). Phytoplankton in the Coastal Waters of the Arctic Ocean at Point Barrow, Alaska. *Arctic*, 16:239–262.

Campbell, J. W. and Aarup, T. (1989). Photosynthetically available radiation at high latitudes. *Limnology and Oceanography*, 34(8):1490–1499.

Carmack, E. and Chapman, D. C. (2003). Wind-driven shelf / basin exchange on an Arctic shelf : The joint roles of ice cover extent and shelf-break bathymetry. *Geophysical Research Letters*, 30(14):3–6.

Carr, M., Friedrichs, M., Schmeltz, M., Noguchiaita, M., Antoine, D., Arrigo, K., Asanuma, I., Aumont, O., Barber, R., and Behrenfeld, M. (2006). A comparison of global estimates of marine primary production from ocean color. *Deep Sea Research Part II: Topical Studies in Oceanography*, 53(5-7):741–770.

Chisholm, S. (1992). Phytoplankton size. In Falkowski, P., Woodhead, A., and Vivirito, K., editors, *Primary Productivity and Biogeochemical Cycles in the Sea*, volume 43 of *Environmental Science Research*, pages 213–237. Springer US.

Claustre, H. (1994). The Trophic Status of Various Oceanic Provinces as Revealed by Phytoplankton Pigment Signatures. *Limnology and Oceanography*, 39(5):1206–1210.

Cleveland, J. S. (1995). Regional models for phytoplankton absorption as a function of chlorophyll a concentration. *Journal of Geophysical Research*, 100(C7):13333.

Cloern, J. E. (1977). Effect of light intensity and temperature on cryptomonas ovata (cryptophyceae) growth and nutrient uptake rates. *Journal of Phycology*, 13(4):389–395.

Cloern, J. E., Grenz, C., and Vidergar-Lucas, L. (1995). An empirical model of the phytoplankton chlorophyll:carbon ratio-the conservation factor between productivity and growth rate. *Limnology and Oceanography*, 40(7):1313–1321.

Comiso, J. C. (2006). Abrupt decline in the Arctic winter sea ice cover. *Geophysical Research Letters*, 33(18):1–11.

Comiso, J. C., Parkinson, C. L., Gersten, R., and Stock, L. (2008). Accelerated decline in the arctic sea ice cover. *Geophysical Research Letters*, 35(1):n/a–n/a.

Cota, G. F., Smith, W. O., and Mitchell, B. G. (1994). Photosynthesis of Phaeocystis in the Greenland Sea. *Limnology and Oceanography*, 39(4):948–953.

Cottrell, M. T. and Kirchman, D. L. (2009). Photoheterotrophic microbes in the Arctic

Ocean in summer and winter. *Applied and environmental microbiology*, 75(15):4958–66.

Coupel, P., Jin, H. Y., Joo, M., Horner, R., Bouvet, H. a., Sicre, M.-a., Gascard, J.-C., Chen, J. F., Garçon, V., and Ruiz-Pino, D. (2012). Phytoplankton distribution in unusually low sea ice cover over the Pacific Arctic. *Biogeosciences*, 9(11):4835–4850.

Cullen, J. J. (1982). The deep chlorophyll maximum: Comparing vertical profiles of chlorophyll a. *Canadian Journal of Fisheries and Aquatic Sciences*, 39(5):791–803.

Cullen, J. J., Franks, P. J., Karl, D. M., and Longhurst, A. (2002). Physical Influences on Marine Ecosystem Dynamics. In Robinson, A., McCarthy, J., and Rothschild, B., editors, *The Sea: Biological-Physical Interactions in the Ocean.*, volume 12, pages 297–336. John Wiley and Sons.

Cullen, J. J. and Lewis, M. R. (1988). The kinetics of algal photoadaptation in the context of vertical mixing. *Journal of Plankton Research*, 10(5):1039–1063.

Cullen, J. J. and Lewis, M. R. (1995). Biological processes and optical measurements near the sea surface: Some issues relevant to remote sensing. *Journal of Geophysical Research*, 100(C7):13255–13266.

Curry, J. A., Schramm, J. L., Rossow, W. B., and Randall, D. (1996). Overview of Arctic Cloud and Radiation Characteristics. *Journal of Climate*, 9(8):1731–1764.

Daufresne, M., Lengfellner, K., and Sommer, U. (2009). Global warming benefits the small in aquatic ecosystems. *Proceedings of the National Academy of Sciences of the United States of America*, 106(31):12788–93.

Davidson, K., Gilpin, L. C., Hart, M. C., Fouilland, E., Mitchell, E., Calleja, I. A., Laurent, C., Miller, A. E. J., and Leakey, R. J. G. (2007). The influence of the balance of inorganic and organic nitrogen on the trophic dynamics of microbial food webs. *Limnology and Oceanography*, 52(5):2147–2163.

Devred, E., Sathyendranath, S., and Platt, T. (2007). Delineation of ecological provinces using ocean colour radiometry. *Marine Ecology Progress Series*, 346:1–13.

Devred, E., Sathyendranath, S., and Platt, T. (2009). Decadal changes in ecological provinces of the northwest Atlantic Ocean revealed by satellite observations. *Methods*, 36:1–6.

Díez, B., Pedrós-Alió, C., and Massana, R. (2001). Study of genetic diversity of eukaryotic picoplankton in different oceanic regions by small-subunit rRNA gene cloning and sequencing. *Applied and environmental microbiology*, 67(7):2932–41.

Dortch, Q. (1990). The interaction between ammonium and nitrate uptake in phytoplankton. *Mar. Ecol. Prog. Ser.*, 61:183–201.

Dubinsky, Z., Falkowski, P. G., and Wyman, K. (1986). Light Harvesting and Utilization by Phytoplankton. *Plant Cell Physiol*, 27(7):1335–1349.

Ehn, J., Mundy, C., Barber, D., Hop, H., Rossnagel, A., and Stewart, J. (2011). Impact of horizontal spreading on light propogation in melt pond covered seasonal sea ice in the Canadian Arctic. *Journal of Geophysical research*.

Eisner, L. B., Twardowski, M. S., Cowles, T. J., and Perry, M. J. (2003). Resolving phytoplankton photoprotective : photosynthetic carotenoid ratios on fine scales using in situ spectral absorption measurements. *Limnology and Oceanography*, 48(2):632–646.

Engelsen, O., Hegseth, E. N., Hop, H., Hansen, E., and Falk-petersen, S. (2002). Spatial variability of chlorophyll-a in the Marginal Ice Zone of the Barents Sea, with relations to sea ice and oceanographic conditions. *J. Mar. Syst.*, 35:79–97.

Eppley, R. W. (1972). Temperature and Phytoplankton Growth in the Sea. *Fishery Bulletin*, 70(4):1063–1085.

Falkowski, P. (1992). Molecular ecology of phytoplankton photosynthesis. In *Primary productivity and biogeochemical cycles in the sea.*, page 4767. Plenum Press, New York.

Falkowski, P. and Raven, J. (1997). *Aquatic photosynthesis*. Blackwell Science Ltd, Oxford, UK.

Falkowski, P. G. and Owens, T. G. (1980). Light-Shade Adaptation : Two Strategies in Marine Phytoplankton. *Plant physiology*, 66(4):592–5.

Fasham, M. (2003). *Ocean biogeochemistry: the role of the ocean carbon cycle in global change*. Global change–the IGBP series. Springer.

Fichot, C. G., Kaiser, K., Hooker, S. B., Amon, R. M. W., Babin, M., Bélanger, S., Walker, S. a., and Benner, R. (2013). Pan-Arctic distributions of continental runoff in the Arctic Ocean. *Scientific reports*, 3:1053.

Field, C. B., Behrenfeld, M. J., Randerson, J. T., and Falkowski, P. (1998). Primary production of the biosphere: Integrating terrestrial and oceanic components. *Science*, 281(5374):237–240.

Finkel, Z. V., Beardall, J., Flynn, K. J., Quigg, A., Rees, T. a. V., and Raven, J. a. (2010).

Phytoplankton in a changing world: cell size and elemental stoichiometry. *Journal of Plankton Research*, 32(1):119–137.

Frouin, R., Franz, B., and Werdell, P. (2003). The SeaWiFS PAR product. *NASA Technical Memorandum 2003-206892*, 22:46–50.

Geider, R. J., Delucia, E. H., Falkowski, P. G., Finzi, A. C., Grime, J. P., Grace, J., Kana, T. M., Roche, J. L. A., Long, S. P., Osborne, B. A., Platt, T., Prentice, I. C., Raven, J. A., Schlesinger, W. H., Smetacek, V., Stuart, V., and Box, P. O. (2001). Primary productivity of planet earth : biological determinants and physical constraints in terrestrial and aquatic habitats. *Global Change Biology*.

Geider, R. J., Macintyre, H. L., Kana, T. M., and Jan, N. (1996). A Dynamic Model of Photoadaptation in Phytoplankton. *Limnology and Oceanography*, 41(1):1–15.

Gilpin, L., Davidson, K., and Roberts, E. (2004). The influence of changes in nitrogen: silicon ratios on diatom growth dynamics. *Journal of Sea Research*, 51(1):21–35.

Gordon, H. and Morel, A. (1983). *Remote Assessment of Ocean Color for Interpretation of Satellite Visible Imagery: A review.* Springer-Verlag. Berlin.

Gordon, H. R. and Morel, A. Y. (1985). Remote Assessment of Ocean Color for Interpretation of Satellite Visible Imagery: A review. *Quarterly Journal of the Royal Meteorological Society*, 111(469):872–872.

Gosselin, M., Levasseur, M., Wheeler, P., Horner, R., and Booth, B. (1997). New measurements of phytoplankton and ice algal production in the Arctic Ocean. *Deep Sea Research Part II: Topical Studies in Oceanography*, 44(8):1623–1644.

Gradinger, R. (1996). Occurrence of an algal bloom under Arctic pack ice. *Marine Ecology Progress Series*, 131(Fig 1):301–305.

Gradinger, R. and Lenz, J. (1995). Seasonal occurrence of picocyanobacteria in the Greenland Sea and central Arctic Ocean. *Polar Biology*, 15(6):447–452.

Ha, S.-Y., Kim, Y.-N., Park, M.-O., Kang, S.-H., Kim, H.-c., and Kyung-Hoon, S. (2012). Production of mycosporine-like amino acids of in situ phytoplankton community in Kongsfjorden, Svalbard, Arctic. *Journal of Photochemistry and Photobiology B: Biology*, 114(0):1 – 14.

Harrison, G. W., Yngve Brsheim, K., Li, W. K., Maillet, G. L., Pepin, P., Sakshaug, E., Skogen, M. D., and Yeats, P. a. (2013). Phytoplankton production and growth regulation in the Subarctic North Atlantic: A comparative study of the Labrador Sea-Labrador/Newfoundland shelves and Barents/Norwegian/Greenland seas and shelves. *Progress in Oceanography*, 114:26–45.

Harrison, W. G. and Platt, T. (1986). Photosynthesis-Irradiance Relationships in Polar and Temperate Phytoplankton Populations. *Marine Ecology*, pages 153 – 164.

Havskum, H., Schlüter, L., Scharek, R., Berdalet, E., and Jacquet, S. (2004). Routine quantification of phytoplankton groups-microscopy or pigment analyses? *Marine Ecology Progress Series*, 273(Willén 1976):31–42.

Hickman, A., Dutkiewicz, S., Williams, R., and Follows, M. (2010). Modelling the effects of chromatic adaptation on phytoplankton community structure in the oligotrophic ocean. *Marine Ecology Progress Series*, 406:1–17.

Hill, V., Cota, G., and Stockwell, D. (2005). Spring and summer phytoplankton commu-

nities in the Chukchi and Eastern Beaufort Seas. *Deep Sea Research Part II: Topical Studies in Oceanography*, 52(24-26):3369–3385.

Hill, V. J., Matrai, P. a., Olson, E., Suttles, S., Steele, M., Codispoti, L., and Zimmerman, R. C. (2013). Synthesis of integrated primary production in the Arctic Ocean: II. In situ and remotely sensed estimates. *Progress in Oceanography*, 110:107–125.

Hill, V. J. and Zimmerman, R. C. (2010). Estimates of primary production by remote sensing in the Arctic Ocean : Assessment of accuracy with passive and active sensors. *Deep-Sea Research Part I*, 57(10):1243–1254.

Hillebrand, H., Dürselen, C.-D., Kirschtel, D., Pollingher, U., and Zohary, T. (1999). Biovolume Calculation for Pelagic and Benthic Microalgae. *Journal of Phycology*, 34:403–424.

Hirata, T., Aiken, J., Hardman-Mountford, N., Smyth, T., and Barlow, R. (2008). An absorption model to determine phytoplankton size classes from satellite ocean colour. *Remote Sensing of Environment*, 112(6):3153–3159.

Hochachka, P. W. and Somero, G. N. (2002). *Biochemical Adaptation: Mechanism and Process in Physiological Evolution.* Oxford University Press, New York.

Hoepffner, N. and Sathyendranath, S. (1992). Bio-optical characteristics of coastal waters : Absorption spectra of phytoplankton and pigment distribution in the western North Atlantic. *Instrumentation*, 37(8):1660–1679.

Holm-Hansen, O., Amos, A., and Hewes, C. (2000). Reliability of estimating chlorophyll a concentrations in Antarctic waters by measurement of in situ chlorophyll a fluorescence. *Marine Ecology Progress Series*, 196:103–110.

Holm-Hansen, O., Lorenzen, C. J., Holmes, R. W., and Strickland, J. D. H. (1965). Fluorometric determination of chlorophyll. *Journal du Conseil*, 30(1):3–15.

Huot, Y., Babin, M., and Bruyant, F. (2013). Photosynthetic parameters in the Beaufort Sea in relation to the phytoplankton community structure. *Biogeosciences*, 10:1551–1576.

IPCC (2007). Climate Change 2007 : Synthesis Report. (November):12–17.

Jeffrey, S. (1997). Application of pigment methods to oceanography. In *Phytoplankton pigments in oceanography: guidelines to modern methods.*, pages 127–165. UNESCO Publishing.

Jeffrey, S. and Wright, S. (1994). Photosynthetic pigments in the Haptophyta. In *The haptophyte algae.*, pages 111–132. Clarendon Press, Oxford.

Johannessen, O. M., Bengtsson, L., Miles, M. W., Kuzmina, S. I., Semenov, V. A., Alekseev, G. V., Nagurnyi, A. P., Zakharov, V. F., Bobylev, L. P., Pettersson, L. H., Hasselmann, K., and Cattle, H. P. (2004). Arctic climate change: observed and modelled temperature and sea-ice variability. *Tellus A*, 56(4):328–341.

Jones, E. P., Anderson, L. G., and Swift, J. H. (1998). Distribution of atlantic and pacific waters in the upper arctic ocean: Implications for circulation. *Geophysical Research Letters*, 25(6):765–768.

Jones, R. I. (2000). Mixotrophy in planktonic protists: an overview. *Freshwater Biology*, 45(2):219–226.

Jordan, R. and Chamberlain, A. (1997). Biodiversity among haptophyte algae. *Biodiversity and Conservation*, 6(1):131–152.

Kahru, M., Brotas, V., Manzano-Sarabia, M., and Mitchell, B. G. (2011). Are phytoplankton blooms occurring earlier in the Arctic? *Global Change Biology*, 17(4):1733–1739.

Kirk, J. (1994). *Light and photosynthesis in aquatic ecosystems*. Cambridge University Press.

Kirk, J. T. O. (1976). A Theoretical Analysis of the Contribution of Algal Cells to the Attenuation of Light Within Natural Waters. III. Cylindrical and Spheroidal Cells. *New Phytologist*, 77(2):341–358.

Kozlowski, W. a., Deutschman, D., Garibotti, I., Trees, C., and Vernet, M. (2011). An evaluation of the application of CHEMTAX to Antarctic coastal pigment data. *Deep Sea Research Part I: Oceanographic Research Papers*, 58(4):350–364.

Kwok, R. (2007). Near zero replenishment of the Arctic multiyear sea ice cover at the end of 2005 summer. *Geophysical Research Letters*, 34(5):L05501.

Kyewalyanga, M., Platt, T., and Sathyendranath, S. (1997). Estimation of the photosynthetic action spectrum:implication for primary production models. *Marine Ecology Progress Series*, 146:207–223.

Latasa, M. (2007). Improving estimations of phytoplankton class abundances using CHEMTAX. *Marine Ecology Progress Series*, 329:13–21.

Laws, E. A. (1991). Photosynthetic quotients, new production and net community production in the open ocean. *Deep Sea Research Part A. Oceanographic Research Papers*, 38(1):143–167.

Laws, E. A., Falkowski, P. G., Smith, W. O., Ducklow, H., and McCarthy, J. J. (2000).

Temperature effects on export production in the open ocean. *Global Biogeochemical Cycles*, 14(4):1231–1246.

Legendre, L. and Rassoulzadegan, F. (1995). Plankton and nutrient dynamics in marine waters. *Ophelia*, 41(1):153–172.

Lewis, M. R., Cullen, J. J., and Platt, T. (1983). Phytoplankton and thermal structure in the upper ocean: Consequences of nonuniformity in chlorophyll profile. *Journal of Geophysical Research: Oceans*, 88(C4):2565–2570.

Li, W. K. W. and Harrison, W. G. (2008). Propagation of an atmospheric climate signal to phytoplankton in a small marine basin. *Limnology and Oceanography*, 53(5):1734–1745.

Li, W. K. W., Mclaughlin, F. A., Lovejoy, C., and Carmack, E. C. (2009). Smallest Algae Thrive As the Arctic Ocean Freshens. *Science*, 326(October):2009–2009.

Light, B., Eicken, H., Maykut, G. A., and Grenfell, T. C. (1998). The effect of included particulates on the spectral albedo of sea ice. *Journal of Geophysical Research*, 103(C12):27739.

Lindsay, R. W., Zhang, J., Schweiger, A., Steele, M., and Stern, H. (2009). Arctic Sea Ice Retreat in 2007 Follows Thinning Trend. *Journal of Climate*, 22(1):165–176.

Longhurst, A. R., Sathyendranath, S., Platt, T., and Caverhill, C. M. (1995). An estimate of global primary production in the ocean from satellite radiometer data. *J. Plankton Res.*, 17(6):1245–1271.

Longhurst.A (1998). *Ecological geography of the sea*. Elsevier.

Lovejoy, C., Vincent, W. F., Bonilla, S., Roy, S., Martineau, M.-J., Terrado, R., Potvin,

M., Massana, R., and Pedrós-Alió, C. (2007). Distribution, Phylogeny, and growth of cold-adapted picoprasinophytes in Arctic seas. *Journal of Phycology*, 43(1):78–89.

Lutz, V., Sathyendranath, S., and Head, E. (1996). Absorption coefficient of phytoplankton:regional variations in the North Atlantic. *Marine Ecology Progress Series*, 135:197–213.

Macdonald, R., Solomon, S., Cranston, R., Welch, H., Yunker, M., and Gobeil, C. (1998). A sediment and organic carbon budget for the Canadian Beaufort Shelf. *Marine Geology*, 144(4):255–273.

Macdonald, R. W., Anderson, L. G., Christensen, J. P., Miller, L. A., Semiletov, I. P., and Stein, R. (2009). The Arctic Ocean, in: Carbon and Nutrient Fluxes in Continental Margins: A Global Synthesis. In Liu, K. K., Atkinson, L., Quinones, R., and Talue-McManus, L., editors, *Global Change The IGBP Series*. Springer.

Mackey, D. and Higgins, H. (2001). Not Just a Black Box. Pigments as a Tool to Estimate the Biomass of Different Phytoplankton Groups. CHEMTAX workshop,Barcelona,Spain.

Mackey, M., Mackey, D., Higgins, H., and Wright, S. (1996). CHEMTAX - a program for estimating class abundances from chemical markers:application to HPLC measurements of phytoplankton. *Marine Ecology Progress Series*, 144:265–283.

Marchant, H., Davidson, A., and Wright, S. (1987). The distribution and abundance of chroococcoid cyanobacteria in the Southern Ocean. *Proc. Natl. Inst. Polar Res. Symp. Polar Biol.*, 1:1–19.

Margalef, R. (1978). Life-forms of phytoplankton as survival alternatives in an unstable environment. *Oceanologica Acta*, 1(4).

Martin, J., Tremblay, J., Gagnon, J., Tremblay, G., Lapoussière, a., Jose, C., Poulin, M., Gosselin, M., Gratton, Y., and Michel, C. (2010). Prevalence, structure and properties of subsurface chlorophyll maxima in Canadian Arctic waters. *Marine Ecology Progress Series*, 412:69–84.

Maslanik, J., Drobot, S., Fowler, C., Emery, W., and Barry, R. (2007). On the Arctic climate paradox and the continuing role of atmospheric circulation in affecting sea ice conditions. *Arctic*, 34:2–5.

Menden-Deuer, S., Lessard, E., and Satterberg, J. (2001). Effect of preservation on dinoflagellate and diatom cell volume, and consequences for carbon biomass predictions. *Marine Ecology Progress Series*, 222:41–50.

Menden-Deuer, S. and Lessard, E. J. (2000). Carbon to volume relationships for dinoflagellates, diatoms, and other protist plankton. *Limnology and Oceanography*, 45(3):569–579.

Mignot, a., Claustre, H., D'Ortenzio, F., Xing, X., Poteau, a., and Ras, J. (2011). From the shape of the vertical profile of in vivo fluorescence to Chlorophyll-¡i¿a¡/i¿ concentration. *Biogeosciences*, 8(8):2391–2406.

Milutinović, S. and Bertino, L. (2011). Assessment and propagation of uncertainties in input terms through an ocean-color-based model of primary productivity. *Remote Sensing of Environment*, 115(8):1906–1917.

Mitchell, B. G., Brody, E. A., Yeh, E.-N., McClain, C., Comiso, J., and Maynard, N. G. (1991). Meridional zonation of the barents sea ecosystem inferred from satellite remote sensing and in situ bio-optical observations. *Polar Research*, 10(1):147–162.

Mobley, C., Stramski, D., Bissett, P., and Boss, E. (2004). Optical Modeling of Ocean

Waters: Is the Case 1 - Case 2 Classification Still Useful? *Oceanography*, 17(2):60–67.

Mock, T. and Thomas, D. N. (2008). Microalgae in Polar Regions : Linking Functional Genomics and Physiology with Environmental Conditions. *Measurement*, pages 285–312.

Montagnes, D. J. S., Berges, J. A., Harrison, P. J., and Taylor, F. J. R. (1994). Estimating carbon, nitrogen, protein, and chlorophyll a from volume in marine phytoplankton. *Limnology and Oceanography*, 39(5):1044–1060.

Montagnes, D. J. S. and Franklin, D. J. (2001). Effect of temperature on diatom volume, growth rate, and carbon and nitrogen content: Reconsidering some paradigms. *Limnology and Oceanography*, 46(8):2008–2018.

Moore, C. M., Suggett, D. J., Hickman, A. E., Kim, Y.-N., Tweddle, J. F., Sharples, J., Geider, R. J., and Holligan, P. M. (2006). Phytoplankton photoacclimation and photoadaptation in response to environmental gradients in a shelf sea. *Limnology and Oceanography*, 51:936–949.

Moore, L. R., Goericke, R., and Chisholm, S. W. (1995). Comparative physiology of synechococcus and prochlorococcus: influence of light and temperature on growth, pigments, fluorescence and absorptive properties. *Marine ecology progress series*, 116(1):259–275.

Morel, A. (1988). Optical modeling of the upper ocean in relation to its biogenous matter content (case I waters). *Journal of Geophysical Research*, 93(C9):10749.

Morel, A. and Berthon, J.-F. (1989). Surface pigments, algal biomass profiles, and

potential production of the euphotic layer: Relationships reinvestigated in view of remote-sensing applications. *Limnology and Oceanography*, 34(8):1545–1562.

Morel, A. and Bricaud, A. (1981). Theoretical results concerning light absorption in a discrete medium, and application to specific absorption of phytoplankton. *Deep Sea Research Part A. Oceanographic Research Papers*, 28(11):1375 – 1393.

Morel, A. and Prieur, L. (1977). Analysis of variations in ocean color. *Limnology and Oceanography*, 22(4):709–722.

Muggli, D. L. and Smith, W. O. (1993). Regulation of nitrate and ammonium uptake in the Greenland Sea. *Marine Biology*, 115(2):199–208.

Mundy, C. J., Gosselin, M., Ehn, J., Gratton, Y., Rossnagel, A., Palmer, M., Barber, D. G., Martin, J., Arrigo, K. R., Fortier, L., Else, B., and Papakyriakou, T. (2009). Contribution of under-ice primary production to an ice-edge upwelling phytoplankton bloom in the Canadian Beaufort Sea. 36:1–5.

Mustapha, S., Bélanger, S., and Larouche, P. (2012). Evaluation of ocean color algorithms in the southeastern Beaufort Sea, Canadian Arctic: New parameterization using SeaWiFS, MODIS, and MERIS spectral bands. *Canadian Journal of Remote Sensing*, (5):535–556.

Nair, A., Sathyendranath, S., Platt, T., Morales, J., Stuart, V., Forget, M.-h., Devred, E., and Bouman, H. (2008). Remote sensing of phytoplankton functional types. *Remote Sensing of Environment*, 112:3366–3375.

Newton, G. (2007). Climate Change Impacts on Australias Coast and Oceans. *Waves*, 13(1):1–32.

Nielsen, T. and Hansen, B. (1999). Plankton community structure and carbon cycling on the western coast of Greenland during the stratified summer situation. *Aquatic Microbial Ecology*, 16(3):205–216.

Not, F., del Campo, J., Balagué, V., de Vargas, C., and Massana, R. (2009). New insights into the diversity of marine picoeukaryotes. *PloS one*, 4(9):e7143.

of Marine Research, N. I. (2002). Report no. 12 to the storting. Technical report, Norwegian Ministry of the Environment.

Osburn, C. L., Retamal, L., and Vincent, W. F. (2009). Photoreactivity of chromophoric dissolved organic matter transported by the Mackenzie River to the Beaufort Sea. *Marine Chemistry*, 115(1-2):10–20.

Overland, J. E. and Wang, M. (2007). Future regional Arctic sea ice declines. *Geophysical Research Letters*, 34(17):L17705.

Pabi, S., van Dijken, G. L., and Arrigo, K. R. (2008). Primary production in the Arctic Ocean, 1998–2006. *Journal of Geophysical Research*, 113(C8):1–22.

Palmer, M. a., Arrigo, K. R., Mundy, C. J., Ehn, J. K., Gosselin, M., Barber, D. G., Martin, J., Alou, E., Roy, S., and Tremblay, J.-E. (2011). Spatial and temporal variation of photosynthetic parameters in natural phytoplankton assemblages in the Beaufort Sea, Canadian Arctic. *Polar Biology*, 34(12):1915–1928.

Parsons, T. and Blackbourn, D. (1968). Pigments of the ciliate *Mesodimium rubrum* (Lohmann). *Neth. J. Sea Res.*, 4:27–31.

Perovich, D. K., Richter-Menge, J. a., Jones, K. F., and Light, B. (2008). Sunlight,

water, and ice: Extreme Arctic sea ice melt during the summer of 2007. *Geophysical Research Letters*, 35(11):L11501.

Perrette, M., Yool, A., Quartly, G. D., and Popova, E. E. (2011). Near-ubiquity of ice-edge blooms in the arctic. *Biogeosciences*, 8(2):515–524.

Platt, T., Caverhill, C., and Sathyendranath, S. (1991). Basin-scale estimates of oceanic primary production by remote sensing: The north atlantic. *Journal of Geophysical Research: Oceans*, 96(C8):15147–15159.

Platt, T., Gallegos, C. L., and Harrison, W. G. (1980). Photoinhibition of photosynthesis in natural assemblages of marine phytoplankton. *Journal of Marine Research*, 38:687–701.

Platt, T. and Jassby, A. (1976). The Relationship Between Photosynthesis and Light for Natural Assemblages of Coastal Marine Phytoplankton. *Journal of Phycology*, 12:421–430.

Platt, T. and Sathyendranath, S. (1988). Oceanic primary production: Estimation by remote sensing at local and regional scales. *Science*, 241(4873):1613–1620.

Platt, T. and Sathyendranath, S. (1999). Spatial structure of pelagic ecosystem processes in the global ocean. *Ecosystems*, 2:384394.

Platt, T. and Sathyendranath, S. (2002). Modelling primary production — i. *Limnology*.

Platt, T., Sathyendranath, S., Forget, M.-h., White, G. N., Caverhill, C., Bouman, H., Devred, E., and Son, S. (2008). Operational estimation of primary production at large geographical scales. *Remote Sensing of Environment*, 112:3437–3448.

Platt, T., Sathyendranath, S., and Ravindran, P. (1990). Primary Production by

Phytoplankton: Analytic Solutions for Daily Rates per Unit Area of Water Surface. *Proceedings of the Royal Society of London. Series B: Biological Sciences*, 241(1301):101–111.

Platt, T., Sathyendranath, S., White, G. N., and Ravindran, P. (1994). Attenuation of visible light by phytoplankton in a vertically structured ocean: solutions and applications. *Journal of Plankton Research*, 16(11):1461–1487.

Pokrovsky, O. S., Viers, J., Dupré, B., Chabaux, F., Gaillardet, J., Audry, S., Prokushkin, A. S., Shirokova, L. S., Kirpotin, S. N., Lapitsky, S. a., and Shevchenko, V. P. (2012). Biogeochemistry of carbon, major and trace elements in watersheds of northern Eurasia drained to the Arctic Ocean: The change of fluxes, sources and mechanisms under the climate warming prospective. *Comptes Rendus Geoscience*, 344(11-12):663–677.

Polyakov, I. V., Alekseev, G. V., Bekryaev, R. V., Bhatt, U., Colony, R. L., Johnson, M. A., Karklin, V. P., Makshtas, A. P., Walsh, D., and Yulin, A. V. (2002). Observationally based assessment of polar amplification of global warming. *Geophysical Research Letters*, 29(18):25–1–25–4.

Polyakov, I. V. and Johnson, M. A. (2000). Arctic decadal and interdecadal variability. *Geophysical Research Letters*, 27(24):4097–4100.

Pope, R. M. and Fry, E. S. (1997). Absorption spectrum (380700 nm) of pure water. II. Integrating cavity measurements. *Applied Optics*, 36(33):8710.

Popova, E. E., Yool, A., Coward, A. C., Dupont, F., Deal, C., Elliott, S., Hunke, E., Jin, M., Steele, M., and Zhang, J. (2012). What controls primary production in the Arctic Ocean? Results from an intercomparison of five general circulation models with biogeochemistry. *Journal of Geophysical Research*, 117:C00D12.

Prieur, L. and Sathyendranath, S. (1981). An optical classification of coastal and oceanic waters based on the specific spectral absorption curves of phytoplankton pigments, dissolved organic matter, and other particulate materials. *Limnology and Oceanography*, 26(4):671–689.

Ptacnik, R., Solimini, A. G., Andersen, T., Tamminen, T., Brettum, P., Lepisto, L., Willen, E., and Rekolainen, S. (2008). Diversity predicts stability and resource use efficiency in natural phytoplankton communities. *Proceedings of the National Academy of Sciences*, 105(13):5134–5138.

Qian, P.-Y., Wang, Y., Lee, O. O., Lau, S. C. K., Yang, J., Lafi, F. F., Al-Suwailem, A., and Wong, A. (2011). Vertical stratification of microbial communities in the Red Sea revealed by 16S rDNA pyrosequencing. *The International Society for Microbial Ecology Journal*, pages 507–518.

Quere, C. L., Harrison, S. P., Prentice, I. C., Buitenhuis, E. T., Aumont, O., Bopp, L., Claustre, H., Cotrim Da Cunha, L., Geider, R., Giraud, X., Klaas, C., Kohfeld, K. E., Legendre, L., Manizza, M., Platt, T., Rivkin, R. B., Sathyendranath, S., Uitz, J., Watson, A. J., and Wolf-Gladrow, D. (2005). Ecosystem dynamics based on plankton functional types for global ocean biogeochemistry models. *Global Change Biology*, 11:2016–2040.

Reilly, J. E. O., Maritorena, S., Mitchell, B. G., Siegel, D. A., Carder, K. L., Garver, S. A., Kahru, M., and Mcclain, C. (1998). Ocean color chlorophyll algorithms for SeaWiFS encompassing chlorophyll concentrations between. *October*, 103(Cll).

Richardson, K., Beardall, J., and Raven, J. A. (1983). Adaptation of Unicellular Algae to Irradiance : An Analysis of Strategies. *New Phytologist*, 93(2):157–191.

Roy, S. (2011). *Phytoplankton pigments: characterization, chemotaxonomy and applications in oceanography*. Cambridge University Press.

Roy, S., Chanut, J., Gosselin, M., and Sime-Ngando, T. (1996). Characterization of phytoplankton communities in the lower St. Lawrence Estuary using HPLC-detected pigments and cell microscopy. *Marine Ecology Progress Series*, 142:55–73.

Sackmann, B. S., Perry, M. J., and Eriksen, C. C. (2008). Seaglider observations of variability in daytime fluorescence quenching of chlorophyll-a in Northeastern Pacific coastal waters. *Biogeosciences Discussions*, 5(4):2839–2865.

Sakshaug, E., Bricaud, a., Dandonneau, Y., Falkowski, P. G., Kiefer, D. a., Legendre, L., Morel, a., Parslow, J., and Takahashi, M. (1997). Parameters of photosynthesis: definitions, theory and interpretation of results. *Journal of Plankton Research*, 19(11):1637–1670.

Sakshaug, E. and Slagstad, D. (1991). Light and productivity of phytoplankton in polar marine ecosystems: a physiological view. *Polar Research*, 10(1):69–86.

Sakshaug, E. and Slagstad, D. (1992). Sea Ice and Wind : Effects on Primary Productivity in the Barents Sea. *PoLAR*, 30(4):579–591.

Sarmiento, J. L. and Gruber, N. (2004). *Chapter 5: Organic Matter Export and Remineralization*, pages 173–226. Princeton University Press.

Sarmiento, J. L., Slater, R., Barber, R., Bopp, L., Doney, S. C., Hirst, A. C., Kleypas, J., Matear, R., Mikolajewicz, U., Monfray, P., Soldatov, V., Spall, S. A., and Stouffer, R. (2004). Response of ocean ecosystems to climate warming. *Global Biogeochemical Cycles*, 18.

Sathyendranath, S., Cota, G., Stuart, V., and Maass, H. (2001). Remote sensing of phytoplankton pigments : a comparison of empirical and theoretical approaches. *International Journal of Remote Sensing*, 22(2):249–273.

Sathyendranath, S., Lazzara, L., and Prieur, L. (1987). Variations in the spectral values of specific absorption of phytoplankton. *Limnology and Oceanography*, 32(2).

Sathyendranath, S., Longhurst, A., Caverhill, C. M., and Platt, T. (1995). Regionally and seasonally differentiated primary production in the North Atlantic. *Deep-Sea Res. I*, 42:1773–1802.

Sathyendranath, S. and Platt, T. (1993). Remote sensing of water-column primary production. measurement of primary production from the molecular to the global scale. 197:236–243.

Sathyendranath, S. and Platt, T. (2001). Primary Production Distribution. In in Chief:John H. Steele, E., Turekian, K. K., and Thorpe, S. A., editors, *Encyclopedia of Ocean Sciences*, pages 572 – 577. Academic Press, Oxford, second edition edition.

Sathyendranath, S., Platt, T., Caverhill, C. M., Warnock, R. E., and Lewis, M. R. (1989a). Remote sensing of oceanic primary production: computations using a spectral model. *Deep Sea Research Part A. Oceanographic Research Papers*, 36(3):431 – 453.

Sathyendranath, S., Platt, T., and Forget, M.-H. (2007). Oceanic primary production: Comparison of models. In *OCEANS 2007 - Europe*, pages 1–3.

Sathyendranath, S., Prieur, L., and Morel, A. (1989b). A 3 component model of ocean

color and its application to remote-sensing of phytoplankton pigments in coastal waters. *International Journal of Remote Sensing*, 10:1373–1394.

Sathyendranath, S., Watts, L., Devred, E., Platt, T., Caverhill, C., and Maass, H. (2004). Discrimination of diatoms from other phytoplankton using ocean-colour data, Mar. *Ecol. Prog. Ser*, 272:59–68.

Saux-Picart, S., Sathyendranath, S., Dowell, M., Moore, T., and Platt, T. (2012). Remote sensing of assimilation number for marine phytoplankton. *Remote Sensing of Environment*.

Schlüter, L. and Møhlenberg, F. (2003). Detecting presence of phytoplankton groups with non-specific pigment signatures. (1998):465–476.

Schlüter, L., Møhlenberg, F., Havskum, H., and Larsen, S. (2000). The use of phytoplankton pigments for identifying and quantifying phytoplankton groups in coastal areas:testing the influence of light and nutrients on pigment/chlorophyll a ratios. *Marine Ecology Progress Series*, 192:49–63.

Sieburth, J. and Smetacek, V. (1978). Pelagic ecosystem structure : Heterotrophic compartments of the plankton and their relationship to plankton size fraction. *Limnology and Oceanography*, 23(6):1256–1263.

Siegel, D. A., Buesseler, K. O., Doney, S. C., Sailley, S. F., Behrenfeld, M. J., and Boyd, P. W. (2014). Global assessment of ocean carbon export by combining satellite observations and food-web models. *Global Biogeochemical Cycles*.

Simon, N., Lebot, N., Marie, D., Partensky, F., and Vaulot, D. (1995). Fluorescent in situ hybridization with rRNA-targeted oligonucleotide probes to identify small phyto-

plankton by flow cytometry . *APPLIED AND ENVIRONMENTAL MICROBIOLOGY*, 61(7).

Slovacek, R., Crowther, D., and Hind, G. (1980). Relative activities of linear and cyclic electron flows during chloroplast CO2-fixation. *Biochim Biophys Acta*, 592(3):495–505.

Smetacek, V. and Nicol, S. (2005). Polar ocean ecosystems in a changing world. *Nature*, 437(7057):362–8.

Smetacek, V. and Passow, U. (1990). Spring bloom initiation and Sverdrup's critical-depth model. *Limnology and Oceanography*, 35(1):228–234.

Smith, R. C., Baker, K. S., Limnology, S., Mar, N., Smith, R. C., and Baker, K. S. (1978). Optical classification of natural waters. *Limnology and Oceanography*, 23(2):260–267.

Smyth, T. J., Tyrrell, T., and Tarrant, B. (2004). Time series of coccolithophore activity in the Barents Sea , from twenty years of satellite imagery. *Time*, 31:2–5.

Soares, M. C., Lobao, L., Vidal, L., Noyma, N., Barros, N., Cardoso, S., and Roland, F. (2011). *Light Microscopy in Aquatic Ecology: Methods for Plankton Communities Studies*, volume 689 of *Methods in Molecular Biology*.

Sosik, H. A. L. and Mitchell, B. G. (1991). Absorption, fluorescence, and quantum yield for growth in nitrogen-limited Dunaliella tertiolecta. *Limnology and Oceanography*, 36(5):910–921.

Sosik, H. M. (1999). Storage of marine particulate samples for light-absorption measurements. *Limnology and Oceanography*, 44(4):1139–1141.

Sosik, H. M. and Mitchell, B. G. (1994). Effects of temperature on growth, light absorption, and quantum yield in Dunaliella Tertiolecta (Chlorophyceae). *Journal of Phycology*, 30(5):833–840.

Steffen, W. L. (1996). A periodic table for ecology? a chemist's view of plant functional types. *Journal of Vegetation Science*, 7(3):425–430.

Stein, R. and MacDonald, R. (2004). *The Organic Carbon Cycle in the Arctic Ocean*. Springer.

Steinberg, D., Nelson, N., Carlson, C., and Prusak, a. (2004). Production of chromophoric dissolved organic matter (CDOM) in the open ocean by zooplankton and the colonial cyanobacterium Trichodesmium spp. *Marine Ecology Progress Series*, 267:45–56.

Stroeve, J. C., Kattsov, V., Barrett, A., Serreze, M., Pavlova, T., Holland, M., and Meier, W. N. (2012). Trends in Arctic sea ice extent from CMIP5, CMIP3 and observations. *Geophysical Research Letters*, 39(16):1–7.

Stuart, V. (2011). Difficulties and limitations in the use of ocean colour remote sensing in polar regions. *IOCCG working group on Ocean Colour Remote Sensing in Polar Seas*.

Stuart, V., Sathyendranath, S., Head, E. J. H., Platt, T., Irwin, B., and Maass, H. (2000). Bio-optical characteristics of diatom and prymnesiophyte populations in the Labrador Sea. *Marine Ecology Progress Series, in press.*

Stuart, V., Sathyendranath, S., Platt, T., Maass, H., and Irwin, B. D. (1998). Pigments and species composition of natural phytoplankton populations: effect on the absorption spectra. *Journal of Plankton Research*, 20(2):187–217.

Stuart, V., Ulloa, O., Alarcon, G., Sathyendranath, S., Major, H., Head, E., and Platt, T. (2004). Bio-optical characteristics of phytoplankton populations in the upwelling system off the coast of Chile. (443):87–105.

Suggett, D., Moore, C., Hickman, A., and Geider, R. (2009). Interpretation of fast repetition rate (FRR) fluorescence: signatures of phytoplankton community structure versus physiological state. *Marine Ecology Progress Series*, 376:1–19.

Sverdrup, H. U. (1953). On Conditions for the Vernal Blooming of Phytoplankton. *ICES Journal of Marine Science*, 18(3):287–295.

Tabita, F. R., Hanson, T. E., Satagopan, S., Witte, B. H., and Kreel, N. E. (2008). Phylogenetic and evolutionary relationships of RubisCO and the RubisCO-like proteins and the functional lessons provided by diverse molecular forms. *Philosophical transactions of the Royal Society of London. Series B, Biological sciences*, 363(1504):2629–40.

Tamelander, T., Reigstad, M., and Hop, H. (2009). Ice algal assemblages and vertical export of organic matter from sea ice in the Barents Sea and Nansen Basin (Arctic Ocean). *Polar Biology*, pages 1261–1273.

Tassan, S. and Ferrari, G. M. (1995). An alternative approach to absorption measurements of aquatic particles retained on filters. *Limnology and Oceanography*, 40(8):1358–1368.

Thekaekara, M. P. (1977). *Solar irradiance, total and spectral*, pages 37–59.

Thomson, R. E. and Fine, I. V. (2003). Estimating Mixed Layer Depth from Oceanic Profile Data. *Journal of Atmospheric and Oceanic Technology*, 20(2):319–329.

Tilstone, G., Figueiras, F., Fermín, E., and Arbones, B. (1999). Significance of nanophytoplankton photosynthesis and primary production in a coastal upwelling system (Ría de Vigo, NW Spain). *Marine Ecology Progress Series*, 183(Mann 1993):13–27.

Tilstone, G., Figueiras, F., Lorenzo, L., and Arbones, B. (2003). Phytoplankton composition, photosynthesis and primary production during different hydrographic conditions at the Northwest Iberian upwelling system. *Marine Ecology Progress Series*, 252:89–104.

Tilzer, M. M., von Bodungen, B., and Smetacek, V. (1985). Light-dependence of phytoplankton photosyn thesis in the Antarctic Ocean: Implications for phytoplankton productivity. In Siegfried, W. R., Condy, P. R., and Laws, R. M., editors, *Antarctic Nutrient Cycles and Food Webs*, pages 60 – 69. Springer.

Tjernström, M. (2007). Is There a Diurnal Cycle in the Summer Cloud-Capped Arctic Boundary Layer? *Journal of the Atmospheric Sciences*, 64(11):3970–3986.

Tremblay, J.-E., Michel, C., Hobson, K. a., Gosselin, M., and Price, N. M. (2006). Bloom dynamics in early opening waters of the Arctic Ocean. *Limnology and Oceanography*, 51(2):900–912.

Tyrrell, T. (1999). The relative influences of nitrogen and phosphorus on oceanic primary production. *Nature*, 400:525–531.

Uitz, J., Claustre, H., Gentili, B., and Stramski, D. (2010). Phytoplankton class-specific primary production in the world's oceans: Seasonal and interannual variability from satellite observations. *Global Biogeochemical Cycles*, 24(3):1–19.

Uitz, J., Claustre, H., Morel, A., and Hooker, S. B. (2006). Vertical distribution of phy-

toplankton communities in open ocean: An assessment based on surface chlorophyll. *Journal of Geophysical Research*, 111(C8).

Vassiliev, I. R., Prasil, O., Wyman, K. D., Kolber, Z., Hanson, A. K., Prentice, J. E., and Falkowski, P. G. (1994). Inhibition of PS II photochemistry by PAR and UV radiation in natural phytoplankton communities. *Photosynthesis Research*, 42(1):51–64.

Vellinga, M. and Wood, R. (2002). Global climatic impacts of a collapse of the atlantic thermohaline circulation. *Climatic Change*, 54:251–267.

Vidussi, F., Roy, S., Lovejoy, C., Gammelgaard, M., Thomsen, H. A., Booth, B., Tremblay, J.-e., and Mostajir, B. (2004). Spatial and temporal variability of the phytoplankton community structure in the North Water Polynya, investigated using pigment biomarkers. *Canadian Journal of Fisheries and Aquatic Sciences*, 61(11):2038–2052.

Vincent, W. F. (2010). Microbial ecosystem responses to rapid climate change in the Arctic. *The ISME journal*, 4(9):1087–90.

Wassmann, P., Duarte, C. M., Agustí, S., and Sejr, M. K. (2011). Footprints of climate change in the Arctic marine ecosystem. *Global Change Biology*, 17(2):1235–1249.

Wassmann, P. and Reigstad, M. (2011). Future Arctic Ocean seasonal ice zones and implications for pelagic-benthic coupling. *Oceanography*, 24(3):220–231.

Waterbury, J. B., Watson, S. W., Valois, F. W., and Franks, D. G. (1986). Biological and ecological characterization of the marine unicellular cyanobacterium synechococcus. *Can. Bull. Fish. Aquat. Sci*, 214:71–120.

Wheeler, P., Watkins, J., and Hansing, R. (1997). Nutrients, organic carbon and or-

ganic nitrogen in the upper water column of the Arctic Ocean: implications for the sources of dissolved organic carbon. *Deep Sea Research Part II: Topical Studies in Oceanography*, 44(8):1571–1592.

Wright, S. and Jeffrey, S. (2006). Pigment markers for phytoplankton production. In Volkman, J., editor, *Marine Organic Matter: Biomarkers, Isotopes and DNA*, volume 2N of *The Handbook of Environmental Chemistry*, pages 71–104. Springer Berlin Heidelberg.

Wright, S., Thomas, D., Marchant, H., Higgins, H., Mackey, M., and Mackey, D. (1996). Analysis of phytoplankton of the Australian sector of the Southern Ocean: comparisons of microscopy and size frequency data with interpretations of pigment HPLC data using the CHEMTAX matrix factorisation program. *Marine Ecology Progress Series*, pages 285–298.

Wright, S. and van den Enden, R. (2000). Phytoplankton community structure and stocks in the East Antarctic marginal ice zone (BROKE survey, JanuaryMarch 1996) determined by CHEMTAX analysis of HPLC pigment signatures. *Deep-Sea Res. Part II: Top. Stud. Oceanogr.*, pages 2363–2400.

Wu, J. (2000). Phosphate Depletion in the Western North Atlantic Ocean. *Science*, 289(5480):759–762.

Yentsch, C. S. (1981). Vertical Mixing, A Constraint to Primary Production: An Extension of the Concept Of an Optimal Mixing Zone. In Nihoul, J. C., editor, *Ecohydrodynamics Proceedings of the 12th International Liege Colloquium on Ocean Hydrodynamics*, volume 32 of *Elsevier Oceanography Series*, pages 67–78. Elsevier.

Zhang, J., Spitz, Y. H., Steele, M., Ashjian, C., Campbell, R., Berline, L., and Matrai,

P. (2010). Modeling the impact of declining sea ice on the Arctic marine planktonic ecosystem. *Journal of Geophysical Research*, 115(C10):1–24.

Zubkov, M., Sleigh, M., and Burkill, P. (2000). Assaying picoplankton distribution by flow cytometry of underway samples collected along a meridional transect across the Atlantic Ocean. *Aquatic Microbial Ecology*, 21(1996):13–20.